Coastal and Hydraulics Laboratory

US Army Corps of Engineers®
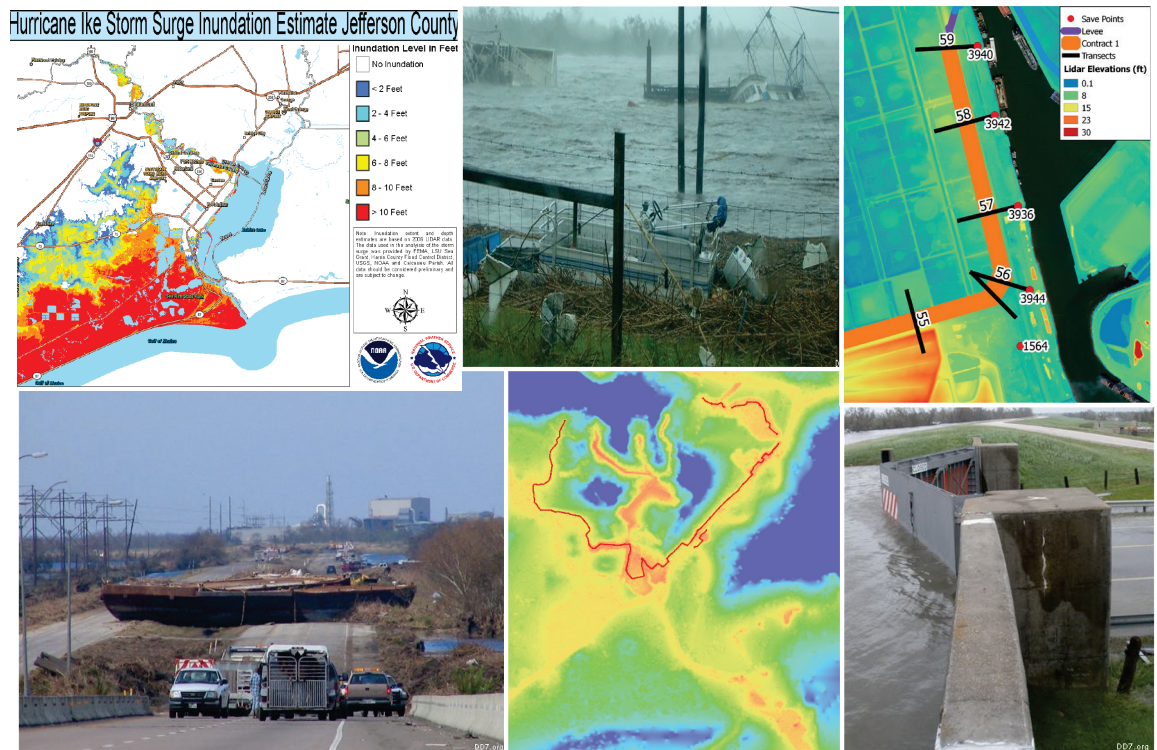Engineer Research and
Development Center

Sabine Pass to Galveston Bay, TX Pre-Construction, Engineering and Design (PED): Coastal Storm Surge and Wave Hazard Assessment

Report 1 – Background and Approach

Jeffrey A. Melby, Thomas C. Massey, Abigail L. Stehno, Norberto C. Nadal-Caraballo, Shubhra Misra, and Victor Gonzalez

August 2021

The US Army Engineer Research and Development Center (ERDC) solves the nation's toughest engineering and environmental challenges. ERDC develops innovative solutions in civil and military engineering, geospatial sciences, water resources, and environmental sciences for the Army, the Department of Defense, civilian agencies, and our nation's public good. Find out more at www.erdc.usace.army.mil.

To search for other technical reports published by ERDC, visit the ERDC online library at https://erdclibrary.on.worldcat.org/discovery.

Sabine Pass to Galveston Bay, TX Pre-Construction, Engineering and Design (PED): Coastal Storm Surge and Wave Hazard Assessment

Report 1 – Background and Approach

Jeffrey A. Melby, Thomas C. Massey, Abigail L. Stehno, Norberto C. Nadal-Caraballo, and Victor Gonzalez

Coastal and Hydraulics Laboratory
US Army Engineer Research and Development Center
3909 Halls Ferry Road
Vicksburg, MS 39180-6199

Shubhra Misra

US Army Engineer District, Galveston
CESWG-EC-H
2000 Fort Point Road, Galveston, TX 77550

Report 1 of a series

Abstract

The US Army Corps of Engineers, Galveston District, is executing the Sabine Pass to Galveston Bay Coastal Storm Risk Management (CSRM) project for Brazoria, Jefferson, and Orange Counties regions. The project is currently in the Pre-construction, Engineering, and Design phase. This report documents coastal storm water level and wave hazards for the Port Arthur CSRM structures. Coastal storm water level (SWL) and wave loading and overtopping are quantified using high-fidelity hydrodynamic modeling and stochastic simulations. The CSTORM coupled water level and wave modeling system simulated 195 synthetic tropical storms on three relative sea level change scenarios for with- and without-project meshes. Annual exceedance probability (AEP) mean values were reported for the range of 0.2 to 0.001 for peak SWL and wave height (H_{m0}) along with associated confidence limits. Wave period and mean wave direction associated with H_{m0} were also computed. A response-based stochastic simulation approach is applied to compute AEP runup and overtopping for levees and overtopping, nappe geometry, and combined hydrostatic and hydrodynamic fluid pressures for floodwalls. CSRM structure crest design elevations are defined based on overtopping rates corresponding to incipient damage. Survivability and resilience are evaluated. A system-wide hazard level assessment was conducted to establish final recommended system-wide CSRM structure elevations.

Contents

Figures and Tables

Figures

Tables

Preface

The study summarized in this report was conducted at the request of the Galveston District (SWG), US Army Corps of Engineers (USACE). The portion of the study reported herein was funded by SWG, under a Cross Charge Labor Code, and primarily conducted at the US Army Engineer Research and Development Center (ERDC), Coastal and Hydraulics Laboratory (CHL), Vicksburg, MS, during the period October 2018–April 2020.

SWG project leadership included Mr. Eddie Irigoyen, SWG Project Manager (PM) for Freeport; Mr. Charles Wheeler, SWG PM for Port Arthur; and Mr. Orlando Ramos-Gines, SWG PM for Orange County. Dr. Shubhra Misra was SWG project technical lead and primary engineering point of contact at SWG. At the time of this study, Mr. Robert Thomas was Chief, Engineering and Construction, SWG. Mr. James Gutshall was Chief of Harbors, Entrances, and Structures Branch within the Navigation Division, led by Dr. Jackie S. Pettway, Chief. Ms. Ashley Frey was Chief of Coastal Processes Branch within the Flood and Storm Protection Division, led by Dr. Cary A. Talbot, Chief. Mr. Jeffrey R. Eckstein was Deputy Director, CHL, and the Director was Dr. Ty V. Wamsley.

At the time of publication of this report, COL Teresa Schlosser was Commander of ERDC, and Dr. David Pittman was Director.

Acknowledgement

Executive Summary

The US Army Corps of Engineers (USACE), Galveston District, is executing the Sabine Pass to Galveston Bay (S2G) Coastal Storm Risk Management (CSRM) project for Brazoria, Jefferson, and Orange Counties regions. The project is currently in the Pre-construction, Engineering, and Design (PED) phase. As identified during the Final Integrated Feasibility Report – Environmental Impact Statement, the S2G Project CSRM formulated measures consist of reducing risks of tropical storm water level (SWL) impacts by constructing the new Orange 3 CSRM system in Orange County and increasing the level of risk reduction and resiliency of the existing Port Arthur and Vicinity and Freeport and Vicinity Hurricane Flood Protection systems.

As part of the ongoing PED phase of the project, this report documents the methods used to develop coastal SWL and wave hazards for an analysis focused on evaluation of the entire CSRM systems for Jefferson, Brazoria, and Orange Counties. Coastal SWL, wave loading, and wave and SWL overtopping rate are quantified using state of the art hydrodynamic modeling and stochastic simulations.

A joint probabilistic model of historical hurricane parameters was developed that spans the full range of tropical storm hazards from frequent, low-intensity storms to very rare, very intense storms. The probabilistic model describes the continuous spatial and temporal hazard. This probabilistic model was sampled efficiently to develop a suite of 195 synthetic tropical storms that effectively capture the flood hazard for the region from Freeport to the Louisiana-Texas border. Wind and pressure fields were developed for these 195 storms using the Planetary Boundary Layer model.

The CSTORM coupled circulation, SWL, and wave modeling system was used to accurately quantify SWL and wave hazards. New model meshes were developed from very-high-resolution land and sub-aqueous surveys for with- and without-project scenarios. With-project meshes include the new Orange CSRM features, deepening of Sabine-Neches Waterway, and increased levee and floodwall elevations as authorized under the S2G feasibility study. The new meshes provide the highest-resolution regional surge and wave modeling done to date for the region. The CSTORM model was validated against historical storms and then used to model the 195

synthetic tropical storms. The storms were run on three relative sea level change (RSLC) scenarios for with- and without-project meshes. These RSLC scenarios are (1) SLC0 corresponding to project completion in 2027 and an associated "Low" RSLC projection, (2) SLC1 corresponding to the end of a 50 yr service lifecycle in 2077 and an associated "Intermediate" RSLC projection, and (3) SLC2 corresponding to the end of a 100 yr service lifecycle in 2127 and an associated "Intermediate" RSLC projection. A "High" RSLC projection over a period of 50 yr is approximately the same as an "Intermediate" RSLC projection over a period of 100 yr, so SLC2 corresponds closely with the end of a 50 yr service life in 2077 under a "High" RSLC projection.

Flood hazard exposure of the project features was quantified by computing hazard curves for the CSTORM output near the structures. Annual exceedance probabilities (AEP) were computed for the range of 1 to 0.0001 for peak SWL and wave height (H_{m0}) but reported out in tables only between 0.2 to 0.001. Wave period (T_p) and mean wave direction associated with H_{m0} were also computed. Both mean values and confidence limits (CL) are summarized herein. In this case, CLs are used to describe epistemic uncertainty or levels of assurance. For hazard curves contained herein, the mean and median are indistinguishable. Therefore, only mean values are reported.

Five different workflows for stochastic assessment of wave runup and overtopping rate of the levees and floodwalls were developed. These range from relatively simple event-based (EB) or frequency-based approaches to complex time-dependent response-based (RB) approaches. In the EB approaches, inputs to runup and overtopping rate calculations are single AEP SWL and H_{m0} values (statistical *events*) with associated T_p and wave direction. For RB approaches, peak run-up and overtopping rate responses are computed for each storm, and then hazard relations were computed from the results. Event-based approaches only yield constant forcing hazard but inconsistent response hazards and therefore inconsistent risk while RB approaches can produce consistent response hazards and resulting risk over project area. It is shown that a peaks-based RB approach yielded an accurate stochastic response with a reasonable computational requirement and is, therefore, the preferred approach to assess and present run-up and overtopping rate response results in this report.

Assessment of crest design elevations was based on peak overtopping rates corresponding to incipient damage. Limit states for peak levee overtopping rate of q = 0.01 cfs/ft for the 50% CL and q =0.1 cfs/ft for the 90% CL were based on the start of erosion for a good-quality grass cover on a clay levee. Limit states for floodwall overtopping rate of q = 0.03 cfs/ft for the 50% CL and q =0.1 cfs/ft for the 90% CL were based on the start of erosion of soils in the unprotected leeside of the floodwall. These limit states are accepted standard of practice within the USACE and internationally. An additional survivability or resilience limit state of q = 1 cfs/ft was checked. In addition to overtopping rate and optimized crest elevations associated with non-exceedance of the limit states, peak overtopping nappe geometry and combined hydrostatic and hydrodynamic peak fluid pressures on vertical structures (e.g., floodwalls) were also calculated and reported at various AEPs.

1 Introduction

1.1 Background

The US Army Corps of Engineers (USACE), Galveston District (SWG), is executing the Sabine Pass to Galveston Bay (S2G), Coastal Storm Risk Management (CSRM), project for Brazoria, Jefferson and, Orange Counties regions. The project is currently in the Pre-construction, Engineering, and Design (PED) phase.

1.2 Objective

The Final Integrated Feasibility Report – Environmental Impact Statement (USACE 2017a) identified measures for reducing risks of tropical storm inundation impacts. The S2G CSRM PED project incorporates additions and modifications of Hurricane Flood Protection (HFP) systems in Orange, Jefferson, and Brazoria Counties, Texas (Figure 1). These measures consist of the following:

- Constructing the new 26.7 mi[1,2] levee/floodwall at the edge of the Sabine and Neches river floodplains from Orange County to the vicinity of Orangefield, Texas (Orange 3 CSRM).
- Increasing the level of risk reduction and resiliency of existing Port Arthur and Vicinity HFP by raising or reconstructing 11.6 mi of existing levees and floodwalls.
- Increasing the level of risk reduction and resiliency of existing Freeport and Vicinity HFP by raising or reconstructing 18.2 mi of existing levees and floodwalls.
- Replacing vehicular closure structures.
- Constructing navigable surge gate structures.
- Increasing resiliency of the CSRM project by installing erosion and scour protection as necessary.

---

[1] For a full list of the spelled-out forms of the units of measure used in this document, please refer to *US Government Publishing Office Style Manual*, 31st ed. (Washington, DC: US Government Publishing Office 2016), 248-52, https://www.govinfo.gov/content/pkg/GPO-STYLEMANUAL-2016/pdf/GPO-STYLEMANUAL-2016.pdf.

[2] For a full list of the unit conversions used in this document, please refer to *US Government Publishing Office Style Manual*, 31st ed. (Washington, DC: US Government Publishing Office 2016), 345-7, https://www.govinfo.gov/content/pkg/GPO-STYLEMANUAL-2016/pdf/GPO-STYLEMANUAL-2016.pdf.

As part of the ongoing PED phase of the project, this report documents the methodology to analyze coastal storm surge and wave hazards and is part of a larger analysis focused on evaluating the entire CSRM systems for Jefferson, Brazoria, and Orange Counties. Coastal storm surge, wave loading, and wave and surge overtopping are quantified using state-of-the-art hydrodynamic modeling and stochastic simulations.

Figure 1. CSRM systems for Brazoria (left), Orange (middle), and Jefferson (right) regions.
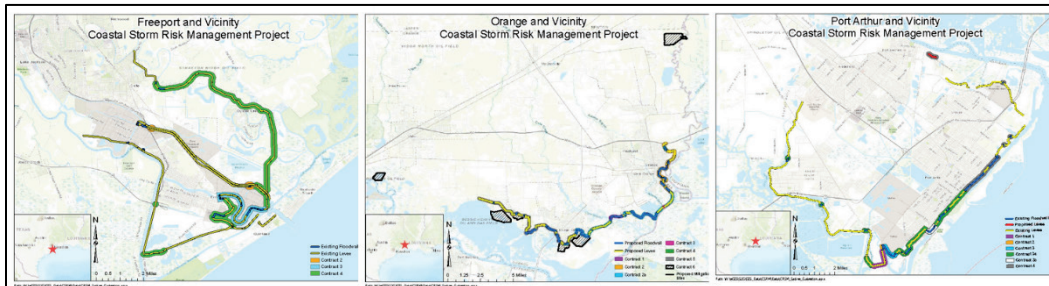
The USACE Chief of Engineers S2G Report is reproduced in Appendix J. Two recommendations should be restated:

> The recommended plan is intended to prevent damages to structures and content and critical infrastructure from coastal storm surge and waves.

and

> In accordance with USACE Sea Level Change (SLC) Guidance, Engineer Regulation (ER) 1100-2-8162, the study evaluated potential impacts in SLC in its plan formulation and engineering of the recommended plan. Three levels of Relative Sea Level Change (RSLC) were considered for both the without-project and with-project conditions. The risk reduction system has been designed to provide a risk reduction against a 1% annual chance exceedance probability storm event based on the 2070 (50-year service life after completion of construction) jntermediate RSLC forecast condition. In recognition of the uncertainty presented by sea level rise, adaptation capacity has been incorporated into the final feasibility-level design to maximize the systems' overall usefulness over the life of the project. The adaptability will allow for limited overtopping of wave and minor still water

overtopping that would then be mitigated for using interior drainage features or height increases to the floodwall if required.

Herein, four levels of protection were addressed for three RSLC scenarios as follows:

1. Existing: present day existing CSRM structure elevations.
2. Authorized: CSRM structure elevations as authorized under the S2G feasibility study.
3. Optimized: CSRM structure elevations that just meet the limit state overtopping criteria.
4. Adaptability: CSRM structure elevations as authorized elevation plus 2 ft.

1.3   Approach

The analysis approach summarized herein took advantage of previous regional modeling completed under the Federal Emergency Management Agency (FEMA) flood information study (FIS) within the FEMA Risk Mapping, Assessment, and Planning program that followed Hurricane Ike[1] (USACE 2017a), and Coastal Texas Comprehensive Study (CTXCS)[3,4] (see Appendix A for description of prior modeling and analysis studies). However, all of the storm wave and water level forcing used herein for levee and floodwall design was based on new modeling done specifically for this project. The analysis includes hurricane surge and wave hydrodynamic regional modeling, nearshore wave modeling, and CSRM stochastic structure response modeling. Extremal

---

[1] FEMA (Federal Emergency Management Agency). 2011 (Unpublished). *Flood Insurance Study: Coastal Counties, Texas. Intermediate Submission 2: Scoping and Data Review*. Joint Report prepared for Federal Emergency Management Agency by the Department of the Army, US Army Corps of Engineers, Washington DC.

[2] Melby, J. A., N. C. Nadal-Caraballo, J. Ratcliff, T. C. Massey, and R. Jensen. 2015 (Unpublished). *Sabine Pass to Galveston Bay Wave and Water Level Modeling*, ERDC/CHL Technical Report, Vicksburg, MS: US Army Engineer Research and Development Center.

[3] Massey, T. C., R. Jensen, M. Cialone, Y. Ding, M. Owensby, and N. C. Nadal-Caraballo. 2019. *A Brief Overview of the Coastal Texas Protection and Restoration Feasibility Study: Coastal Storm Model Simulations of Waves and Water Levels*. ERDC/CHL LR-19-7. Vicksburg, MS: US Army Engineer Research and Development Center. NOTE: For access to this document, contact the author.

[4] Nadal-Caraballo, N. C., A. B. Lewis, V. M. Gonzalez, T. C. Massey, and A. T. Cox. Draft. Coastal Texas Protection and Restoration Feasibility Study, Probabilistic Modeling of Coastal Storm Hazards. ERDC/CHL Technical Report, Vicksburg, MS: US Army Engineer Research and Development Center.

statistics were computed for storm responses. The process used in the present analysis was as follows:

1. Developed a joint probability model of tropical storm parameters for S2G PED.
   a. This included defining storm recurrence rates for the coastline and mapping previously defined synthetic tropical storms developed within CTXCS onto the new joint probability model.
   b. These storms had a frequency range based on storm water levels of approximately one in 1 yr to one in 2000 yr.
2. Adopted a genetic algorithm optimization storm water level (SWL) hazard curve matching technique to determine an optimal suite of 195 storms from the 660 synthetic tropical storms from CTXCS.
   a. The 660 CTXCS storms impacted the Texas coast and spanned the practical probability space.
   b. The 195 S2G storms characterized the flood hazard for the entire S2G region.
3. Adopted wind and pressure fields for all storms developed within CTXCS study using Planetary Boundary Layer (PBL) TC96 Model. Associated TROP files, which contain time series of hurricane parameters at 1 hr intervals, from the CTXCS study were used to define storm parameters.
4. Revised without-project and with-project ADCIRC and Steady State Wave (STWAVE) grids by refining the CTXCS base mesh and adding new bathymetry and topography, as well as significantly higher spatial resolution, in the areas of the S2G CSRM systems.
   a. CSTORM includes coupled ADCIRC surge/circulation and STWAVE wave models.
   b. New bathymetry included surveys of Taylor and Hillebrand bayous, Sabine-Neches Waterway (SNWW), and the Taylor Bayou turning basin.
   c. New topography incorporated regional LiDAR survey at 1 ft resolution.
   d. With-project grids incorporated authorized USACE projects, including the SNWW 48' project, Freeport Dow Canal floodgate, Orange County levee system with authorized topographic and bathymetric changes, and authorized design elevations for the existing CSRM systems.

5. Revalidated surge response against observations using historical Hurricanes Ike (2008), Carla (1961), Rita (2005), Harvey (2017), and Bret (1999). Computed bias and uncertainty for the models.
6. Completed CSTORM simulations for all synthetic joint probability method with Optimal Sampling (JPM-OS) storms for with- and without-project conditions and three RSLC scenarios.
   a. CSTORM modeling output at ADCIRC mesh and STWAVE grid locations.
   b. CSTORM modeling included output model nodes and at 5148 save points (SPs) to cover the areas around the CSRM structures and seaward to the 15 m depth contour in the Gulf of Mexico.
7. Computed extremal statistics and confidence limits for waves and water levels using StormSim (Nadal-Caraballo et al. 2015; Melby et al. 2015; Melby et al. 2017) and the joint probability method (JPM).
   a. Adjusted responses for bias.
   b. Mean peak SWL and peak significant wave height (H_{m0}) annual exceedance probabilities (AEP) characterize a wide range of probabilities. Mean peak wave period and mean wave direction directly correspond to SWL and H_{m0} AEP values. Mean and median are indistinguishable; therefore, only the mean is reported herein.
   c. The resulting probabilistic model of storm responses was conditionally joint with JPM-OS storm parameters.
   d. Uncertainty included the standard deviation of epistemic uncertainty as well as upper 90% and lower 10% confidence limits (CL).
8. Conducted simulations to determine the local stochastic response of the CSRM system.
   a. Response simulation included wave runup and steady overflow and wave overtopping for levees; steady overflow and wave overtopping, combined hydrostatic and hydrodynamic pressures and overtopping nappe characteristics for floodwalls; and included epistemic uncertainty.
   b. Computed overtopping rates were compared to limit states.
   c. Four different crest elevation categories were evaluated:
      (1) Existing: present day existing (without-project) levee and floodwall elevations.
      (2) Authorized: with-project levee and floodwall elevations as authorized under the S2G feasibility study.
      (3) Optimized: with-project levee and floodwall elevations that just meet the limit state overtopping criteria.

   (4) Adaptability: with-project levee and floodwall elevations as authorized elevation plus 2 ft.

9. Reported results at various AEPs and CL at each critical section for the with- and without-project alternatives for the three RSLC scenarios.

  a. Results included combined overflow and overtopping rates, combined hydrostatic and hydrodynamic wall pressures, and overtopping nappe geometry for authorized CSRM structure elevations.

  b. Damage initiation overtopping criteria and resilience and survivability criteria provide reference to "tolerable" overtopping rates.

  c. Evaluation of existing and authorized elevations.

  d. Calculation and evaluation of optimized elevations for design and adaptability

The project has been authorized for a design scenario that is a 50 yr intermediate RSLC scenario and for adaptability at 100 yr intermediate or, equivalently, 50 yr high RSLC scenarios. These timelines are discussed in more detail in Chapter 3, "Relative sea level change (RSLC)" section. All coastal hazard response parameters are determined for these three RSLC scenarios. The project authorization for design is for a 50 yr intermediate RSLC scenario, beginning in year 2027 and ending in year 2077, with considerations of adaptability including 100 yr intermediate/50 yr high RSLC rates.

2 Storm Hazard Development

2.1 Joint Probability Method (JPM)

The lack of adequate storm data in hurricane-prone areas has been a known weakness in design of coastal flood control systems for decades. This led to probabilistic synthetic storm modeling. The JPM has become the dominant probabilistic model used to assess the coastal storm hazard in hurricane-prone areas of the United States. Although the JPM approach has been in development since the 1970s, recent advancements in technology have made it possible to reduce the necessary number of synthetic storms resulting in improved sampling techniques and the development of the JPM-OS (e.g., Nadal et al. 2015). Recent JPM studies have considered uncertainty throughout the process stemming from the probabilistic model, the meteorological and hydrodynamic numerical models, and the climatological and oceanic observations. The developmental progression of the JPM-OS methodology for USACE projects, including storm selection and uncertainty quantification, culminating in the approach taken during the CTXCS study, is described in Appendix A.

2.2 Storm selection for Sabine Pass to Galveston Bay (S2G)

A total of 660 storms was developed for the CTXCS study using the JPM-OS approach[1]. The storm tracks align with idealized master tracks shown in Figure 2 and Figure 3.

For the S2G PED study, a metamodel or surrogate model using a genetic algorithm optimization approach selected an optimal subsample of the 660 CTXCS storms. The method is described in detail in Appendix C. The full suite of 660 storms had already been modeled using CSTORM, so results across the region had been output at SPs surrounding the Brazoria and Sabine CSRM systems and extending offshore. The peak SWLs from the 660 events were used as the primary parameter for optimization.

---

[1] Nadal-Caraballo, N. C., A. B. Lewis, V. M. Gonzalez, T. C. Massey, and A. T. Cox. Draft. *Coastal Texas Protection and Restoration Feasibility Study, Probabilistic Modeling of Coastal Storm Hazards.* Unpublished. ERDC/CHL Technical Report. Vicksburg, MS: US Army Engineer Research and Development Center.

Figure 2. Map of storm tracks for JPM storms.
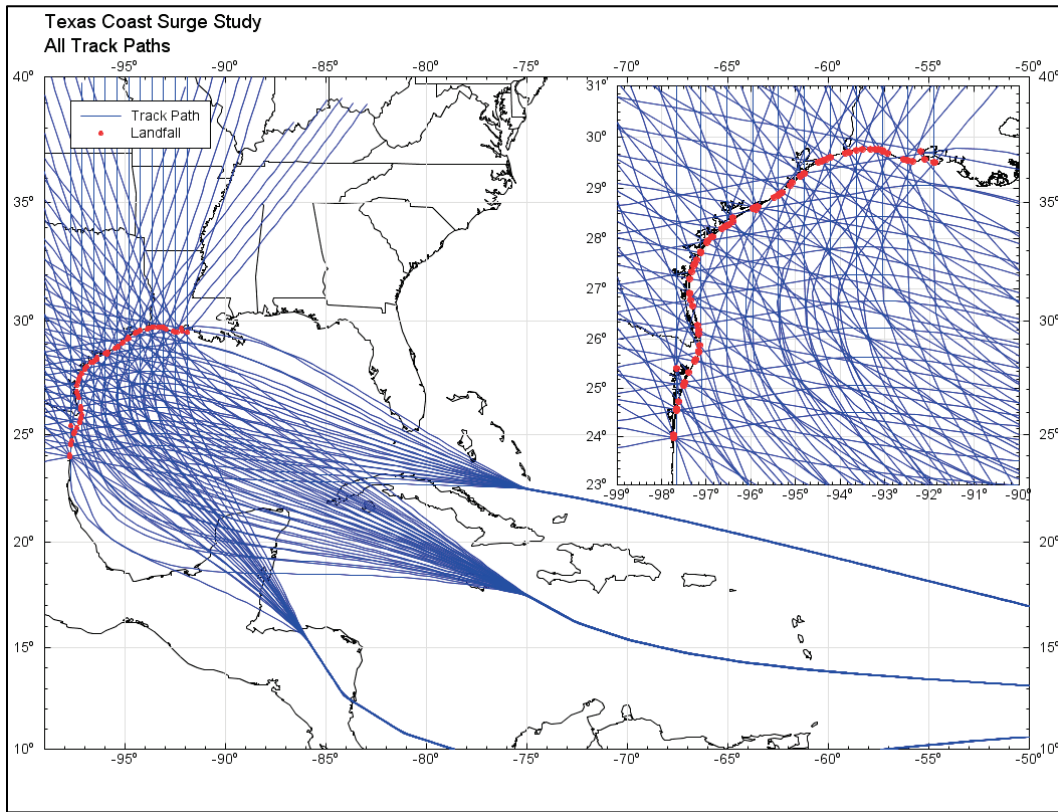
Figure 3. Zoomed-in map of master tracks of storms for entire region (left) and storms that significantly influence project (right).
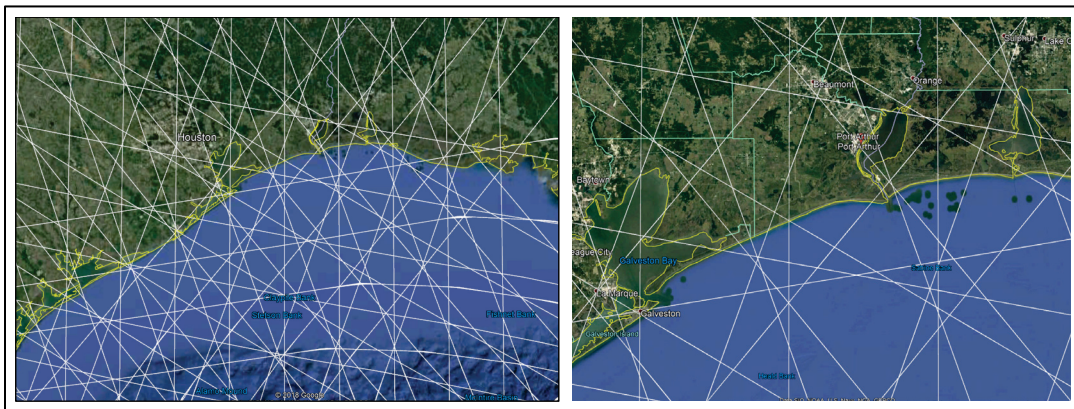
In this approach, an initial sample of storms is obtained and tested against the base condition. The SWL hazard curves are computed for each of the save locations, and the reduced sample hazard curve is compared against the full sample. The best storm sample set is determined by minimizing the difference in hazard curves using a genetic algorithm. The optimal set of events that minimizes the error is selected. While 195 storms were initially selected using this procedure, some of the storms would not run

reliably in CSTORM, so only 189 storms were selected. Figure 4 shows the results of the process where the Genetic Algorithm penalty value is the error of the objective function defined by the normalized hazard curve difference. The horizontal axis shows the number of generations or groups of storms that are iteratively approaching the optimal. On the right is the water level hazard curve for both the full storm set and the reduced optimized storm set of 189 storms. The figures illustrate that the sample of 189 storms converged and the ultimate hazard curve error is very close to zero. Here, convergence describes the fact that the error reduces to nearly zero as the sample size approaches 189. Note that the error between sample and original is small for samples much smaller than 189 storms when considering specific regions such as Port Arthur. However, a larger sample was required to span the large region of north Texas and achieve convergence for overtopping because relatively few storms overtop the CSRM features. The reduced sets of 195 and 189 S2G storms and the original 660 CTXCS storms are summarized in Appendix D. The final set of 189 S2G storms includes representative storms from virtually all of the master tracks shown in Figure 2 and includes all of the headings. Only a few of the tracks that extend into Mexico were omitted. In addition, the 189 S2G tracks span the full range of other hurricane parameters in the full suite of 660 storms. A sample size of 60 storms was used to investigate different local project alternatives. In this case, samples were selected to best characterize the full SWL hazard curve for select small areas.

Figure 4. Genetic Algorithm penalty value plotted as a function of Genetic Algorithm generation (left) and full and reduced storm sets water level hazard curves for CTXCS SP 17396 (S2G SP 1094) in center of Taylors Bayou Turning Basin, Port Arthur (right).
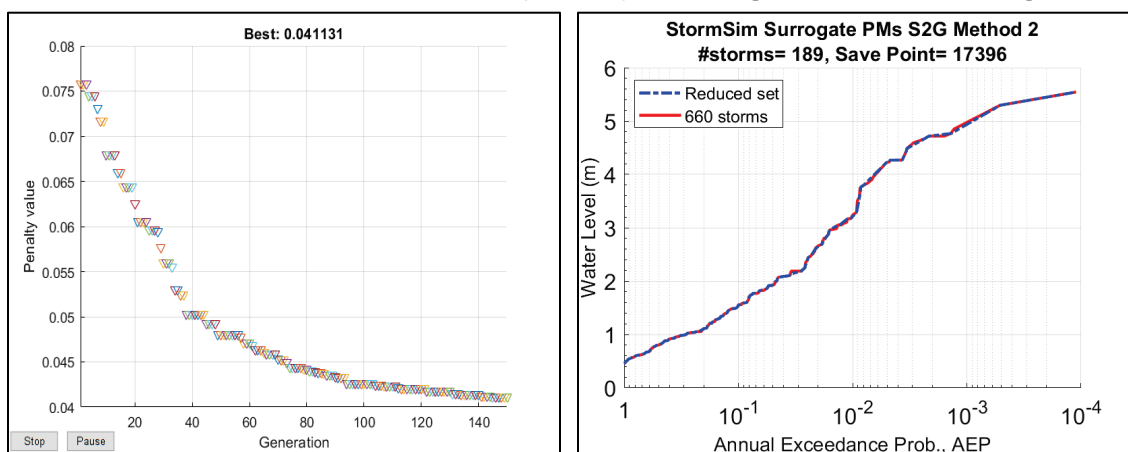
3   Regional Surge and Wave Modeling

3.1   CSTORM model domain, topography, bathymetry, and mesh

Regional wind and surface pressure fields were produced for three wind/pressure field grids for each storm (Figure 5). The Level1 (also referred to as WNAT, or Western Northern Atlantic) grid boundaries extended from 5.0° to 47.2° north latitude and from 99.0° to 54.8° west longitude and used a 0.20° by 0.20° grid spacing. The Level2 (referred to as the GOM for Gulf of Mexico) grid boundaries centered on the Gulf of Mexico and extended from 18.0° to 31.04° north latitude and 98.0° to 79.92° west longitude and used a 0.08° by 0.08° grid spacing. The third set of wind/pressure files had grid boundaries centered on the landfall location of the storm (as such the grid was referred to as the Landfall domain). Since landfall locations changed by storm, this domain was not fixed in any one location as the other two domains were, but the spatial grid resolution and domain size were fixed for every storm. A grid spacing of 0.02° by 0.02° was used, and each domain covered a 3.0° by 3.0° square.

Figure 5. Map showing the three grid boundary extents for the regional wind and pressure files in (red) and the ADCIRC model domain shown in black.

3.2 Wave model (WAM)

The wave modeling technology used to generate the offshore wave estimates for both CTXCS and S2G is the third-generation wave model WAM (Komen et al. 1994). WAM is similar to other third-generation wave models like WaveWatch III[1] or SWAN[2]. WAM makes no a priori assumptions governing the spectral shape of the waves, and the source term solution is formulated to the wave model's frequency/directional resolution. WAM was selected based on its use for previous tropical cyclone simulations as part of the Interagency Performance Evaluation Task Force (USACE 2009a), the Louisiana Coastal Protection and Restoration Project (LACPR) (USACE 2006), and Hurricane Katrina and Rita simulations (Bunya et al. 2010; Dietrich et al. 2010).

Accurately estimating the offshore wave conditions for the entire coastal area of Texas required developing the wave field grid for the entire Gulf of Mexico and extending into the Caribbean Sea and a small part of the western basin of the Atlantic Ocean. However, all synthetic tropical storms used are confined to the area west of 75° west longitude. The bounding box defining the bathymetry used for the offshore wave generation is shown in Figure 6. Open water gaps occur between the Straits of Florida and Cuba and between the western tip of Cuba and the Yucatan Peninsula of Mexico. Portions of the synthetic storm tracks population reside in these areas. Therefore, wind-waves will initially develop outside the gulf, and the resulting energy penetrates into the Gulf of Mexico.

The color-contoured bathymetry shown in Figure 6 was derived from the General Bathymetric Chart of the Oceans (Becker et al. 2009). The WAM grid boundary extents were from 18.0° to 31.0° north latitude and from 98.0° to 75.0° west longitude. A grid spacing of 0.05° by 0.05° was used for discretizing the domain. Defining the wave model grid at this resolution provides accuracy levels for the Caribbean Islands and shoreline features.

---

[1] User manual and system documentation of WAVEWATCH III® version 6.07, 2019. Tech. Note 333, NOAA/NWS/NCEP/MMAB, College Park, MD, USA, 465 pp.

[2] Scientific and Technical Documentation for SWAN Cycle III version 41.20. 2017. Technical report from Delft University of Technology.

Figure 6. Offshore wave generation domain. Water depth color contours are given in meters.
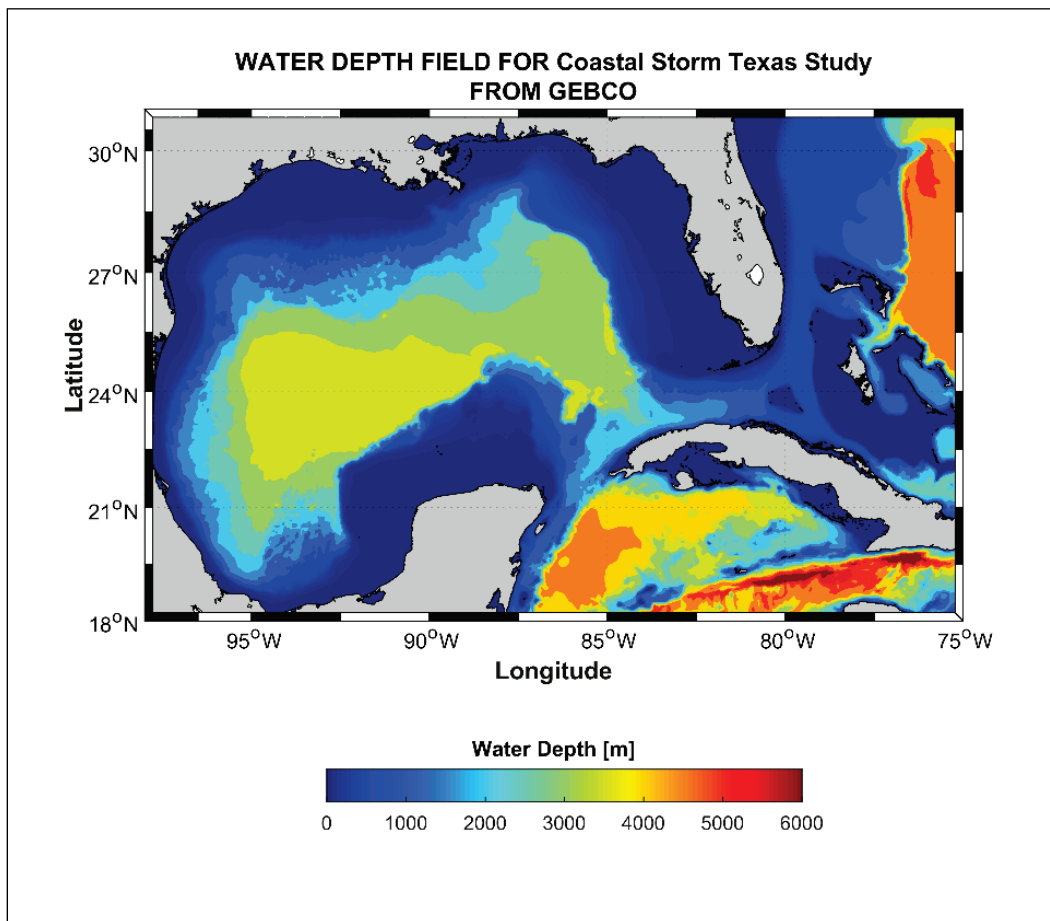
3.3 Nearshore waves: the Steady State Wave (STWAVE) model

Like the WAM model, STWAVE is a finite-difference model that is formulated on a Cartesian grid. STWAVE grids have the x-axis oriented in the cross-shore direction (I) and the y-axis oriented alongshore (J). Wave angles are measured counterclockwise from the x-axis. As a starting point, three STWAVE grids originally developed based on those of the FEMA FIS[1] were analyzed for use: TX-S, TX-C, and TX-N. A fourth grid was added to better bridge the Texas-Louisiana border: TX-LA (Figure 7). It was determined that the TX-S grid was located too far away from any of the project locations to have any significant influence on the computed

---

[1] FEMA (Federal Emergency Management Agency). 2011. Unpublished. *Flood Insurance Study: Coastal Counties, Texas. Intermediate Submission 2: Scoping and Data Review.* Joint Report prepared for Federal Emergency Management Agency by the Department of the Army, US Army Corps of Engineers, Washington DC.

solutions in the project areas. Therefore, the TX-S grid was not used. The STWAVE grids span two State Plane coordinate systems, Louisiana Offshore (FIPS 1703) and Texas South Central (FIPS 4204). The bathymetry, topography, and Manning's n bottom friction values were interpolated from the ADCIRC mesh. A grid spacing of 656 ft was selected for the TX-C grid as its domain did not intersect directly with any project areas. The TX-N grid, which encompasses Freeport, Galveston Bay, and Port Arthur, used a 328 ft grid spacing. The TX-LA grid, which overlaps the TX-N grid and encompasses parts for Port Arthur and Orange County, also used a 328 ft grid spacing. Previous studies of Hurricanes Katrina, Rita, Gustav, and Ike in the Gulf of Mexico as well as the North Atlantic Coast Comprehensive Study used similar resolutions (656 ft in coastal areas, 328–656 ft in nested bays) and demonstrated good agreements with measurements (Dietrich et al. 2011; Hope et al. 2013; Bunya et al. 2010; Dietrich et al. 2010; Cialone et al. 2015). These past studies showed that a 656 ft resolution sufficiently resolved the surf zone to capture the wave-breaking processes that drive wave radiation stresses and wave setup. The TX-N and TX-LA grids used a 328 ft resolution spacing to better resolve with- and without-project configurations and other local topographic features near the project areas.

Figure 7 shows the location of STWAVE grids with respect to the WAM grid and the ADCIRC mesh along with a close-up view of the STWAVE grids with color contours of bathymetry/topography. Note that the location of the TX-S grid in Figure 7 illustrates its significant distance away from the nearest project area, Freeport. The grid geometries are listed in Table 1. The full names of the grids are based on their relative regional location within Texas, moving from north to south. The grids' offshore boundaries were extended into depths of at least 131 ft, which is considered deep by STWAVE standards. Wave interactions with the bottom at this offshore extent are relatively small, particularly in comparison to the importance of wave generation.

STWAVE has two modes available: half-plane and full-plane. Half-plane mode allows wave energy to propagate only from the offshore towards the nearshore ($\pm$ 87.5^o from the x-axis of the grid). STWAVE half-plane grids are typically aligned with the dominant wave direction, since all waves traveling in the negative x-direction, such as those generated by offshore-blowing winds, are neglected in half-plane simulations. Full-plane mode allows wave generation and transformation in all directions. Due to the

large number of storm simulations and possible variations in the dominant wave direction, all simulations used the full-plane mode of STWAVE.

Figure 7. Maps showing the STWAVE grid boundaries in relation to the WAM boundary (a) and a close-up view along the Texas/Louisiana coastline with color contours of bathymetry/topography in (b).

(a)   (b)
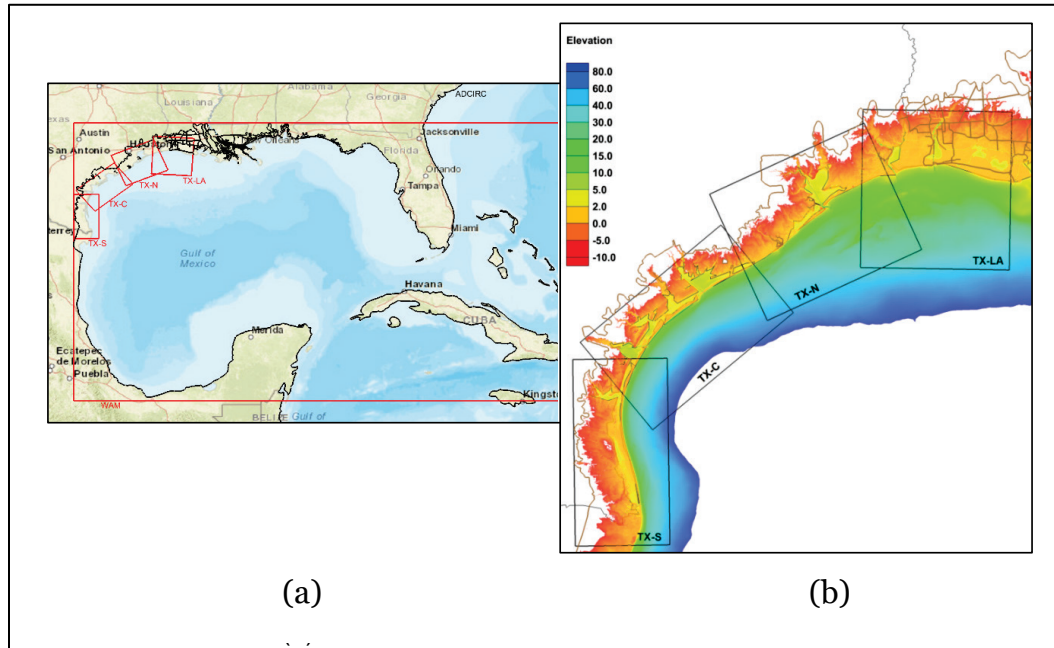
Table 1. Grid properties for the three STWAVE domains.

Grid	Projection	Grid Origin (x,y) (m)	Azimuth (deg)	Resolution (ft)	Number of Cells	
					I	J
Texas-Louisiana (TX-LA)	Louisiana Offshore (FIPS 1703)	(891818.0, 339821.0)	85.8	328.1	1958	1852
Texas-North (TX-N)	Texas South Central (FIPS 4204)	(1132495.0, 4123323.0)	115.0	328.1	1721	2111
Texas-Central (TX-C)	Texas South Central (FIPS 4204)	(973560.0, 4044100.0)	130.0	656.2	705	1137

3.4   Circulation and water levels: The Advanced Circulation (ADCIRC) model

The computational domain for storm-surge modeling by ADCIRC contains the western North Atlantic, the Gulf of Mexico, and the Caribbean Sea (Figure 8). It covers an approximately 38° by 38° square area in longitudinal (from 98° W to 60° W) and latitudinal (from 8.0° N to 46° N)

directions. The mesh consists of approximately 4.6 million computational nodes and 9.2 million unstructured triangular elements with an open ocean boundary specified along the eastern edge (60° W longitude). The largest elements are in the deep waters of the Atlantic Ocean and the Caribbean Sea, with element sizes of approximately 36 mi as measured by the longest triangular edge length. The smallest elements resolve detailed geographic features such as tributaries and control structures like levees and roadways. The minimum element size is approximately 39 ft. Color contour maps of the ADCIRC mesh resolution are shown in Figure 9 and Figure 10. Water depths range from approximately 26,000 ft in the deep Atlantic to over 328 ft of land elevation (above mean sea level).

Figure 8. Map showing the computation domain for the ADCIRC model.
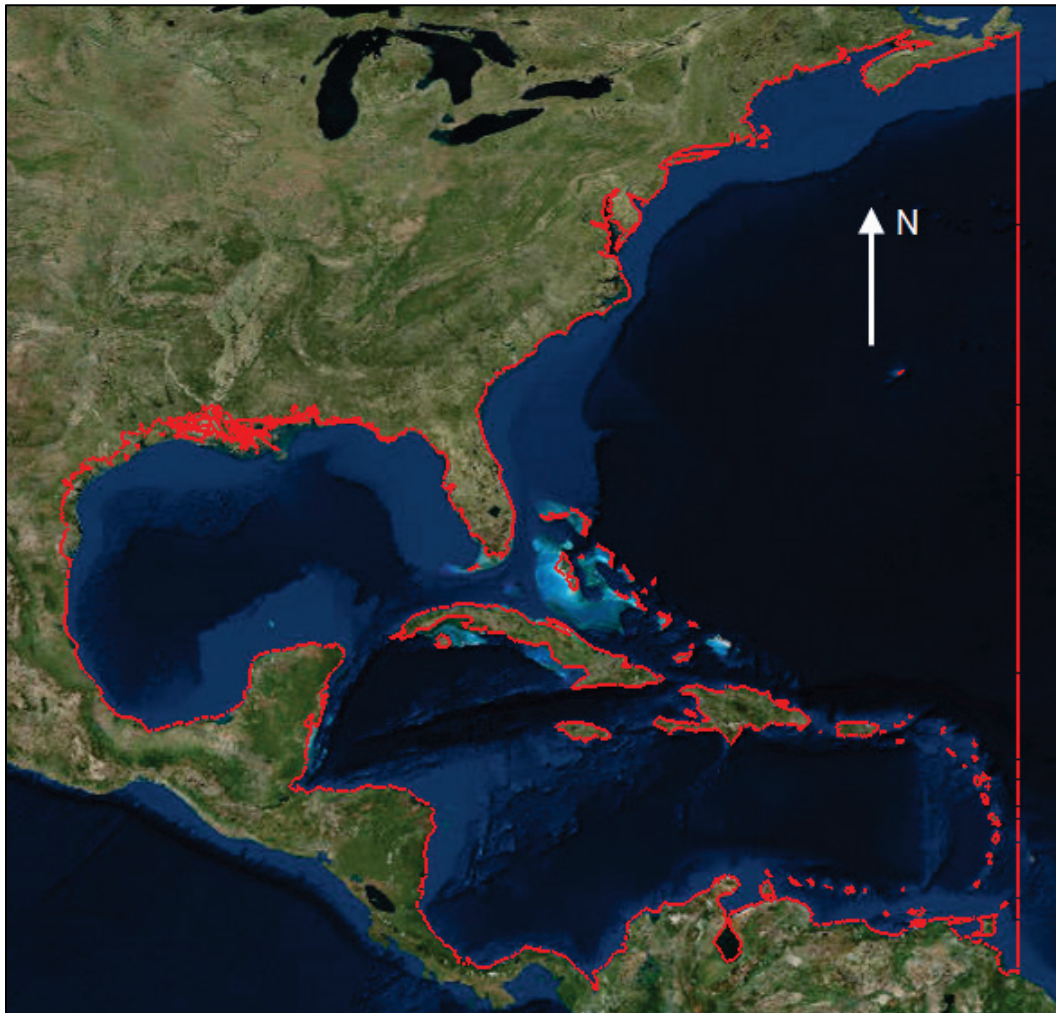
Figure 9. Map showing the ADCIRC mesh with color contours representing the element resolution.
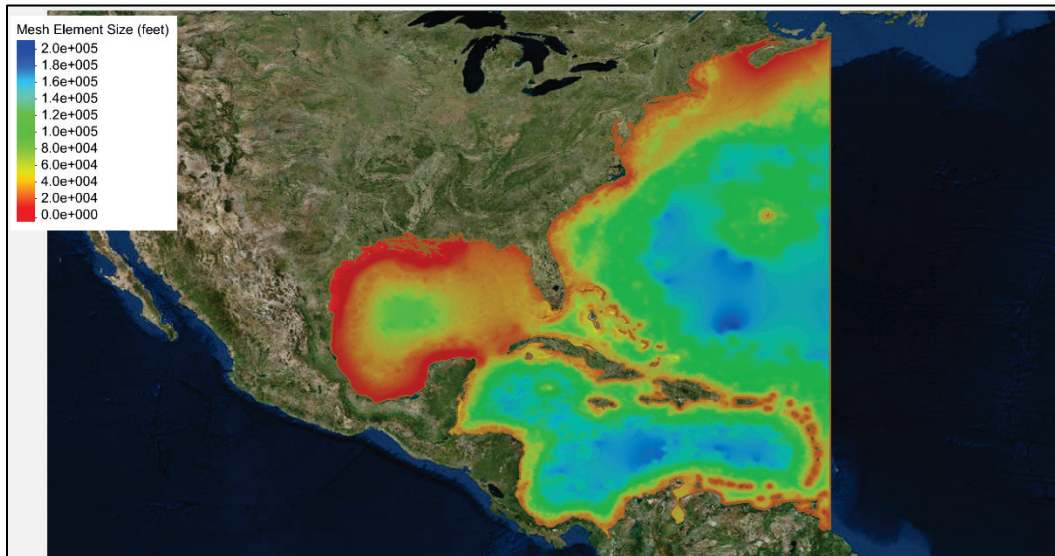
Figure 10. A close-up view of the ADCIRC mesh in the northern Gulf of Mexico showing element sizes as color contours.
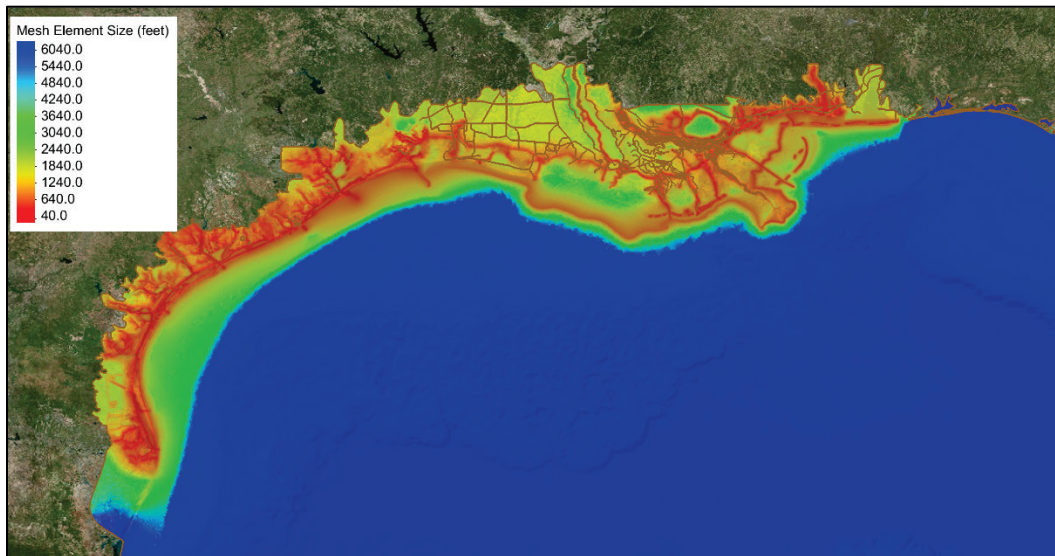
The ADCIRC mesh was adapted from a combination of previously developed and validated ADCIRC meshes. As shown in Figure 11, the Texas FEMA FIS mesh was used along the entire Texas coastline. At the Texas-Louisiana border and continuing eastward along the coast past Mobile, AL, portions of a mesh for southern Louisiana developed for both FEMA and USACE (USACE 2011) and most recently used in the post-Hurricane Isaac investigation of the Hurricane Storm Damage Risk Reduction System (HSDRRS) (USACE 2013) were used. In the Atlantic

and Caribbean, grid EC95, which was originally created for computing tidal databases (Hench et al. 1995), served as the base mesh and was used with some localized refinements to improve response and robustness around some of the islands and shallower depths. After the three main meshes had their respective high-resolution areas extracted, they were stitched together, and the deeper water areas of the Gulf of Mexico were recreated to smooth the transitions between the meshes and to reduce the number of nodes and elements in that area.

Figure 11. Composite map showing the approximate areas where different ADCIRC meshes were combined and created to produce a seamless high-resolution mesh for the entire Texas-Louisiana-Mississippi coastline.
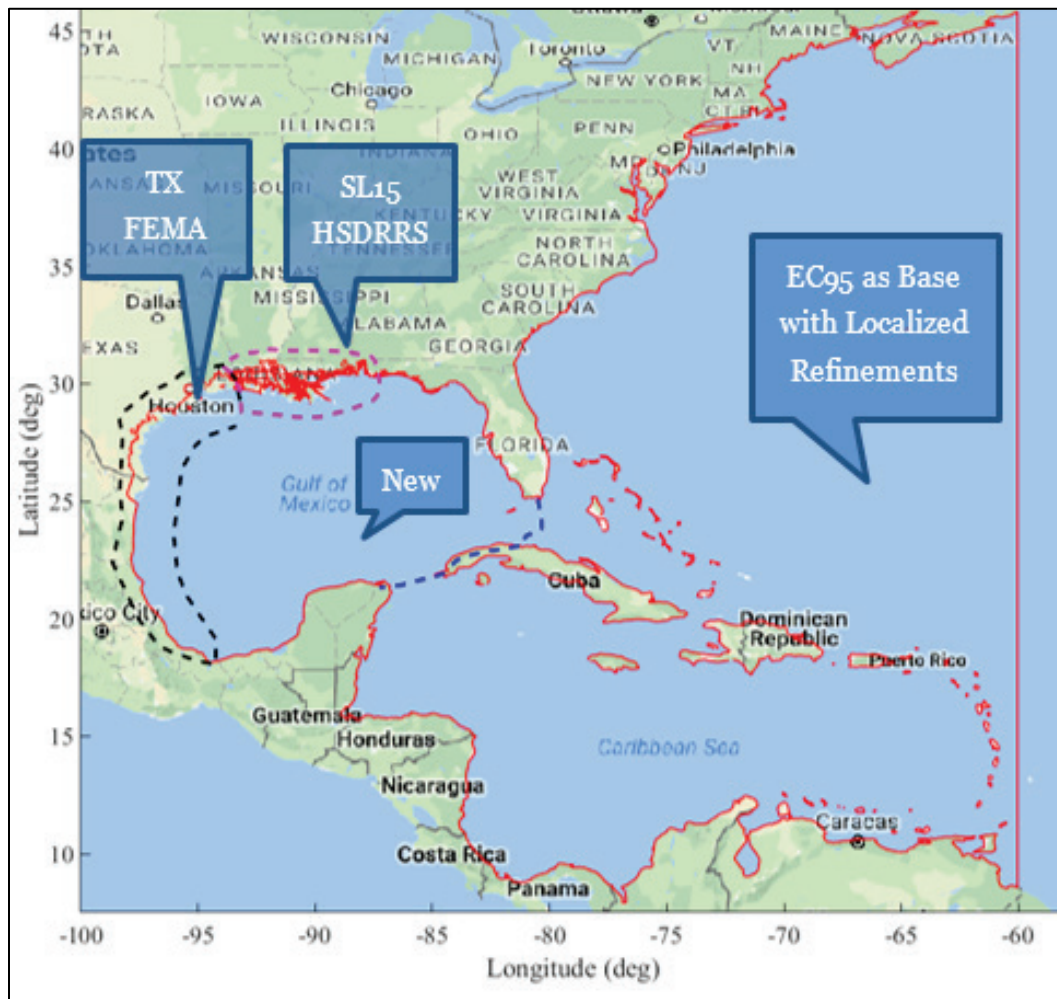
The bathymetries from the Texas FEMA and SL15-HSDRRS meshes were given relative to NAVD88[1]. The two sources of bathymetry/topography were maintained for the final meshes in their respective areas. The bathymetry from the Texas FEMA mesh was used in the Gulf of Mexico and the areas derived from the EC95 mesh. As described in the next section, recent LiDAR data for Brazoria, Jefferson, and Orange Counties were developed into a digital elevation model (DEM) and then used to update the ADCIRC and STWAVE topography in those areas. A view of the bathymetry and topography from the ADCIRC mesh in the Texas-Louisiana border area is shown in Figure 12.

Figure 12. A color contour map showing the seamless topography and bathymetry contained in the ADCIRC mesh along the Texas-Louisiana border.
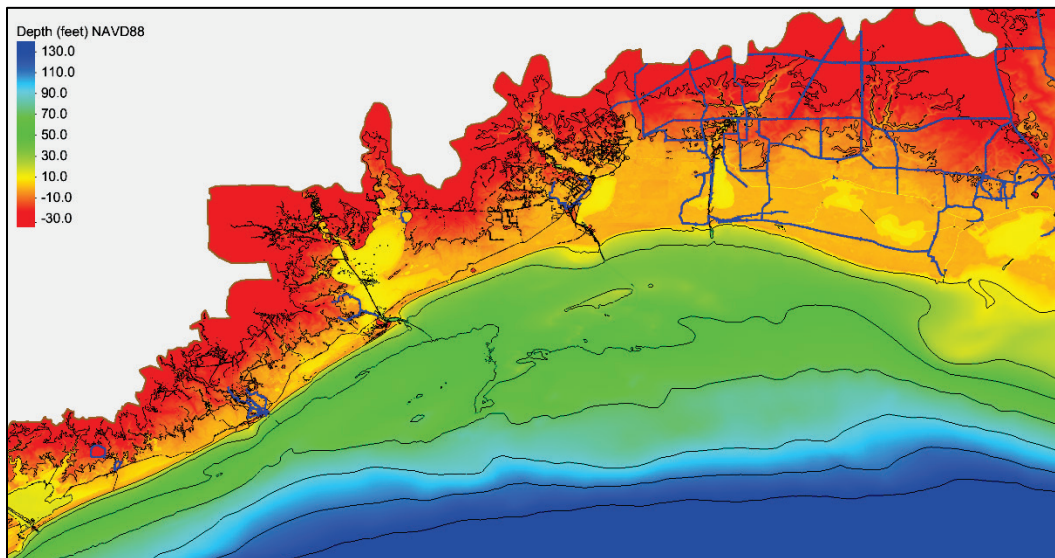
3.5   Topography and bathymetry

LiDAR data collected during 2018 were processed to construct a bare-earth DEM for the area. Excerpts from the metadata are given in Appendix E that describe data collection, data processing, and quality control. Note that throughout this study, datum references followed requirements published in EM 1110-2-6056 (USACE 2010a), including those specifically stated in Chapter 5 of that manual: "Procedures for Referencing Datums on Coastal Hurricane and Shore Protection Projects."

---

[1] North American Vertical Datum of 1988.

LiDAR data were obtained from the Texas Water Development Board (TWDB) with DEM divided into smaller tiles. These tiles were mosaicked into county-wide DEMs. The LiDAR was collected by Fugro January 12–March 22, 2018, during leaf off season with Riegl sensors. Once tiles for each county were located and mosaicked, the raster calculator projector tools in Microstation v8.5.2.55 were used to transform the DEM into Texas South Central State Plane (feet) coordinate system and NAVD88 Geoid12B.

3.5.1   Taylor/Hillebrand Bayou bathymetric data

In February 2019, the SWG survey crew collected single-beam bathymetric data along cross sections within Hillebrand and Taylor Bayous (Figure 13 and Figure 14). The Hydrolite echo sounder was attached to a flat-bottom boat and linked with a Trimble receiver for horizontal location of the depth readings. These points were reported relative to NAVD88 (feet) State Plane Texas South Central Geoid12B. Bare-earth real-time kinematic Global Positioning System (GPS) data were obtained from boat on bank to tie field data with LiDAR. When these ground shots were compared to the DEM derived from LiDAR, there was an average difference of under 0.1 ft with a standard deviation of 1 ft.

Figure 13. Extent (in blue) of 2019 bathymetric surveys of Taylor and Hillebrand bayous.
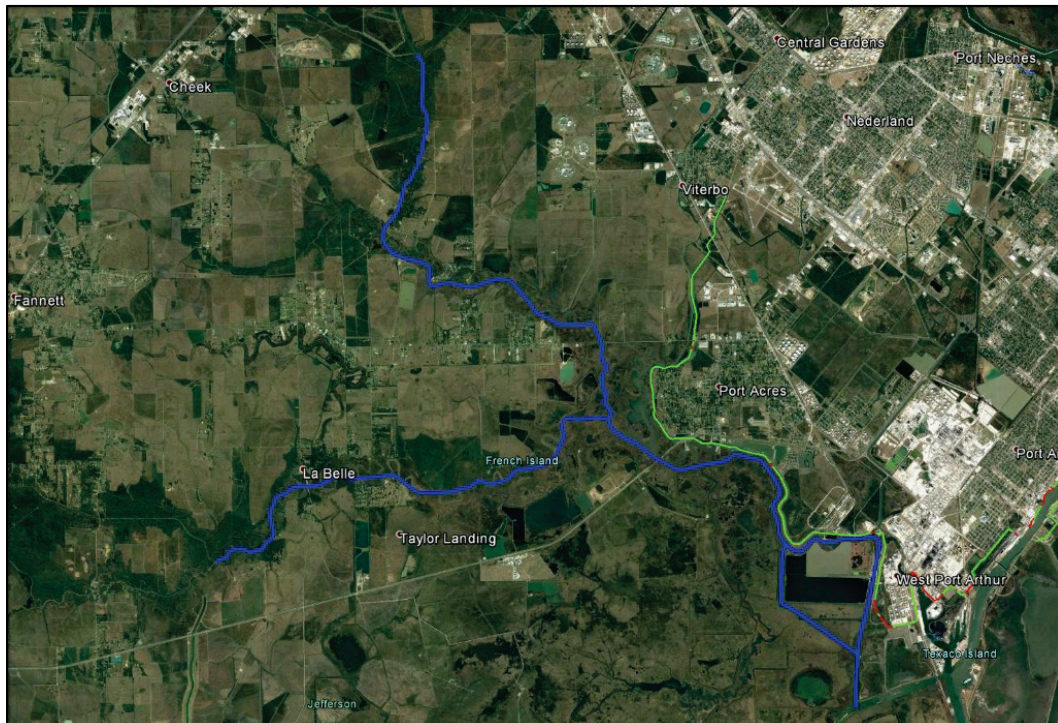
Figure 14. Survey cross-section for 2019 bathymetry surveys of Taylor and Hillebrand bayous.
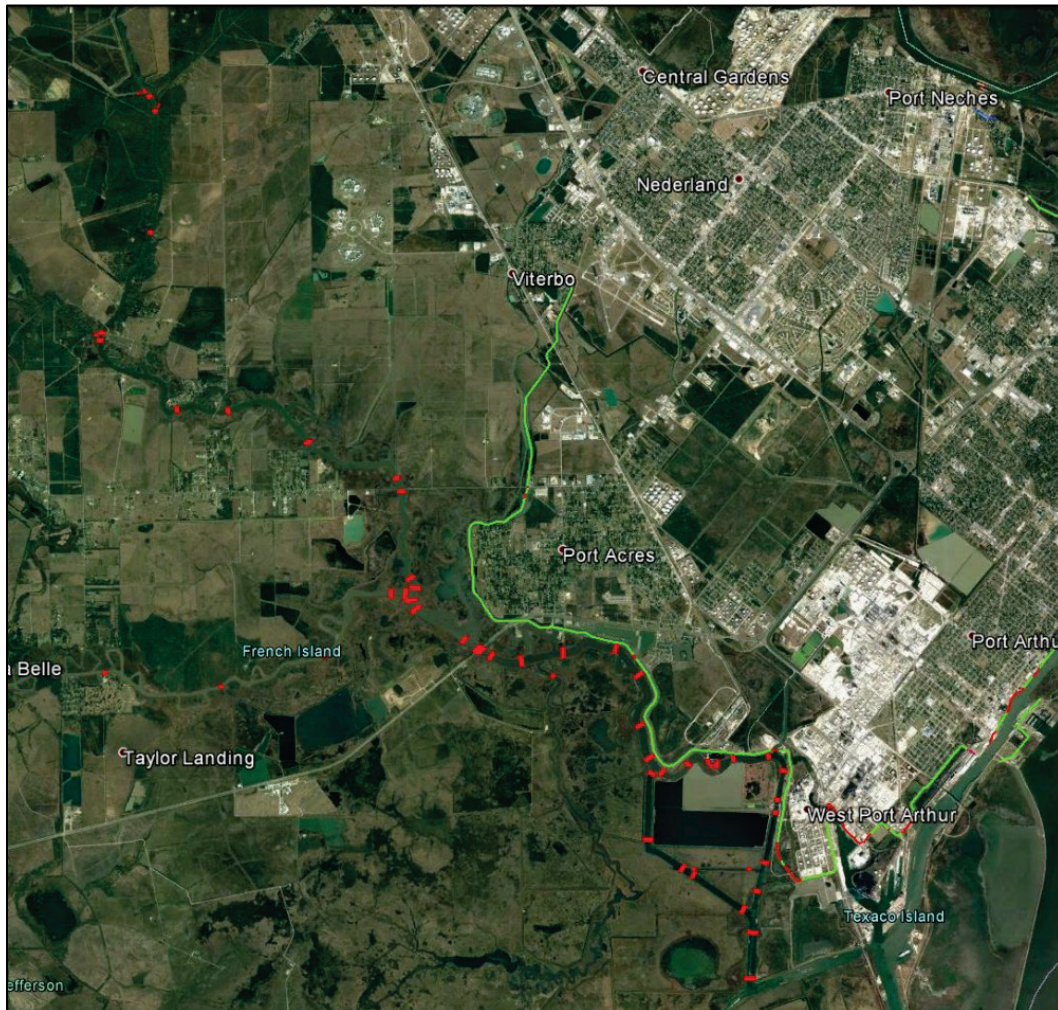
3.5.2   Detailed ADCIRC mesh refinements

The existing CSRM systems in the ADCIRC mesh and STWAVE grids used for the CTXCS were not sufficiently resolved to provide the level of detail required for the PED phase of S2G. Therefore, the ADCIRC mesh and STWAVE grids were modified from the ones in CTXCS to more accurately capture the existing and proposed flood protection measures. The STWAVE grid specifications listed previously in Table 1 reflect the updated conditions used for S2G. Modifications included adding more resolution along the CSRM systems. The CTXCS ADCIRC mesh has element sizes in the range of 300 to 600 ft in these areas whereas the updated S2G ADCIRC mesh has element sizes in the range of 40 to 200 ft. Levees and floodwalls were represented in the mesh as weir pairs. In each of the three project areas, mesh resolution and alignments were adjusted to more

closely represent other hydraulically important features, such as open drainage canals and barge canals, along with roads and non-federal levees. Figure 15 and Figure 16 present details of the ADCIRC mesh refinements made in the project areas. Figure 17 shows the mesh elevations for CTXCS, S2G existing and S2G with-project meshes. Figure 18 shows the elevation (topography/bathymetry) difference between with- and without-project S2G meshes.

Figure 15. Port Arthur, TX, area ADCIRC mesh lines. Top is CTXCS mesh and bottom is S2G mesh.
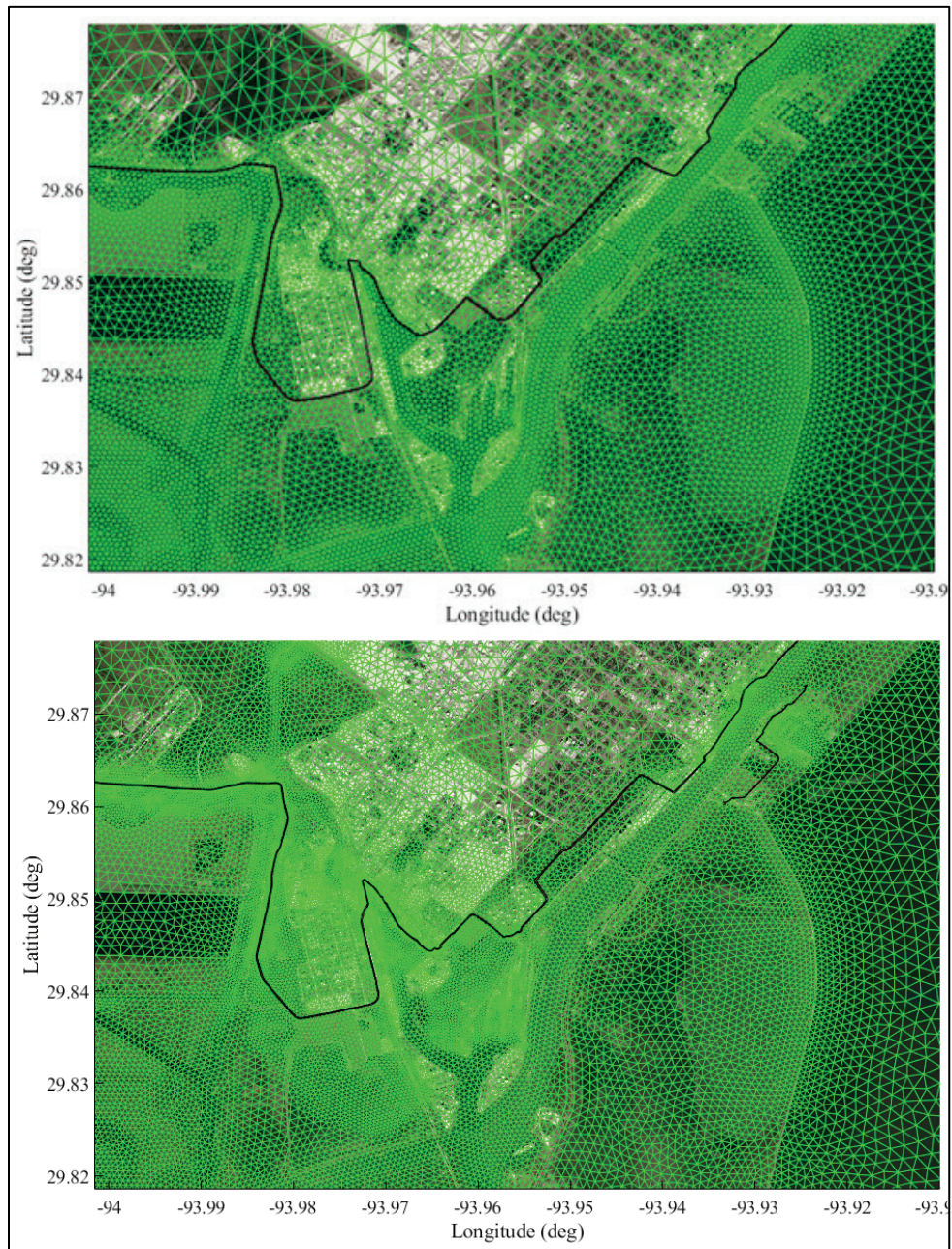
Figure 16. ADCIRC mesh resolution (element size in feet) for Port Arthur, TX. Top is
CTXCS mesh, and bottom is S2G mesh.
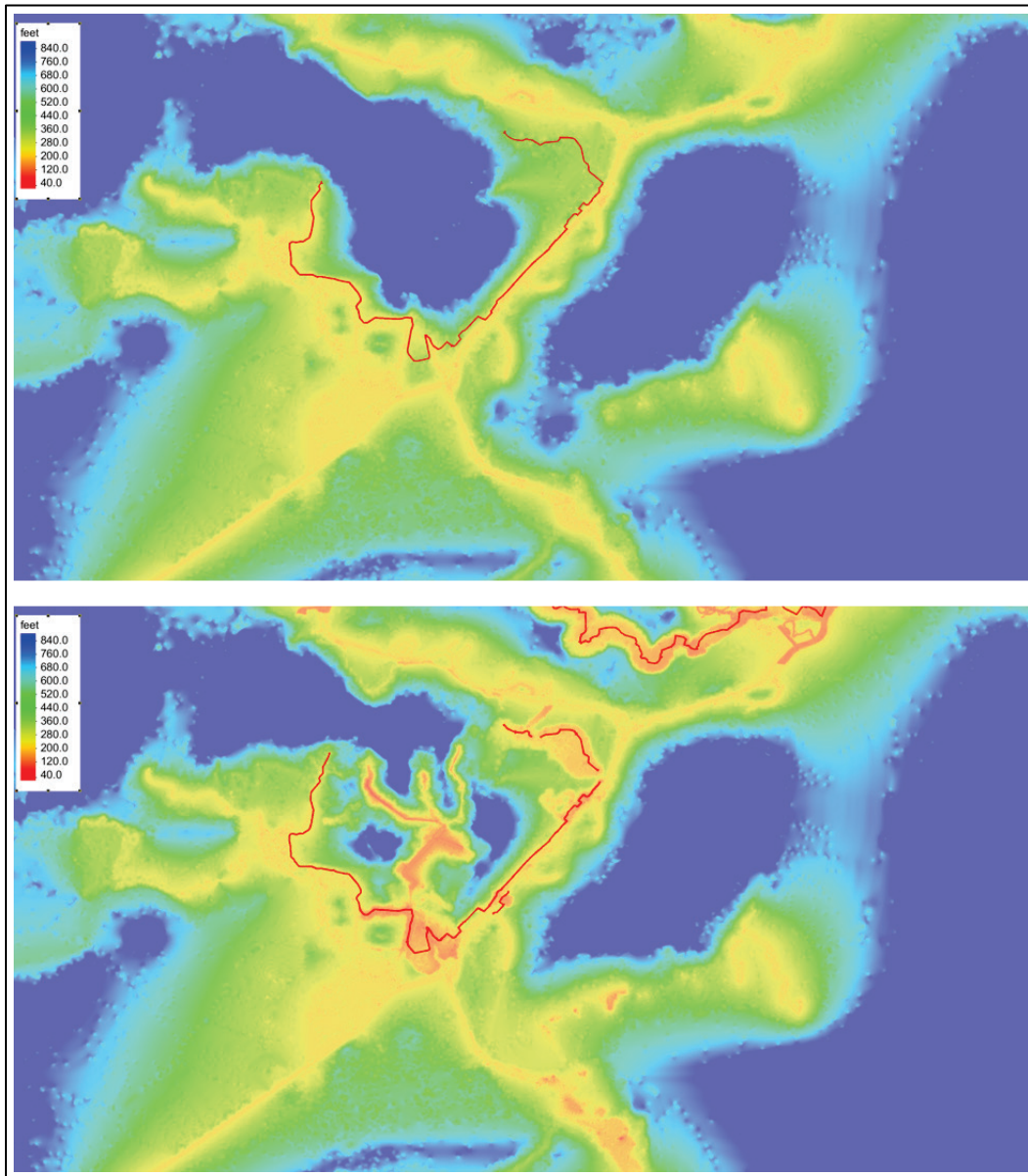
Figure 17. Topography and bathymetry values in the ADCIRC mesh. Top left is CTXCS mesh, middle, top right is S2G existing conditions mesh, and bottom is the S2G with-project conditions mesh in the Port Arthur area.
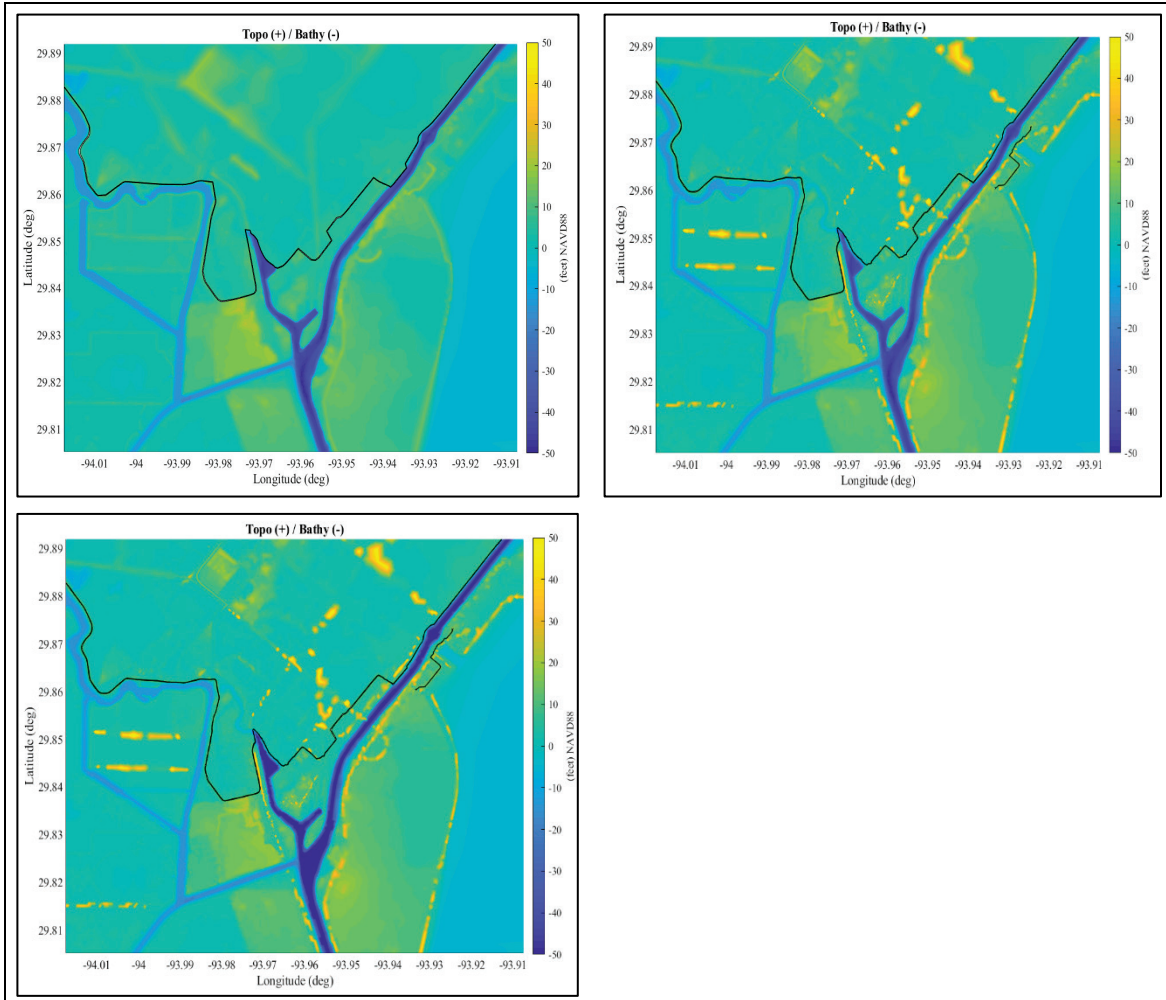
Figure 18. Difference (with-project minus existing) plot of bathymetry/topographic values between the existing conditions S2G ADCIRC mesh and the with-project conditions for the S2G ADCIRC mesh, in the Port Arthur area.
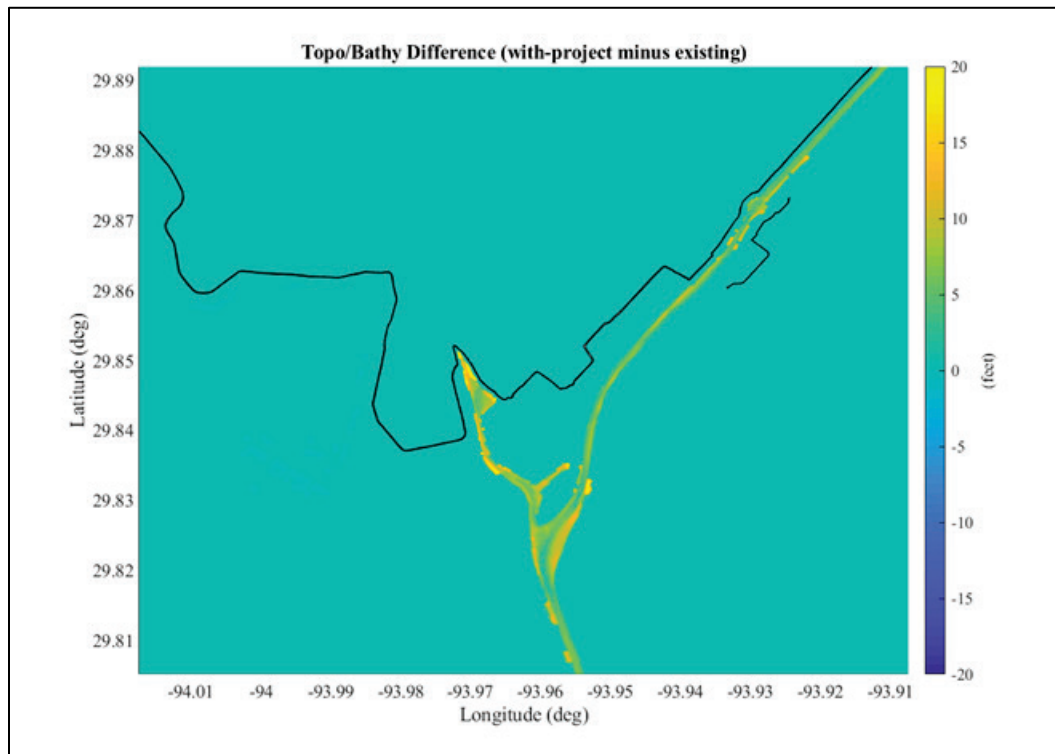
For the with-project condition versions of the ADCIRC mesh and STWAVE grids, the SNWW authorized project water depths were also incorporated, deepening the waterway to 50 ft (USACE 2011). In the Freeport area, an authorized project for deepening of the channel was also included (USACE 2018).

Compared to CTXCS, for S2G PED, both ADCIRC and STWAVE models decreased cell size by approximately a factor of 2 in and around the CSRM systems. CSRM features were carefully recreated in the mesh to model the surge and waves accurately in the vicinity.

3.6   Save points (SP)

The CSTORM model peak SWLs are typically saved at ADCIRC mesh nodal locations. These files are massive and cumbersome to manage. Therefore, reduced data sets of responses at select spatial locations called *save points* (SP) were also saved at run time. For S2G PED, 5148 SPs were defined that span Freeport, Port Arthur, and Orange CSRM areas from inland to offshore. Figure 19 and Figure 20 show the SP locations for Port

Arthur and Orange County area. Figure 21 and Figure 22 show the SP locations for the Freeport area. SP spatial density is high in the immediate vicinity of the CSRM features. In addition, SPs were identified to coincide with the seaward and leeward locations of the analysis transects. For most areas, SPs were located both on dry land and in nearby water bodies. SP results were used for design of levee and floodwall reaches while nodal results were used to describe flooding in the vicinity of CSRM features.

Figure 19. S2G SPs in the area of Port Arthur and Orange County CSRM systems.
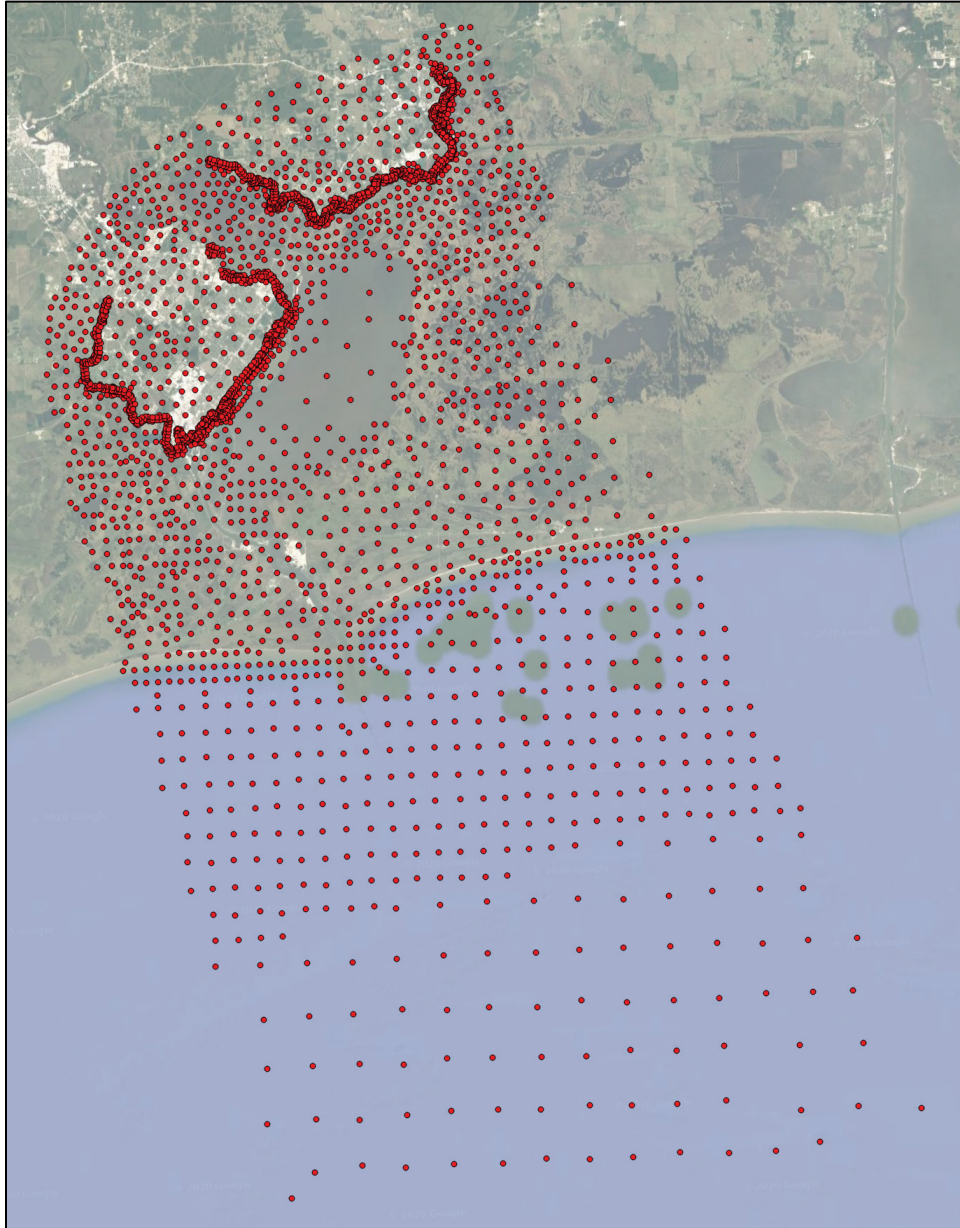
Figure 20. S2G SPs around Port Arthur (top) and Orange County (bottom) CSRM systems.
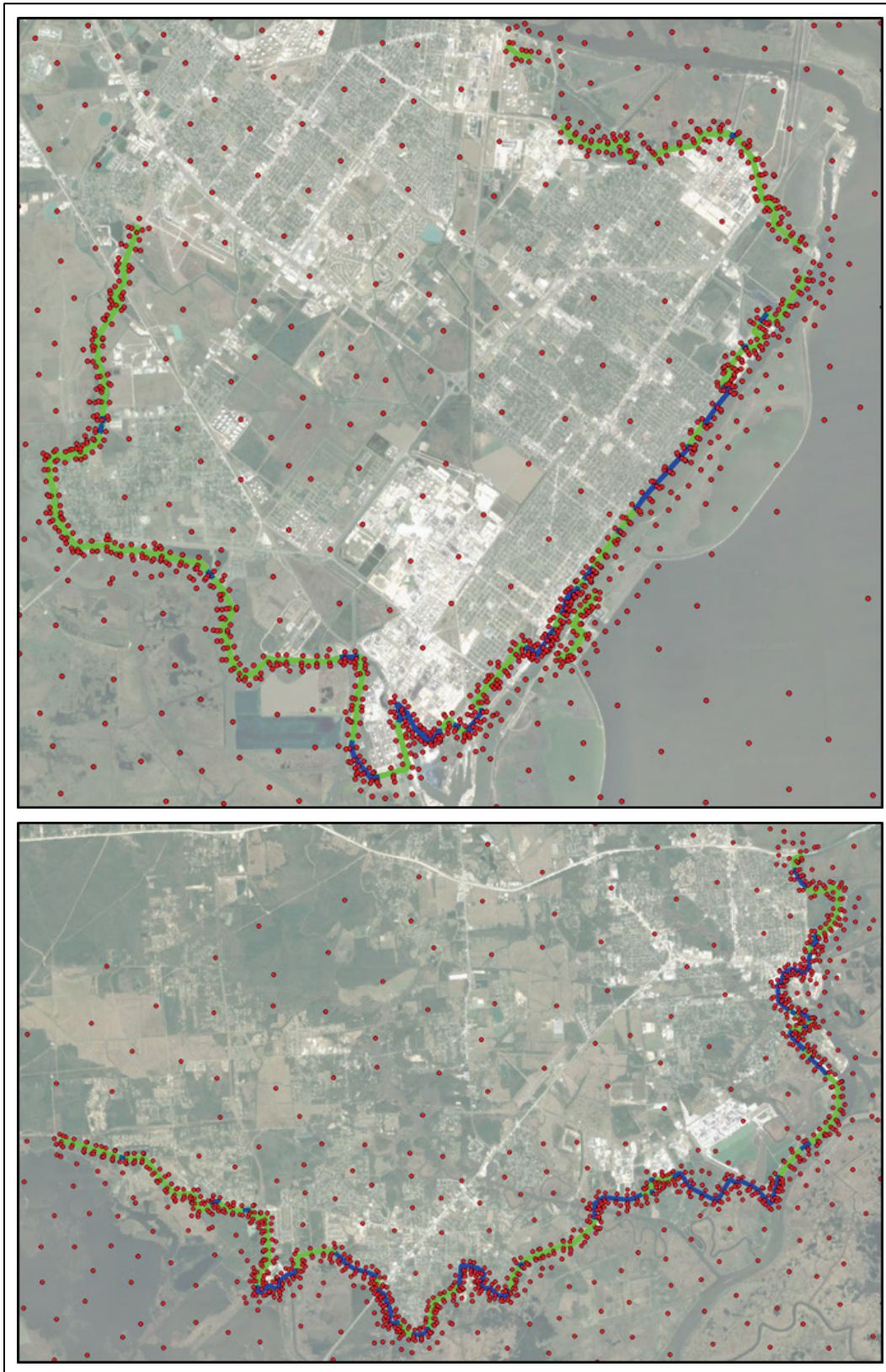
Figure 21. S2G SPs in the area of Freeport CSRM system.
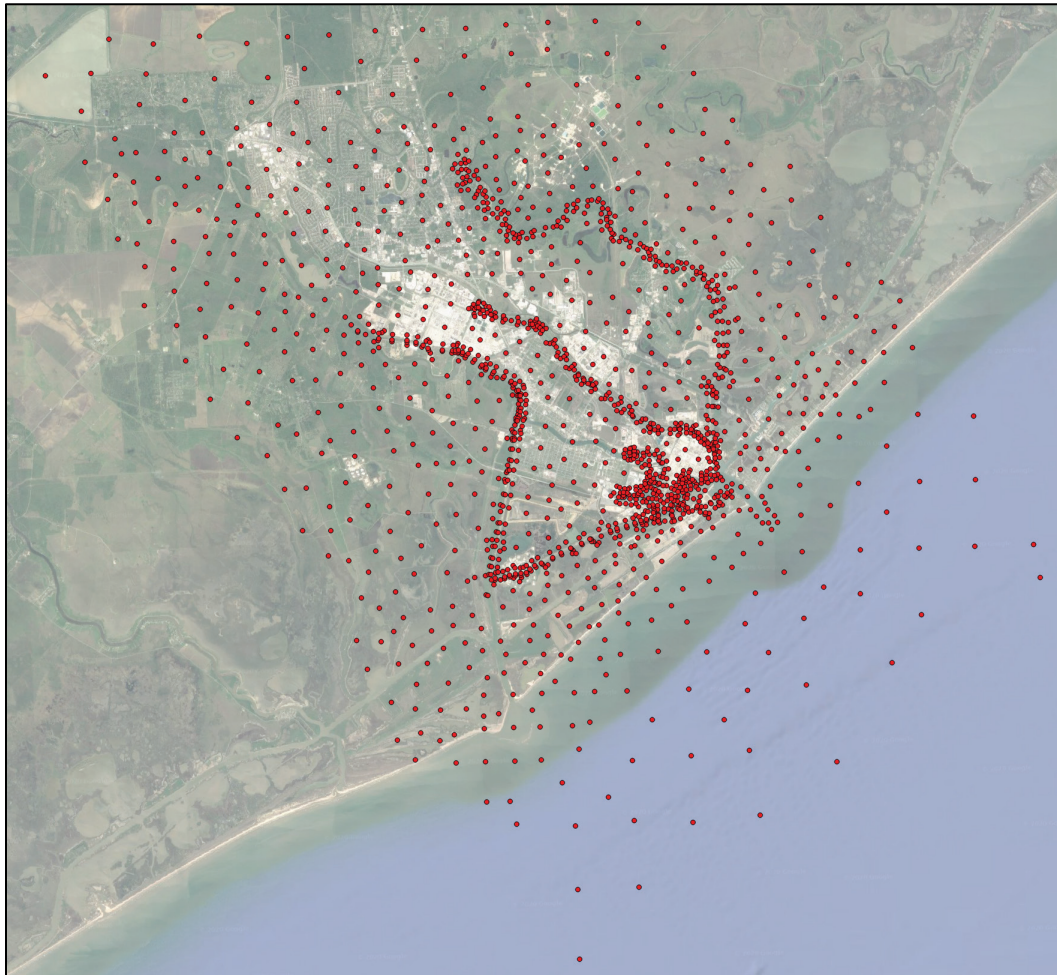
Figure 22. S2G SPs near Freeport CSRM system.
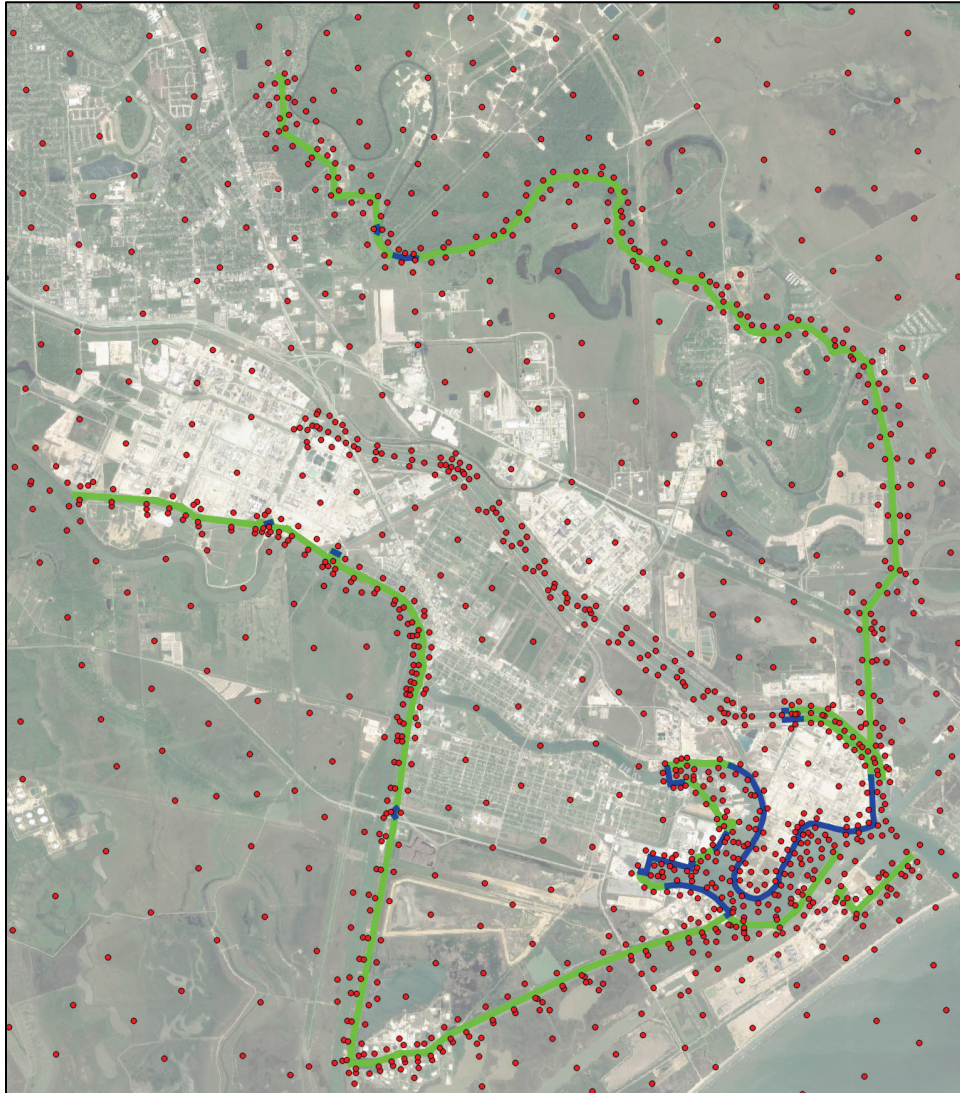
3.7 Additional model settings

ADCIRC also makes use of a nodal attribute file (fort.13) that specifies spatially variable model parameters like Manning's n for bottom roughness. Many of the nodal attribute parameters are derived from land cover and land use (LCLU) data that provide classification systems for what is on Earth's surface at a given location. For wind and coastal hydrodynamic modeling by ADCIRC, LCLU data were used to determine spatially distributed values of bottom friction coefficients (or Manning's n), canopy coefficients, and surface roughness length for directional wind reduction. These parameters were updated for the CTXCS using the most recent LCLU data and, in general, were not changed for the S2G project. However, Manning's n values in the open waters of the Gulf of Mexico were decreased

from 0.02 to 0.015 to improve agreement between ADCIRC simulated water levels and measured high water marks in inland areas for historical severe hurricanes, such as Hurricanes Ike and Carla.

Two sets of LCLU data were used to specify the above-mentioned model parameters over the entire coasts of Gulf of Mexico. The first LCLU dataset is the USGS 2011 National Land Cover Database (NCLD) (NLCD 2016; Homer et al. 2015), which covers the Gulf Coast of the United States. The NCLD is the most recent national land cover product created by the Multi-Resolution Land Characteristics Consortium. The NLCD uses a 29-class land cover classification scheme at a spatial resolution of 98 ft.

The second set of LCLU dataset used for the study is the Global Land Cover Characterization (GLCC) (GLCC 2017), which is a series of global land cover classification datasets. The spatial resolution of GLCC is 3281 ft, much coarser than that in the NLCD dataset. Therefore, the GLCC dataset was used only for defining land cover properties in the areas beyond the NLCD data coverage. GLCC uses a 20-class land cover classification scheme.

Two river inflows from the Mississippi River and the Atchafalaya River are included in the storm-surge simulations. The inflow boundary (or the river cross section) of the Mississippi River is located near the US Geological Survey (USGS) gage #07374000 Mississippi River at Baton Rouge, LA. The boundary for the Atchafalaya River is placed near the USGS gage #07381490 Atchafalaya River at Simmesport, LA. Constant river inflows were used for all simulations. A value of approximately 160,000 cfs was used for the Mississippi River, and a value of 68,000 cfs was used for the Atchafalaya River. No riverine inflows within the Texas coast (e.g., Sabine, Neches, and Brazos) were included in the model. Note that extensive riverine analysis (Sabine and Neches) has been conducted, and compound flooding impacts have been assessed separately – both statistically and by including riverine flows (for both Sabine and Neches) in ADCIRC. However, for a given AEP, the design elevations are dominated by hurricane storm surge and wave contributions, not by riverine flows or by the compounding effect of the two. The joint probability of surge and rainfall runoff impacts AEP water levels that are much rarer than would be a consideration for CSRM design.

A few model runtime parameters for ADCIRC were also adjusted, compared to the CTXCS setup for the model to compare better with measured high water mark data along the study areas and to be more aligned with values used for the feasibility study for S2G. ADCIRC includes a wind multiplier model setting. This setting is sometimes used as an adjustment parameter for historical storms, particularly when the input wind fields do not match observation data. It is also used to adjust wind fields from a 30 min averaging window to a 10 min averaging window. A wind multiplier value of 1.09 was used in S2G instead of the 1.0 in the CTXCS study; however, both values are considered within the normal range. The wind drag formulation was also changed from a Garratt formula to the Powell formulation (Powell et al. 2003, 2010). The Powell formula is specially designed for tropical cyclone events by identifying the storm center location and then dividing the storm area into three sections around the center, where different algorithms are used to better capture the naturally occurring structure of a storm. In conjunction with these two changes, the ADCIRC model's upper limit for wind drag coefficient was set to a value of 0.002 in S2G, instead of the 0.003 used in the CTXCS study, where it is noted that 0.0035 is the default value in the ADCIRC model. The 0.002 value was also used in the FEMA FIS for the area. To better capture the storm forerunner development for Hurricane Ike, the lower limit of bottom friction coefficient was decreased to 0.001 for S2G, instead of the 0.003 used in the CTXCS study, and the Manning's *n* values in the open Gulf of Mexico were decreased from 0.02 in CTXCS to 0.015 in S2G. The above model settings were used for all storms and both with- and without-project scenarios.

3.8   Tides

For modeling coupled responses, including tides, for validation storms, the open ocean boundary (60 deg west longitude in Westerink et al. (2011) was forced with eight tidal constituents. Time-varying tidal elevations specified at nodes along the open ocean boundaries were synthesized using the M2, S2, N2, K1, O1, Q1, P1, and K2 tidal constituents. Constituent information was extracted from a database developed from the TOPEX 7 satellite measurements. Because the model domain is of sufficient size that celestial attraction induces tide within the mesh proper, tide-generating potential functions were included in the simulations and corresponded to the constituents listed above. Tidal forcing was only included for the historical storms and was not used for CSTORM modeling of synthetic storms.

While tides were not included explicitly in the CSTORM synthetic storm modeling, they were included as a statistic in the simulation modeling. This is consistent with recent flood protection studies in the Gulf of Mexico. An error assessment was conducted to determine if this approach was reasonable. Stochastic simulation of water levels to determine an SWL hazard curve was done (1) without tides, (2) with tide as a statistic, and (3) with historical tides explicitly sampled using Monte Carlo simulation. For all three simulations, CSTORM synthetic storm peak water levels were sampled based on the associated storm rates, and over 1 million samples were obtained to construct a hazard curve. Tidal statistics were based on a 5 yr sample from National Oceanic and Atmospheric Administration (NOAA) tide gage 877570 Sabine Pass North. The S2G suite of 189 storm simulations was used for this evaluation. CSTORM with-project simulations from S2G SP 707 near the Sabine Pass North gage were used in the simulation of water levels. Epistemic uncertainty of the models was included as described in detail in Appendix G.

Details of method 1, no tide: The discrete JPM integral (Equation A.1, Appendix A) for SWL was solved numerically with the 189 storms and with all uncertainties except no tide was included.

Details for Method 2, tide as a statistic: The discrete JPM integral for SWL was solved numerically with the 189 storms and all uncertainties and tide was included as an additional statistic. For the statistical evaluation, the square root of the sum of the squares of all error standard deviations was computed as presented in Appendix G. Measured tide standard deviation was included in the error budget.

Details of method 3, historical tides explicitly sampled using Monte Carlo simulation: For explicitly sampled tides, the 5 yr predicted tide record was randomly sampled for all storms. A hydrograph was created for each storm by linearly superimposing the randomly phased tidal time series on the storm water level hydrograph. For this brief evaluation, the storm hydrograph was a scaled unit hydrograph with the same shape as Hurricane Ike. A combined tide and surge peak SWL was extracted for each storm, and the hazard curve was computed using the same JPM integration as above.

The results of this analysis are shown in Figure 23. It is evident from the figures that all three methods yield virtually identical hazard curves and

uncertainty bands at 10% and 90% confidence limits. For the 1% AEP mean water level, the difference between explicitly including tides and including tides as a statistic was 0.1% for both the mean and the 90% upper CL. The conclusion from this investigation was that tides can be included as a statistic (Method 2) for all S2G computations with no significant impact on results.

Figure 23. Tidal simulation results with no tides (upper left), tide as statistic (upper right), and explicit tide (bottom). Mean hazard curve is shown as black solid line while 90% and 10% CLs are shown as red dotted lines.
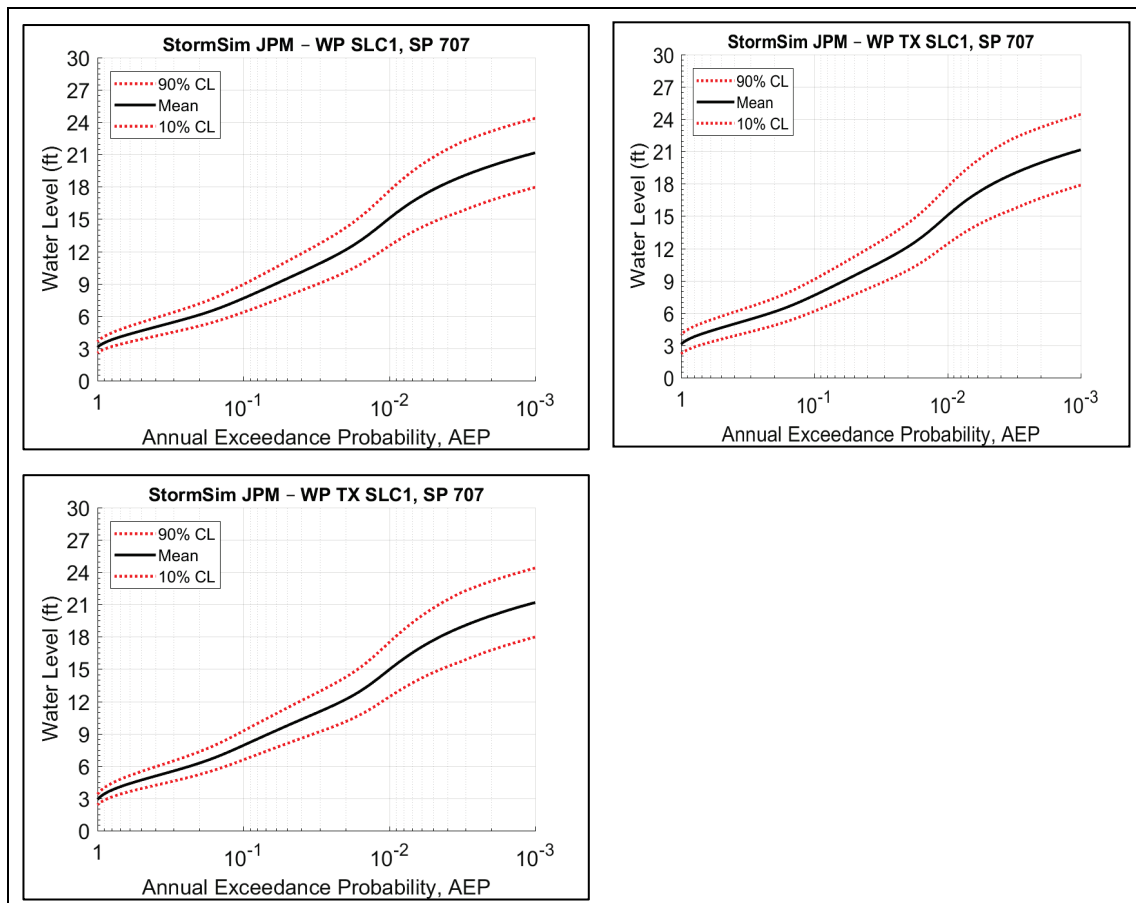
3.9   Relative sea level change (RSLC)

The RSLC scenarios were defined according to sea level change (SLC) guidance set forth in USACE ER 1100-2-8162 (USACE 2019a) and EP 1100-2-1 (USACE 2019b). SLC over periods longer than a month is a result of global (eustatic), regional, and local changes with time. The global mean sea level (GMSL) increased between 1975 and 2005, and prescribed for project design was 0.067 in. (1.7 mm/yr) and is a result of thermal expansion and melting ice sheets and glaciers. However, the global trend is

non-linear with clear acceleration since the 1990s with global mean water level rising by 0.14 in. (3.6 mm) per year from 2006 to 2015[1]. Therefore, while the present regulation prescribes 1.7 mm/yr for GMSL, it is possible that this will be increased in the future. Significant regional sea level changes occur due to seasonal variations in water levels due to Gulf of Mexico thermal variations and local subsidence. Regional seasonal thermal variations in sea level range up to approximately 6 in. Liu et al. (2020) quantified the subsidence component of RSLC in Galveston to be approximately 30% of the total SLC in 2018. However, subsidence is a decreasing proportion of RSLC due to the increasing rate of GMSL increase, as discussed by Liu et al.

For this project, RSLC scenarios were defined according to the above USACE regulations. USACE (2017a) provides a detailed description as follows:

> Floodwall sections will be constructed to the 50-year intermediate RSLC and will be designed for the greatest hydraulic loading out of the 50-year intermediate, the 50-year high and the 100-year intermediate. These load cases will ensure that the wall will meet all design criteria for the 50 year intermediate and still survive and not suffer a brittle failure under hydraulic loading from the 50-year high or the 100-year intermediate RSLC. All levee sections will be designed to the 50-year intermediate RSLC, with the assumption that they can be more easily adapted to future SLC than the floodwall. The recommended plan for the floodwall will allow for future increases in wall height due to its current robust structural design in the floodwall base and stem.

> The limits of 50-year high or the 100-year intermediate RSLC were recognized due to the constraints of high ground tie in, levee footprint impacting ultimate levee height, and adaptability constraints on closure structures, navigation gates, and pump stations. The adaptability concept for the RSLC scenarios above the 50-year intermediate will allow for limited overtopping of waves and minor still water

---

[1] See for example, https://www.climate.gov/news-features/understanding-climate/climate-change-global-sea-level

overtopping that would then be mitigated for using interior drainage features. This approach also minimizes the initial cost of the floodwall while still allowing for adaptation. The recommended plan for the floodwall will allow for future increases in wall height due to its current robust structural design in the floodwall base and stem. (USACE 2017a)

The base year for the calculations was 1992 as this was the midpoint of the last National Tidal Datum Epoch, which spans 1983 to 2001. The scenarios use a global mean sea level rise of 1.7 mm/yr and add criteria for different sea level rise acceleration rates. While the curves start in 1992, they are differenced against the project beginning of service life year 2027. Calculations were performed with the USACE Sea-Level Change Curve Calculator (vers. 2017.55). There are three RSLC curves as follows, and shown in Figure 24:

1. Low curve representing the linear historical SLC (USACE Low).
2. National Research Council (NRC) Curve I (USACE Intermediate or USACE Int).
3. Modified NRC Curve III (USACE High).

Figure 24. Relative SLC curves for Sabine project area (top) and Freeport (bottom).
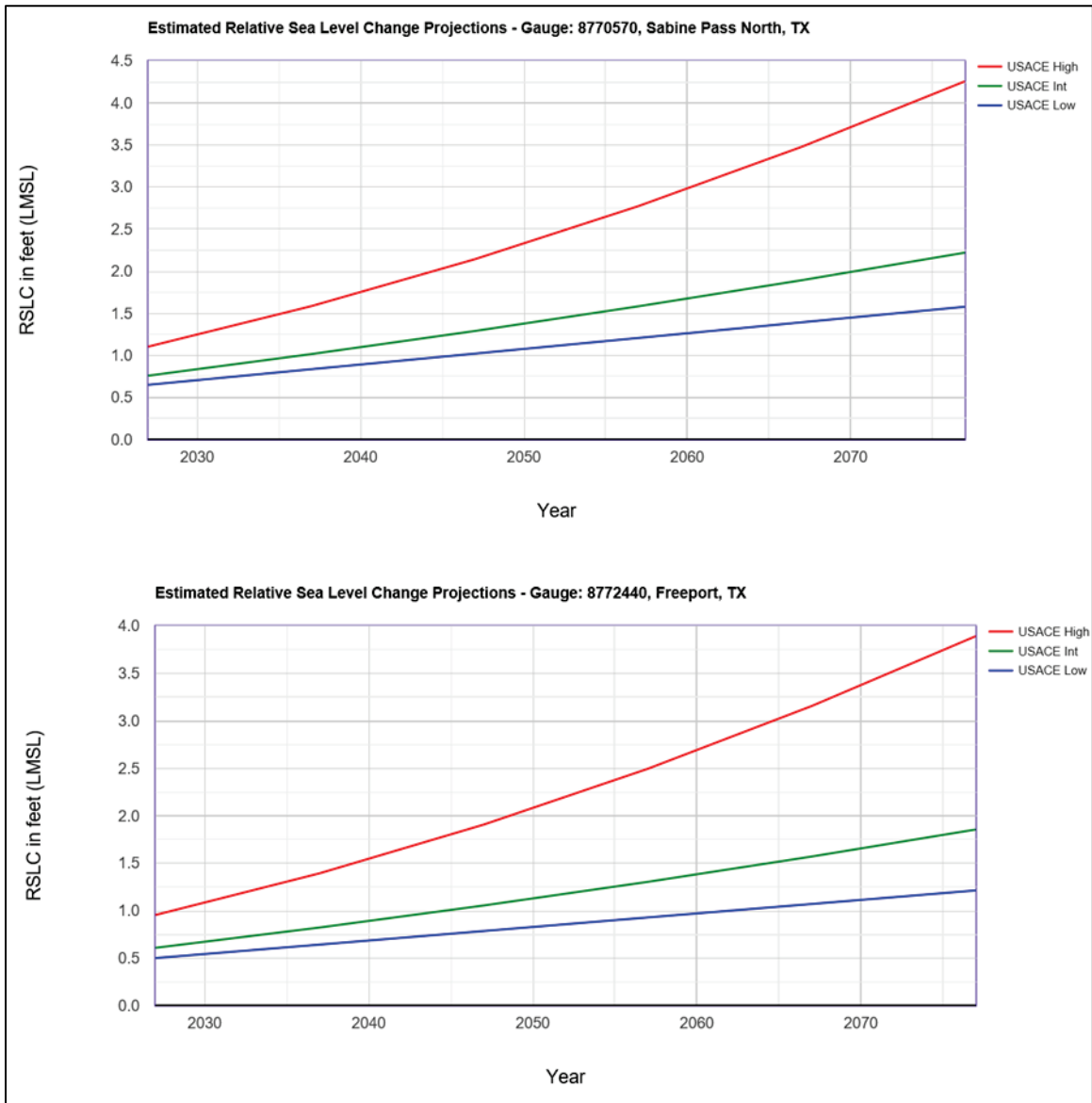
To account for the SLC from the time of topography/bathymetry data collection (2017) and beginning of service life (2027), an additional SLC was added based on historical gage data. The long-term SLC at the NOAA Sabine Pass water level gage is shown in Figure 25.

Figure 25. Long-term time-series plot for NOAA Gage 8770570 at Sabine Pass area (top) and Freeport (bottom). Note that Freeport gage data extend only through 2008 and include an apparent datum shift in 1972.
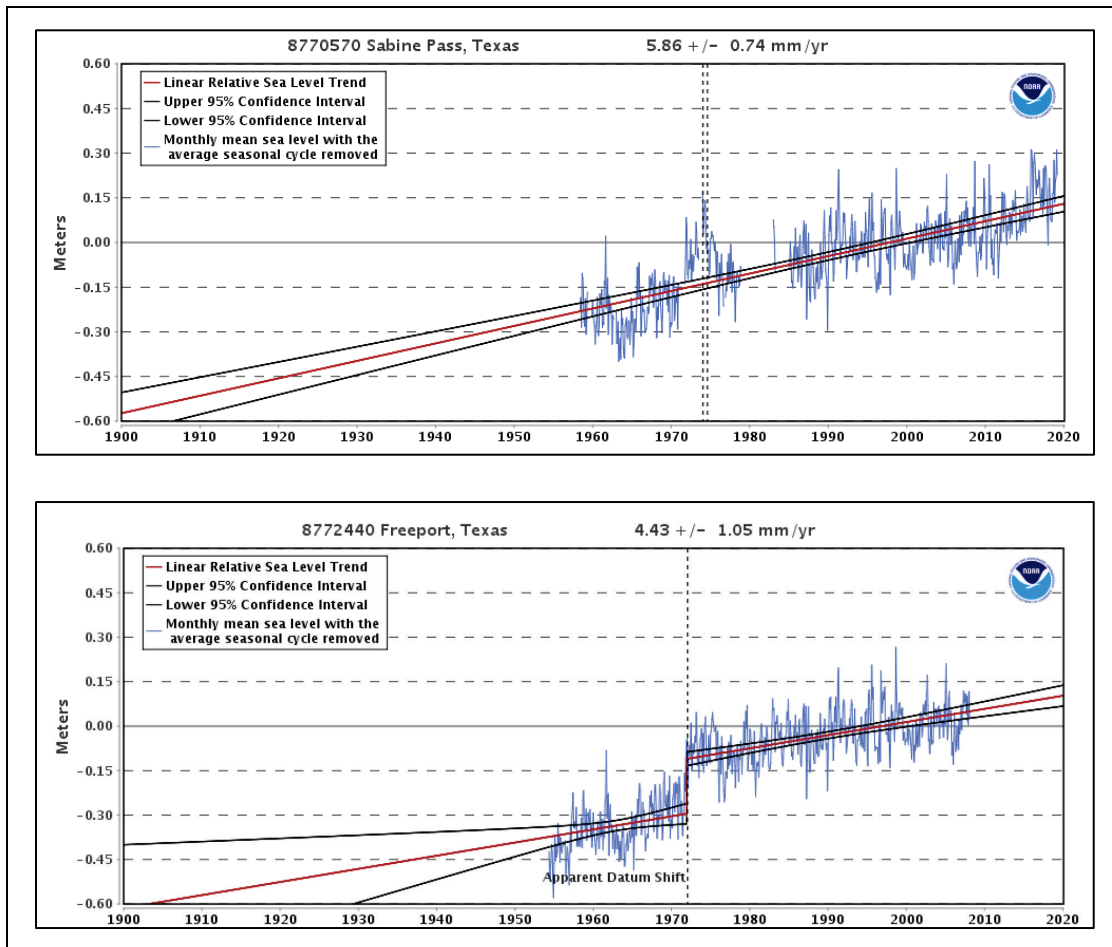
The detailed calculations of RSLC and Geoid offsets for CSTORM simulation scenarios are given in Appendix H. The RSLC plus other sea level adjustments were used to compute the final geoid offset for the CSTORM simulations. Besides SLC, a steric adjustment of 0.39 ft was added to account for regional and seasonal variations to sea level. The steric adjustment was selected as a spatial and temporal average of seasonal variations observed in the water levels due to baroclinic effects that are not directly modeled by ADCIRC (e.g., thermal expansion of water due to increased temperatures during the hurricane season). The ADCIRC model can apply only a single steric adjustment over the entire domain,

otherwise artificial flows would be induced at the onset of the simulation. The 0.39 ft value was computed as an average of the peak seasonal water level increase based on the NOAA long-term sea-level trends at gages along the Texas coast for the period from July to November, when most hurricanes occur along the Texas coast. FEMA[1] gives a thorough analysis of the steric adjustment. For the S2G project area, the average water level peaks in September, and the 0.39 ft adjustment is approximately equal to the average of the September peaks. The standard deviation of the September peak is approximately 0.1 ft, so using a lower statistic would produce an inconsequential effect on the design CSRM structure elevations. Also, an adjustment to convert from local mean sea level (LMSL) datum to NAVD88 was added as summarized in Appendix H. The total RSLC and final geoid offsets for the CSTORM simulations were as follows:

- SLC0, Beginning of Service Life
  - RSLC = 0.17 ft
  - Geoid offset=0.39 ft steric+(0.96 ft LMSL-NAVD88)+0.17 ft=1.52 ft
- SLC1, 50 yr Service Life
  - RSLC = 0.22 + 1.36 ft = 1.58 ft
  - Geoid offset=0.39 ft steric+(0.96 ft LMSL-NAVD88)+1.58 ft=2.93 ft
- SCL2, 100 yr Service Life
  - RSLC = 0.22 + 3.16 ft = 3.38 ft
  - Geoid offset=0.39 ft steric+(0.96 ft LMSL-NAVD88)+3.38 ft=4.73 ft.

In the preceding calculations, the USACE low curve yielded the 0.17 ft adjustment for RSLC while the USACE Intermediate curve yielded the 0.22 ft adjustment. As only a single water level can be used as an initial water level over the entire model domain in the ADCIRC-STWAVE simulations, an average of the total RSLC and geoid offsets at Sabine Pass North and Freeport is used. The final "design" SWLs for a given project area are adjusted as per the difference between this average value and the values at the Sabine Pass North and Freeport gages for the Sabine and Freeport areas, respectively. For example, presented in Appendix H, the difference between the LMSL at Sabine Pass North gage, and the average LMSL (used to initialize the numerical model

---

[1] FEMA (Federal Emergency Management Agency). 2011 (Unpublished). *Flood Insurance Study: Coastal Counties, Texas. Intermediate Submission 2: Scoping and Data Review*. Joint Report prepared for Federal Emergency Management Agency by the Department of the Army, US Army Corps of Engineers, Washington DC.

simulations) is 0.11 ft (1.07 ft – 0.96 ft). As such, final design SWLs in the Sabine area include this additional 0.11 ft to reflect the larger "local" LMSL compared to the "regional" average LMSL used to initialize the simulations. Details are provided in Appendix H.

3.10 Final CSTORM scenarios

The final list of scenarios for CSTORM with Geoid offset was as follows:

1. Without-project, SLC0.
2. Without-project, SLC1.
3. Without-project, SLC2.
4. With-project, SLC0, with Orange County CSRM system.
5. With-project, SLC1, with Orange County CSRM system.
6. With-project, SLC2, with Orange County CSRM system.

4   Local Wave and Water Level Response

4.1   Storm peak responses

The output of the S2G regional surge and wave modeling at 5148 SPs included the storm peak responses. Save point 3936 (Figure 26) provides an example of storm responses for the region. Table 2 lists the top-10 synthetic storms ranked by SWL for SP 3936 for without- and with-project conditions. The mean wave direction (MWD) column is mean wave direction and is Euclidean (0 is east; counterclockwise is positive). Spectral peak wave period T_p and MWD are values associated with significant wave height H_{m0} peak. With-project SWL and H_{m0} peaks for all storms are plotted against without-project conditions in Figure 27. Figure 28 shows the peak SWL for 189 S2G storms for without-project and with-project, SLC0, SLC1, and SLC2 scenarios. Figure 29 shows H_{m0} peaks for without-project and with-project SLC0, SLC1, and SLC2.

Figure 26. S2G CSRM SPs in the Port Arthur (Taylor Bayou Turning Basin) area.
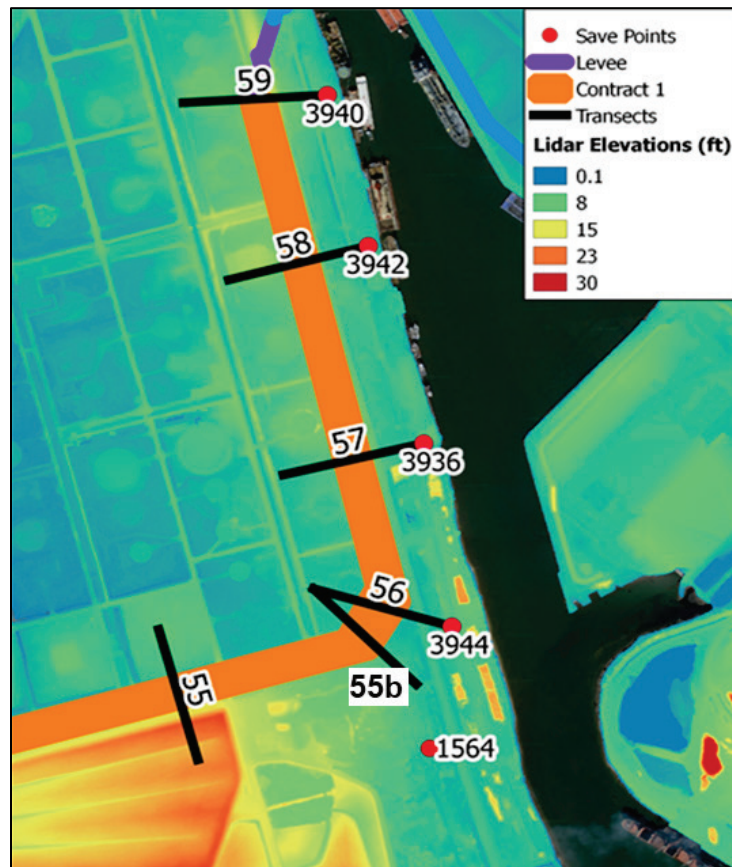
Table 2. CSTORM output peaks for top-10 synthetic storms ranked by SWL for without-project scenario (left side) and for with-project scenario (right side) at SP 3936.

SLC0 – Without-Project					SLC0 – With-Project				
Storm Identifier (ID)	SWL (ft, NAVD88)	H_{m0} (ft)	T_p (s)	MWD (deg, Eucl)	Storm ID	SWL (ft, NAVD88)	H_{m0} (ft)	T_p (s)	MWD (deg, Eucl)
461	19.01	4.02	3.24	127.9	461	18.16	4.16	3.91	127.9
633	18.46	3.13	3.24	161.9	447	17.64	2.20	2.94	141.7
357	17.96	2.63	2.94	140.7	633	17.48	3.22	3.56	161.8
447	17.88	2.25	2.94	141.7	357	17.45	2.43	2.94	140.7
464	16.36	2.19	2.94	139.4	589	16.69	2.09	2.94	109.3
342	16.17	1.66	2.94	146.6	464	16.51	2.19	2.94	139.4
598	15.96	2.36	2.94	138.1	342	16.38	1.76	2.94	146.6
589	15.88	1.94	3.24	115.9	598	16.16	2.38	2.94	138.1
159	15.04	1.96	2.94	127.3	529	15.90	1.82	3.24	118.6
529	14.64	1.85	3.24	118.6	634	15.51	2.15	3.56	178.3
SLC1 – Without Project					SLC1 – With Project				
Storm ID	SWL (ft, NAVD88)	H_{m0} (ft)	T_p (s)	MWD (deg, Eucl)	Storm ID	SWL (ft, NAVD88)	H_{m0} (ft)	T_p (s)	MWD (deg, Eucl)
461	20.14	4.28	3.56	127.9	461	19.52	4.28	3.56	127.9
633	19.38	3.87	3.56	163.8	447	19.46	2.46	2.94	144.5
447	19.27	2.47	2.94	141.7	357	19.21	2.73	2.94	140.7
357	19.08	2.75	2.94	140.7	633	19.19	3.75	3.56	163.8
589	18.64	2.25	2.94	97.5	589	18.50	2.14	2.94	126.0
598	18.45	2.87	2.94	138.1	464	18.01	2.59	2.94	139.4
342	18.29	2.02	2.94	149.4	342	17.93	2.00	2.94	149.4
464	18.27	2.67	3.24	154.7	598	17.82	2.86	3.24	148.7
529	16.52	2.28	3.24	118.6	529	16.97	2.25	3.24	118.6
159	16.40	2.19	2.94	129.6	159	16.64	2.24	2.94	129.6
SLC2 – Without Project					SLC2 – With Project				
Storm ID	SWL (ft, NAVD88)	H_{m0} (ft)	T_p (s)	MWD (deg, Eucl)	Storm ID	SWL (ft, NAVD88)	H_{m0} (ft)	T_p (s)	MWD (deg, Eucl)
461	21.76	5.01	3.56	147.3	416	21.79	4.79	3.56	147.3
366	21.40	4.43	3.56	163.8	447	21.54	2.72	3.24	150.2
447	21.37	2.67	3.24	152.9	357	21.36	3.02	3.24	148.7
357	21.17	2.97	3.24	152.4	366	21.35	4.47	3.56	163.8
589	20.38	2.51	2.94	97.5	589	20.49	2.50	2.94	97.5
464	20.22	3.03	3.24	154.7	464	20.28	3.03	3.24	154.7
598	20.14	3.36	3.24	148.7	598	20.08	3.35	3.24	148.7
342	19.96	2.30	2.94	152.5	342	20.04	2.32	2.94	152.5
529	19.50	2.60	3.56	129.5	529	19.24	2.65	3.24	118.6
595	19.21	3.77	3.56	118.6	532	18.74	2.22	2.94	145.2

Figure 27. With-project SWL and H_{m0} peaks for all storms plotted against without-project conditions for SP 3936. Upper row is SLC0, middle row is SLC1, and bottom row is SLC2.
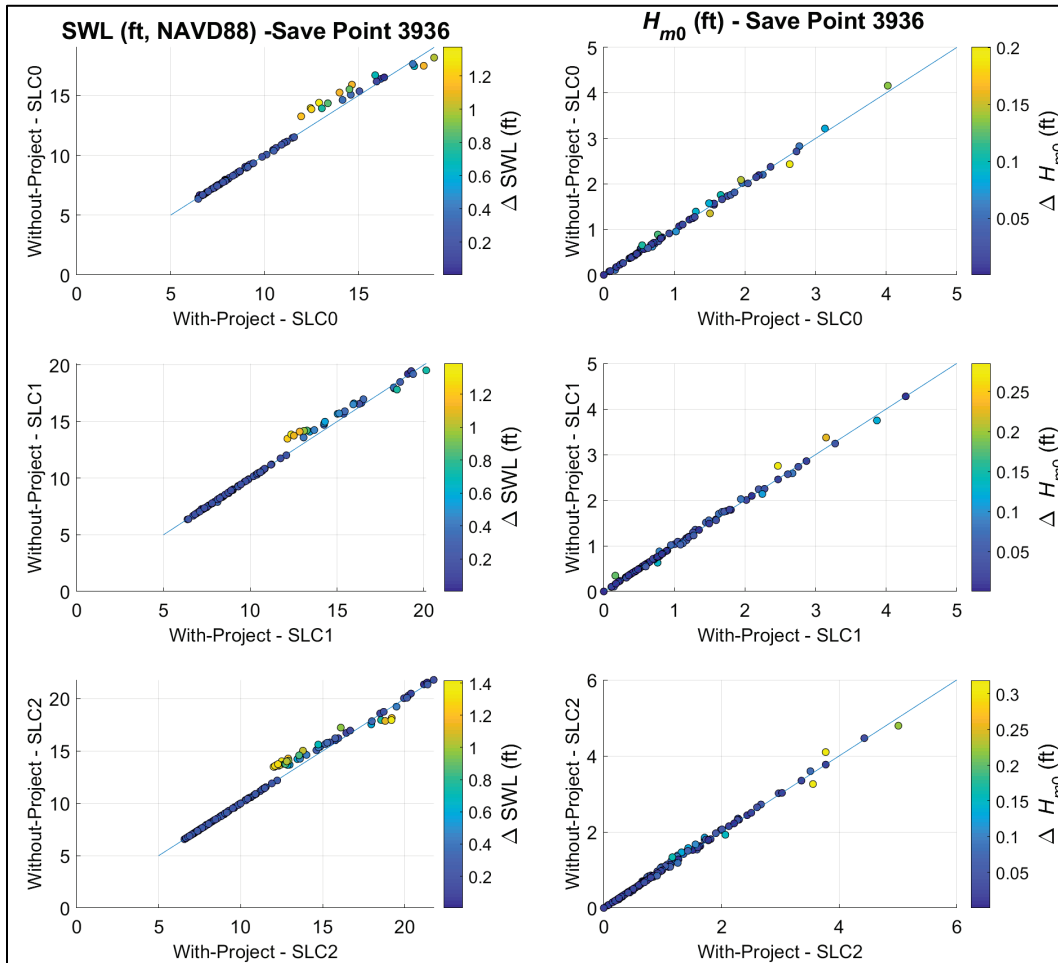
Figure 28. Storm number vs. peak SWL for SP 3936. The top three plots are for the existing structure conditions under scenarios SLC0, SLC1, and SLC2, respectively. The bottom three plots are for the with-project conditions under scenarios SLC0, SLC1, and SLC2, respectively.
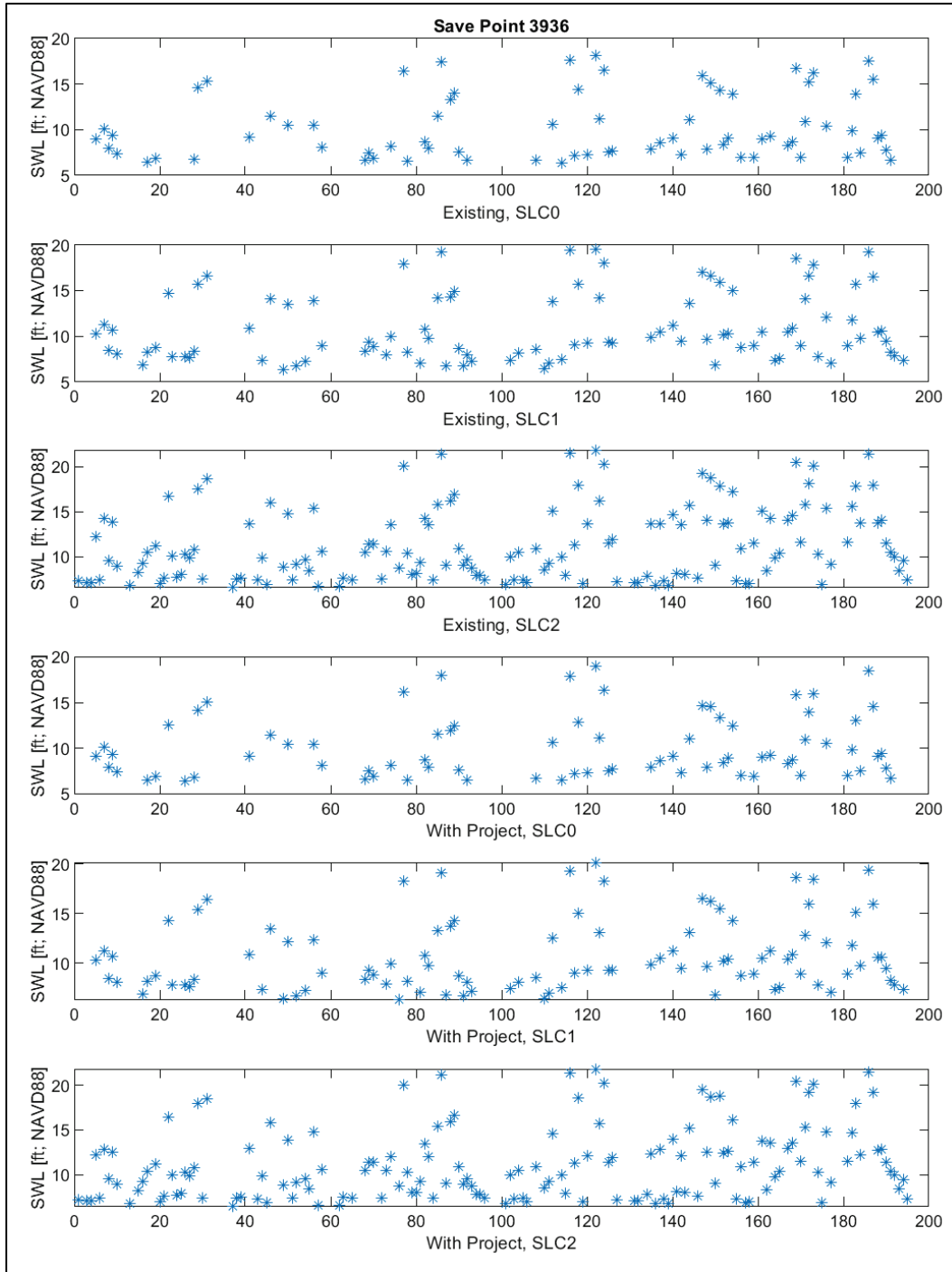
Figure 29. Storm number vs. peak H_{m0} for SP 3936. The top three plots are for the without-project structure conditions under scenarios SLC0, SLC1, and SLC2, respectively. The bottom three plots are for the with-project conditions under scenarios SLC0, SLC1, and SLC2, respectively.
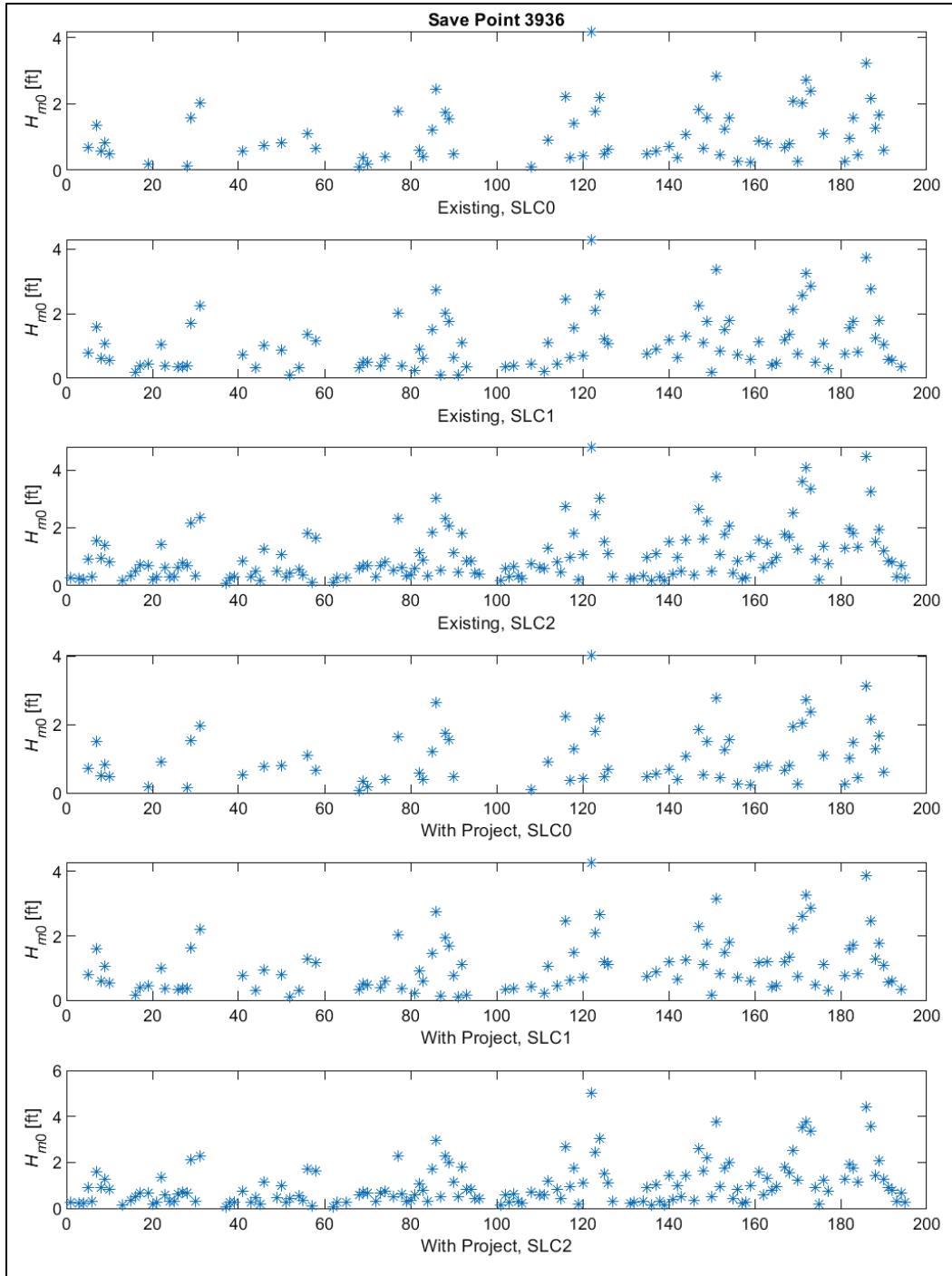
4.2   Nonlinear residual

For the typical coastal engineering project, it is common to linearly superimpose water level components (e.g., surge, tide, wave setup, wind setup, RSLC). The alternative is to model the hydrodynamics with a coupled modeling system like CSTORM. *Nonlinear residual* (NLR) is defined as the difference between the SWL computed using the coupled model and that computed using linear superposition. Therefore, NLR is the error that results from linear superposition. As shown Appendix I, the NLR can be large due to not including important physics that are the result of wave and wind setup along with the effects from currents and other localized effects. Individual storm response can be used to illustrate the NLR. For example, the SWL difference between SLC conditions for SP 3936, Storm ID 461, is $SWL_{SLC1} - SWL_{SLC0} = 20.14 - 19.01$ ft $= 1.13$ ft. Likewise, the difference for Storm ID 633 is 0.92 ft. These are compared to the difference between CSTORM starting geoid offset, which is $SLC1 - SLC0 = 1.58 - 0.17$ ft $= 1.41$ ft. The largest difference is 2.76 ft for Storm ID 589. At SP 3936, six of the top-ten storms have NLR greater than the difference between SLC0 and SLC1. NLR can be either positive or negative.

Appendix I has a summary of NLR for the study region. NLR is shown to be a significant issue for these areas represented by flooding extending inland many miles. Locations near structures and in confined areas can have larger NLR. Nadal-Caraballo et al. (2015) reported similar responses for the northeast US coast. In Appendix I, it is shown that NLR can be up to 2-3 times the linear increment between the RSLC scenarios. Note that wave parameters are depth-dependent so the NLR impacts both flood depth and waves. In addition, larger increments (e.g., SLC0 – SLC2) will have larger NLR. The NLR is usually a variable bias, and so it is difficult to accurately account for in the stochastic simulation. This provides a significant justification for coupled wave and surge modeling for all scenarios with RSLC incorporated into the initialized water level in the model, and not relying on linear superposition of RSLC scenarios in stochastic simulation, as was applied for this study.

4.3   Probability masses

The JPM-OS methodology was used to define the CTXCS storm suite and the associated storm probability masses (Nadal-Caraballo et al. 2015,

2019). The computation was completed for CTXCS[1]. These probability masses provide the relative probabilities of the synthetic tropical cyclones and are required to construct the hazard curves. They are closely related to the storm rates shown in the discrete version of Equation A.1 in Appendix A. The exceedance probability of response, such as storm water level, is the summation over all storms of the product of storm probability mass and conditional joint probability of storm parameters (Equation A.1). Probability masses were computed from the JPM analysis of CTXCS modeling output for 660 storms and 18332 SPs. The CTXCS probability masses were computed for the smaller number of S2G storms using the methods discussed in Appendix C. In this case, the matching was optimized for the hazard range from AEP=0.025 to 0.00167. An example unsmoothed hazard curve is shown in Figure 30 where the estimated SWL hazard curve for the S2G reduced storm set nearly exactly matches that of the full set of CTXCS storms. The method provides a very accurate estimate of the reduced sample probability masses and accurately reproduces the SWL hazard curve with errors less than 0.1%.

Figure 30. Example hazard curve for a single SP generated from 189 storms vs. the benchmark generated using 660 storms.
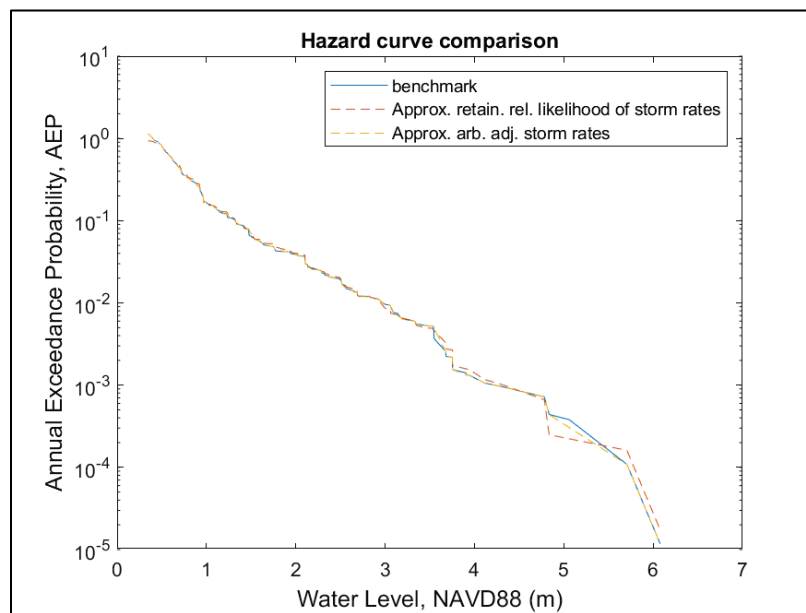
[1] Nadal-Caraballo, N. C., A. B. Lewis, V. M. Gonzalez, T. C. Massey, and A. T. Cox. Draft. *Coastal Texas Protection and Restoration Feasibility Study, Probabilistic Modeling of Coastal Storm Hazards*. ERDC/CHL Technical Report, Vicksburg, MS: US Army Engineer Research and Development Center.

4.4   Storm response hazard

Probability mass surfaces were constructed for without- and with-project alternatives for each RSLC scenario using the exceedance distributions for 18332 CTXCS points and then mapped onto the 5148 S2G points for the 189 S2G storms resulting in accurate storm probability masses. The probability masses were used with the individual storm peaks to develop hazard curves for both SWL and H_{m0} for all S2G SPs solving Equation A.1 and including uncertainty. Gonzalez et al. (2019) summarized efforts to quantify uncertainty in probabilistic storm surge models. The uncertainty that is incorporated in this analysis follows these methods. The application is introduced in Appendix A and discussed in more detail in Appendix G. The stochastic simulation strategy with uncertainty is described in detail in Appendix G. The uncertainties that are considered in the hazard computation for SWL and H_{m0} have been used in recent JPM-OS studies:

1. Errors in hydrodynamic modeling and grids associated with epistemic uncertainty.
2. Errors in meteorological modeling associated with simplified PBL winds.
3. Random variations in the Holland B parameter (shape of wind profile).
4. Storm track variations not captured in synthetic storm set.
5. Random astronomical tide phase.

The bias-corrected uncertainty associated with each error is normally distributed. The total uncertainty is represented by the standard deviation of errors (σ_ε), where the total associated uncertainty is computed as the square root of the sum of the squares of the standard deviations of each uncertainty (σ_i) where σ_ε is the total standard deviation of errors and σ_i is the standard deviation of error i. The total error is capped to avoid large unreasonable error estimates.

Figure 31 shows example SWL and H_{m0} hazard curves for without-project and with-project scenarios for SLC0, SLC1 and SLC2, with the 50% and 90% CL shown. Here, the 90% CL represents the influence of the summation of the epistemic uncertainties listed above. The individual AEP values are listed in Table 3 (without-project) and Table 4 (with-project). The H_{m0} values are listed in Table 5 (without) and Table 6 (with).

Figure 31. AEP vs. SWL and Hm0 for SP 3936. Top row is SLC0, middle row is SLC1, and bottom is SLC2.
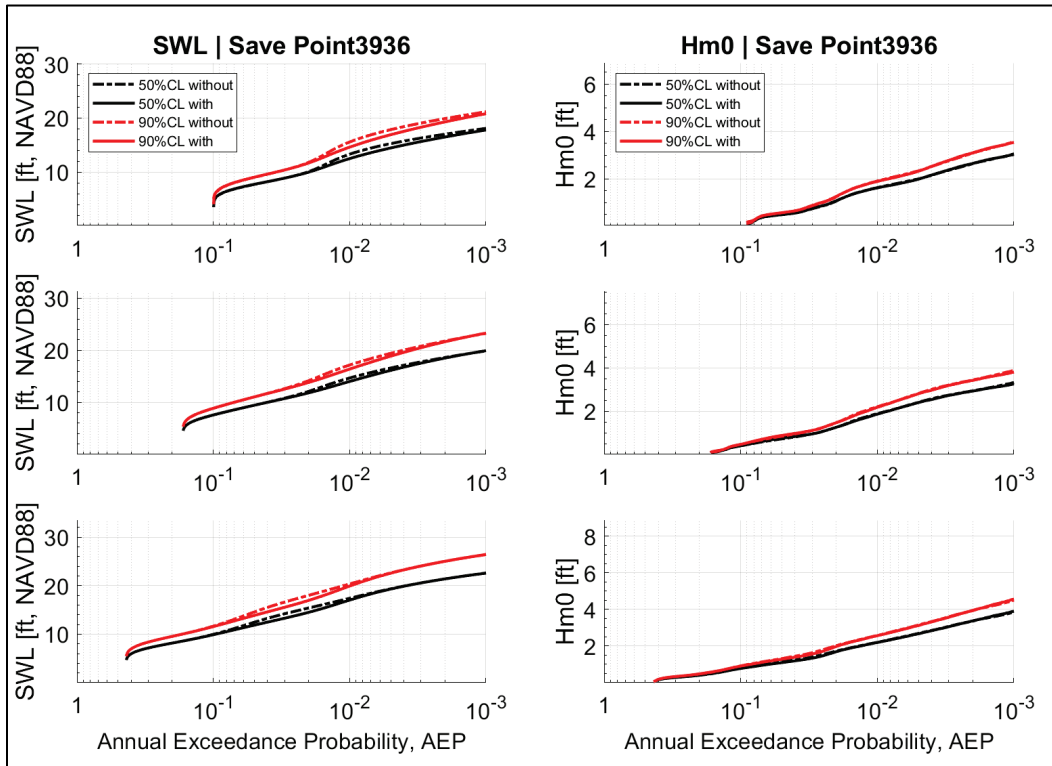
Table 3. AEP SWL in feet for SP 3936, without-project.

Scenario	CL	Annual Exceedance Probability									
		0.2	0.1	0.05	0.02	0.01	0.005	0.003	0.002	0.0013	0.001
Without-Project SLC0	50%	0.0	0.0	7.7	10.1	13.3	15.3	16.1	17.0	17.7	18.1
Without-Project SLC0	90%	0.0	0.0	9.0	11.8	15.6	17.9	18.8	19.9	20.7	21.2
Without-Project SLC1	50%	5.0	6.6	9.0	11.4	13.2	15.1	16.2	17.5	18.5	19.1
Without-Project SLC1	90%	5.8	7.8	10.5	13.3	15.5	17.7	18.9	20.5	21.6	22.3
Without-Project SLC2	50%	8.2	10.0	12.5	15.4	17.4	19.4	20.3	21.4	22.1	22.6
Without-Project SLC2	90%	9.5	11.7	14.6	18.0	20.4	22.6	23.8	25.0	25.9	26.4

Table 4. AEP SWL in feet for SP 3936, with-project.

Scenario	CL	Annual Exceedance Probability									
		0.2	0.1	0.05	0.02	0.01	0.005	0.003	0.002	0.0013	0.001
With-Project SLC0	50%	0.0	0.0	7.7	10.0	12.5	14.5	15.4	16.5	17.3	17.8
With-Project SLC0	90%	0.0	0.0	9.1	11.7	14.6	16.9	18.0	19.3	20.2	20.8
With-Project SLC1	50%	0.0	7.6	9.4	11.8	14.0	16.1	17.3	18.5	19.4	19.9
With-Project SLC1	90%	0.0	8.9	11.0	13.8	16.4	18.9	20.2	21.6	22.7	23.3
With-Project SLC2	50%	8.2	9.9	11.9	14.5	17.0	19.3	20.3	21.4	22.1	22.6
With-Project SLC2	90%	9.5	11.6	13.9	17.0	19.9	22.6	23.8	25.0	25.9	26.4

Table 5. AEP H_{m0} in feet for SP 3936, without-project.

Scenario	CL	Annual Exceedance Probability									
		0.2	0.1	0.05	0.02	0.01	0.005	0.003	0.002	0.0013	0.001
Without-Project SLC0	50%	0.0	0.0	0.5	1.1	1.6	2.0	2.3	2.6	2.9	3.0
Without-Project SLC0	90%	0.0	0.0	0.6	1.2	1.9	2.3	2.7	3.1	3.4	3.5
Without-Project SLC1	50%	0.0	0.4	0.7	1.2	1.9	2.4	2.7	3.2	3.7	4.2
Without-Project SLC1	90%	0.0	0.5	0.8	1.5	2.2	2.8	3.1	3.5	3.7	3.9
Without-Project SLC2	50%	0.4	0.8	1.1	1.7	2.2	2.7	3.0	3.3	3.6	3.8
Without-Project SLC2	90%	0.5	0.9	1.3	2.0	2.6	3.2	3.5	3.9	4.3	4.5

Table 6. AEP H_{m0} in feet for SP 3936, with-project.

Scenario	CL	Annual Exceedance Probability									
		0.2	0.1	0.05	0.02	0.01	0.005	0.003	0.002	0.0013	0.001
With-Project SLC0	50%	0.0	0.0	0.5	1.1	1.6	2.0	2.3	2.6	2.9	3.0
With-Project SLC0	90%	0.0	0.0	0.6	1.2	1.9	2.3	2.7	3.1	3.3	3.5
With-Project SLC1	50%	0.0	0.4	0.8	1.3	1.9	2.4	2.7	2.9	3.1	3.3
With-Project SLC1	90%	0.0	0.5	0.9	1.5	2.2	2.8	3.1	3.4	3.6	3.8
With-Project SLC2	50%	0.4	0.8	1.1	1.7	2.2	2.7	3.0	3.4	3.7	3.9
With-Project SLC2	90%	0.5	0.9	1.3	2.0	2.6	3.1	3.5	4.0	4.3	4.5

4.5 Historical hurricane average recurrence intervals (ARIs)

Within CSRM projects, and especially within the JPM-OS framework where synthetic storm events define coastal hazards, it is useful to provide perspective for design SWLs by comparing them to the response from historical events. Historical tropical cyclones for Texas are listed in Appendix D.

An analysis of the locally highest surge-producing recent tropical cyclones, Hurricanes Carla and Ike, was conducted to determine ARI for peak SWLs. Each historical storm was modeled using CSTORM with geoid set to model the steric water level at the time of the storm. Tidal fluctuations at the time of the event were included. Without-project (existing) mesh was used. The storm modeling of historical events is described in Appendix B. Peak SWLs from the model are shown to be reasonably well predicted when compared with peak NOAA water level gage measurements near the area (NOAA gage 8770475 located at Port Arthur, TX).

Figure 32 shows peak SWL for Hurricane Carla (1961) for the Sabine region, and the corresponding ARIs are plotted in Figure 33. Similar SWL and ARI plots for Freeport area are shown in Figure 34 and Figure 35, respectively. Similarly, Hurricane Ike (2008) is plotted in Figure 36 through Figure 39. Hurricane Carla produced peak SWLs near the CSRM systems in the Sabine area of 7 to 9 ft, NAVD88, corresponding to ARIs of approximately 20 to 30 yr. Carla produced peak SWLs near the CSRM system in Freeport area of 9 to 13 ft, NAVD88, corresponding to ARIs of approximately 25 to 70 yr. Hurricane Ike produced peak SWLs near the CSRM systems in Sabine area of 12 to 17 ft, NAVD88, corresponding to ARIs of approximately 120 to 300 yr. Ike produced peak SWLs near the CSRM system in Freeport area of 5 to 8 ft, NAVD88, corresponding to ARIs of approximately 4 to 13 yr. These values are consistent with synthetic storm hazard curves discussed in the prior section.

Table 7 presents ARI for historical storm SWL for Taylor Bayou Turning Basin area.

Figure 32. Peak SWL color-fill contour plot of peak SWL for Hurricane Carla for Sabine area. SWL is in feet, NAVD88.
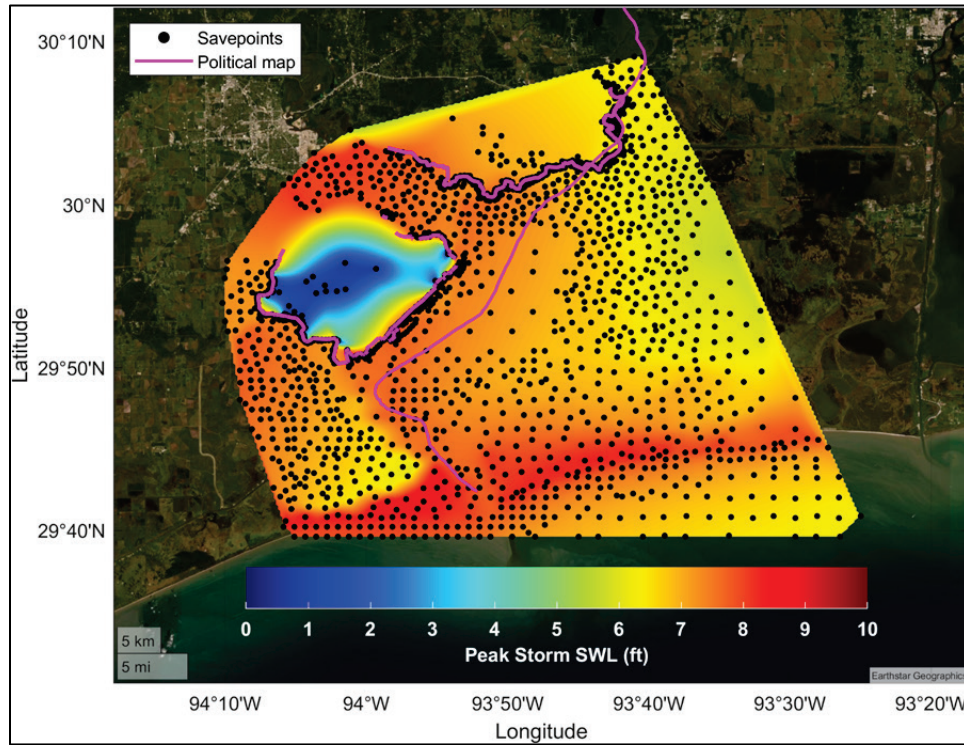
Figure 33. ARI for peak SWL color-fill contour plot of peak SWL for Hurricane Carla for Sabine area.
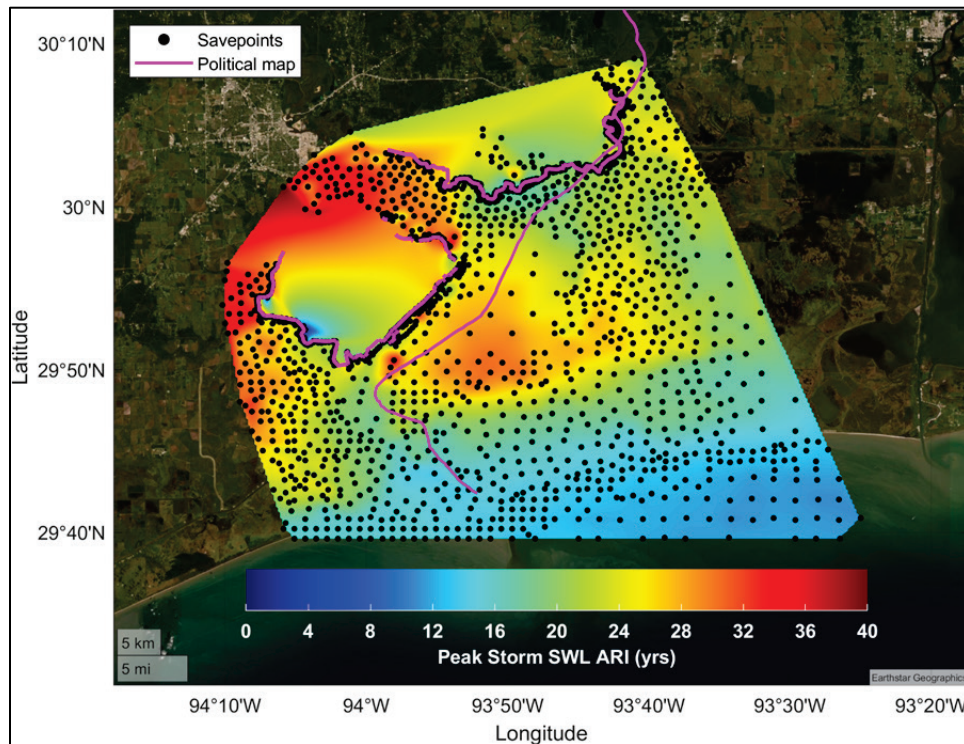
Figure 34. Peak SWL color-fill contour plot of peak SWL for Hurricane Carla for Freeport area. SWL is in feet, NAVD88.
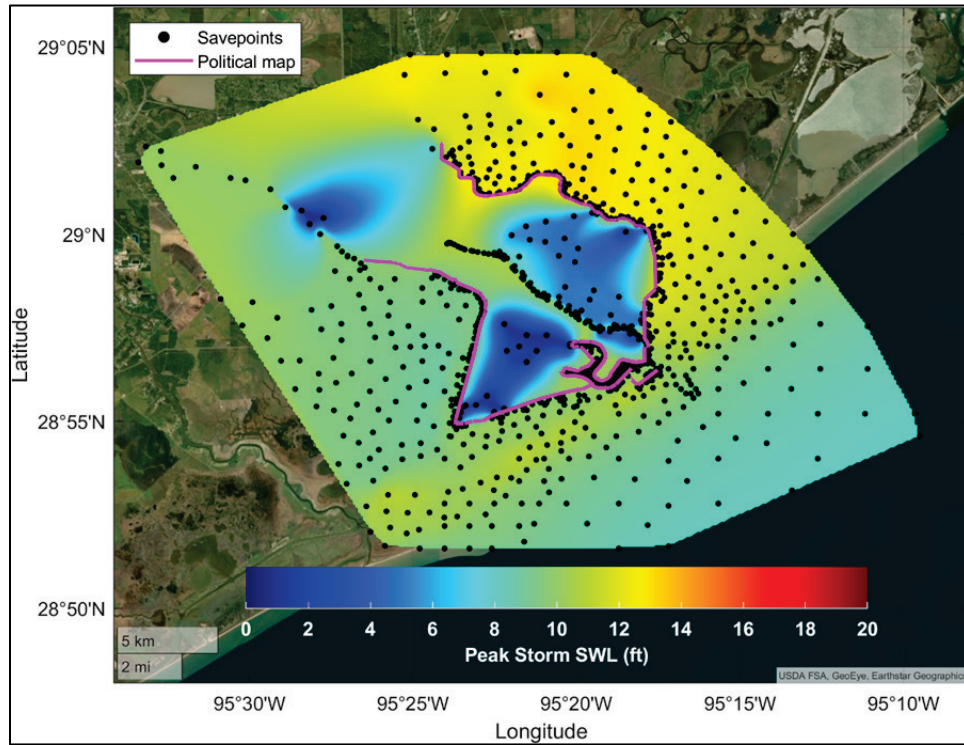
Figure 35. ARI for peak SWL color-fill contour plot of peak SWL for Hurricane Carla for Freeport area.
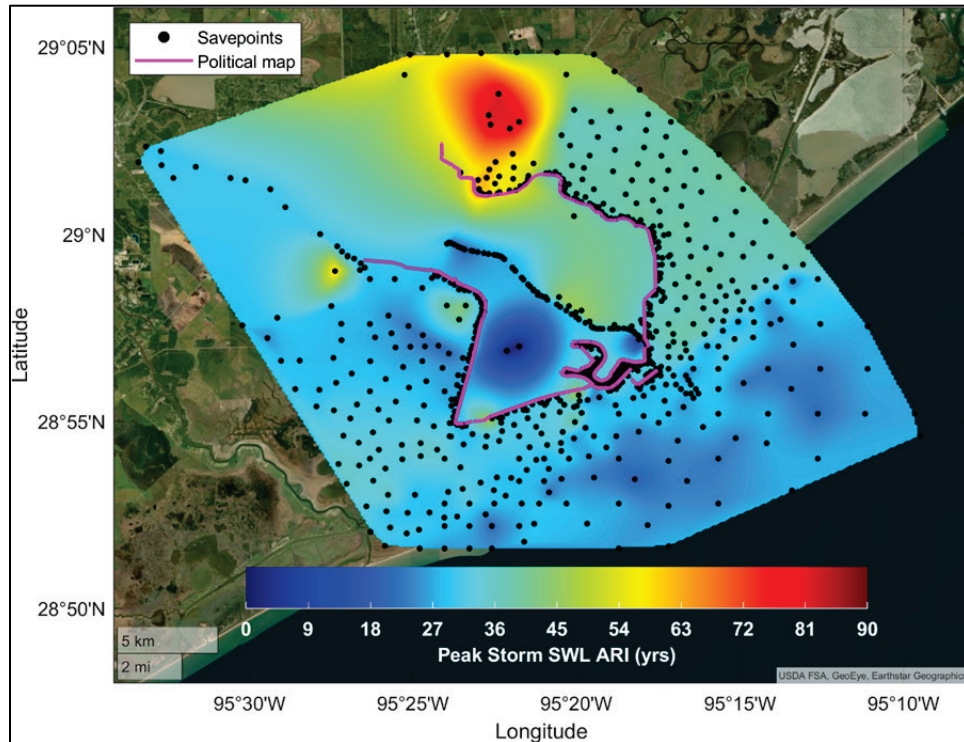
Figure 36. Peak SWL color-fill contour plot of peak SWL for Hurricane Ike for Sabine area. SWL is in feet, NAVD88.
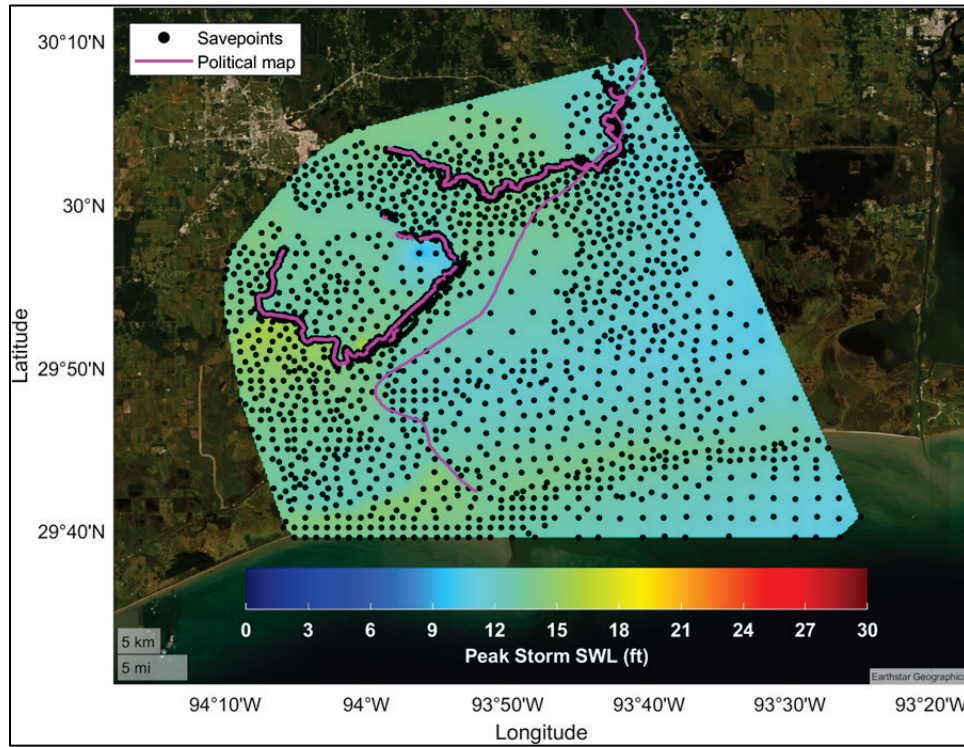
Figure 37. ARI for peak SWL color-fill contour plot of peak SWL for Hurricane Ike for Sabine area.
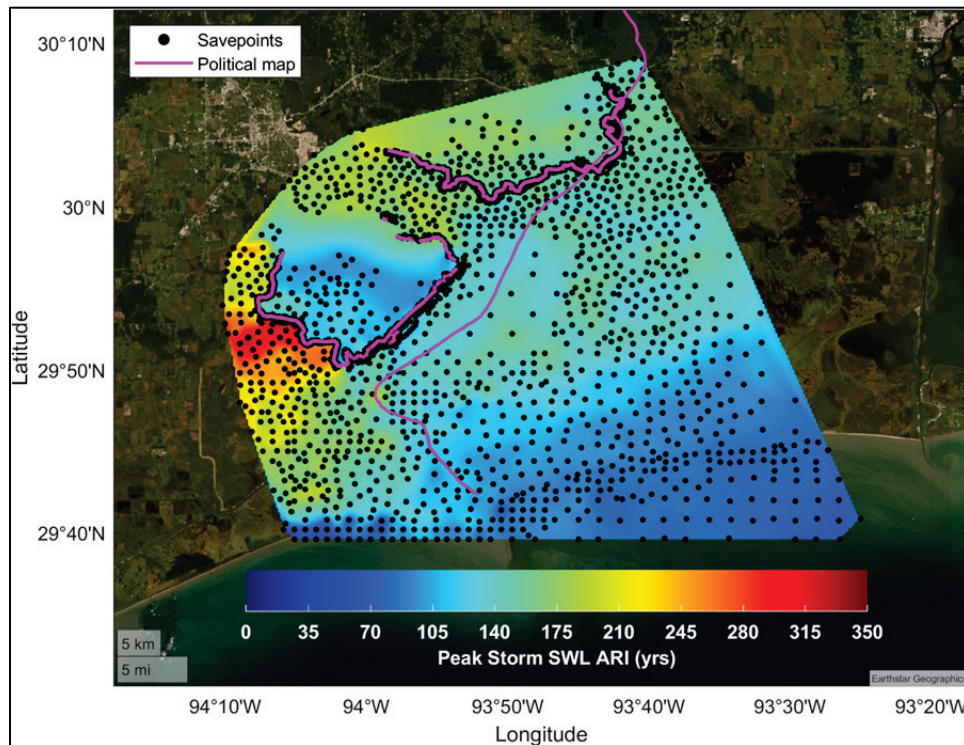
Figure 38. Peak SWL color-fill contour plot of peak SWL for Hurricane Ike for Freeport area. SWL is in feet, NAVD88.
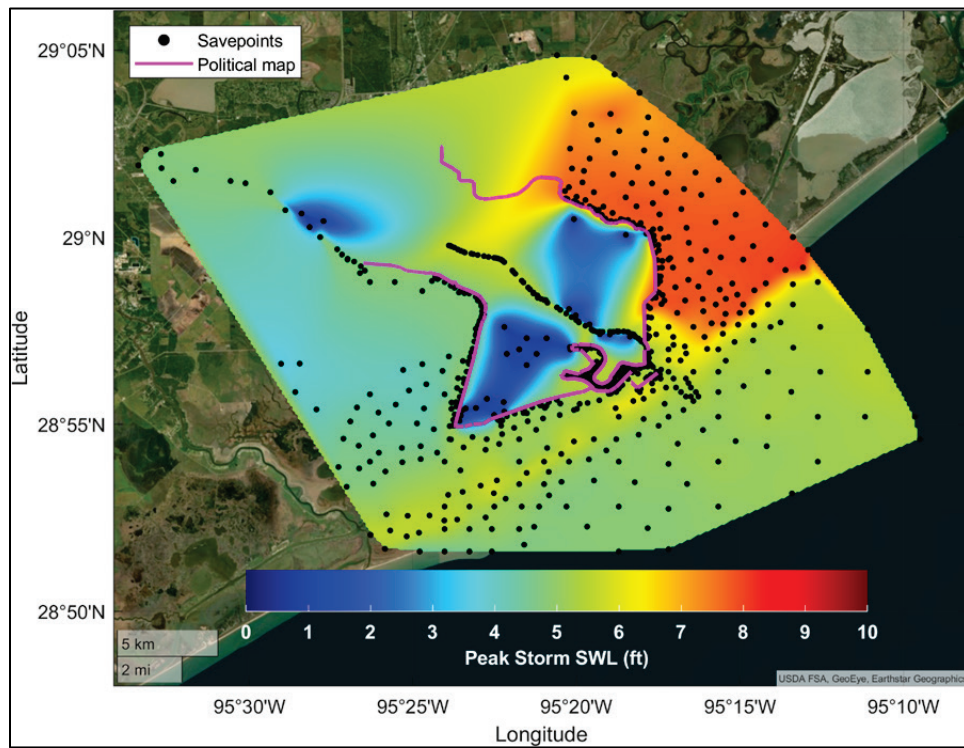
Figure 39. ARI for peak SWL color-fill contour plot of peak SWL for Hurricane Ike for Freeport area.
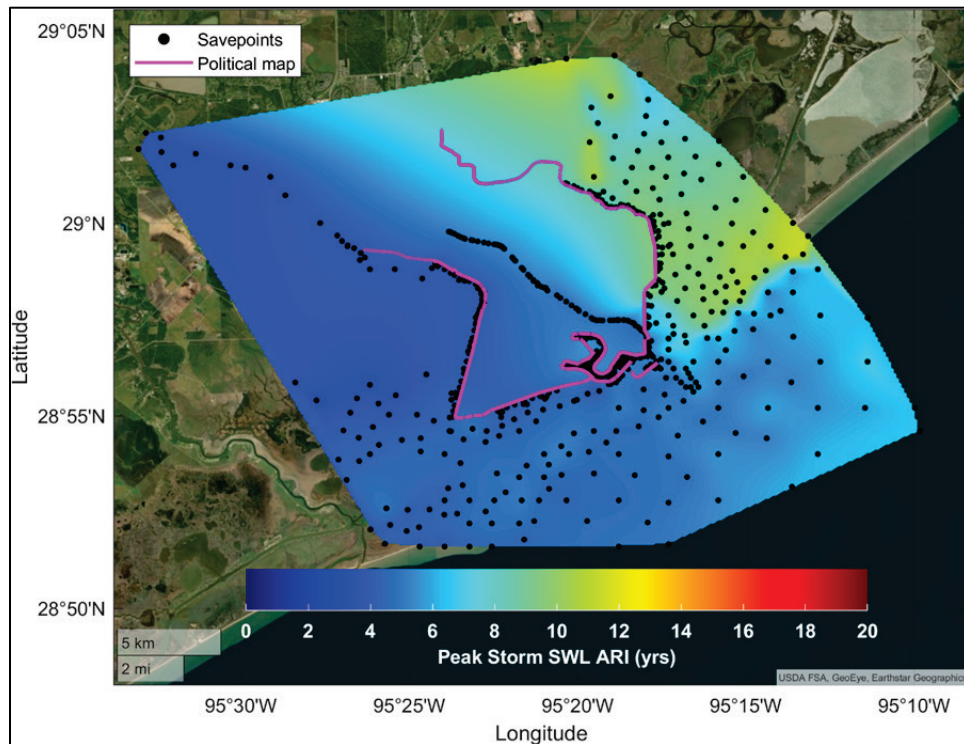
Table 7. ARI for historical storm SWL for Taylor Bayou Turning Basin area.

Storm	Landfall Date	Landfall Location	Cp (mbar)	SWLmax (ft, NAVD88)	ARI in years	
					50% CL	90% CL
Harvey	26 Aug 2017	San Jose Is., TX	937	3	1.6	1.3
Ike	30 Sep 2008	NE end of Galveston Island, TX	950	11.7	74	45
Rita	24 Sep 2005	Near TX-LA border	937	5	5	4
Carla	1961	Near Port O'Connor	935	7.3	22	18

4.6 Drawdown

Where needed, an analysis of minimum water level probabilistic hazard was conducted to provide input for geotechnical stability related to drawdown. Drawdown on a day-to-day basis occurs as a result of tidal fluctuations and relatively minor climate events (sub-tropical storms, frontal systems, etc.). Water level minima can occur from storm-related anti-surge where the wind blows the water away from shore. Extreme minima can occur during tropical cyclones when very strong winds blow water offshore and pressure lobes increase water levels in some areas but decrease water levels in others. For example, if the cyclone center of pressure is just to the east of Sabine (e.g., Hurricane Rita, Hurricane Isaac), strong winds will blow water offshore in Sabine area, and increased water levels under the center of pressure in western Louisiana will reduce surrounding water levels in the Sabine area of eastern Texas.

To compute the probability distribution of water level minima, the combination of relatively frequent localized minima from tides and general weather systems and the infrequent extremes due to tropical cyclones must be combined. Herein, the assumption is that these two statistical populations are independent. As an example, for the Port Arthur area, the analysis methodology was as follows:

1. Analyze measured water levels.
   a. Download Sabine Pass North Gage (8770570) continuous recoded hourly and monthly water levels from NOAA Tides and Currents website. This gage had a 33 yr record length.
   b. Detrend time series by rotating raw time series about center of epoch and subtracting out bias. Remove tropical storm events.

      c. Compute nontidal residual (NTR): NTR = measured η – predicted η, where η is the time varying water level.

      d. Invert NTR time series so time series minima become peaks. Perform standard peaks-over-threshold analysis. Save the most extreme "peaks" or minima.

      e. Perform extremal analysis of these negative peaks and fit to generalized Pareto distribution.

2. Analyze JPM synthetic tropical cyclone (TC) minimum water levels.

      a. Select SP 1094 (Figure 26), which is in center of Taylors Bayou Turning Basin.

      b. Find minimum water level for each storm and invert sample so all minima are positive SWL.

      c. Subtract out steric water level of 0.39 ft that was added as a seasonal average increase in sea level due to primarily seasonal thermal fluctuations.

      d. Compute TC minima probability distribution for selected location.

3. Combine hazard curves of positive SWL minima peaks.

Figure 40 shows the measured SWL and resulting minima hazard curve. Note that the tropical storms were removed from this record before processing for the extremal distribution but are still present in the left hand side of Figure 40 (e.g., Hurricane Ike in 2008 is clearly visible). Also, values in the time series in the left plot have not been inverted, but values in the distribution on the right have been. Figure 41 shows time series of two synthetic TCs with extreme minima highlighted. Here, extreme minima are the result of that location being on the left side of storm where winds are blowing offshore. Minima for all 189 TCs are shown in Figure 42 for with-project SLC0 scenario. Figure 43 shows the resulting TC minima hazard curves for with- and without-project SLC0 scenarios. Figure 44 shows the combined hazard curve. Select values of drawdown at various AEPs are shown in Table 8.

Figure 40. Water level gage 877570 recorded 33 yr time series (left) and
resulting inverted minima hazard curve (right).
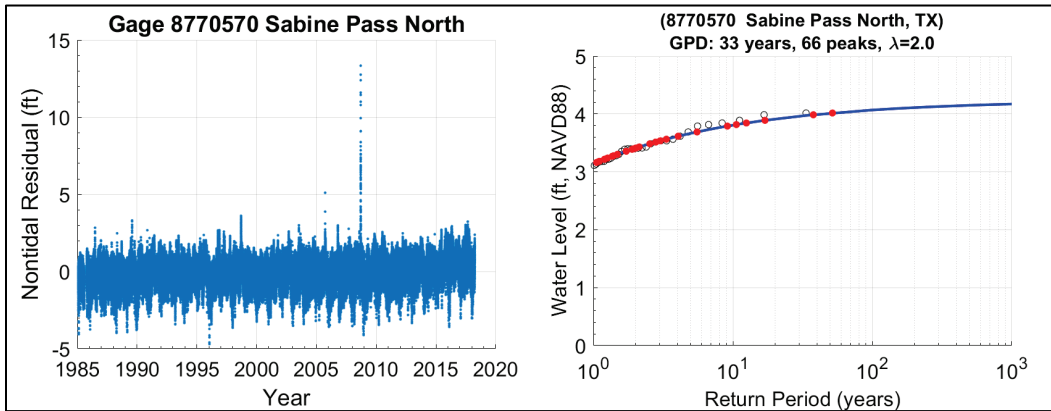
Figure 41. Example SWL time series and minima (red circle) for synthetic TC
at SP 1094 for with-project SLCO scenario.
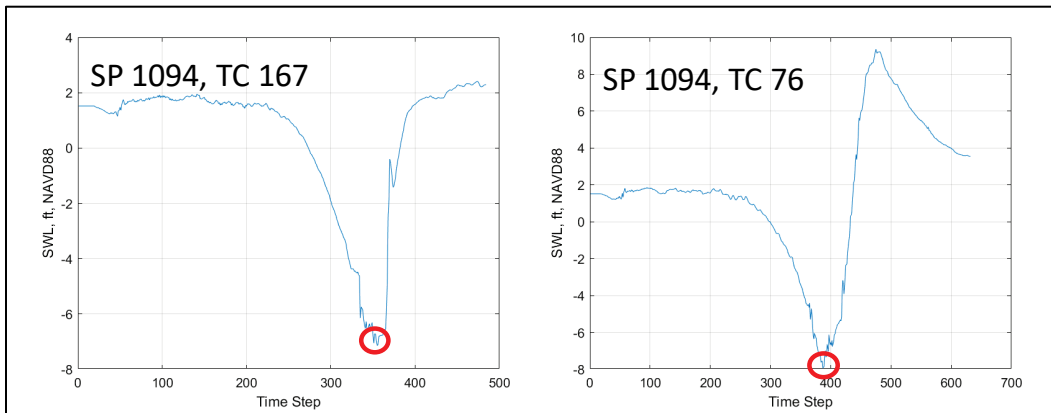
Figure 42. All TC minima for synthetic TCs at SP 1094
for with-project SLCO scenario.
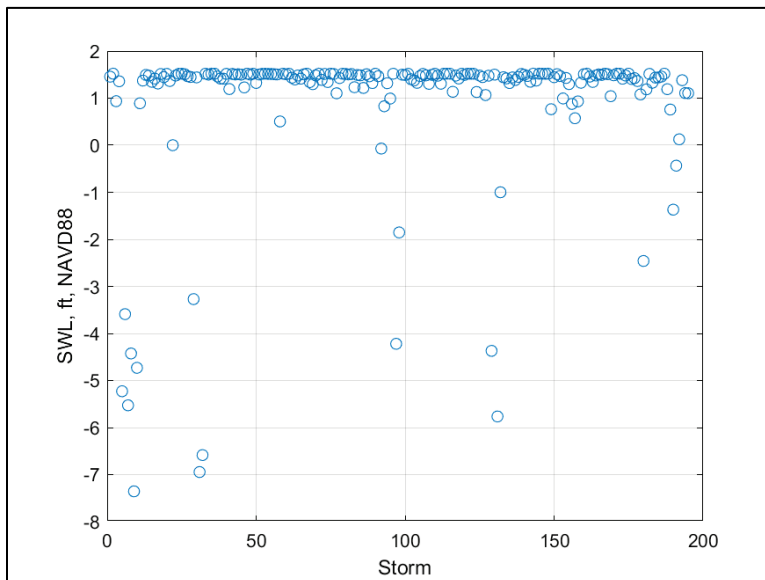
Figure 43. Hazard curves for synthetic TC minima at SP 1094 for without-project (left) and with-project (right) and SLC0 scenarios.
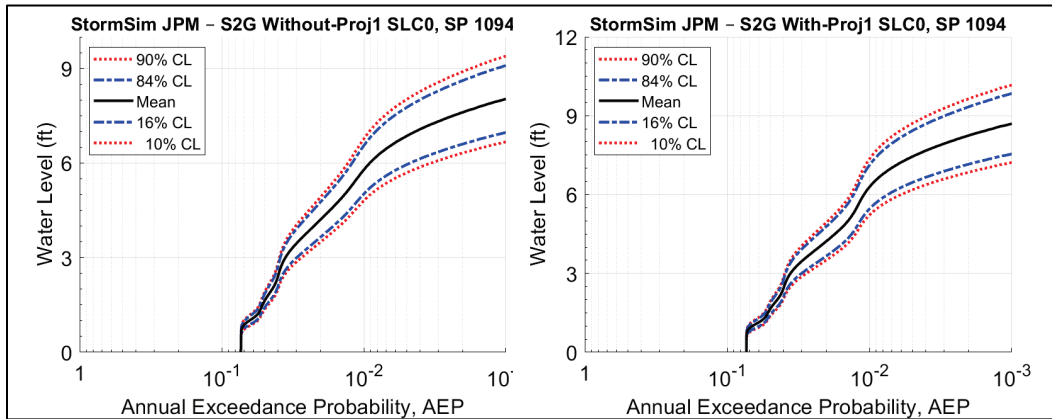
Figure 44. Hazard curves for combined measured and TC minima at SP 1094 for with-project SLC0 scenario.
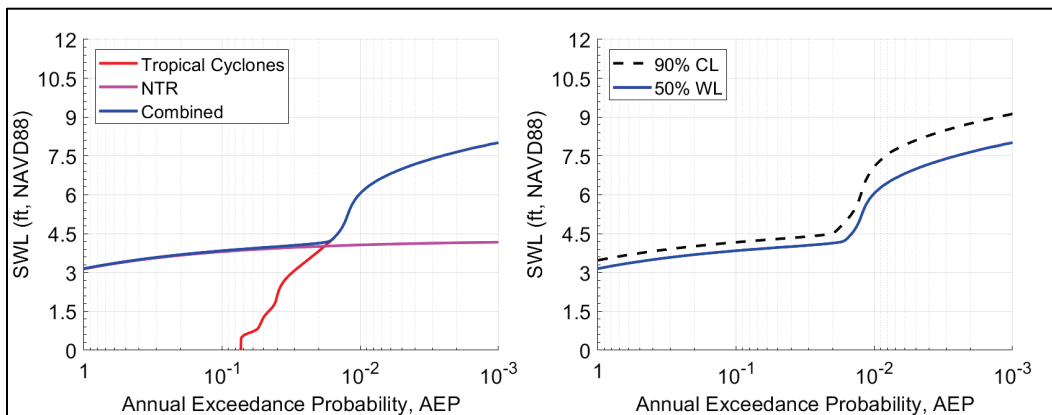
Table 8. Inverted minimum water levels for several AEPs for drawdown at SP 1094 in Taylors Bayou Turning Basin. Water levels are in feet, NAVD88.

Scenario	Annual Exceedance Probability					
	1	0.1	0.02	0.01	0.002	0.001
Without-Project SLC0 50% CL	3.1	3.8	4.1	5.5	7.1	7.5
Without-Project SLC0 90% CL	3.5	4.2	4.5	6.4	8.2	8.6
With-Project SLC0 50% CL	3.1	3.8	4.2	6.0	7.6	8.0
With-Project SLC0 90% CL	3.5	4.2	4.5	7.1	8.7	9.1

5 Local Coastal Storm Risk Management (CSRM) Response Modeling

5.1 Hydraulic responses

5.1.1 Wave runup

Wave runup has historically been used for coastal structure design as it is an indicator of the landward extent of wave action. Wave runup and setup are illustrated in Figure 45 where η_{max} = maximum setup and R = runup. Wave setup is the increase of the still water level as a result of radiation stresses from wave breaking in the nearshore zone. Wave runup and rundown are the time-varying vertical extent of the water level along the shoreline. Wave runup typically includes wave setup. Because runup is a time-varying quantity, a representative statistical value is required. Usually, runup is represented as a relatively extreme probability of exceedance, say $R_{1\%}$ or $R_{2\%}$, computed from about one-half hour of continuous water surface recordings, where 1% and 2% indicated percent exceedance values. For coastal structures, the run-up statistic is typically computed as the sum of runups divided by the number of waves as opposed to the number of runups, primarily because the number of waves is more consistent and definitive.

Figure 45. Illustration of wave setup and runup from Melby (2012).
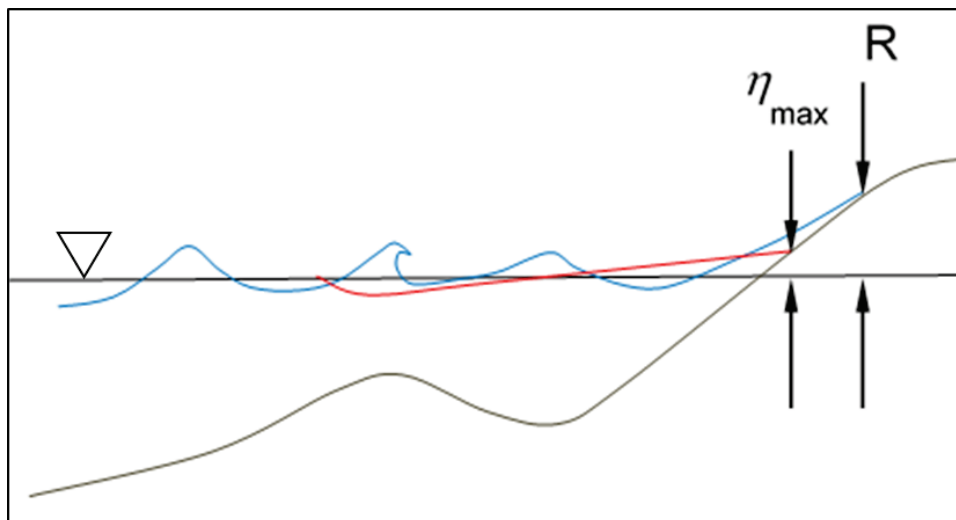
The runup height statistic $R_{2\%}$ above the still water level which is that exceeded by 2% of incident irregular waves is the typical parameter used for defining runup. It is defined using wave and water level inputs from

the toe of the structure. $R_{2\%}$ is most closely associated with an overtopping rate of 0.001 cfs/ft, although this depends on the water levels, wave height, and wave period (EC 1110-2-6067; USACE [2010b]). This is a very small amount, approximately equal to 2 tablespoons of water per foot per second. A number of empirical formulas have been proposed to estimate $R_{2\%}$ (USACE 2008) and more recently in the EurOtop II (2018) manual. The recent formulas include a few dimensionless constants that can be calibrated for different applications. The primary relation used herein for computing runup is discussed in detail in Appendix F.

5.1.2 Overflow

For the no-wave condition when the SWL is above the crest of the structure, the broad-crested weir equation is typically used to compute overtopping rate. This equation is discussed in Appendix F.

5.1.3 Wave overtopping

Wave overtopping rate defines different limit states for design, and these are somewhat loosely tied to degrees of erosion. Wave overtopping rate q per unit alongshore length of the structure crest is used for design. Wave overtopping rate for sloping structures is given in the Coastal Engineering Manual (CEM) (USACE 2008). Relatively minor updates to the wave overtopping equations based on significantly more laboratory and field data have been recently published in the EurOtop II (2018) manual. These equations are used in this study as they include options for addressing a wider variety of structure conditions including berms and walls, variable friction, variable roughness, and variations in wave direction. Overtopping equations used herein are discussed in detail in Appendix F.

5.1.4 Combined overflow and wave overtopping

Recent advances in wave overtopping have improved the reliability of empirical overtopping estimates for coastal applications. A relatively simple empirical equation that combines overflow and wave overtopping rates was used based on guidance in the EurOtop (2018) manual. Again, the equation used herein is given in Appendix F.

All of the above runup and overtopping equations are empirical mean fits to primarily small-scale laboratory data. These data also include mid- to large-scale physical model tests as well as full-scale experiments. The

important consideration used herein is that these equations are not based on basic physics but are mean fits to measurements with considerable scatter. As such, there is considerable uncertainty in these relations. This uncertainty is accounted for herein by including the equation uncertainty in the stochastic simulations as described below and in Appendix G.

5.2 Structure configurations

Transects associated with reaches along each of the CSRM systems were selected due to their location and structure geometries. Save point locations were also associated with each transect. LiDAR-based ground elevations and existing CSRM structure elevations (provided by USACE SWG) were used to define the existing levee and floodwall elevations. Additional structure geometry details were computed from the LiDAR DEMs or provided by USACE SWG. As examples, Figure 46 shows schematized analysis transects, required for application of response empirical equations, for a levee and a floodwall transect. The with-project levee raises shown in Figure 46 have steeper slopes than existing. These are shown in Appendix F to have lower overtopping than shallower slopes. They also result in reduced construction material quantities and therefore reduced cost.

Figure 46. Example of a with-project analysis levee transect with measured topography (black), schematized without-project (blue), and levees with authorized elevation (red), and example floodwall transect with measured topography (black) and floodwalls with authorized elevation (blue). Elevations are in feet, NAVD88.
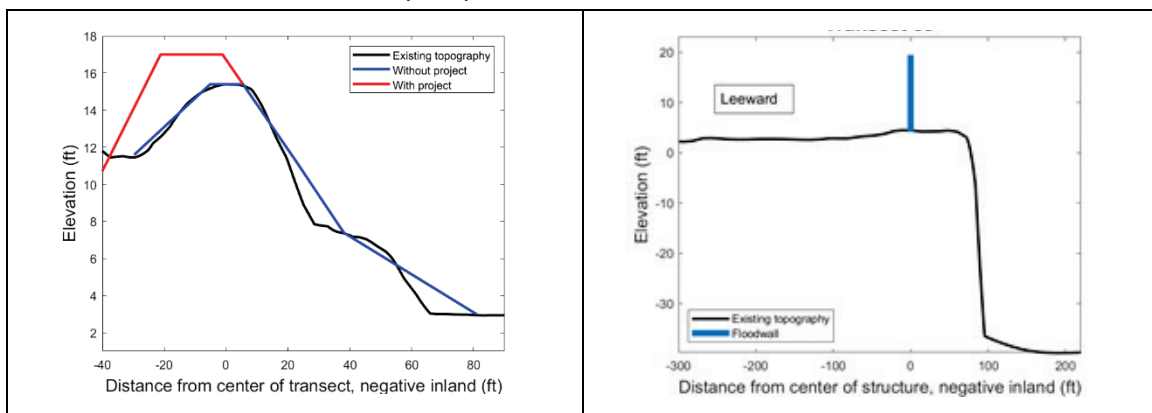
5.3 Deterministic validation

The empirical formulations for $R_{2\%}$ and q have been integrated into StormSim (Nadal-Caraballo et al. 2015; Melby et al. 2015, 2017). The runup and overtopping subroutines were validated against the EurOtop

example cases provided in the manual and the EurOtop artificial neural network (ANN) overtopping database. The training data used in the ANN are limited to mostly idealized experimental laboratory results. The combination of very high surge, small waves, complex bathymetry/topography and complex structure geometry for levees and floodwalls that comprise the S2G CSRM systems makes the project somewhat unique. The majority of storm and structure geometry combinations at Port Arthur were outside of the domain of the ANN. Twelve storms that were within the domain of the ANN were selected for comparison between the empirical deterministic code and the ANN output. Storms used for validation were CTXCS CSTORM simulations 357, 447, 456, 461, 525, 537, 538, 595, 598, and 633 (see Appendix D for storm details) with responses at SP 14499, shown in Figure 47. The structure geometries used were from transects 113, 114, 115, 118, 119, 120, 122, 126, 128, and 149. These transects, shown in Figure 48, lay along the SNWW for Port Arthur, shown in Figure 47. The comparison between the empirical equation and the ANN output is shown in Figure 49.

Figure 47. Locations of transects along the SNWW used for validation of runup and overtopping StormSim module.

Figure 48. Transects along the SNWW used for validation of runup and overtopping StormSim module.
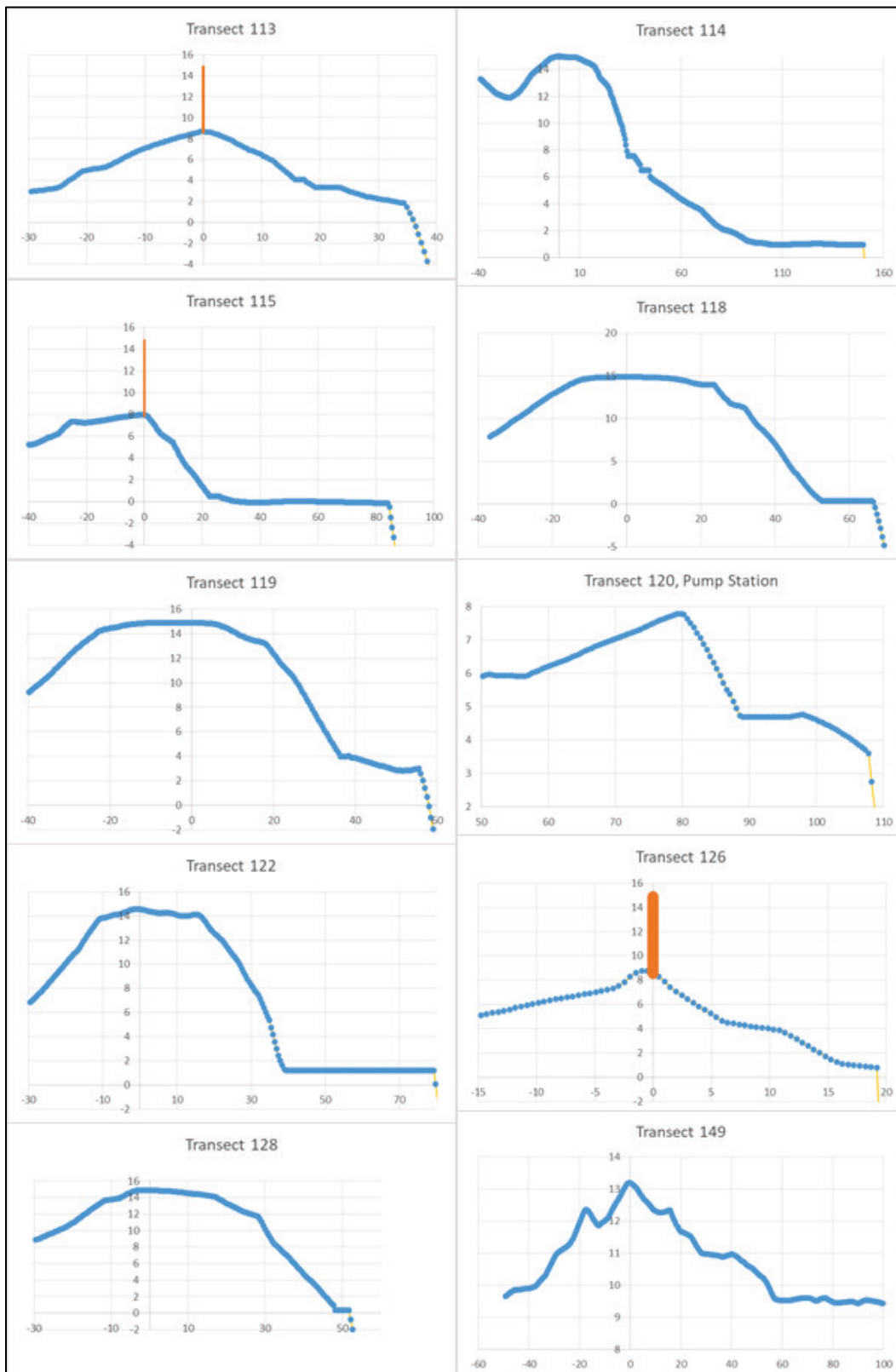
Figure 49. Validation plot from EurOtop ANN – Outputs of the validation transects.
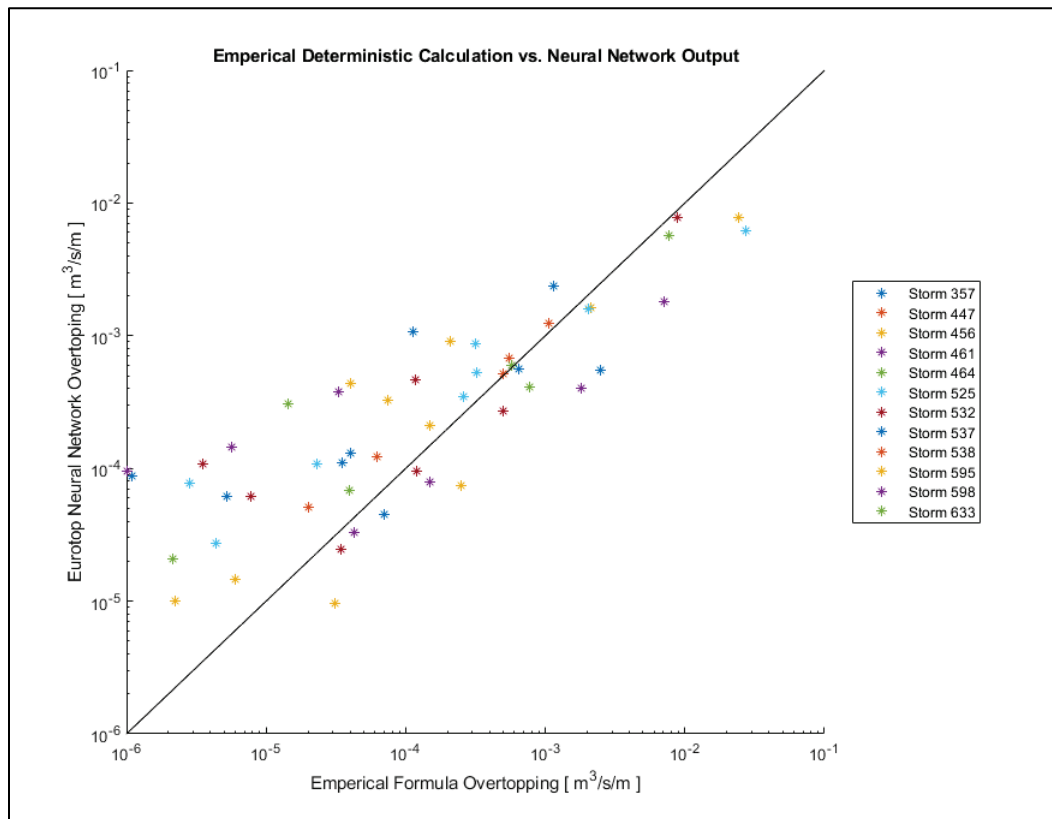
The empirical equations produced similar results to the ANN. There was some scatter; however, the differences are within the uncertainty of the empirical equations. As the overtopping rate decreases, the ANN overpredicts, compared to the empirical equation. This may be because these very small overtopping rates are difficult to measure in laboratory experiments or not physically possible. In general, the very small overtopping rates are not physically significant.

Additional validation of the software was completed using the examples in the EurOtop II (2018) manual. These examples assume one standard deviation is added to each coefficient, which was adjusted during this validation in the empirical equation codes. The empirical equation output from StormSim matched the output of the EurOtop II examples exactly.

5.4   Runup and overtopping computation

The empirical response equations discussed above can be incorporated into statistical simulations using standard software, such as Matlab. Herein, StormSim is used for this. StormSim is a suite of statistical

software tools for coastal engineering produced by the Coastal Hazards Group of the US Army Engineer Research and Development Center (ERDC), Coastal and Hydraulics Laboratory. For this study, StormSim stochastic simulation architecture was adapted to include the response empirical equations, wave and water level uncertainty, and response uncertainty. Within the primary simulation code, the storms are sampled according to their probability masses, which were defined using the previously described JPM technique. CSTORM output for each storm is used as input to the response computation. For empirical runup and overtopping, the CSTORM response SWL, H_{m0}, T_p, and MWD is defined near the structure toe. These are the hydraulic inputs to the above empirical equations. The relation $T_{m-1,0} = T_p/1.1$ is adopted to determine the integral mean period. This assumes a single peaked wave spectral density function.

As discussed in Appendix F, the coefficients in the $R_{2\%}$ and q empirical equations are mean values and are assumed to be normally distributed, as recommended in EurOtop (2018). In simulations, the uncertainty in the equation can be included explicitly by sampling from a normal distribution using a random number generator. To ascertain whether or not this generates a reasonable representation of the uncertainty, the smooth levee runup data from the recent EurOtop II (2018) update were used. The 113 laboratory and full-scale data points included both uniform slopes and bermed slopes. The data are shown in Figure 50. In this case, the empirical equation best-mean-fit coefficient 1.65 was reduced to 1.5 to better fit the data and eliminate bias. This data set was resynthesized with randomized coefficients. A total of 10 sets of 113 points were synthesized. The result is shown in Figure 51. The mean and bias are similar to those of the base data set and the range of deviation from the mean is similar. Therefore, the stochastic simulation using empirical equations like Equation E.1 will produce a reasonable approximation of the mean, the variation, and the range.

As seen in Figure 46 and Figure 48, the without-project structure slopes are highly variable from reach to reach and are not uniform. During stochastic simulations, an average slope is computed at each time-step over the vertical distance of $\pm H_{m0}$ above and below the instantaneous SWL using a weighted average of the slope segments. This provides a reasonable approximation of the slope for the empirical equations. A slope uncertainty coefficient of variation of 10% has been used to account for

slope uncertainty; however, it was found that including this additional uncertainty had no measurable influence on the AEPs for runup or overtopping hazards.

Figure 50. Runup measurements on smooth slope vs. prediction using Equation E.1.
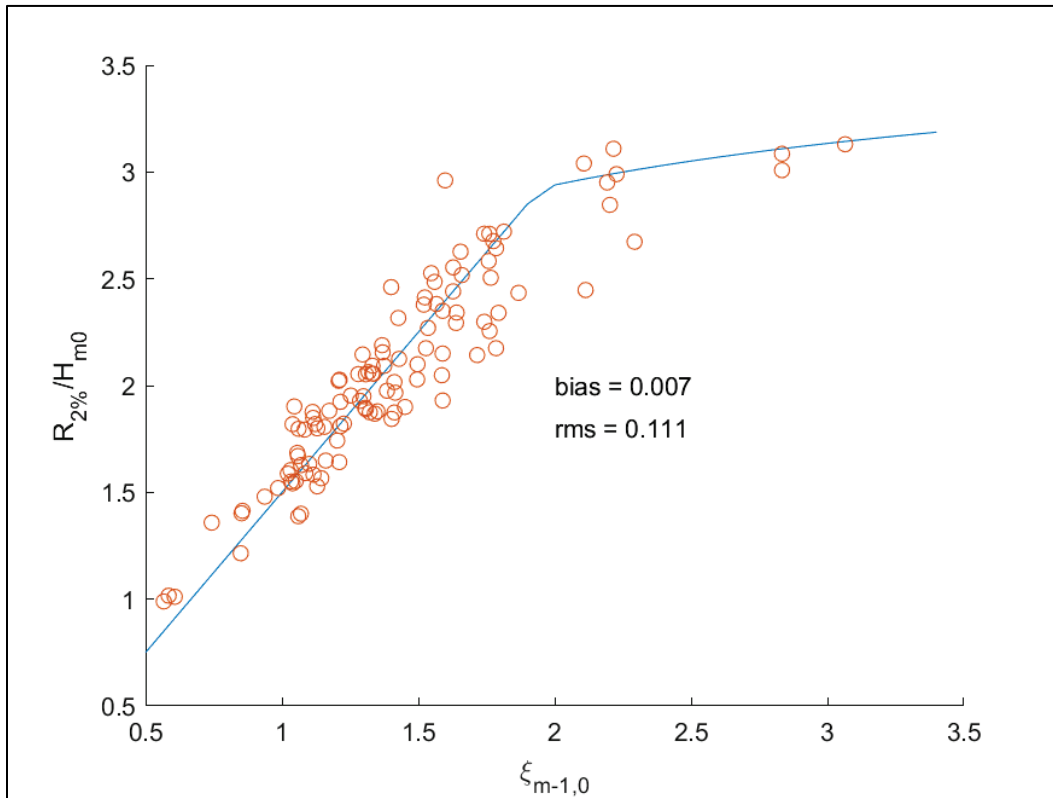
Figure 51. Synthesized runup data for smooth slope vs. prediction using Equation E.1.
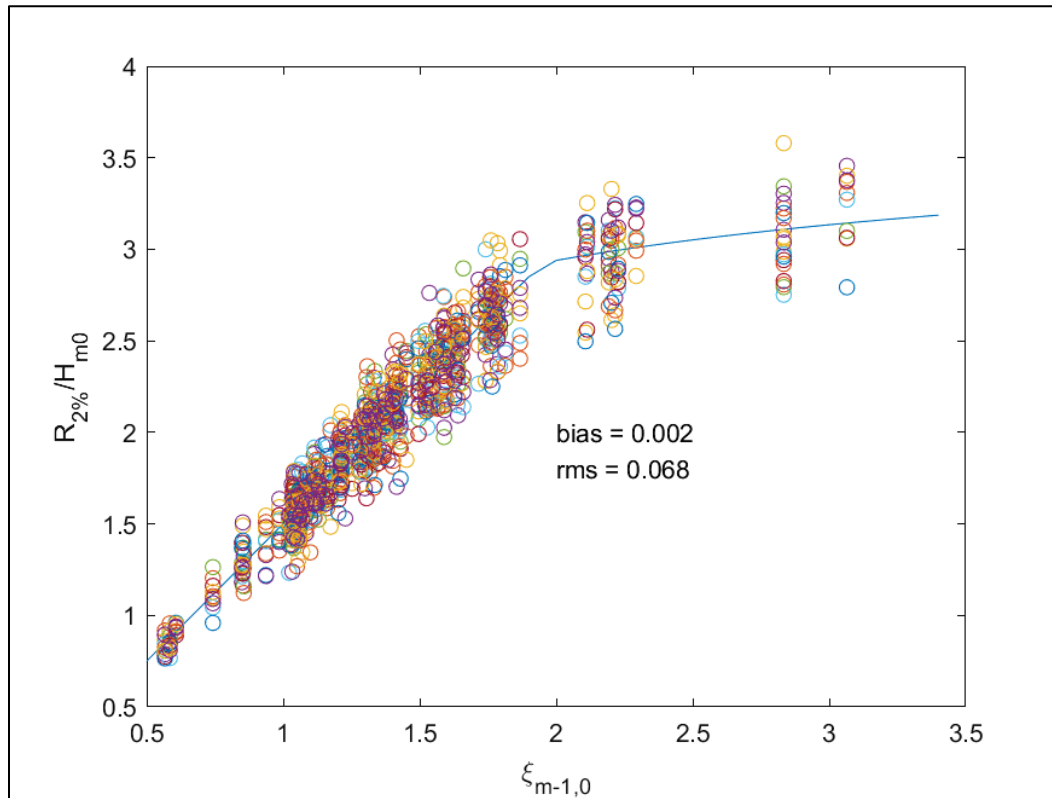
5.5 Limit states for overtopping design and resilience

The average wave overtopping rate q is between 0.01 and 0.1 cfs/ft for the start of damage to an earthen grass-covered levee (USACE 2008). There should be no damage for q less than 0.001 cfs/ft. In addition, q=0.001 cfs/ft is a start-of-damage criterion that should be appropriate for poorly constructed levees with little grass cover (e.g., sandy soils), q=0.01 cfs/ft is appropriate for most normal levees with consolidated clayey soils and good grass cover while the highest criteria q=0.1 cfs/ft should be reserved for levees with consolidated clay and thick grass covers. Note that 0.1 cf is just over 2 L while 0.01 cf is approximately 10 oz. Higher overtopping rates are allowed for levees with reinforced or armored surfaces. A task within the S2G project provided a review of overtopping limit states[1].

---

[1] Melby, J. A., S. Misra, A. Stehno, R. Thomas, A. Nelson, and B. Arcement. 2020 (unpublished). *Sabine Pass to Galveston Bay Pre-construction, Engineering and Design (PED) Project, State-of-Practice Review of Wave Overtopping and Steady Overflow Levee Erosion Guidance*. White Paper. US Army Engineer Research and Development Center, Vicksburg, MS.

Defining overtopping design criterion for floodwalls is empirical, and exact guidance does not exist. The CEM (USACE 2008) provides some general criterion, but there is considerable uncertainty due to a wide variation of potential structure configurations and quality of surrounding soil and ground cover. A wall on a grass levee would likely be designed for overtopping rates consistent with grass levees while a floodwall on a concrete wharf or quaywall would be designed for overtopping rates consistent with concrete armoring.

Damage here refers to the impact on surrounding soils near a floodwall due to overtopping. If the surrounding area is entirely concrete, the damage risk would be dramatically less than a wall on an earthen levee. Damage, in this sense, does not include settlement, damage to the wall, or geotechnical failure due to wall separation or levee slip circle failure. Herein, damage is defined only in relation to erosion of the leeside surrounding soil that supports the structure components. As such, levee and wall elevations defined in final design may need to be higher than the optimized elevations defined within this study to account for settlement.

For recent USACE projects referenced in this document, grass-covered clay levees are designed for the 1% AEP at the 50% and 90% CL: $q_{50\%} = 0.01$ cfs/ft and $q_{90\%} = 0.1$ cfs/ft, respectively. Similarly, floodwalls are designed for the 1% AEP at the 50% and 90% CL: $q_{50\%} = 0.03$ cfs/ft and $q_{90\%} = 0.1$ cfs/ft, respectively. These q limit states are used herein. This assumes that levees have, or will be reconstructed with, a compacted clay base, a relatively thin layer of topsoil and finally a good-quality grass armor layer, at a minimum. The turf roots should penetrate into the clay layer. Turf reinforcements and other more hardened armoring products are now common practice for levees that do not meet the above overtopping criterion or where added resilience is required.

The above limit states represent conservative start-of-damage overtopping limit states. Based on past physical testing related to USACE levees (e.g., Thornton 2010), it is likely that the levees can sustain higher levels of overtopping, but raising the limit states would require site-specific physical testing of the S2G levees. Hughes and Thornton (2015) discuss levee vulnerability, and a referenced quote from Hewlett et al. (1987) is useful: "The condition when soil is directly exposed to flowing water is classified as the onset of failure and is unacceptable." This suggests two vulnerabilities: one for the forcing (flow) and one for the quality of grass

cover. Without grass cover, duration of overflow is not particularly relevant because there is little resistance to erosion. With a good grass cover, the slope is likely to be able to sustain at least minor levels of overtopping for hours. The design level forcing for the S2G CSRM system consists mostly of small, short wind waves on an SWL that is close to the structure crest. When exposed to this forcing condition, it is likely that levees with even medium-quality soil and grass cover will remain undamaged. For the condition where the SWL exceeds the crest, the levees are vulnerable to breaching, particularly in locations where the grass cover is not optimal or the underlying soils are not high quality compacted clay. Because the design condition has little freeboard, there is a relatively small margin of safety between the design condition discussed above and significant vulnerability for breaching in areas with suboptimal levee conditions. This relatively small safety margin is exacerbated by the fact that the existing levee erosion resistance capacity is not explicitly known because there has been no physical testing of the levees. This further justifies the use of the conservative overtopping limit states. Levee design techniques based on excess work (e.g., Dean et al. [2010]), as summarized in Melby et al. (2020), would better incorporate storm duration and erosion estimates, but they require field testing data that were not available for this study. In addition, because of the small safety margin, it is likely that application of the excess work methods with known levee erosion resistance will yield only slightly lower levee elevations. Still, over the entire region, this could yield large savings and better estimates of risk, so it is recommended that the excess work methods be considered in design.

While the above limit states are accepted practice for design, they give little indication of how or under what conditions a levee will actually fail. Levee failure can proceed from minor erosion through to breaching quite rapidly if significant overtopping persists for hours. Figure 52 shows some examples of minor levee damage through to major head cutting. Full-scale tests of levees have become popular to discern this ultimate failure limit state. The HSDRRS and Morganza-to-Gulf projects conducted full-scale tests of failure of good quality grass cover layers (Thornton 2010). Based on these tests, USACE (2012, 2013) recommended to use 1 cfs/ft for the limit state for failure of non-federal levees and 2 cfs/ft for federal levees,

and the failure probability was set, somewhat arbitrarily, at 95%. USACE[1] has the following recommendation based on the HSDRRS full scale tests:

> The Levee Armoring Research Documentation Report (HSDRRS, USACE 2012) recommends that for average wave overtopping discharges up to 1.0 cfs/ft, unreinforced Bermuda grass may be appropriate provided a minimum of 2-year-old grass quality is attained. Definitions of grass quality are included in the report. For average overtopping discharges between 1.0 and 2.7 cfs/ft, Bermuda grass established from sod reinforced with a high performance turf reinforcement mat (HPTRM) may be adequate on the crown, down the landside slope, and 15 ft past the slope-to-berm transition, provided the grass is established from sod and follows a regimen of watering if rainfall is less than the minimum required, and required fertilizing during the growing season. Additional checks for landside armoring should consider the duration of overtopping, effects of vegetation, the presence of manmade structures, and the characteristics of the overtopping.

> Turf reinforced with high performance turf reinforcement mats (HPTRM) is required where the maximum time-averaged wave overtopping discharge is 4.0 cfs/ft. The HPTRM system is a combination of HPTRM, securing pins, cable anchors and a fully developed grass turf. The specifications for an HPTRM system, including overlap, roll size, securing pins, delivery storage and handling, installation requirements, trenching and anchoring requirements, and Bermuda grass sod specs and installation methods, can be found in HSDRRS (USACE 2012).

For S2G PED, a resiliency ultimate limit state of q=1 cfs/ft at 90% CL was used.

---

[1] *Evaluation,* Design, and Construction of Levees. EM 1110-2-1913. Post Grand Summit Draft. September 2017. Washington, DC: Department of the Army, US Army Corps of Engineers.

Figure 52. Levee erosion surrounding New Orleans area after Hurricane Katrina (from USACE 2009b).
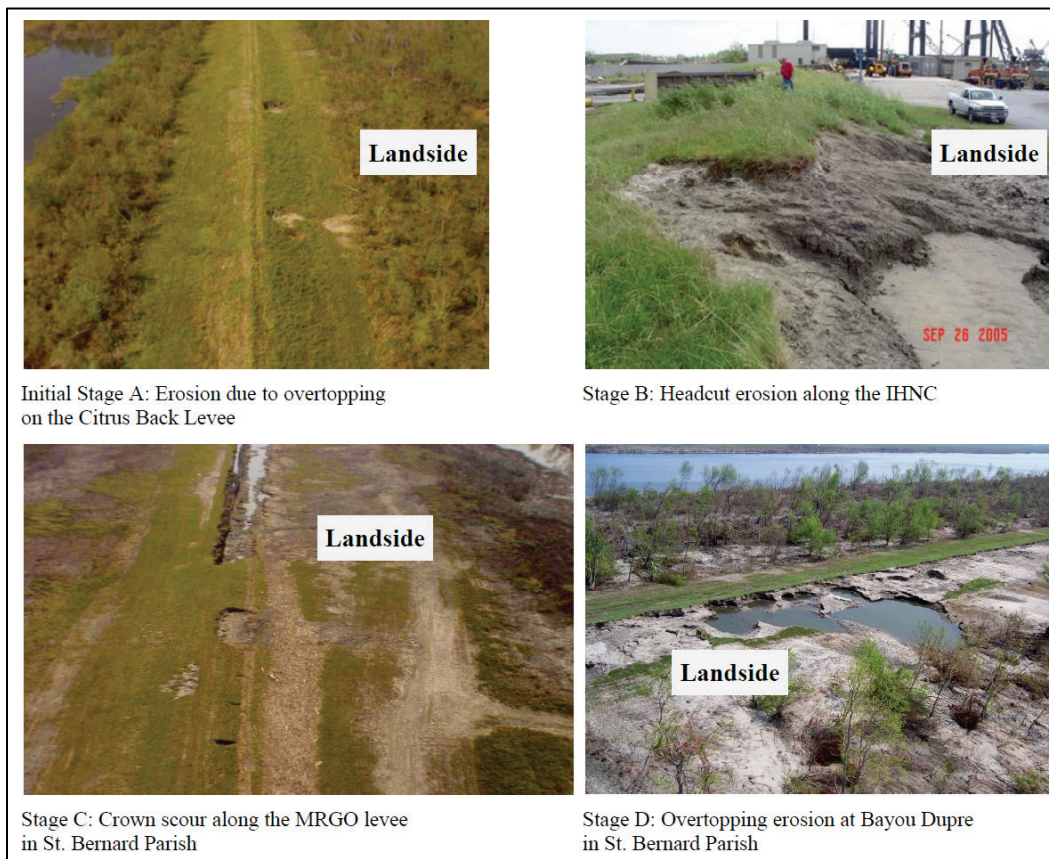
An additional risk-related parameter is overtopping volume. This is pertinent to the amount of flooding and consequences. The feasibility study investigated this in detail, so it is not presented here. Also, for the conservative limit states defined herein, there would be little overtopping accumulation in the lee as long as the levees and floodwalls were not breached or flanked during a storm. However, it will be useful to quantify overtopping volume for the worst-case SLC2 conditions related to survivability and adaptability. Cumulative overtopping volume can be estimated with the data presented herein.

5.6 Overtopping nappe geometry analysis

Computation of the overtopping nappe characteristics is required to design the splash pad on the leeside of the CSRM floodwalls to protect from scour. The nappe geometry is based on HSDRRS (USACE 2012) and the computation approach is described in Appendix F. At very low overtopping rates, the overtopping flow runs down the leeside of the wall. For higher flow rates, the nappe will separate from the wall and form a jet.

The transition from flow down the wall to jet is difficult to predict for time-varying flows and not an important criterion for wall and splash pad design. What is critical is to predict the maximum possible distance from the wall of the jet impact on the splash pad and the condition where jet produces the highest forces on the splash pad. The geometry of the nappe jet is shown in Figure 53 where x_C is the center of the jet impact and x_U and x_L are the jet impact bounds measured from the flood side of the seawall. For this analysis, the seaward edge of the crest is considered the crest of a sharp-edged weir. The average geometric width of the impinging jet normal to the flow streamlines is B_J. There is an expectation that a splash pad will exist or be constructed on the leeside of all floodwalls regardless of the characteristics of the overtopping flow for the overtopping limit state and that the splash pad will extend from the wall past the region of high flow rates from the impinging jet. This is required to prevent erosion that can occur for unarmored leeside areas even for low overtopping rates where the nappe does not separate from the wall. As occurred in New Orleans during Hurricane Katrina, the erosion resulting from overflow of a wall can be severe enough to cause leeside soil erosion and dramatically increase the risk of failure due to wall failure.

For with-project conditions, calculations were done for the angle of jet impact area, θ_c, the jet velocity parallel to the flow streamlines, V_J, and the total force exerted by the overtopping jet on the leeside impact area, F_J. The nappe geometry parameters are based on SWL and wave conditions, and these are calculated for a range of AEPs. The combination of overflow and wave overtopping creates a pulsating overtopping flow, and estimates of these parameters using the given equations tend to be biased low but are reasonable approximations.

Figure 53. Nappe geometry diagram.
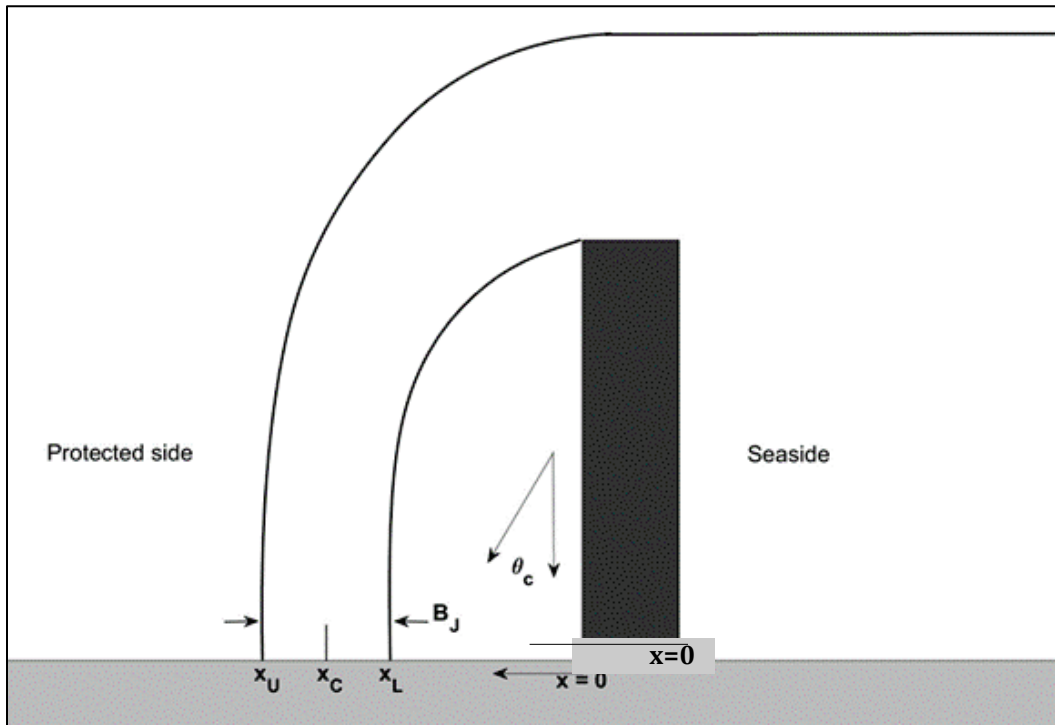
5.7 Floodwall fluid pressures

For with-project conditions, the hydrostatic and hydrodynamic pressures on the seaside face of the CSRM floodwall were computed with the equations of Goda (USACE 2008), which are described in Appendix F. Figure 54 shows the diagram of the pressures on the seaside of a floodwall. The pressure at the SWL is p_1, the pressure at the crest of the structure is p_2, and the pressure at the toe of the structure is p_3.

The pressures for each floodwall transect were computed at the three RSLC conditions. For conditions where SWL is greater than the crest elevation, only the p_2 and p_3 pressures are influencing the floodside of the wall; therefore, p_1 is not presented for these cases (Appendix F).

Figure 54. Goda pressure diagram for a floodwall.
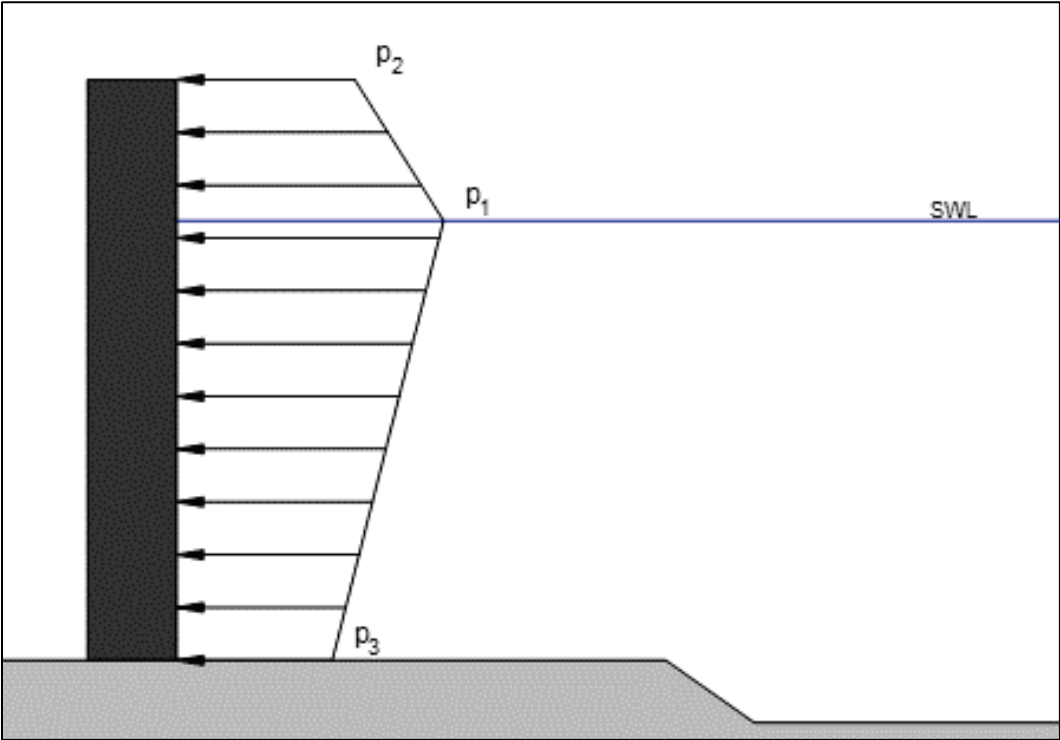
6   Stochastic Simulation of Response

6.1   Stochastic response simulation approach

Five different approaches for stochastic simulation of runup and overtopping response were evaluated for this study ranging from relatively simple event-based (EB) approaches where a single return interval *event* is specified (e.g., 100 yr ARI) to a complex response-based (RB) time-dependent method. Appendix G discusses the different stochastic simulation approaches and how they compare. The final method chosen was the following RB approach:

1. Previously discussed synthetic tropical storms are sampled based on their respective probability masses.
2. Peak SWL and H_{m0} associated with each storm and each SP are retrieved from storm input files.
3. Average T_p and MWD associated with the peak H_{m0} are computed.
4. Uncertainty is sampled from normal distributions and applied.
5. Structure slope, crest elevation (for without- and with-project) and roughness are retrieved from user input files.
6. Above inputs are used to compute runup, overtopping, pressure, and overtopping nappe using the empirical equations summarized in Appendix F for thousands of uncertainty samples.
7. Discrete JPM integral (Equation A.1, Appendix A) is solved numerically to compute SWL, H_{m0}, $R_{2\%}$, q pressure, and nappe geometry hazard curves.
8. SWL, H_{m0}, $R_{2\%}$, q, pressure distribution, and nappe geometry/force at various AEP values at 50% and 90% CL are reported.

In this approach, the uncertainties discussed earlier are applied for each storm by sampling normal distributions for each uncertainty component. The constants in the empirical equations for runup and overtopping are uncertain, and those uncertainties are also sampled from normal distributions for each storm.

The authorized elevations from the feasibility study and the actual structure slopes are used to determine the associated AEP runup $R_{2\%}$ and overtopping q at 50% and 90% CL. The optimized levee crest elevation that would meet overtopping criteria at 1% AEP was also determined for each transect. The design level of risk reduction of the CSRM components corresponds to the start of damage, or serviceability limit state, and is

characterized by the non-exceedance of the overtopping rate limit states at 50% and 90% CL. These values are q=0.01 cfs/ft at 50% CL (upper confidence limit) and q=0.1 cfs/ft at 90% CL for grass-covered earthen levees, and q=0.03 cfs/ft at 50% CL (upper confidence limit) and q=0.1 cfs/ft at 90% CL for floodwalls. In addition, a resiliency ultimate limit state of q=1 cfs/ft at 90% CL was also computed. Using RB analysis, it is possible that q at 90% CL is below the limit state, and the 1% SWL is above the structure crest because overtopping uncertainty is very large compared to SWL uncertainty. Therefore, an additional limit state was applied that assured that the 1% AEP SWL at 90% be at or below the crest elevation. These limit states have been used in prior Gulf of Mexico studies including USACE (2009b) and USACE (2012a). This specification of uncertainty is consistent with the requirements set forth in ER 1105-2-101 (USACE 2017b) that stipulate that stage-frequency relations be provided with associated assurance (conditional non-exceedance probability) and long-term exceedance probability (LTEP). For coastal engineering, stage-frequency is insufficient to describe forcing. Herein, the AEP relationships for both wave and water level parameters are provided. In addition, CLs are provided to characterize assurance, and LTEP is given below.

As noted in Appendix G, an EB approach maintains constant forcing (wave and water level) statistics across the CSRM system, but response statistics will vary. EB approaches produce variable reliability and therefore variable risk along the length of the structure. The RB simulation approach overcomes these limitations but usually requires more computational effort than EB approaches because thousands of storm simulations are required to achieve a statistically stable solution. Fortunately, as noted in Appendix G, the peaks-based RB approach yields an accurate approximation of the more complex time-dependent approaches and requires little additional computational effort than an EB approach that also samples uncertainty. Therefore, the RB peaks-based stochastic simulation was used within this study.

In addition, RB stochastic approaches often include less subjective judgment about the multivariate statistical relationships that may be contrary to physics. For example, EB techniques require selecting water level, wave height, wave period, wave direction, and storm duration corresponding to a specific statistic (e.g., AEP = 1%). This particular statistic is multivalued and has many possible permutations. That is, the 1% event may have a very high SWL and small wave, a moderately high

SWL and moderately large wave, a small wave with a long wavelength, or a large wave with a relatively short wavelength. Of course, there are infinite possibilities, and the entire 1% AEP hyper-surface must be analyzed to determine the worst-case 1% event. These parameters also interact nonlinearly in shallow water, and the statistical *event* may not reflect these physical processes. There is also no guarantee that the assumptions required in an EB approach are conservative. Wave overtopping is a function of wave height cubed, so any error in the joint probability model will be magnified in the response computation.

The primary wave-related limitation of the method used in S2G is its dependence on the STWAVE model output. Nonlinear wave propagation physics, such as wave diffraction and infragravity wave propagation, were not modeled. A simple analysis of nonlinear wave effects was conducted to determine the impact of not including these effects. A Boussinesq model (FUNWAVE) was developed for the area from Sabine Lake to the CSRM system along the SNWW. This area is the most exposed section of the Port Arthur and Orange County CSRM systems. The waves were shown to dissipate to the degree that only local wind waves were present at the structure. These local wind waves are modeled by STWAVE. Therefore, it was concluded that for Orange County and Port Arthur CSRM systems, no phase-resolving-type wave modeling was required. For Freeport, the CSRM system is much closer to the Gulf of Mexico, and infragravity waves can be important. A combined-STWAVE and Boussinesq modeling strategy is being employed along with the more traditional STWAVE-only approach there.

As an added conservatism, for this study the waves were considered normally incident, even in areas where they would likely be reduced by diffraction. In general, the wave heights were larger than would be expected for these enclosed and confined inland areas but were considered reasonably conservative. Most of the design waves for S2G were wind waves in the range of 1 to 3 ft. These waves are highly directional and could be from a variety of directions.

6.2   Runup and overtopping hazard

Runup and overtopping hazard results for each transect for the CSRM structures were analyzed. Runup+SWL was only provided for information and was not used for design. AEP plots and tables for each of the responses

were generated. The overtopping rates were compared to the no-damage limit states.

Examples of runup and overtopping results from the RB analysis are shown in Figure 55, Table 9, and Table 10 for a levee transect in the Port Arthur area.

Figure 55. Runup+SWL and q AEP for Transect 55b in the Port Arthur area. Upper row is SLC0, second row is SLC1, and bottom is SLC2.
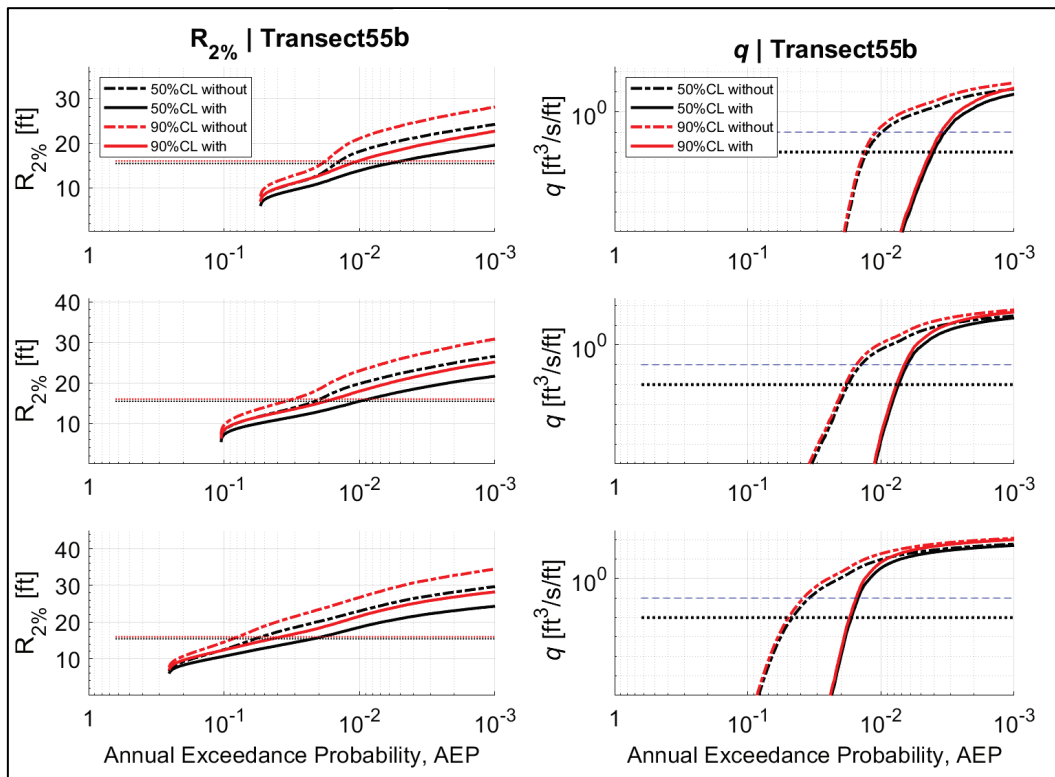
Table 9. $R_{2\%}$+SWL in ft, NAVD88, for a range of AEPs for transect 55b. Red values exceed the structure crest elevation. The without-project crest elevations are 14.5 ft, NAVD88, and the with-project design crest elevations are 16.0 ft, NAVD88. Transect 55b is associated with SP 1564.

Scenario	CL	Annual Exceedance Probability									
		0.2	0.1	0.05	0.02	0.01	0.005	0.003	0.002	0.0013	0.001
Without-Project SLC0	50%	0	0	8.6	12.9	18.1	20.5	21.6	22.7	23.7	24.2
Without-Project SLC0	90%	0	0	10.0	15.0	21.0	23.8	25.1	26.4	27.5	28.1
Without-Project SLC1	50%	0	8.2	12.1	15.9	19.8	22.3	23.6	25.0	26.0	26.6
Without-Project SLC1	90%	0	9.6	14.0	18.4	23.0	25.9	27.4	29.0	30.1	30.9
Without-Project SLC2	50%	9.2	12.5	16.3	20.1	23.0	25.7	27.0	28.2	29.0	29.6
Without-Project SLC2	90%	10.7	14.5	19.0	23.3	26.7	29.8	31.3	32.7	33.6	34.4
With-Project SLC0	50%	0	0	7.4	10.9	13.9	16.0	17.0	18.2	19.0	19.5
With-Project SLC0	90%	0	0	8.6	12.7	16.1	18.5	19.7	21.1	22.1	22.6
With-Project SLC1	50%	0	7.2	10.3	12.9	15.4	17.8	18.9	20.2	21.1	21.7
With-Project SLC1	90%	0	8.4	11.9	15.0	17.9	20.6	22.0	23.4	24.5	25.2
With-Project SLC2	50%	8.3	10.7	12.9	15.8	18.6	21.0	22.0	23.1	23.9	24.3
With-Project SLC2	90%	9.6	12.4	15.0	18.3	21.6	24.3	25.5	26.9	27.7	28.3

Table 10. q in cfs/ft for a range of AEPs for without-project scenario for transect 55b. Red values exceed q = 0.01 cfs/ft for 50% CL or 0.1 cfs/ft for 90% CL. Bold purple values exceed 1 cfs/ft. The without-project crest elevations are 14.5 ft, NAVD88, and the with-project design crest elevations are 16.0 ft, NAVD88. Transect 55b is associated with SP 1564.

Scenario	CL	Annual Exceedance Probability									
		0.2	0.1	0.05	0.02	0.01	0.005	0.003	0.002	0.0013	0.001
Without-Project SLC0	50%	0	0	0	0	0.087	1.0	2.8	7.1	11	14
Without-Project SLC0	90%	0	0	0	0	0.173	2.1	5.5	14	22	28
Without-Project SLC1	50%	0	0	0	0.0017	0.598	5.1	10	18	25	30
Without-Project SLC1	90%	0	0	0	0.0034	1.2	10	21	37	49	59
Without-Project SLC2	50%	0	0	0.005	1.1	10	24	34	45	53	59
Without-Project SLC2	90%	0	0	0.0096	2.1	19	49	67	90	107	118
With-Project SLC0	50%	0	0	0	0	0	0.0005	0.086	1.7	4.9	7.7
With-Project SLC0	90%	0	0	0	0	0	0.0009	0.171	3.3	9.8	15
With-Project SLC1	50%	0	0	0	0	0	0.848	4.7	12	18	23
With-Project SLC1	90%	0	0	0	0	0	1.7	9.3	24	37	46
With-Project SLC2	50%	0	0	0	0.0001	3.5	18	27	37	45	50
With-Project SLC2	90%	0	0	0	0.0002	6.9	35	53	74	90	100

6.3 Long-term exceedance probability (LTEP)

According to the requirements of ER 1105-2-101 (USACE 2017b), residual risk, which includes consequences of project performance or capacity exceedance, needs to be evaluated and reported for the system as a whole over the system's given lifecycle and for each component that makes up that system. In addition to AEP and associated CL, as an additional metric

to assess system performance, LTEP, is also provided. LTEP, also referred to as *Encounter Probability*, is a measure of system performance that establishes the likelihood of exceedance of a given AEP event at least once in the specified duration and is computed as $1 - (1 - AEP)N$, where $N =$ duration/number of years. The number of years, N, considered in this report includes 10, 20, 30, 50, and 100 yr. LTEP for various AEPs and durations/number of years are shown in Figure 56 and Table 11. As an example, the red arrows in Figure 56 show that the probability of an event with an AEP of 0.01 (i.e., a 100 yr event) being equaled or exceeded at least once in a duration of 50 yr is approximately 0.4. This example is also illustrated in Table 11.

Figure 56. Graphical depiction of LTEP and duration/number of years.
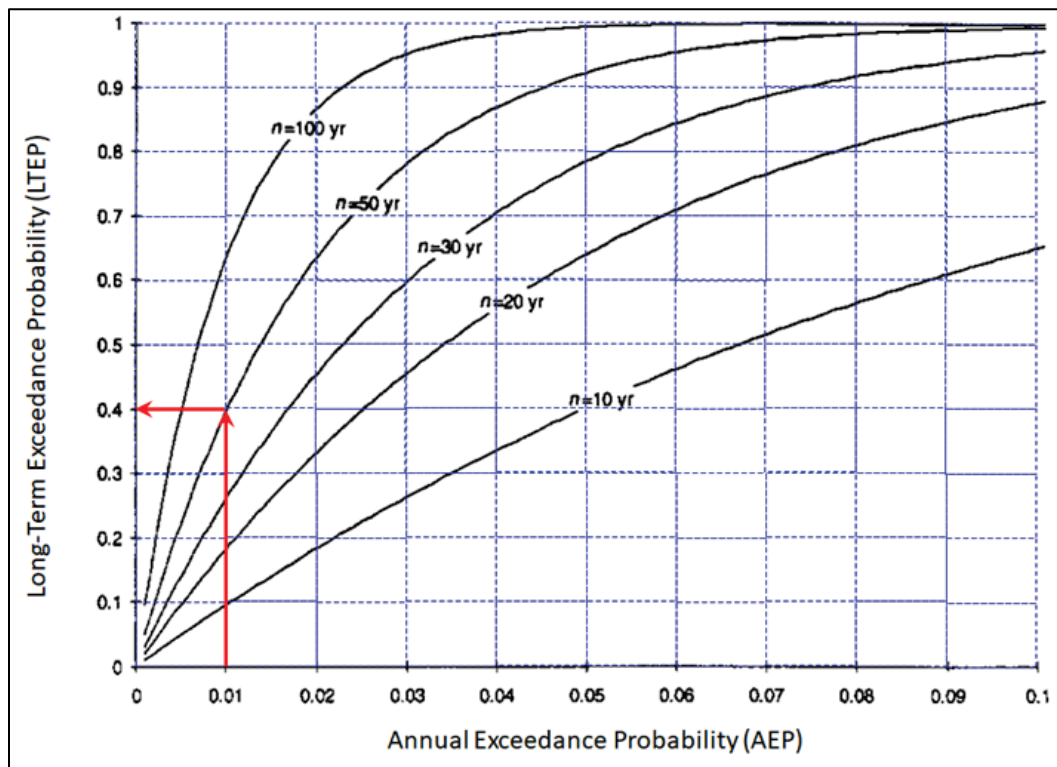
Table 11. Tabulated values of LTEP associated with AEP and duration/number of years.

Annual Exceedance Probability (AEP)	Duration/Number of Years (N)				
	10	20	30	50	100
0.5	1.00	1.00	1.00	1.00	1.00
0.2	0.89	0.99	1.00	1.00	1.00
0.1	0.65	0.88	0.96	0.99	1.00
0.05	0.40	0.64	0.79	0.92	0.99
0.02	0.18	0.33	0.45	0.64	0.87
0.01	0.10	0.18	0.26	**0.39**	0.63
0.005	0.05	0.10	0.14	0.22	0.39
0.002	0.02	0.04	0.06	0.10	0.18
0.001	0.01	0.02	0.03	0.05	0.10

6.4   Optimized crest elevations

An optimized levee and floodwall crest elevation was calculated to match the no-damage limit states. The StormSim RB stochastic simulation was run starting below the existing levee or floodwall elevation. The crest elevation was increased in increments of 0.5 ft until the overtopping rate was less than the no-damage limit states of q = 0.01 cfs/ft for levees and q = 0.03 cfs/ft for floodwalls at a 50% CL or q = 0.1 cfs/ft at 90% CL for both levees and floodwall. Only the with-project scenarios were run. The optimized crest elevation results are shown in Table 12 for Transect 55. These can be compared to the existing elevation of 14.5 ft, the authorized design elevation (at SLC1) of 16.0 ft, and authorized adaptability elevation (at SLC2) of 18.0 ft.

Table 12. Optimized levee crest elevations in feet, NAVD88, that
most nearly match the no-damage overtopping limit states.

Transect	Optimized levee crest elevations in ft, NAVD88		
	SLC0	SLC1	SLC2
55	13.5	15.0	18.0

6.5   CSRM system flanking

Flanking of the CSRM system was investigated by observing the modeled
1% AEP SWL in the neighborhood of the ends of the CSRM systems. In
most cases, this consisted of comparing the high ground elevation to the
SWL for various scenarios. In some cases, this included analyzing roadway
overpasses and canals that could be conduits for flooding beyond the ends
of the CSRM systems. ADCIRC nodal outputs were used for this
evaluation. Results were reported separately from this report.

7   Summary and Conclusions

The US Army Corps of Engineers Galveston District (SWG) is executing the Sabine Pass to Galveston Bay (S2G) Coastal Storm Risk Management (CSRM) project for Brazoria, Jefferson, and Orange Counties regions. The project is currently in the Pre-construction, Engineering, and Design (PED) phase. As identified during the *Final Integrated Feasibility Report – Environmental Impact Statement* (USACE 2017a), the S2G Project CSRM formulated measures consist of reducing the risks of tropical storm surge impacts by constructing the new Orange 3 CSRM system in Orange County and increasing the level of risk reduction and resiliency of the existing Port Arthur and Vicinity and Freeport and Vicinity Hurricane Flood Protection systems in Jefferson and Brazoria Counties, Texas.

As part of the ongoing PED phase of the project, this report documents the methodology for analyzing coastal storm surge and wave hazards for an analysis focused on evaluation of the entire CSRM systems for Jefferson, Brazoria, and Orange Counties. Coastal storm surge, wave loading, and wave and surge overtopping are quantified using state-of-the-art hydrodynamic modeling and stochastic simulations.

A joint probabilistic model of historical hurricane parameters was developed that spans the full range of tropical storm hazards from frequent, low-intensity storms to very rare, very intense storms. The probabilistic model describes the continuous spatial and temporal hazard. This probabilistic model was sampled efficiently to develop a suite of 195 synthetic tropical storms that effectively capture the flood hazard for the region from Freeport to the Louisiana-Texas border. Wind and pressure fields were developed for these storms using the Planetary Boundary Layer model.

The CSTORM coupled surge and wave modeling system was used to accurately quantify the surge and wave responses. New model meshes were developed from very-high-resolution land and sub-aqueous surveys for with- and without-project scenarios. With-project meshes include the new Orange County CSRM system, deepening of Sabine-Neches Waterway, and increased levee and floodwall elevations as authorized under the S2G feasibility study. The new meshes provide the highest-resolution regional surge and wave modeling done to date for the region. The CSTORM model was validated against historical storms and then used to model the 195

synthetic tropical storms. Of the 195 storms, 189 were modeled reliably for all scenarios, and these storms were used for all analyses. The storms were run on three relative sea level change (RSLC) scenarios for the with- and without-project meshes. These RSLC scenarios are referred to as SLC0 corresponding to project completion in 2027, SLC1 corresponding to the end of a 50 yr service lifecycle in 2077, and SLC2 corresponding to the end of a 100 yr service lifecycle in 2127. Nonlinear residual is shown to be significant in several areas, as much as 2 to 3 times the linear increment, further justifying the use of coupled surge and wave modeling.

The flood hazard exposure of the project features was quantified by computing hazard curves for the CSTORM output near the structures. Annual exceedance probabilities (AEP) were computed for the range of 1 to 0.0001 for peak storm water level (SWL) and wave height (H_{m0}) and reported in Microsoft Excel tables for AEP of 0.2 to 0.001. Wave period (T_p) and wave direction associated with peak H_{m0} were also reported. Both mean values and confidence limits were included.

Five different workflows for stochastic simulation of wave runup and overtopping of the levees were compared. These range from relatively simple EB approaches to complex time-dependent RB approaches. In the EB approaches, inputs to overtopping calculations are single AEP SWL and H_{m0} values (statistical *events*) with associated T_p and wave direction. For RB approaches, the run-up and overtopping responses are computed for each storm and then hazard relations are computed from the results. It was shown that a peaks-based RB approach yielded accurate stochastic responses, so this was used to compute the design. It was also shown that the less accurate EB approaches can yield accurate solutions but often yield answers that are highly inaccurate and unacceptable for design.

Limit states for overtopping of q = 0.01 cfs/ft for the 50% CL and q =0.1 cfs/ft for the 90% CL were based on the start of erosion for a good-quality grass cover on a clay levee. For floodwalls, based on the erodibility potential of leeside soils, limit states for overtopping of q = 0.03 cfs/ft for the 50% CL and q =0.1 cfs/ft for the 90% CL were used. An additional ultimate limit state of q=1 cfs/ft was evaluated to determine the vulnerability to severe damage including head cutting and potential breaching of levees, and floodwall failure due to erosion of leeside soils. These limit states are accepted standard of practice within the US Army Corps of Engineers and internationally. In addition to overtopping rate,

and optimized crest elevations associated with non-exceedance of the limit states, overtopping nappe geometry and combined hydrostatic and hydrodynamic fluid pressures on vertical floodwalls are also calculated and reported at various AEPs.

References

Becker, J. J., D. T. Sandwell, W. H. Smith, J. Braud, B. Binder, J. Depner, D. Fabre, J. Factor, S. Ingalls, S.-H. Kim, R. Ladner, K. Marks, S. Nelson, A. Pharaoh, R. Trimmer, J. Von Rosenberg, G. Wallace, and P. Weatherall. 2009. "Global Bathymetry and Elevation Data at 30 Arc Seconds Resolution: SRTM30_PLUS." *Marine Geodesy* 32(4): 355–371.

Bunya, S., J. Westerink, J. C. Dietrich, H. J. Westerink, L. G. Westerink, J. Atkinson, B. Ebersole, J. M. Smith, D. Resio, R. Jensen, M. A. Cialone, R. Luettich, C. Dawson, H. J. Roberts, and J. Ratcliff. 2010. "A High-Resolution Coupled Riverine Flow, Tide, Wind, Wind Wave and Storm Surge Model for Southern Louisiana and Mississippi: Part I-Model Development and Validation." *Monthly Weather Review* 138(2): 345–377.

Cialone, M. A., T. C. Massey, M. E. Anderson, A. S. Grzegorzewski, R. E. Jensen, A. Cialone, D. J. Mark, K. C. Pevey, B. L. Gunkel, and T. O. McAlpin. 2015. *North Atlantic Coast Comprehensive Study (NACCS) Coastal Storm Model Simulations: Waves and Water Levels*. ERDC/CHL TR-15-14. Vicksburg, MS: US Army Engineer Research and Development Center.

Dean, R. G., J. D. Rosati, T. L. Walton, and B. L. Edge. 2010. "Erosional Equivalences of Levees: Steady and Intermittent Wave Overtopping." *Ocean Engineering* 2010(37): 104–113.

Dietrich, J. C., S. Bunya, J. J. Westerink, B. A. Ebersole, J. M. Smith, J. H. Atkinson, R. Jensen, D. T. Resio, R. A. Luettich, C. Dawson, V. J. Cardone, A. T. Cox, M. D. Powell, H. J. Westerink, and H. J. Roberts. 2010. "A High-Resolution Coupled Riverine Flow, Tide, Wind, Wind Wave and Storm Surge Model for Southern Louisiana and Mississippi: Part II-Synoptic Description and Analysis of Hurricanes Katrina and Rita." *Monthly Weather Review* 138: 378–404.

Dietrich, J. C., J. J. Westerink, A. B. Kennedy, J. M. Smith, R. E. Jensen, M. Zijlema, L. H. Holthuijsen, C. Dawson, R. A. Luettich Jr, M. D. Powell, V. J. Cardone, A. T. Cox, G. W. Stone, H. Pourtaheri, M. E. Hope, S. Tanaka, L. G. Westerink, H. J. Westerink, and Z. Corbell. 2011. "Hurricane Gustav (2008) Waves and Storm Surge: Hindcast, Synoptic Analysis, and Validation in Southern Louisiana." *Monthly Weather Review* 139(8): 2488–2522.

EurOtop. 2018. *Wave Overtopping of Sea Defences and Related Structures: Assessment Manual*, August 2018. http://www.overtopping-manual.com

GLCC (Global Land Cover Data Base). 2017. https://prd-wret.s3.us-west-2.amazonaws.com/assets/palladium/production/s3fs-public/atoms/files/GlobalLandCoverCharacteristicsDataBaseReadmeVersion2.pdf

Gonzalez, V. M., N. C. Nadal-Caraballo, J. A. Melby, and M. A. Cialone. 2019. *Quantification of Uncertainty in Probabilistic Storm Surge Models: Literature Review*. ERDC/CHL SR-19-1. Vicksburg, MS: US Army Engineer Research and Development Center.

Hench, J. L., R. A. Luettich, Jr., J. J. Westerink, and N. W. Scheffner. 1995. *ADCIRC: An Advanced Three-Dimensional Circulation Model for Shelves, Coasts and Estuaries, Report 6: Development of a Tidal Constituent Data Base for the Eastern North Pacific*. DRP-92-6. Vicksburg, MS: US Army Corps of Engineers, Waterways Experiment Station.

Hewlett, H. W. M., L. A. Boorman, and M. E. Bramley. 1987. *Design of Reinforced Grass Waterways*. CIRIA Report 116. London, UK: Construction and Industry Research and Information Association.

Homer, C. G., J. A. Dewitz, L. Yang, S. Jin, P. Danielson, G. Xian, J. Coulston, N. D. Herold, J. D. Wickham, and K. Megown. 2015. "Completion of the 2011 National Land Cover Database for the Conterminous United States-Representing a Decade of Land Cover Change Information." *Photogrammetric Engineering and Remote Sensing* 81(5): 345–354.

Hope, M. E., J. J. Westerink, A. B. Kennedy, P. C. Kerr, J. C. Dietrich, C. Dawson, C. Bender, J. M. Smith, R. E. Jensen, M. Zijlema, L. H. Holthuijsen, R. A. Luettich, M. D. Powell, V. J. Cardone, A. T. Cox, H. Pourtaheri, H. J. Roberts, J. H. Atkinson, S. Tanaka, H. J. Westerink, and L. G. Westerink. 2013. "Hindcast and Validation of Hurricane Ike (2008) Waves, Forerunner, and Storm Surge." *Journal of Geophysical Research* 118(9): 4424–4460.

Hughes, S.A., and C. L. Thornton. 2015. "Tolerable Time-Varying Overflow on Grass-Covered Slopes." *Journal of Marine Science and Engineering* 2015(3): 128–145

Komen, G. J. L. Cavaleri, M. Donelan, K. Hasselmann, S. Hasselmann, and P. A. E. M. Janssen. 1994. *Dynamics and Modeling of Ocean Waves*. United Kingdom: Cambridge University Press.

Liu, Y., J. Li, J. Fasullo, D. L. Galloway (2020). Land Subsidence Contributions to Relative Sea Level Rise at Tide Gauge Galveston Pier 21, Texas, *Scientific Reports* 10(1) (2020): 1-11.

Melby, J. A. 2012. *Wave Runup Prediction for Flood Hazard Assessment*. ERDC/CHL TR-12-24. Vicksburg, MS: US Army Engineer Research and Development Center.

Melby, J. A., F. Diop, N. C. Nadal-Caraballo, D. Green, and V. M. Gonzalez. 2015. *Coastal Hazards System, Coastal Structures and Solutions to Coastal Disasters Joint Conference* (COPRI), 9–11 September 2015, Boston, MA, USA.

Melby, J. A., N. C. Nadal-Caraballo, V. M. Gonzalez. 2017. "Uncertainty in Coastal Structure Reliability." *Coasts, Marine Structures and Breakwaters 2017 Conference, ICE*, Liverpool, UK.

Nadal-Caraballo, N. C., J. A. Melby, V. M. Gonzalez, and A. T. Cox. 2015. *Coastal Storm Hazards from Virginia to Maine*. ERDC/CHL TR-15-5. Vicksburg, MS: US Army Engineer Research and Development Center.

Nadal-Caraballo, N. C., V. M. Gonzalez, and L. Chouinard. 2019. *Storm Recurrence Rate Models for Tropical Cyclones: Report 1 of a Series on the Quantification of Uncertainties in Probabilistic Storm Surge Models*. ERDC/CHL TR-19-4. Vicksburg, MS: US Army Engineer Research and Development Center.

NLCD (National Land Cover Database). 2016. National Land Cover Database 2016 (NLCD 2016). https://www.mrlc.gov/viewerjs/.

Powell, M. D., P. J. Vickery, and T. A. Reinhold. 2003. "Reduced Drag Coefficient for High Wind Speeds in Tropical Cyclones." *Nature* 422: 279–283.

Powell, M. D., S. Murillo, P. Dodge, E. Uhlhorn, J. Gamache, V. Cardone, A. Cox, S. Otero, N. Carrasco, B. Annane, and R. St. Fleur. 2010. "Reconstruction of Hurricane Katrina's Wind Fields for Storm Surge and Wave Hindcasting." *Ocean Engineering* 37(1): 26–36.

Taflanidis, A. A., J. Zhang, N. C. Nadal-Caraballo, and J. A. Melby. 2017. "Advances in Surrogate Modeling for Hurricane Risk Assessment: Storm Selection and Climate Change Impacts. *12th Int. Conf. on Structural Safety and Reliability*, TU-Verlag, 552–561. TU Wien, Vienna, Austria.

Thornton, C., B. N. Scholl, S. R. Abt. 2010. *Wave Overtopping Simulator Testing of Proposed Levee Armoring Materials*. Fort Collins, CO: Colorado State University.

USACE (US Army Corps of Engineers). 2006. *Louisiana Coastal Protection and Restoration (LACPR) Preliminary Technical Report*. New Orleans, LA: US Army Corps of Engineers District. https://www.mvn.usace.army.mil/Portals/56/docs/environmental/LaCPR/LACPRFinalTechnical ReportJune2009.pdf

_____. 2008. *Coastal Engineering Manual*. EM-1110-2-1100. Washington, DC: Department of the Army, US Army Corps of Engineers.

_____. 2009a. *Interagency Performance Evaluation Task Force (IPET). Performance Evaluation of the New Orleans and Southeast Louisiana Hurricane Protection System*. Final Report of the Interagency Performance Evaluation Task Force. Washington, DC: Department of the Army, US Army Corps of Engineers.

_____. 2009b. *Louisiana Coastal Protection and Restoration (LACPR) Final Technical Report*. New Orleans, LA: US Army Corps of Engineers District.

_____. 2010a. *Standards and Procedures for Referencing Project Elevation Grades to Nationwide Vertical Datums*. EC 1110-2-6056. Washington, DC: Department of the Army, US Army Corps of Engineers.

_____. 2010b. *USACE Process for the National Flood Insurance Program (NFIP) Levee System Evaluation*. EC 1110-2-6067. Washington, DC: Department of the Army, US Army Corps of Engineers.

_____. 2011. *Sabine-Neches Waterway Channel Improvement Project, Southeast Texas and Southwest Louisiana*. CEMP-SWD (1105-2-10-a). Galveston, TX: US Army Corps of Engineers District.

_____. 2012. *Hurricane and Storm Damage Reduction System Design Guidelines, New Orleans, LA*. US Army Corps of Engineers District.

_____. 2013. *Post Authorization Change Report Appendices, Morganza to the Gulf of Mexico, Louisiana*. New Orleans, LA: US Army Corps of Engineers District.

_____. 2017a. *Final Integrated Feasibility Report – Environmental Impact Statement. Galveston, TX*. US Army Corps of Engineers District. https://www.glo.texas.gov/coastal-grants/_documents/grant-project/1523-final-rpt-may-2017.pdf

_____. 2017b. *Risk Assessment for Flood Risk Management Studies*. ER-1105-2-101. July 17. Washington, DC: Department of the Army, US Army Corps of Engineers.

_____. 2018. *Freeport Harbor Channel Improvement Project, Brazoria County, Texas, Final Integrated General Reevaluation Report and Environmental Assessment*. CESWD-PDP, Galveston, TX: US Army Corps of Engineers District.

_____. 2019a. *Incorporating Sea Level Change in Civil Works Programs*. ER-1100-2-8162. Washington, DC: Department of the Army, US Army Corps of Engineers.

_____. 2019b. *Procedures to Evaluate Sea Level Change: Impacts, Responses, and Adaptation*. EP-1100-2-1. Washington, DC: Department of the Army, US Army Corps of Engineers.

References for Appendix F

EurOtop. 2018. EurOtop - Wave Overtopping of Sea Defences and Related Structures: Assessment Manual, August 2018. http://www.overtopping-manual.com/eurotop.pdf

Kobayashi, N., and B. K. Jacobs. 1985. "Stability of Armor Units on Composite Slopes." J. *Waterway, Port, Coastal, and Ocean Engineering* 111(5): 880–894.

Goda Y. 2010. *Random Seas and Design of Maritime Structures*, 3rd Edition. Hackensak, New Jersey: World Scientific.

Hughes, S. A., and N. C. Nadal. 2009. "Laboratory Study of Combined Wave Overtopping and Storm Surge Overflow of a Levee." *Journal of Coastal Engineering* 56 (2009), Elsevier.

Mase, H., T. Tamada, T. Yasuda, T. S. Hedges, and M. T. Reis. 2013. "Wave Runup and Overtopping at Seawalls Built on Land and in very Shallow Water." *Journal of Waterway, Port, Coastal, and Ocean Engi*neering 139(5): 346–357.

Melby, J. A. 2012. *Wave Runup Prediction for Flood Hazard Assessment*. ERDC CHL TR-12-24. Vicksbug, MS: US Army Engineer Research and Development Center.

References for Appendix G

Jacobsen, R. W., N. L. Dill, A. Herrin, and M. Beck. 2015. "Hurricane Surge Hazard Uncertainty in Coastal Flood Protection Design." *The J. of Dam Safety* 13(3): 21–38.

Melby, J. A., N. C. Nadal-Caraballo, V. M. Gonzalez. 2017. "Uncertainty in Coastal Structure Reliability." *Coasts, Marine Structures and Breakwaters 2017 Conference, ICE*, Liverpool, UK.

Nadal-Caraballo, N. C., J. A. Melby, V. M. Gonzalez, and A. T. Cox. 2015. *Coastal Storm Hazards from Virginia to Maine*. ERDC/CHL TR-15-5. Vicksburg, MS: US Army Engineer Research and Development Center.

Resio, D. T., S. J. Boc, L. Borgman, V. Cardone, A. T. Cox, W. R. Dally, R. G. Dean, D. Divoky, E. Hirsh, J. L. Irish, D. Levinson, A. Niedoroda, M. D. Powell, J. J. Ratcliff, V. Stutts, J. Suhada, G. R. Toro, and P. J. Vickery. 2007. *White Paper on Estimating Hurricane Inundation Probabilities*. Consulting Report prepared by USACE for FEMA. Vicksburg, MS: US Army Engineer Research and Development Center.

Resio, D. T., J. L. Irish, J. J. Westerink, and N. J. Powell. 2013. "The Effect of Uncertainty on Estimates of Hurricane Surge Hazards." *Natural Hazards* 66: 1443–1459.

Stehno, A. 2021. *Coastal Structure Overtopping and Overflow Stochastic Simulation Method Comparison*. M.S. thesis. Clinton, MS: Mississippi College.

Appendix A: White Paper on Prior Studies

Pre-Construction Engineering and Design Modeling of Coastal Hazards (Storm Surge and Waves) for *Sabine to Galveston* Hurricane Flood Protection System

November 26, 2018

Jeffrey Melby, Chris Massey, Norberto Nadal-Caraballo, Victor Gonzalez

US Army Engineer R&D Center, Vicksburg, MS
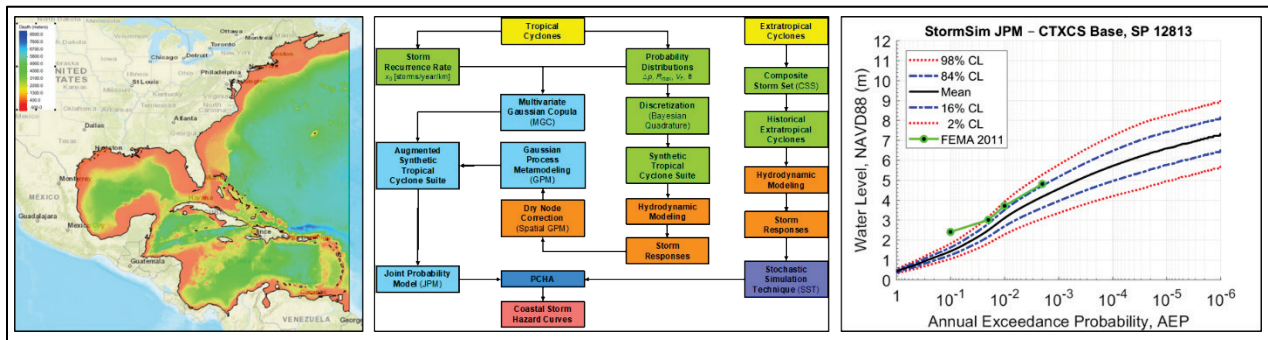
Executive Summary

This white paper presents a summary of recent coastal storm modeling supporting Sabine-to-Galveston coastal flooding analysis. The primary studies are the Federal Emergency Management Agency (FEMA) Region VI Risk Mapping, Analysis and Planning (Risk MAP) study using 2008 conditions (FEMA 2011); the US Army Corps of Engineers (USACE) feasibility study for flood risk management on the Sabine to Galveston portion of the Texas coast (S2G2015) (Melby et al. 2015); and the USACE Coastal Texas Protection and Restoration Feasibility Study (CTXCS) (Massey et al. 2018, Nadal-Caraballo et al. 2018).

Each of these studies took advantage of modern joint probability analysis of tropical storm parameters to develop a suite of tropical storms that adequately reflects the coastal storm hazard. Each study also used modern numerical hydrodynamic modeling of these storms to characterize the regional waves and water levels. However, each study did not fully characterize the hazard. The limitations or weaknesses related to the above modeling can be summarized as follows:

FEMA 2011

- Used separate technologies for Louisiana and Texas modeling creating a discontinuity in statistical response, such as 1% annual chance exceedance surge and wave height, near the LA-TX border
- Older uncoupled surge and wave modeling technologies
- Limited parameter sampling for JPM-OS resulting in poor parameter space resolution
- Limited response surface resulted in poor parameter space resolution in some cases
- Simple windowing approach with 333 km kernel size to determine alongshore spatial variation of storm probability. Estimated frequency of land-falling hurricanes at 1-deg of longitude increments starting at latitude 29.5 deg N which yielded inconsistent frequency distribution.
- Probability masses computed in a crude way, including errors in discretization, and not actual joint probability distribution using a correlation tree.
- Model uncertainty computed for known uncertainty (epsilon) terms but only half of the computed values were used. Uncertainty included in probability integration so result was a hazard curve near the 84% upper confidence limit (one standard deviation above the mean).

- High-fidelity modeling was not conducted in close proximity to hurricane flood protection systems (CSRM).
- Risk assessment of CSRM based primarily on 100 year average recurrence interval water level. Wave impacts, detailed wave analysis in the vicinity of CSRM, and multi-variate probability analysis of hazard was not done.
- Inland wave modeling produced intermittent output and lacked consistent quality to the point that it was not useful to define hazards over the entire flood protection system for engineering design.

S2G2015

This study mostly used FEMA 2011 modeling so the study suffered from some of the same problems as FEMA 2011. However storms where the primary influence was in the Sabine region near the TX-LA border were remodeled using updated surge and wave modeling software and consistent technologies from Louisiana to Texas. Risk assessment of CSRM was still based primarily on 100 year average recurrence interval water level. Wave impacts, detailed wave analysis in the vicinity of CSRM, and multi-variate probability analysis of hazard was limited.

CTXCS

The CTXCS modeling provided significant improvements in both the storm characterization through the JPM-OS and the regional storm surge and wave modeling. The related primary problems mentioned above were resolved in the CTXCS study. In particular, wave modeling is both continuous and of consistent quality throughout the region. The CTXCS modeling will provide a strong foundation for doing with-project regional modeling, detailed wave modeling in the vicinity of the CSRM, multi-variate probability analysis of the hazard, and accurate estimation of CSRM response and related flood risk.

Approach for Present S2G PED Study

The focus in this study is the Freeport, Port Arthur, and Orange County CSRMs. The approach for assessing the flood hazard will utilize the CTX base regional modeling for without-project waves and water levels. It is expected that a response-based approach will be used with the forcing for the hazard being defined by average annual exceedance values from a multivariate probability model. The multivariate response probability model will be conditioned on the JPM-OS storm probability model. Both aleatory and epistemic uncertainties will be included. Event-based modeling will be done with specific modeling components to validate response-based results. Some details of the approach are

being worked out in the first phase of the study but, in general, the expected study approach is as follows:

1. Sample CTX without-project CSTORM modeling corresponding to CSRM reaches (both storm-wise and from the multivariate statistical model.)
2. Refine CTX mesh/grids near CSRMs and include with-project alternatives.
3. Select subset of storms from original CTX modeling that influence statistical responses near CSRMs.
4. Compute with-project regional responses using CSTORM for subset of storms,
5. Construct multi-modal spectra from CTX modeling.
6. Construct Boussinesq near-structure two-dimensional models for CSRMs.
7. Compute response-based hazards (runup, overtopping, forces on walls, shear stresses on levees, etc.) using Boussinesq models and spectra from step 5. This will be done for specific statistical forcing conditions (e.g., 1% annual chance exceedance) and for specific extreme events. A surrogate of the Boussinesq model may be developed if time and funding allow. Empirical response models will be integrated where appropriate.
8. Compute simpler one-dimensional response near structure for both response-based and event-based approaches and compare to step 7 results. Goal is to develop simpler approach that provides adequate accuracy.
9. Sea level rise (SLR) will be incorporated by using the CTX simulations at 3 SLR levels. In this way, nonlinearities from the combination of SLR and surge will be included explicitly.
10. Compare computed hazards to limit states and compute reliability for different CL.
11. Iterate with variations of alternatives if required.

Introduction

The USACE is beginning Preconstruction, Engineering and Design (PED) of Hurricane Flood Protection Systems (CSRM) in the Sabine to Galveston, Texas (S2G) region. A number of flood risk studies have been completed for this region since Hurricane Ike in 2008. This whitepaper discusses modeling needs for the present PED of CSRM. Evaluation of the need focusses on prior flood risk studies conducted for the region since Hurricane Ike and their applicability to the present CSRM study. Three prior studies covered in the paper are the Federal Emergency Management Agency (FEMA) Region VI Risk Mapping, Analysis and Planning (Risk MAP) study using 2008 conditions (FEMA 2011); the US Army Corps of Engineers (USACE) feasibility study for flood risk management on the Sabine to Galveston portion of the Texas coast (S2G2015) (Melby et al. 2015); and the USACE Coastal Texas Protection and Restoration Feasibility Study (CTXCS) (Massey et al. 2018, Nadal-Caraballo et al. 2018). Other studies have been conducted for the region, but they either use the above study results for their base flood level or they use something similar. For example, various Galveston barrier studies conducted by Texas A&M-Galveston, Rice University (SSPEED Center), and Jackson State University-ERDC used specific storms for scenario analysis and to represent univariate return intervals.

Additional studies have been conducted by the various flood districts and FEMA (e.g., FEMA 2012a, Lynett 2018, Orange County 2012). Most of the above flood risk assessment studies were based on FEMA 2011 base flood elevations and some included updates to this analysis. Various regional flood risk studies also used specific univariate return interval event-based or scenario approaches primarily based on FEMA 2011 modeling (e.g., USACE SQRA, 2014). So the issues discussed herein are generally applicable to all flood risk studies conducted recently for the region.

While prior S2G region CSRM studies sought to understand flood risk, accurate quantification of risk and resilience was not possible for many reasons. First, most studies have used the FEMA 2011 modeling that has significant weaknesses when applied for engineering design purposes. The primary weaknesses are discussed in this whitepaper. Model uncertainty has not been fully quantified in prior studies. This includes climatology, flood hydrodynamic, and statistical numerical models as well as bathymetric and topographic data and hydrodynamic measurements. Our understanding of, and ability to model, coastal storm flood physics and storm probability combined with improvement of numerical technologies has advanced significantly in the last 15 years, leading to a reduction of uncertainty. However, perhaps more importantly, only in the last few years has

there been increased confidence that the complete range of uncertainty can be included in risk estimates.

Prior studies were founded in event-based analysis. Usually, event-based approaches are in the context of FEMA NFIP studies where a 1% annual chance exceedance (ACE) water level is defined. So the hazards are based on a 1% water level. These hazards include flood depths, wave and steady flow overtopping, hydraulic loads, scour, debris loading, and other responses. For coastal studies where wind and waves are important contributors to these hazards, infrastructure performance prediction for a range of hazards is required for understanding risk and resilience and an NFIP approach is far too simple to properly characterize risk. Hydraulic loads, overtopping, and erosion computation on CSRM structures require careful consideration of the nonlinear hydrodynamic physics and joint probability of wind, waves, and water levels. Event-based approaches often include computation of wave height from a wave height-water level joint probability model and sometimes include computation of wave period, wave direction, and storm duration but this joint probability model is complex. A single statistic, such as the 1% ACE response, is multi-valued for hazards derived from waves and water levels and selection of the worst case requires computation over the entire hyper-surface. While this is not infeasible, it is always challenging, and it is common to assume parameter independence or other simplifying assumptions that introduce unknown uncertainty. The focus for many coastal engineering studies is on numerical hydrodynamic models, but errors in computing statistics often overwhelm the numerical model accuracy, as will be discussed in this white paper. The Coastal Hazards System (Melby et al. 2015) (CHS) includes coastal storm climatological and hydrodynamic modeling simulations that span practical probability space. It also includes response statistics that are multi-variate, conditioned on the tropical storm parameters. These data can be leveraged for more accurate event-based design.

Recent advances in hurricane probabilistic modeling and computational capabilities have changed the flood risk paradigm. It is now practical to use response-based approaches to evaluate flood risk and resilience and include known significant uncertainties. Recent response-based approaches facilitate accurate risk and resilience assessment over the continuum of practical probability space. A wide variety of studies have been successfully implemented using response-based modeling including Gravens et al. (2007), Males and Melby (2012), Melby (2009), Melby et al. (2015a), USACE (2009a), and USACE (2012). The CHS was specifically designed to facilitate the above types of response-based simulations. The above references include discussion of USACE software systems

that can read CHS storm simulations and their relative probabilities and perform accurate flood risk computations. These software systems include Beach-fx, Generation II Coastal Risk Model (G2CRM), and StormSim. In addition, HEC-FIA is a response-based risk analysis software package that does similar analysis for inland flooding. This type of approach is a transformational development in flood risk evaluation and its application for S2G using the most recent modeling strategies will guarantee a significant improvement in flood risk understanding and improved actions in mitigating flood risk for the S2G region.

FEMA Region VI's Risk MAP Study

Comprehensive coastal storm modeling was completed for coastal Texas under FEMA Region VI Risk Mapping, Analysis and Planning (Risk MAP) study using storms and bathymetry and topography data available through 2008 (FEMA 2011). This study utilized what has become a standard approach for flood risk studies involving coastlines exposed to tropical cyclones. The study began with Joint Probability Method of Optimum Sampling (JPM-OS) methodology to characterize the probabilistic nature of coastal tropical storms and associated responses including storm wind and pressure fields, surge, and waves. The HURDAT2 database of historical tropical storm climatology was used to define a joint probability model of hurricane parameters. The particular approach utilized a response surface technique and included a fair amount of subjective analysis (FEMA 2011) and this model was sampled to yield a set of 446 synthetic tropical storms, 223 for Texas North and 223 for Texas South.

Characteristics of the JPM-OS approach for FEMA 2011:

- Storm tracks created at regular spacing.
- HURDAT2 database sample 1941 – 2005 landfalling storms. Parameters sampled were landfall location (latitude and longitude), central pressure (C_p), radius to maximum wind speed (R_{max}), translational speed (V_t), and heading direction (θ). As is typical, central pressure deficit $\Delta_p = 1013 - C_p$ was used instead of C_p to describe storm intensity. Joint probability distribution created using these parameters.
- "Optimal sampling" based on engineering judgment. JPM discretization and weights assigned based on expert judgement. Four storm intensities: 900, 930, 960 (high intensity) and 975 hPa (low intensity) resulting in poor parameter space resolution. The storm suite included 152 low frequency and 71 high frequency storms for TX North and TX South regions.
- Limited response surface (RS) that interpolated surge as a function of central pressure and radius of maximum winds, omitting impacts from

- other relevant parameters such as translational speed, heading direction, Holland B parameter.
- Initial storm suite on the order of 100-500 tropical cyclones. Increased central pressure and R_{max} parameter resolution through response surface.
- Simple windowing approach with 333 km kernel size to determine alongshore spatial variation of storm probability. Estimated frequency of landfalling hurricanes at 1-deg of longitude increments starting at latitude 29.5 deg N which yielded inconsistent frequency distribution.
- Probability masses computed in a crude way, including errors in discretization, and not actual joint probability distribution using a correlation tree.
- Model uncertainty computed for known uncertainty (epsilon) terms but only half of the computed values were used. Uncertainty included in probability integration so result was a hazard curve near the 84% upper confidence limit (one standard deviation above the mean). This is described below.

Wind and pressure fields for the 446 synthetic storms were created in collaboration between Ocean Weather Inc. (OWI) and ERDC using the Planetary Boundary Layer (PBL) TC96 Model. The model was driven with TROP files of hurricane parameters at 1 hour intervals. A single set of wind and pressure files was created for each storm that covered the Gulf of Mexico (GOM) domain. The GOM domain extended between longitudes -98.0 degrees west to -80.0 degrees west and from 18.0 degrees north to 31.0 degrees north latitude at 0.05 degree resolution. A 15.0-minute time step between fields for the wind and pressure files was used. The wind and pressure fields were used as forcing for both the wave and surge modeling. Five historical tropical events, Hurricane Carla 1961, Hurricane Allen 1980, Hurricane Bret 1999, Hurricane Rita 2005, and Hurricane Ike 2008 were modeled.

The FEMA study utilized Texas-specific modeling for most of the region but also took advantage of prior modeling that was done for the Louisiana FEMA Risk MAP study (USACE 2009a). Water levels and waves were computed using three different models: 1) the deep water Wave Model (WAM) model (Komen et al. 1994), used for producing offshore wave boundary conditions for use with 2) the nearshore Steady-state Wave (STWAVE) model (Smith et al. 2001, Massey et al. 2011), and 3) the Advanced Circulation (ADCIRC) model (ADCIRC 2017, Luettich et al. 1992, Kolar et al. 1994), which was used to simulate two-dimensional depth-averaged surge and circulation responses to the storm conditions. The computational domain for storm-surge modeling by ADCIRC contained the western North Atlantic, the Gulf of Mexico, and the Caribbean Sea. It covered an

approximately 38° by 38° square area in longitudinal (from 98° W to 60° W) and latitudinal (from 8.0° N to 46° N) directions. The mesh consisted of approximately 3.35 million computational nodes and 6.68 million unstructured triangular elements with an open ocean boundary specified along the eastern edge (60° W longitude). The largest elements were in the deep waters of the Atlantic Ocean and the Caribbean Sea (Figure A-1, Figure A-2), with element sizes of about 58 km as measured by the longest triangular edge length. The smallest elements resolved detailed geographic features such as tributaries and control structures like levees and roadways. The minimum element size was approximately 14 meters. Water depths ranged from almost 8,000 meters in the deep Atlantic to over 100 meters of land elevation (above mean sea level).

For wind and coastal hydrodynamic modeling by ADCIRC, land cover and land use (LCLU) data was used to determine spatially distributed values of bottom friction coefficients (or Manning's *n*), canopy coefficients, and surface roughness length for the effect of directional wind reduction, in response to spatial changes of land cover and land use over the study area. These values were set in ADCIRC's nodal attribute (fort.13) file.

Figure A-1. Map showing the ADCIRC model domain with topographic and bathymetric values represented as color contour plots.
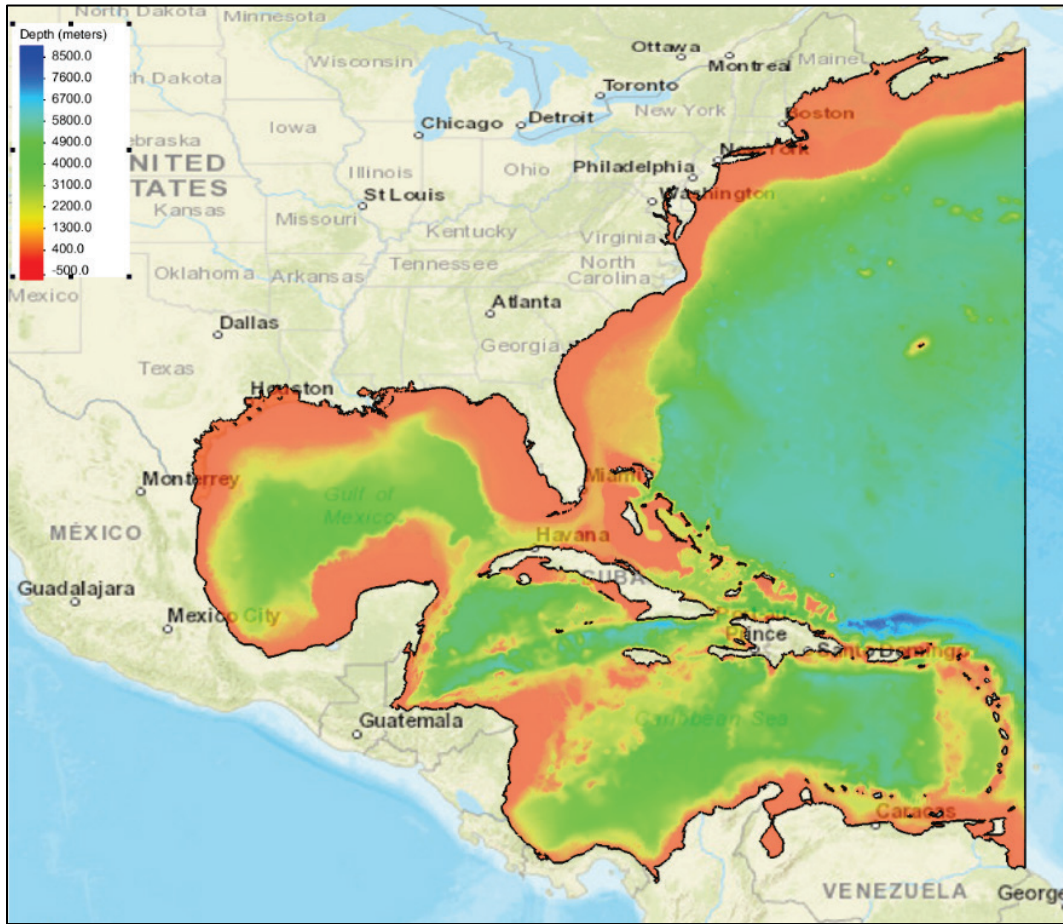
Figure A-2. Map showing a close-up view of the topographic/bathymetric values in the TX/LA area of the TX FEMA ADCIRC mesh.
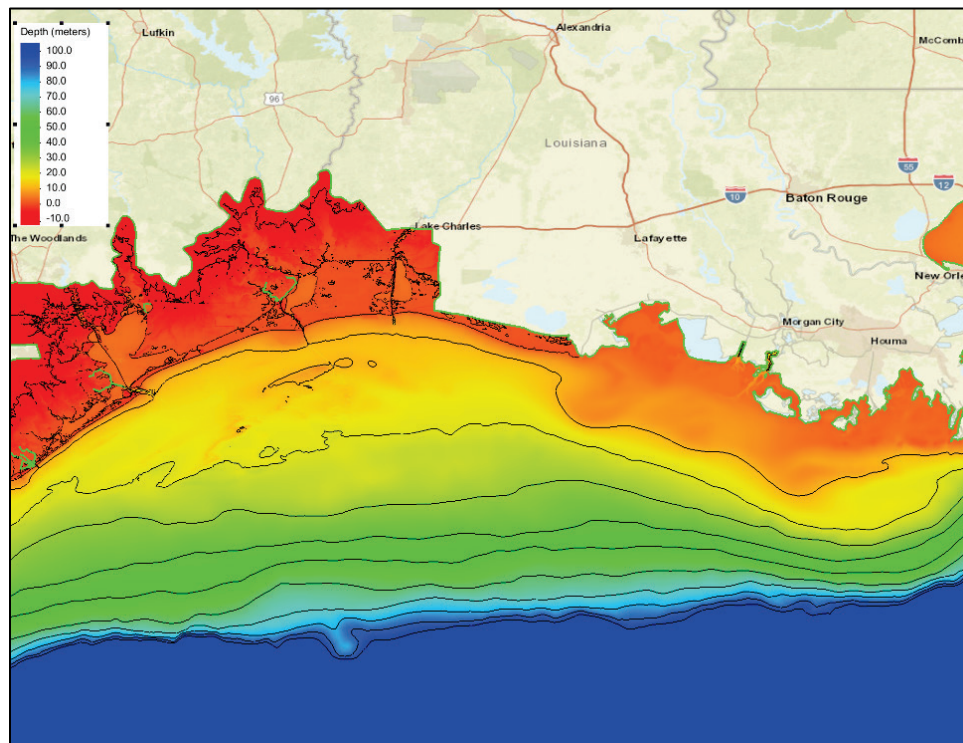
A single WAM grid was used and covered the Gulf of Mexico. Three regional-scale parent grid STWAVE domains covering the coast of Texas were used and were executed in half-plane mode, which is described later, along with two local-scale "child" grids nested within the parent grids. Each child grid used the same spatial resolution as the parent grid but was executed in full-plane mode. This parent-child nesting was required to both save computational time and to allow for full-plane computations in key areas. At the time of that study, STWAVE was not a parallelized code and thus could not solve large computational domains in full-plane mode due to time constraints and computer memory. The ADCIRC and STWAVE simulations were performed using loose coupling, which means that ADCIRC was run first without wave conditions in order to provide an initial water level to STWAVE. ADCIRC-only water levels and wind fields were then interpolated onto the STWAVE domain to be used as input conditions. The STWAVE parent and child grids were then run and the wave radiation stress gradients computed by STWAVE were interpolated onto the ADCIRC domain. Then ADCIRC was run a second time, including wave stress gradient forcing fields computed by STWAVE. STWAVE model runs were two days in duration and wave conditions were computed every 30 minutes. The STWAVE model was typically started approximately one day prior to landfall of the storm and lasted for one (1) day

post landfall. This was standard practice at the time and was done regardless of the size or forward speed of the storm.

Figure A-3. Map showing the wave model domains (WAM) and STWAVE used for the TXFEMA study.
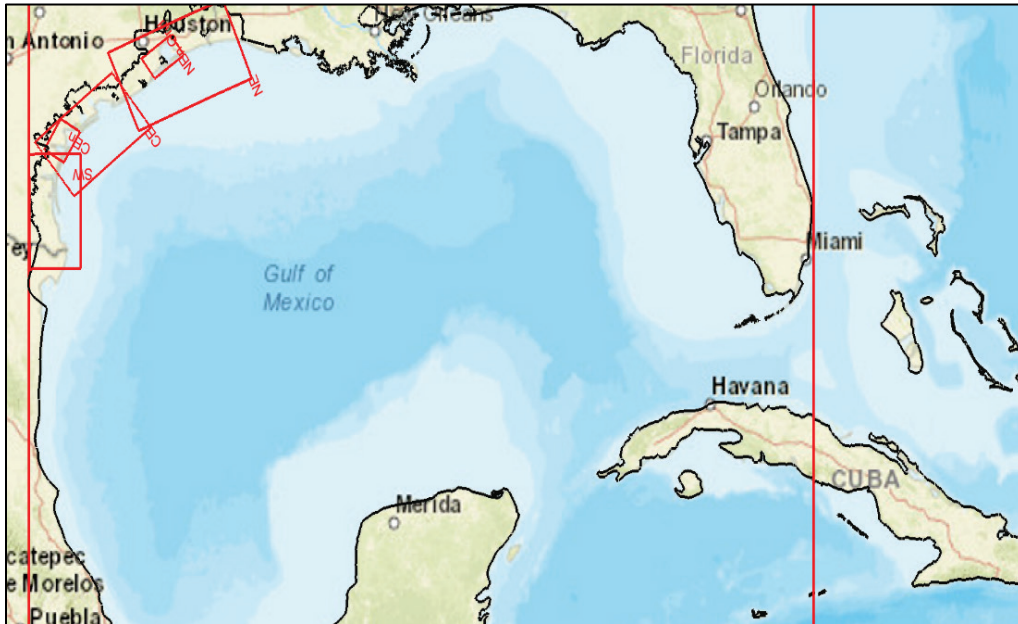
Figure A-4. FEMA study modeling flowchart (FEMA 2011).
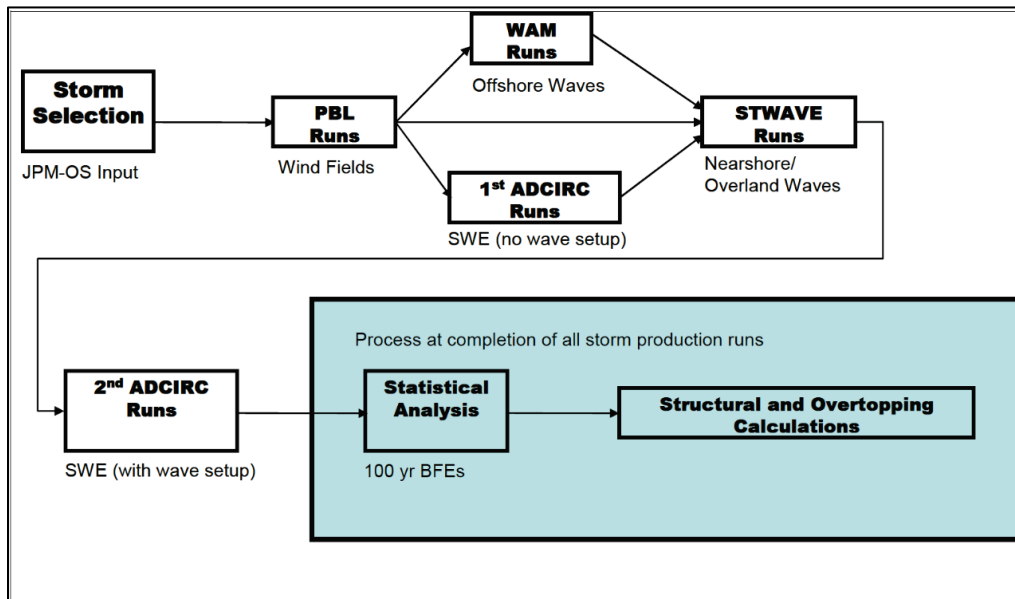
The FEMA Risk MAP Region VI study adopted a set of storms from the Louisiana Risk MAP study known as LA West storms. The modeling and statistics for the LA West region were completed separately from those of Texas and as a result there is a discontinuity in the results that occurs at the TX/LA state lines. Investigations

have revealed that the biggest cause of the discontinuity is the different treatment of the wind drag coefficient in ADCIRC between the two studies, resulting in surge differences of 2 to 5 feet. The Garratt wind drag formula was used in the FEMA Texas study with a cap value of 0.002, instead of ADCIRC's default value of 0.0035 which was used in the LA West study. While this lower cap value was used to validate the ADCIRC setup for Hurricane Ike and a few other Texas storms as part of the FEMA study, it is inconsistent with the values used in the Louisiana IPET (IPET 2009) and other FEMA Risk Map studies as well as what was used in the NACCS (Cialone et al 2015).

The annual exceedance probability (AEP) of coastal storm hazards at a given site is a function of three main components: the recurrence rate of storms, the joint probability of characteristic storm parameters, and the individual storm responses. The joint probability of coastal storm hazards can be summarized by means of the JPM integral:

$$\lambda_{r(\hat{x})>r} = \lambda \int P[r(\hat{x}) + \varepsilon > r|\hat{x}, \varepsilon] \, f_{\hat{x}}(\hat{x}) f_\varepsilon(\varepsilon) d\hat{x} d\varepsilon$$

$$\approx \sum_i^n \lambda_i \, P[r(\hat{x}) + \varepsilon > r|\hat{x}, \varepsilon] \tag{A.1}$$

where $\lambda_{r(\hat{x})>r}$ = AEP of storm response r due to forcing vector $\hat{x}$; ε =unbiased error or epsilon term; $P[r(\hat{x}) + \varepsilon > r|\hat{x}, \varepsilon]$ = conditional probability that storm i with parameters $\hat{x}$ generates a response larger than r. The primary storm parameters commonly accounted for in the forcing vector $\hat{x}$ are: distance to reference location (x_0); central pressure deficit (Δp); radius of maximum winds (R_{max}), translation speed (V_f); and heading direction (θ). Secondary parameters may include: Holland B; and astronomical tide. As is typical, a discrete version of Equation A.1 was employed and a response surface was utilized to achieve a finer computational resolution. In Equation 1, for FEMA studies, it is common practice to include the epistemic uncertainty in the integral so that the AEP is defined at the upper 84% confidence limit. However, in the USACE, this practice has changed to externalize the epistemic uncertainty so that the level of uncertainty can be defined explicitly (Nadal-Caraballo et al. 2015). Epistemic uncertainty arising from modeling inaccuracy was incorporated into the joint probability model. The four uncertainty terms considered were

ε_1: deviation between a storm at a random tide phase and a zero tide level;

ε_2: deviation created by variation of the Holland B parameter;

ε_3: deviation created by variations in tracks approaching the coast; and

ε_4: deviation created primarily by errors in models and grids.

The uncertainties were generally considered independent except ε_4 which was considered to vary linearly with surge.

One of the primary issues that has plagued the reuse of the FEMA 2011 modeling is the inconsistent quality of wave modeling results. Many of the simulated storms had missing wave data. Additionally, it was common for there to be two neighboring points with essentially identical characteristics but very different wave data. These issues occurred in open water and on normally-dry land that was flooded. However, the problems were much more common in interior areas. The reasons for the poor wave data quality is unknown but CTXCS modeling described below did not have these problems.

USACE Sabine to Galveston Feasibility Study (S2G2015)

The following comments apply for both the S2G2015 study and the FEMA Region VI reanalysis for Orange County which were both done by ERDC using the data described below. For the S2G2015 Study, the storm suites, numerical hydrodynamic and statistical models were all updated.

New modeling was conducted for storms that impacted the Sabine region where there was a discontinuity between the Texas and Louisiana modeling as discussed above. The 223 FEMA 2011 TX North storms were used as a basis for the hazard for both Brazoria and Orange Counties. Thirty TX North storms were selected from the original 223 that produced significant flooding in the area of the Orange County CSRM. These storms were remodeled using the Coastal Storm Modeling System (CSTORM-MS) (Massey et al 2011) coupled ADCIRC and STWAVE for both without- and with-project conditions. Additionally, 31 LA West storms were selected that impacted the Sabine region and these were remodeled with CSTORM-MS. Then hazard statistics were computed using the 193 original FEMA-modeled storms, 30 S2G-modeled TX North storms, and 31 S2G-modeled LA West storms for without- and with-project conditions.

The existing ADCIRC and STWAVE setups that were used in the FEMA Risk MAP (FEMA_TX) study were adopted as a starting point, however, modifications to the model input control files were necessary in order to use the newer model source codes, which included the parallel version of STWAVE V6.0 as well as a newer version of ADCIRC's source code, version 50. A further change was that the

coupling framework of the Coastal Storm Modeling System was used to perform dynamic two-way model coupling between ADCIRC and STWAVE, instead of the older and more computationally expensive loose file coupling. Since the updated version of STWAVE was now parallelized, nested child domains were not required. Recall they had the same resolution as the parent grids but were much smaller in domain size and used full-plane physics. With the parallelized version of STWAVE, it was possible to use the full-plane version of STWAVE for the full parent grids. For each of the models, the bathymetry and topographic values were left unchanged from the FEMA_TX study.

The ADCIRC mesh was modified to reflect the required increased resolution around the structures. With-project and without-project meshes/grids were constructed with identical resolutions so alternatives could be compared to the no-project base case. The ADCIRC mesh resolution was increased near the structure and the bathymetry/topography elevations in the original ADCIRC mesh from the FEMA_TX study were linearly interpolated onto the new meshes. In addition, the ADCIRC FEMA_TX nodal attribute values, such as Manning's n values for friction, were also interpolated onto the two new meshes and used without alteration. All the with-project conditions existed within one STWAVE domain, the Texas NE grid. The with-project condition was added to the NE grid by updating the depth file to include the height of the flood wall structures that were a part of the with-project conditions.

Model stability issues were encountered while trying to reproduce the FEMA 2011 ADCIRC model validation results even with no mesh updates. While the ADCIRC model domain was highly resolved, there were issues with some structure features being insufficiently resolved, such as dune systems and jetties, which caused model run time instabilities for ADCIRC. To overcome some of those instabilities, in the FEMA 2011 study, an early form of solution slope limiting was used internally within ADCIRC for some (but not all) of the storms. The exact settings and triggering mechanism for using slope limiting were not able to be recovered for future use so model validations were not reproducible. Another stability issue was that a model setting in ADCIRC that controls the lower limit of bottom friction drag coefficients was set to zero. Setting this limit to zero is physically unrealistic and leads to a major source of model run time instabilities. This setting was employed in order to capture the Hurricane Ike forerunner. By comparison, a more reasonable value of 0.003 was used in the MSCIP study (USACE 2009b), in the Louisiana IPET studies (IPET 2009), and the NACCS study (Cialone et al. 2015). When this latter value is used for Hurricane Ike simulations, the water levels associated with the forerunner do not develop as high as

recorded data and are not as high as when the zero value is used. However, when the 0.003 value is used, no slope limiting is required as the ADCIRC model remains stable. As part of another smaller study done for the same area, a value of 0.00026 was used as the lower limit. This value for the bottom friction coefficient (which depends on both water depth and Manning's n values) is consistent with lower limit values found in surge and tide studies of regions that are characterized by fine grain sediment bottoms. While its use improved the model results for storm surge levels for Hurricane Ike, its use requires that slope limiting be applied due to increased instances of model instabilities. As a compromise between model stability and better resolution of the Ike forerunner, a value of 0.003 was used for the S2G2015 study and did not require the use of slope limiting.

The 254 synthetic storms in the S2G2015 study were remapped onto a new joint probability model. The model was built with the approach shown in Figure A-5 and discussed below.

Characteristics of the JPM-OS approach for S2G2015:

- Storm tracks created at regular spacing.
- HURDAT2 database sample 1940 – 2013 landfalling and bypassing storms. Parameters sampled were landfall location (latitude and longitude), Δ_p, R_{max}, V_t, and θ. Joint probability distribution created using these parameters.
- "Optimal sampling" based on hybrid approach using Bayesian Quadrature combined with structured discretization. Storm Recurrence Rates (SRR) were computed using Gaussian Kernel Function weighting. Weights for computing probability masses assigned to storms using Bayesian Quadrature resulting in a significant improvement in accuracy of the probability masses. All storm recurrence statistics computed at 200 locations along coast.
- Gaussian Kernel Function (GKF) with an optimized kernel size of 200 km was used to define SRR.
- No response surface was computed.
- Improved estimates of uncertainty (epsilon) terms and these were used to compute various confidence limits around mean rather than being included in hazard curve.
- The probability masses were computed in a more accurate way to better represent response hazard curves. The higher accuracy in the statistical approach resulted in over 1 m error correction over much of the coast.

S2G2015 wave simulations suffered from similar problems that plagued FEMA 2011 in that the inland wave modeling produced intermittent output and lacked consistent quality.

Figure A-5. Typical joint probability approach employed by FEMA and USACE (NACCS).
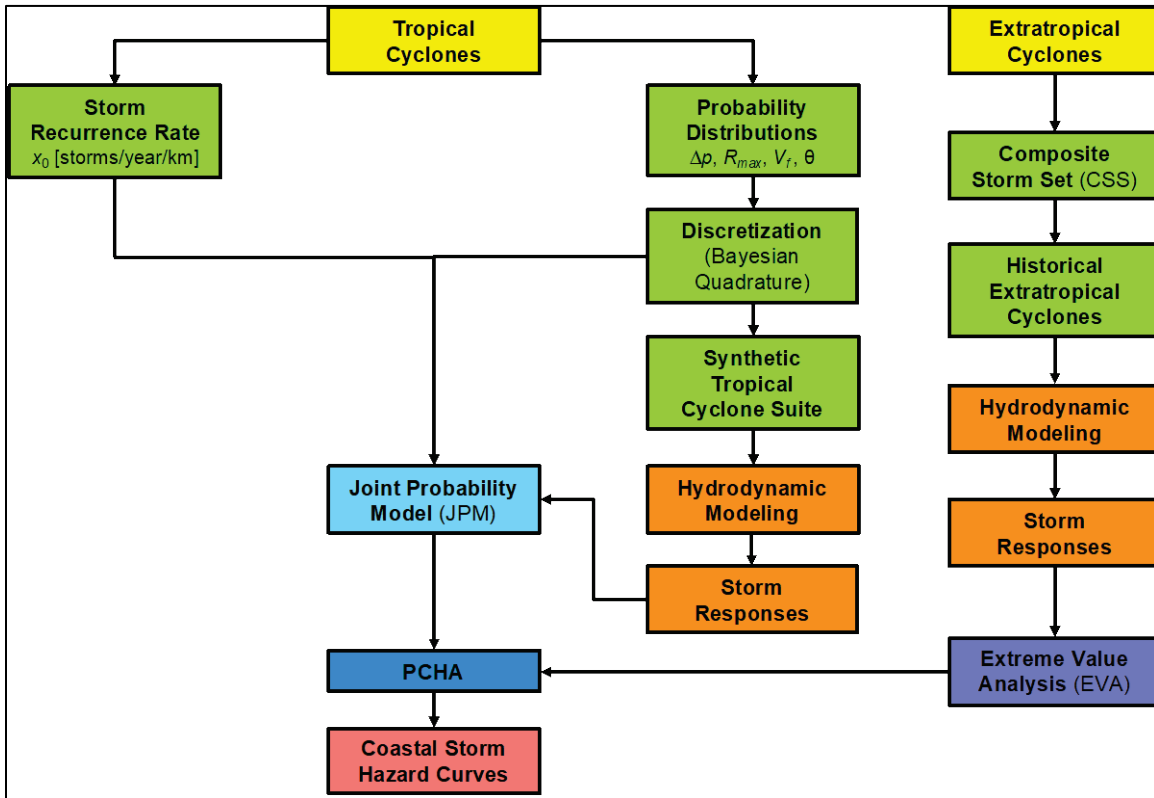
USACE Coastal Texas Protection and Restoration Feasibility Study (CTXCS)

The 2018 CTXCS modeling study was designed to correct the primary deficiencies identified in preceding sections and apply these corrections over the entire TX coastline. The primary improvements included:

- Improved storm climatology physics and modeling technology
- Improved numerical model physics and modeling technology including fully coupled surge, circulation, and wave models and full plane wave model
- Improved bathymetry, topography, land use, ground cover data
- Increased overall resolution of all numerical models
- Used three wind/pressure domains to increase the extents of data and increased resolution
- Span state margins so there are no spatial discontinuities
- Increased model resolution near HPFS's
- Much broader range of validity tests
- Longer duration of hurricane data
- Improved statistical modeling technology
- Increased resolution of storm probability space
- Improved understanding of both aleatory and epistemic uncertainties
- More consistent modeling across entire probability space
- Model reproducibility
- Incorporation of surrogate meta-modeling technology.

The above improvements combine to improve modeling accuracy and reproducibility and allow much more accurate estimation of risk. The surrogate models promote accurate modeling of the continuous storm probability space, which is a new and powerful capability. Further, the CTXCS modeling facilitates improvements in both response-based and event-based risk assessment as a result of the improvements listed above.

The ADCIRC and STWAVE model settings were selected in order to balance model accuracy and stability, while at the same time maintaining consistency with other studies in terms of physical processes. As such, a significant portion of the original ADCIRC mesh from the FEMA_TX Risk MAP study was used without alterations in the nearshore and inland areas. It was necessary to apply localized alterations to the mesh where under-resolved features caused model instabilities. Inland inundation extents were added to the mesh along the entire Louisiana, Mississippi, and Alabama coastlines in order to improve accuracy along the TX-LA

border and to accommodate storm tracks that intersected with that portion of the coast. The STWAVE and WAM grid extents are shown in Figure A-6. A fourth STWAVE grid was added to cover the Texas/LA coast. The Texas NE STWAVE grid was also recreated in order to change grid cell spacing from 200 meters to 150 meters. This allowed for better representation of with-project features and more accuracy.

Consistent ADCIRC model settings and parameters were selected and validated for using wind drag coefficient caps and the lower limit of bottom drag friction coefficients. Specifically, a lower limit coefficient of 0.002 was used for bottom friction and a Garratt wind drag coefficient cap of 0.003 was also used. It was necessary for solution slope limiting to be applied for some of the most intense storm simulations. In those cases, the exact locations, values and procedures for applying it have been documented.

By recording all model changes and using the modern Coastal Storm Modeling System, reproducibility of model results is now certain. Model reproducibility is vitally important for accuracy and quality control, as well as for the current needs of comparing with- and without-project conditions. More details of the changes to the ADCIRC and STWAVE model setup are provided later.

A completely new set of synthetic storm conditions were created for the CTXCS study. In addition, ten historical tropical storms impacting the TX/LA area were selected for model validation and testing. The ten storms are hurricanes Audrey 1957, Carla 1961, Beulah 1967, Allen 1980, Bret 1999, Katrina 2005, Rita 2005, Gustav 2008, Ike 2008 and Isaac 2012. Three sets of wind and pressure fields were created for each of the storms, a Western North Atlantic (WNAT) domain, a Gulf of Mexico domain and a LandFall domain that was allowed to move from one storm track to another. The WNAT domain extended between 99.0 degrees west and 55.0 degrees west longitude and from 5.0 degrees north to 35.0 degrees north at 0.20 degree grid spacing. The GOM mesh extended between 98.0 degrees west to 80.0 degrees west longitude and from 18.0 degrees north to 30.96 degrees north latitude at 0.08 degree grid spacing. The LandFall domains were allowed to move depending on the storm track, however the domain size and resolution was the same for all storms, namely a 0.02 degree grid resolution was specified and the domain size was 3.0 degrees by 3.0 degrees centered on landfall locations. Using three domains with varying degrees of resolution and domain extents allows for proper resolution of deep water waves from outside the Gulf of Mexico, allows for basin to basin scale interactions for circulation and improved resolution/definition of the storm at landfall locations.

As in the studies described above, the JPM-OS was used to characterize the probabilistic nature of coastal storms and associated responses. The HURDAT2 database of historical storms and their associated climatology was used as a data source for the JPM analysis. A joint probability model of hurricane parameters was sampled to yield a set of 660 synthetic tropical storms. Wind and pressure fields for the storms were created in collaboration between OWI and ERDC. The discrete set of storms provides an efficient but complete representation of the full range of potential storms that could impact the Texas coast. A total of 82 master storm tracks were created. For these tracks, four key storm parameters were perturbed: θ, Δ_p, R_{max}, and V_t. Storm intensities ranged from very low intensity storms with Δ_p = 8 mb to catastrophic category 5 hurricanes (on the Saffir-Simpson Wind Scale) with Δ_p = 148 mb. R_{max} ranged from approximately 5 miles (approx. 8 km) for very small storms to 66 miles (approx. 107 km) for very large storms. V_t ranged from 4 mph (approx. 7 km/h) to 27 mph (approx. 44 km/h). Further details of the JPM-OS approach and synthetic storm suite can be found in Nadal et al. (2018).

The Wave Model (WAM) was used to model the deep water wave contributions for each of the storms. The FEMA_TX study setup for the WAM model parameters was used and is considered standard. A single WAM grid system was used but was enlarged. The CTXCS domain is defined for the coastal areas of the state of Texas, in particular from the Texas-Louisiana state line to the US-Mexico border. Accurately estimating the offshore wave conditions for the entire coastal area of Texas required developing the wave field grid for the entire Gulf of Mexico and extending into the Caribbean Sea and a small part of the western basin of the Atlantic Ocean. The WAM model was validated against the ten historical events.

The primary purpose of the WAM offshore wave generation is to provide boundary condition wave estimates to STWAVE as part of the input to the CSTORM simulations. The forms of the boundary condition wave estimates are defined by two-dimensional wave spectra that vary in space (*x* & *y*) and time, covering a discrete range of frequencies *f*, and directions θ. Setting the boundary locations for STWAVE is dependent on the nearshore, local domains defined in the CSTORM simulations, used specifically as input to STWAVE (Massey et al., 2011). As noted earlier, the full-plane version of STWAVE was used for all grid domains. The bathymetry, topography, and Manning's *n* bottom friction values were interpolated from the updated ADCIRC mesh to be described later. A grid resolution of 200 m was selected for all the grids except for the TX-N grid, encompassing Galveston Bay, which used a 150 m value.

Figure A-6. Maps showing the STWAVE grid boundaries in relation to the WAM
boundary used for the CTXCS
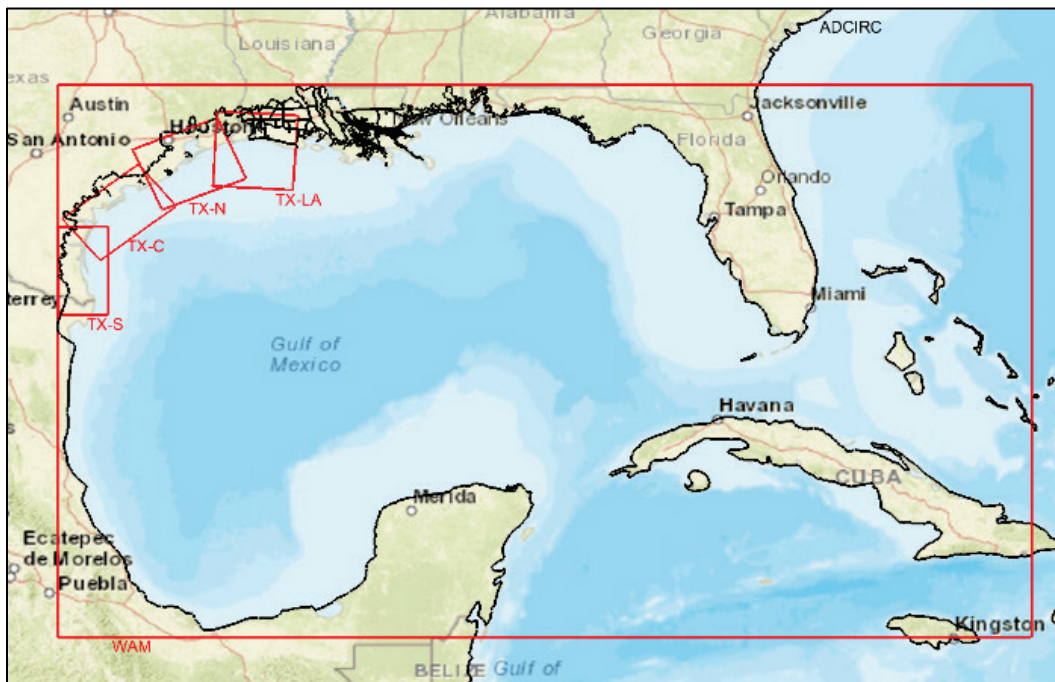
The STWAVE model setups and changes were also validated for the historical
storms. STWAVE model simulation duration and time between wave
computations was allowed to vary depending on the storm characteristics. Storms
were grouped into three categories for nearshore wave conditions, fast moving
storms, moderate forward speed and slow forward speed. Corresponding to these
conditions, STWAVE times between wave computations was 15 minutes, 30
minutes, and 60 minutes. Nearshore wave computations started when the leading
outer edge of the storm center was located at approximately 4 times the radius of
maximum winds away from any STWAVE domain. STWAVE computations were
continued until the trailing outer edge of the storm was located approximately 4
times the radius of the maximum winds away from any STWAVE domain.
Furthermore, all storms had at least 24 wave conditions computed and a
maximum of 265. Roughly 2/3 of all storms used a 30 minute wave snap and the
remaining were evenly split between 15 minute and 60 minute snaps. This
methodology for defining the duration and frequency of nearshore wave
conditions produces significant improvement in accuracy of storm responses over
the Texas FEMA Risk Map study.

The ADCIRC mesh developed and used for the coastal Texas study was adapted
from a combination of previously developed and validated ADCIRC meshes. The
Texas FEMA Risk MAP mesh from the 2011 study was used as a base mesh along

the entire Texas coastline. At the Texas-Louisiana border and continuing eastward along the coast past Mobile, AL, portions of a mesh for southern Louisiana developed for both FEMA and USACE uses (USACE 2011) were used. This mesh is sometimes called the SL15 mesh and was most recently used in the post-Hurricane Isaac investigation of the Hurricane Storm Damage Risk Reduction System (HSDRRS), see USACE (2012b).

Then in the Atlantic and Caribbean, a grid named EC95, which was originally created for computing tidal databases (Hench et al. 1995), served as the base mesh and was used with some localized refinements to improve response and robustness around some of the islands and shallower depths. After the three main meshes (TX FEMA., Southern LA, and EC95) had their respective high resolution areas extracted, they were stitched together and the deeper water areas of the Gulf of Mexico were recreated to smooth the transitions between the meshes and to reduce the number of nodes and elements in that area. The bathymetry from the TX FEMA mesh and SL15-HSDRRS mesh was given in meters relative to NAVD88 and was maintained for the final meshes in their respective areas. The bathymetry from the TX FEMA mesh was used in the Gulf of Mexico and the areas derived from the EC95 mesh.

Figure A-7 shows a color-fill topographic/bathymetric map of the topography/bathymetry values used in the CTXCS ADCIRC mesh. Notice also in Figure A-7 the levee and roadway structures being represented in the ADCIRC mesh in the LA portion of the domain. These structures were not a part of the TX FEMA mesh. The CTXCS ADCIRC mesh has a total of 4.5 million computational nodes and 9.0 million unstructured elements. Maximum and minimum element sizes are in the same range as the TX FEMA mesh, ranging from approximately 14 meters to 58 km.

Figure A-7. A color contour map showing the seamless topography and bathymetry contained in the CTXCS ADCIRC mesh along the TX-LA border
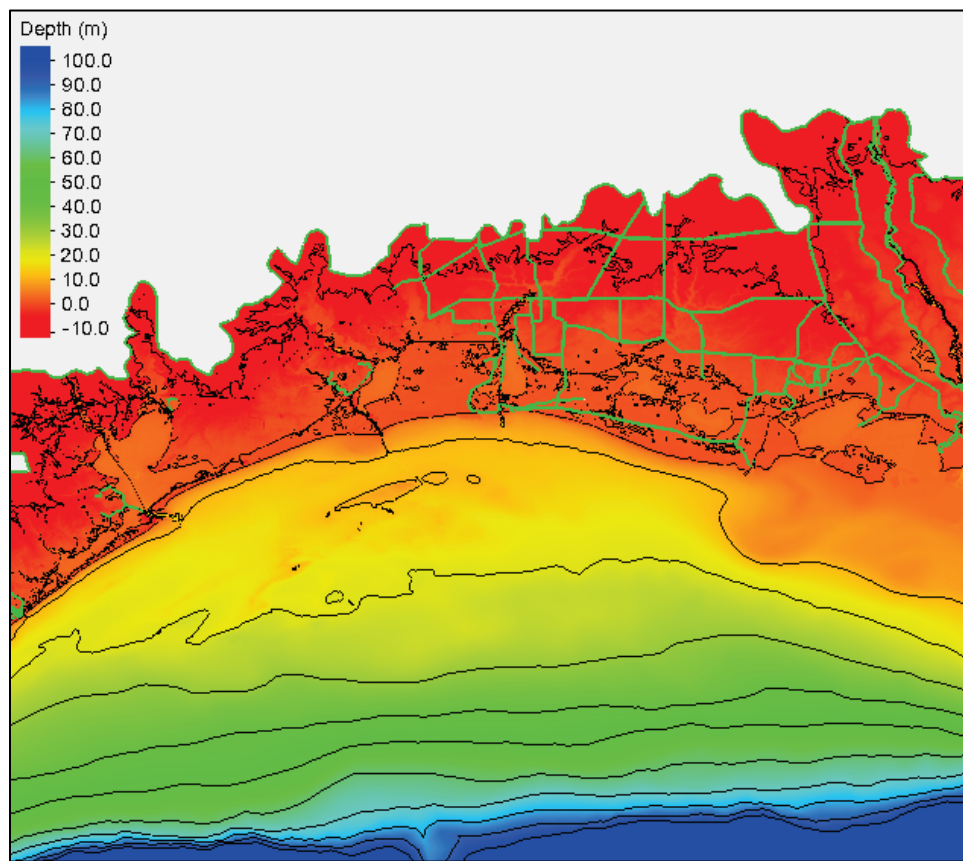
For wind and coastal hydrodynamic modeling by ADCIRC, LCLU data was used to determine spatially distributed values of bottom friction coefficients (or Manning's *n*), canopy coefficients, and surface roughness length for the effect of directional wind reduction, in response to spatial changes of land cover and land use over study areas. These parameters were all updated for the CTXCS using the most recent LCLU data, primarily from the USGS.

Two river inflows from the Mississippi River and the Atchafalaya River are included in the storm-surge simulations. The inflow boundary (or the river cross-section) of the Mississippi River is located near the USGS gage #07374000 Mississippi River at Baton Rouge, LA. The boundary for the Atchafalaya River is placed near the USGS gage #07381490 Atchafalaya River at Simmesport, LA. Constant river inflows were used for all simulations. A value of approximately 160,00 cfs (cubic feet per second) was used for the Mississippi River and a value of 68,000 cfs was used for the Atchafalaya River. Rivers in the TX area of the domain were included in the ADCIRC mesh, but were not forced with any inflow data. The ADCIRC domain

extends so far inland that the rivers at the boundary of the model domain are too small to produce significant forcing.

Validation simulations for the CSTORM coupled ADCIRC + STWAVE were performed for historical hurricanes Brett, Carla, Ike, Rita, Katrina, Gustav, and Isaac. These storms were selected for their historical significance to the Texas coastline and for the availability of measurement data.

Three different sets of water level conditions were modeled for the CTXCS: a base value representing present day conditions, a sea level rise value of 1.5 meters and a sea level rise value of 0.75 meters.

The 660 synthetic storms were sampled from a new joint probability model. The model and storm sampling follow an approach similar to that described above. However significant improvements have been integrated. The approach is illustrated in Figure A-8 and described below.

Figure A-8. USACE's "new" Probabilistic Coastal Hazard Analysis (StormSim-PCHA) (Nadal-Caraballo et al. 2018)
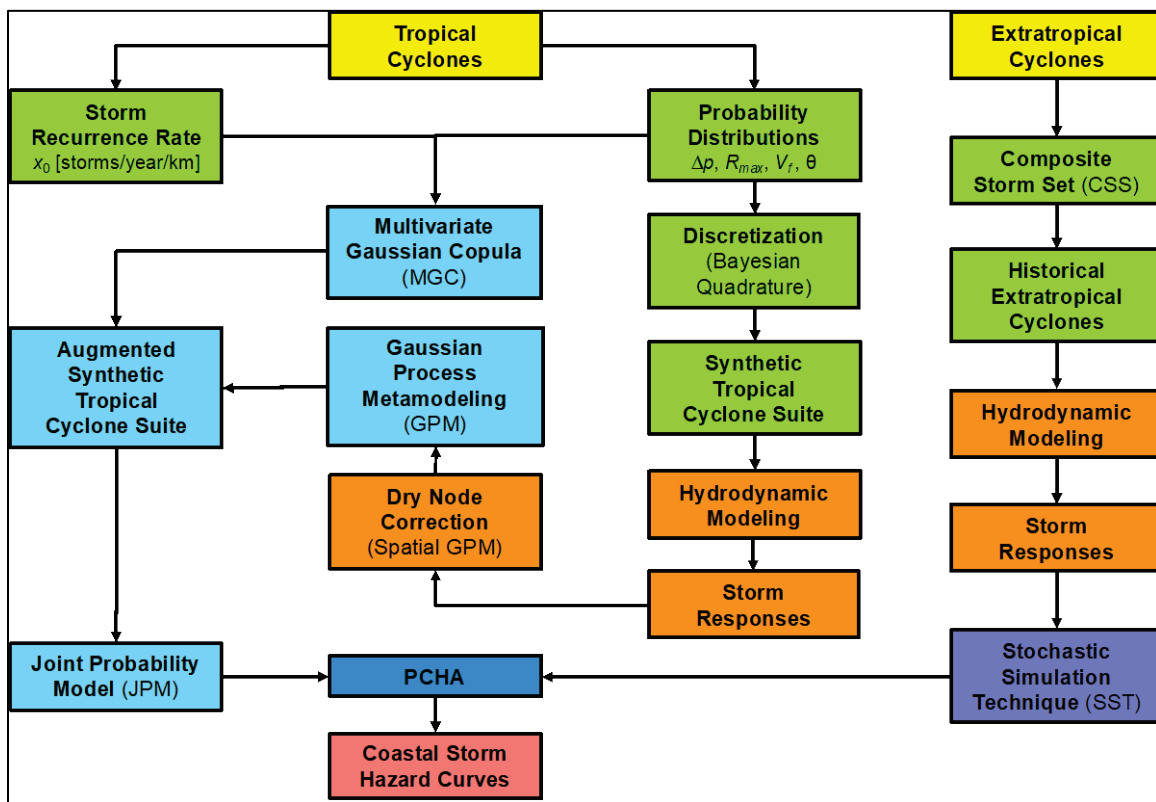
Characteristics of the JPM-OS approach for CTXCS (Nadal-Caraballo et al. 2018):

- Storm tracks created at regular spacing.
- HURDAT2 database sample 1940 – 2017 landfalling and bypassing storms. Parameters sampled were landfall location (latitude and longitude), Δ_p, R_{max}, V_t, and θ. Joint probability distribution created using these parameters.
- A hybrid optimal sampling method was employed for the discretization of the marginal distributions of tropical cyclone parameters. To ensure optimum coverage of both probability and parameter spaces, as well as spatial coverage of the study area, a structured discretization approach was used for the Δ_p and θ marginal distributions. The discretization of the R_{max} and V_t marginal distributions was performed using the Bayesian Quadrature method. Holland B was estimated as a function of Δ_p, R_{max}, and latitude.
- A higher resolution statistical analysis was performed at +200 CRLs throughout the Texas coastline.
- Since intense tropical cyclones (TC) behave differently from weak ones, for CTXCS, storms were separated into three partitions: low-intensity TCs (8 hPa ≤ Δ_p < 28 hPa), medium intensity (28 hPa ≤ Δ_p < 48 hPa) and high-intensity TCs (Δ_p ≥ 48 hPa). Similar partitioning was done by Toro in Mississippi, but had not been done for LA or TX. CTXCS had the following intensities: 148, 138, 128, 118, 108, 98, 88, 78, 68, 58, 48 hPa (high); 38, 28 hPa (medium); 18, 8 hPa (low)
- The GKF was reconceived as a point-based approach accounting for all storms above a given intensity threshold (e.g., all TCs with Δ_p ≥ 8 hPa), each with the appropriate distance-weight. This is different from previous methods used to compute SRR using capture zones (weight of 1 inside; weight of 0 outside), and even from previous applications of the GKF where a capture zone was used first to screen storms and then the SRR computed. The latter can result in underestimation of SRR. Also, the new point-based approach allows for the partitioning of TCs by intensity.
- The distance-weighting GKF methodology was used to compute the TC parameter distance-weighted mean values and marginal probabilistic distributions for each JPM-OS parameter. For each of the TC parameter distributions, a distance-weighted mean was computed based on the distances between the track point of higher intensity and the CRLs. The marginal distributions were fitted to the distance-adjusted TC parameters. The purpose of this Gaussian process is to maximize the use of available

historical data while properly characterizing the storm climatology given the latitude-dependency of the TC parameters.

- Improved estimates of uncertainty (epsilon) terms used to compute various confidence limits around mean rather than being included in hazard curve.

The impact of the increased number of storm intensities can be seen in Figure A-9. Here the base CTXCS is plotted with mean and two sets of confidence limits while the FEMA 2011 plot is the short green line. The FEMA 2011 under-sampling of storm intensities results in the high frequency tail being high by a meter. In addition, by including the epsilon terms in the JPM integral, the curve is close to the 84% upper confidence limit.

Figure A-9. Comparison of hazard curves for FEMA 2011 and CTXCS (Nadal-Caraballo et al. 2018)
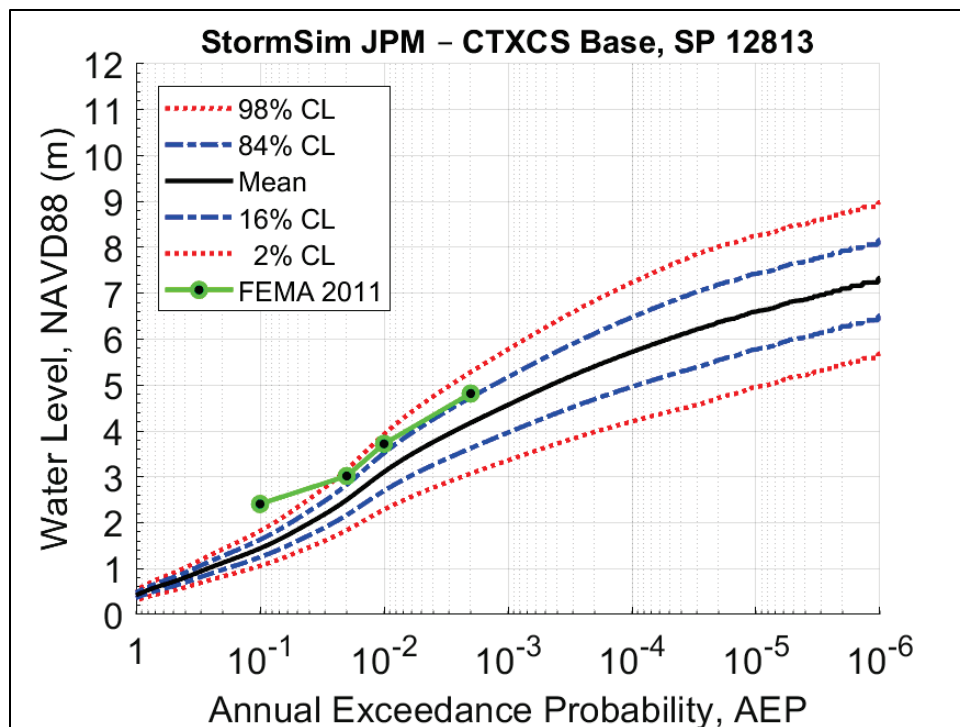
The main improvement of the new PCHA JPM approach used in the CTXCS is incorporation of a surrogate model (Gaussian Process Metamodeling (GPM)) as substitute for a response surface (RS). While the FEMA-TX RS only accounted for Δ_p and R_{max}, GPM accounts for all storm parameters: Δ_p and R_{max}, V_t, θ, and Holland B. The GPM is used to augment the storm sampling by accurately computing parameter values. Where not used, interpolated values have been shown to introduce additional uncertainty in water surface elevations with root-

mean-square deviation on the order of 0.70 m (CPRA 2013). The added uncertainty is seldom quantified in these studies.

Figure A-10 shows a comparison of several JPM approaches for a specific point located in the North Atlantic Coast Comprehensive Study Region. Note the green curve, which was produced using the above method without the GPM, and the top black curve, which was computed with GPM. In this case, the GPM-augmented storm suite consisted of approximately 200,000 storms. Over the range of extremes of interest the difference is roughly 1 m and the method without GPM is not conservative. Of course, much finer (greater) parameter and probability resolution is expected to produce more accurate results, but this could translate to higher or lower surge hazard magnitude compared to standard JPM approaches, depending on location within study area – it will not necessarily be always higher than standard JPM.

Figure A-10. Comparison of hazard curves for several JPM approaches
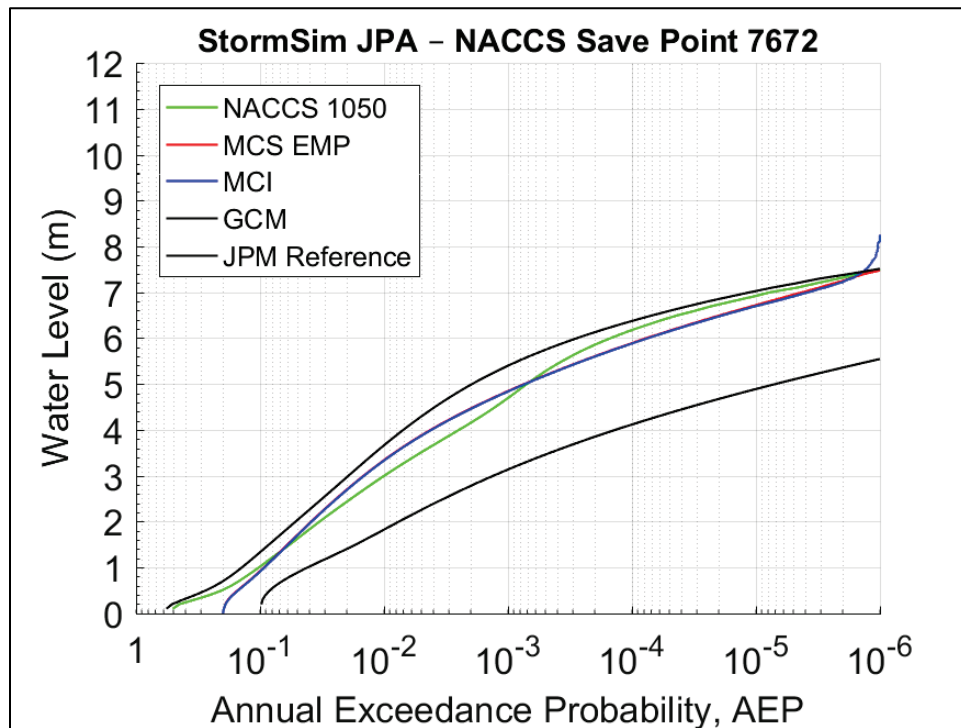
An additional improvement in the methods is the use of Multivariate Gaussian Copula (MGC). Unlike all previous JPM studies, which use 1:1 conditional probabilities, MGC allows to, for the first time, have an explicit joint probability model accounting for the (univariate) extreme value distributions of all storm parameters and their corresponding correlations.

Nearshore hydraulic modeling is complicated by the fact that near to, and within, the surf zone, the processes are highly nonlinear and waves and water levels are strongly correlated. The resulting hazards include wave runup, wave and/or steady flow overtopping and wave forces and these are also relatively complicated processes. Historically, these processes were modeled using empirical relations and simple statistical models (e.g., USACE 1984) and errors were unknown. In particular, most empirical models do not account for spatially varying bathymetry that impacts wave transformation, runup and overtopping and are limited to the ranges of parameter combinations from laboratory studies.

Modern analysis includes numerical modeling of nearshore waves and water levels using either phase averaged models (e.g., STWAVE, CMS-WAVE, SWAN, CSHORE) or phase resolving models (e.g., COULWAVE, BOUSS2D, COBRAS, OpenFOAM, FLUENT, Proteus). FEMA uses WHAFIS for nearshore responses and this is an empirical model that is not typically very accurate. FEMA has begun to apply CSHORE as a replacement for WHAFIS for some projects (FEMA 2012b, Johnson 2012, Johnson et al. 2012, Melby 2012). Most of the phased-averaged models include relatively simple characterizations of wave breaking based on the statistical wave characteristics while phase resolving models attempt to model the surf zone for each wave. In addition, many phase resolving models can model runup and overtopping to some extent. CHSHORE is the only phase averaged model in the list above that can model runup and overtopping and it runs very quickly so it is attractive for risk simulations where thousands of events are required. COULWAVE and BOUSS2D have both been successfully applied to projects within S2G (Lynett 2018, Melby et al. 2015). These Boussinesq models would be expected to be much more accurate than the phase averaged models in the nearshore. They model nonlinear phenomena, such as wave breaking, diffraction and infragravity waves, that are not explicitly modeled by phase averaged models. However, phase resolving may not be more accurate than empirical models for complex phenomena, such as wave overtopping, that are heavily dependent on real fluid effects like friction and dissipation resulting from very rough and porous surfaces unless calibrated. The downside is that they are resource intensive, with both a large computational burden and requiring significant post-processing effort and skill.

Nearshore Boussinesq and RANS models are applied in two horizontal dimensions and in one (transect models). CSHORE is a one-dimensional model. Two-dimensional wave models can take into account wave refraction, diffraction and oblique reflection. Often in the nearshore, waves align with shore-parallel contours and refraction and diffraction are not important. In that case, transect

models are often adequate. In addition, the condition of shore-parallel wave crests is often the worst case, so it is conservative to assume this. However, in areas where diffraction and refraction are predominant, such as the Freeport inlet and Dow thumb area, a two-dimensional Boussinesq model is required. An initial task with the present study is to compare the various approaches for nearshore wave transformation and adopt the best methods.

Lynett (2018) modeled the nearshore area of Freeport with two-dimensional COULWAVE models using a response-based approach. This captured physics not modeled with previous phase resolving models. However, COULWAVE does not include wind-wave generation so wind waves generated on flood waters landward of the coast were not reproduced.

References

ADCIRC (2017). ADCIRC Utility Programs, http://adcirc.org/home/related-software/adcirc-utility-programs/, accessed on Aug. 1, 2017

Cialone, Mary A., Massey, T.C., Anderson, Mary E., Grzegorzewski, Alison S., Jensen, Robert E., Cialone, Alan, Mark, David J., Pevey, Kimberly C., Gunkel, Brittany L., McAlpin, Tate O. (2015). North Atlantic Coast Comprehensive Study (NACCS) Coastal Storm Model Simulations: Waves and Water Levels. ERDC/CHL TR-15-14. Vicksburg, MS: US Army Engineer Research and Development Center.

Federal Emergency Management Agency (FEMA) 2011. Flood Insurance Study: Coastal Counties, Texas: Scoping and Data Review. Joint Report prepared for Federal Emergency Management Agency by the Department of the Army, US Army Corps of Engineers, Washington DC.

_____2012a. Technical Support Data Notebook DFIRM Update for Brazoria County, Texas Coastal Flood Hazard Analysis Deliverable. FEMA Region VI report.

_____2012b. Great Lakes Coastal Guidelines Update. FEMA Region V report.

Gravens, Mark B., Richard M. Males, Richard M., and Moser, David A. (2007). *Beach-fx: Monte Carlo Life-Cycle Simulation Model for Estimating Shore Protection Project Evolution and Cost Benefit Analyses*, Shore and Beach, Vol. 75, No. 1, Winter, pages 12-19.

Hench, J.L., R.A. Luettich, Jr., J.J. Westerink and N.W. Scheffner, 1995, ADCIRC: an advanced three-dimensional circulation model for shelves, coasts and estuaries, report 6: development of a tidal constituent data base for the Eastern North Pacific, Dredging Research Program Technical Report, US Army Corps of Engineers Waterways Experiment Station, Vicksburg, MS.

IPET. 2009. Performance Evaluation of the New Orleans and Southeast Louisiana Hurricane Protection System. Final Report of the Interagency Performance Evaluation Task Force. Department of the Army, US Army Corps of Engineers, Washington, DC.

Johnson, B. D. 2012. Lake Michigan: Prediction of Sand Beach and Dune Erosion for Flood Hazard Assessment. Great Lakes Coastal Flood Study, 2012 Federal Inter-Agency Initiative, ERDC/CHL TR-12-16, US Army Engineer R&D Center, Vicksburg, MS.

Johnson, B. D., Kobayashi, N., Gravens, M. 2012. Cross-Shore Numerical Model CSHORE for Waves, Currents, Sediment Transport and Beach Profile Evolution. Great Lakes Coastal Flood Study, 2012 Federal Inter-Agency Initiative, ERDC/CHL TR-12-22, US Army Engineer R&D Center, Vicksburg, MS.

Kolar, R. L., W.G. Gray, J.J. Westerink, and R.A. Luettich. (1994). Shallow water modeling in spherical coordinates: Equation formulation, numerical implementation, and application. Journal of Hydraulic Research, 32 (1), 3-24.

Komen, G.J. L. Cavaleri, M. Donelan, K. Hasselmann, S. Hasselmann, and P.A.E.M. Janssen, (1994). Dynamics and modeling of ocean waves. Cambridge University Press, United Kingdom. 532 pp.

Luettich, R. A., Jr., J.J. Westerink, N.W. Scheffner, N. W. (1992). ADCIRC: An advanced three-dimensional circulation model for shelves, coasts, and estuaries. Technical Report DRP-92-6, US Army Engineer Research and Development Center, Vicksburg, MS.

Lynett, P.J., Kalligeris, N. (2018). Velasco Drainage District Levee Overtopping, Valesco Drainage District contract report.

Males, R. M., and Melby, J. A. (2012). "Monte Carlo simulation model for economic evaluation of rubble mound breakwater protection in harbors," Frontiers of Earth Science Journal, Springer, vol. 5 issue 4 December 2011. P. 432 – 441.

Massey, T.C., Jensen, R.E., Bryant, M.A., Ding, Y., Owensby, M.E., and Nadal-Caraballo, N.C. (2018). Coastal Texas Protection and Restoration Feasibility Study: Coastal Storm Model Simulations: Waves and Water Levels. Draft ERDC/CHL Technical Report. Vicksburg, MS: US Army Engineer Research and Development Center.

Massey, T. C., M.E. Anderson, J.M. Smith, J. Gomez, and R. Jones. (2011). *STWAVE: Steady-state spectral wave model user's manual for STWAVE, Version 6.0.* ERDC/CHL SR-11-1.US Army Engineer Research and Development Center, Vicksburg, MS.

Melby, J.A., N.C. Nadal-Caraballo, and J. Winkelman. (2015a). Point Judith, Rhode Island, Breakwater Risk Assessment. ERDC/CHL TR-15-13. Vicksburg, MS: US Army Engineer Research and Development Center.

Melby, J.A., Nadal-Caraballo, N.C., Ratcliff, J.J., Massey, C.T., Jensen, R.E. (2015b). Sabine Pass to Galveston Bay Wave and Water Level Modeling, Draft Technical Report, US Army Engineer R&D Center, Vicksburg, MS.

Melby, J.A. (2009). Time-dependent life-cycle analysis of coastal structures," Proc. Coastal Structures 2007, World Scientific, 1842-1853.

Melby, J.A. (2012). "Wave runup prediction for flood hazard assessment," Technical Report ERDC/CHL TR-12-24, US Army Engineer Research and Development Center, Vicksburg, MS. 111 pgs.

Melby, J. A., Thompson, E. F., Cialone, M. A., Smith, J. M., Borgman, L. E., Demirbilek, Z., Hanson, J. L., and Lin, L. (2005). "Life-Cycle Analysis of Mid Bay and Poplar Island Projects, Chesapeake Bay, Maryland," Technical Report ERDC/CHl TR-05-12, US Army Engineer Research and Development Center, Vicksburg, MS.

Melby, J.A., Diop, F., Nadal-Caraballo, N.C.., Green, D., Gonzalez, V. (2015). "Coastal Hazards System", Coastal Structures and Solutions to Coastal Disasters Conference, ASCE, Boston, MA.

Nadal-Caraballo, N.C., Lewis, A.B., Gonzalez, V.M., Massey, T.C. and Cox, A.T. (2018). Coastal Texas Protection and Restoration Feasibility Study, Probabilistic Modeling of Coastal Storm Hazards, Draft Technical Report, US Army Engineer R&D Center, Vicksburg, MS.

Orange County 2012. Flood Protection Planning Study Hurricane Flood Protection System, Orange County, Texas. Report prepared for Orange County, Orange County EDC and The Texas Water Development Board.

Smith, J. M., A.R. Sherlock, and D.T. Resio. (2001). *STWAVE: Steady-state spectral wave model user's manual for STWAVE, Version 3.0*. ERDC/CHL SR-01-1. US Army Engineer Research and Development Center, Vicksburg, MS.

United States Army Corps of Engineers (USACE). (2006). Louisiana Coastal Protection and Restoration (LACPR) Preliminary Technical Report. Provided to United States Congress.

_____. 2009a. *Louisiana Coastal Protection and Restoration (LACPR) Final Technical Report*. New Orleans District, Mississippi Valley Division, USACE.

_____. 2009b. *Mississippi Coastal Improvements Program (MSCIP), Hancock, Harrison, and Jackson Counties, Mississippi*. Mobile, AL: Mobile District, South Atlantic Division, USACE.

_____. 2012. Hurricane and Storm Damage Reduction System Design Guidelines, New Orleans District, Mississippi Valley Division, USACE.

_____. 2014. Freeport Hurricane Flood Protection, Semi-Quantitative Risk Assessment Report. US Army Engineer Galveston District.

Westerink, J.J., R.A. Luettich Jr., J.C. Feyen, J.H. Atkinson, C. Dawson, H.J. Roberts, M.D. Powell, J.P. Dunion, E.J. Kubatko, and H. Portaheri. (2008). A basin- to channel-scale unstructured grid hurricane storm surge model applied to southern Louisiana. Monthly Weather Review, 136, 833–864.

Westerink, J., Dietrich, J., Westerink, H., Tanaka, S., Martyr, R., Hope,M., Westerink, L., Atkinson, J., H. Roberts, R. Clark, S. Zou, Z. Cobell, C. Bender, R. Srinivas, J. Smith, R. Jensen, D. Resio, J. Ratcliff, H. Pourtaheri, N. Powell, D. Elzey, D. Ulm, C. Dawson, J. Proft, C. Szpilka, R. Kolar, K. Dresback, V. Cardone, A. Cox, M. Powell, (2011). Flood Insurance Study: Coastal Counties, Texas, Intermediate Submission 2: Scoping and Data Review, FEMA Region 6, USACE New Orleans District, 15 November 2011.

Appendix B: CSTORM Modeling Validation and Assessment

Validation and bias correction

Validation simulations for the CSTORM coupled ADCIRC + STWAVE were performed for historical Hurricanes Brett, Carla, Ike, Rita, and Harvey. These storms were selected for their historical significance to the Texas coastline and for the availability of measurement data. Due to the brevity of this summary report, only portions of the results will be shown. In Figure B-1, three time-series plot comparisons of measured versus modeled water surface elevations are shown at NOAA gage station (8771450) located at Galveston Pier 21. The time-series comparisons are for Hurricanes Rita, Ike, and Harvey. Modeled water levels for Hurricane Rita are approximately 0.5 ft higher than measured for the peak of the simulation. For Hurricane Ike, the model results are approximately 8 in. low in the 24 hr leading up to the peak of the storm, approximately equal for the peak, and then are approximately 1.6 ft low after the storm peak. Model results are approximately 0.75 ft lower than measured for Hurricane Harvey during the peak of the storm but are approximately the same for the three tidal cycles shown between August 20 and August 23.

Figure B-1. Plots showing time series of water levels (in meters, NAVD88) at the NOAA tide gage station (8771450) located at Galveston Pier 21. Results are shown for (a) Hurricane Rita, (b) Hurricane Ike, and (c) Hurricane Harvey.

(a)

(b)

(c)
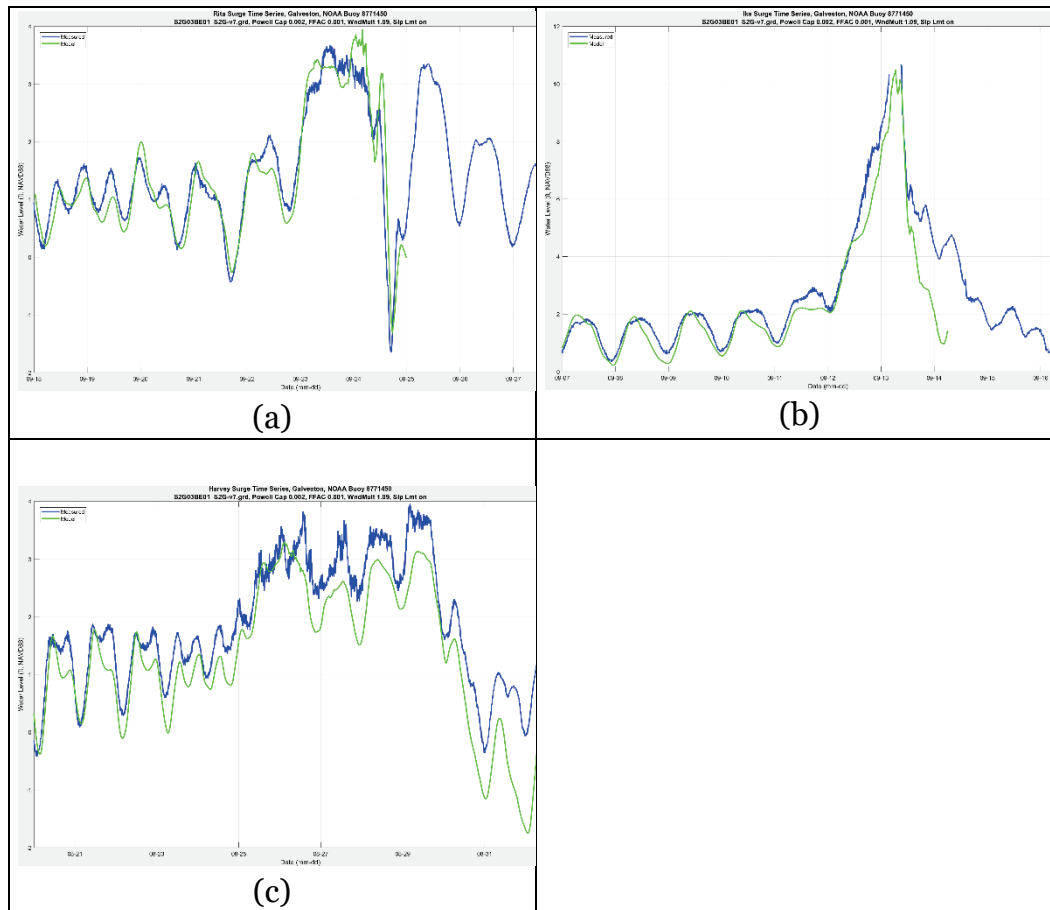
In Figure B-2, three time-series plot comparisons of measured versus modeled water surface elevations are shown at NOAA gage station (8770475) located at Port Arthur, TX, for Hurricanes Rita, Ike, and Harvey. Modeled water levels for Hurricane Rita are approximately 0.5 ft lower than measured leading up to the peak at which point the model underestimates the peak by approximately 1 ft. For Hurricane Ike, the model results are approximately 0.3 ft low leading up to the peak of the storm and then are approximately 1.5 ft high at the peak. For Hurricane Harvey, the model results are approximately 0.5 ft lower than measured leading up to and including the peak of the storm. The measured results continue to increase after about August 27 while the modeled results stay approximately the same until about August 30 after which they significantly decrease. The measurement data continue to increase due to the rainfall/runoff influence from Hurricane Harvey that is not being modeled by ADCIRC. In Figures B1 and B2, vertical axis is SWL (feet, NAVD88) and horizontal axis is date (month-day).

Figure B-2. Plots showing time series of water levels (in meters, NAVD88) at the NOAA tide gage station (8770475) located at Port Arthur, TX. Results are shown for (a) Hurricane Rita, (b) Hurricane Ike, and (c) Hurricane Harvey.

(a)

(b)

(c)
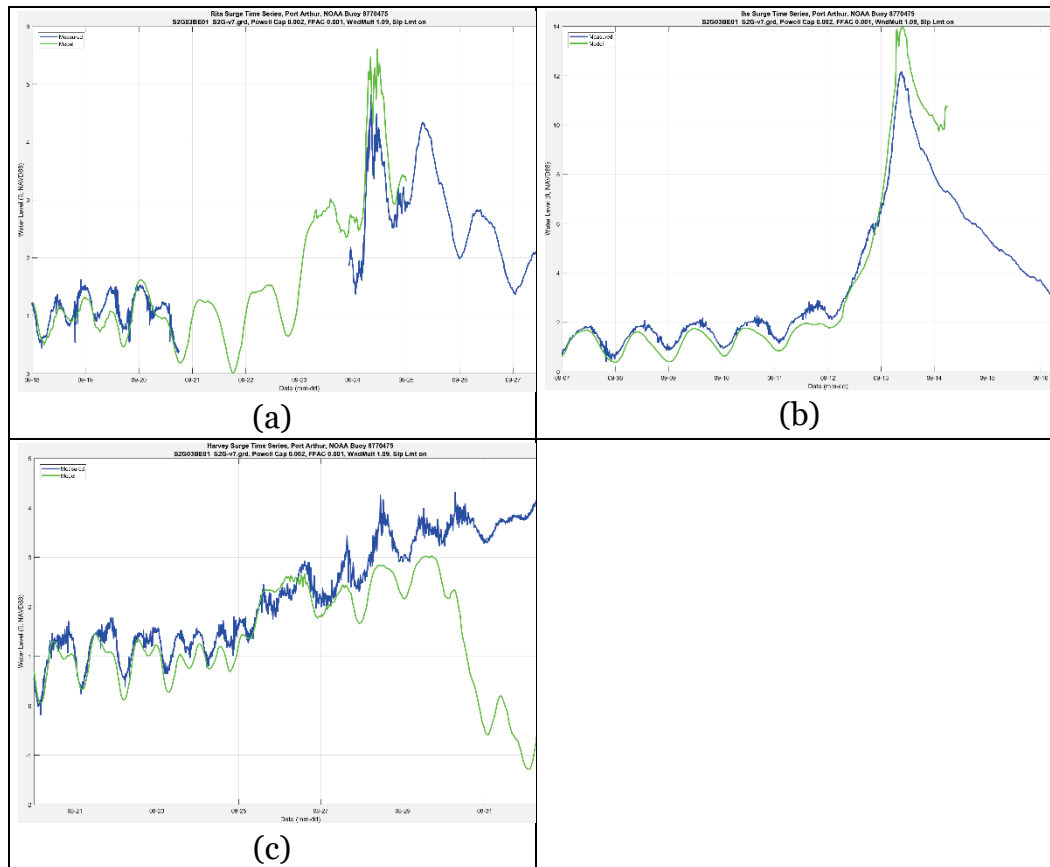
In Figure B-3, peak water level QQ plots and the corresponding point location differences are shown for Hurricanes Brett and Carla. For Hurricane Brett, all measured versus modeled differences are less than 1.6 ft with a correlation coefficient of 0.41. For Hurricane Carla only 20% of the model versus measured result differences are less than 1.6 ft, with the majority of the model results being lower than measured by approximately 3.3 ft. Similarly, in Figure B-4 maximum surge water level QQ plots and corresponding point location differences are shown for Hurricanes Ike and Rita. Approximately 47% of all model versus measurement differences are within 1.5 ft, and an overall correlation coefficient of 0.81 was computed for Hurricane Ike. Again, the model tends to underestimate surge levels by approximately 2.6 ft. For Hurricane Rita, the correlation coefficient is 0.63, and approximately 51% of all locations show modeled versus measured differences of less than 1.5 ft. For Hurricane Rita, only a few measurement locations were located in Texas.

Figure B-3. QQ plots and the corresponding measurement locations plotted on a map for Hurricanes Brett and Carla (results shown in meters).

(a)

(b)

(c)

(d)
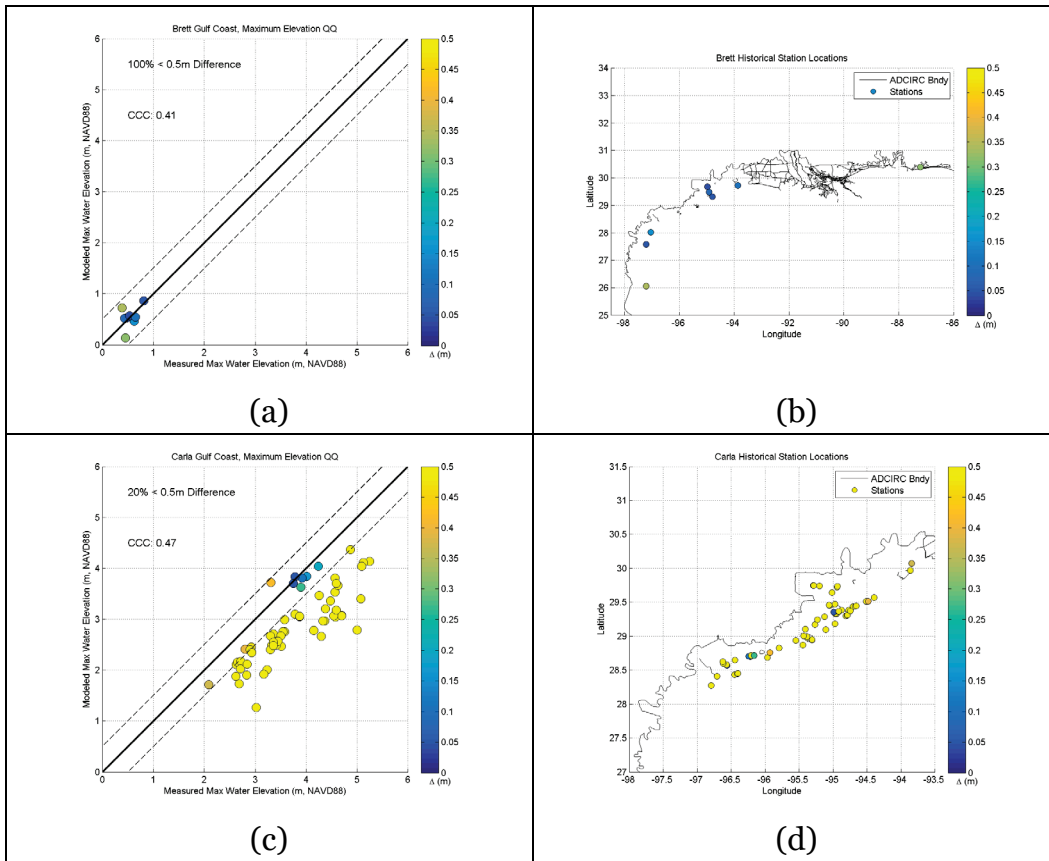
Figure B-4. QQ plots and the corresponding measurement locations plotted on a map for Hurricanes Ike and Rita.

(a)

(b)

(c)

(d)
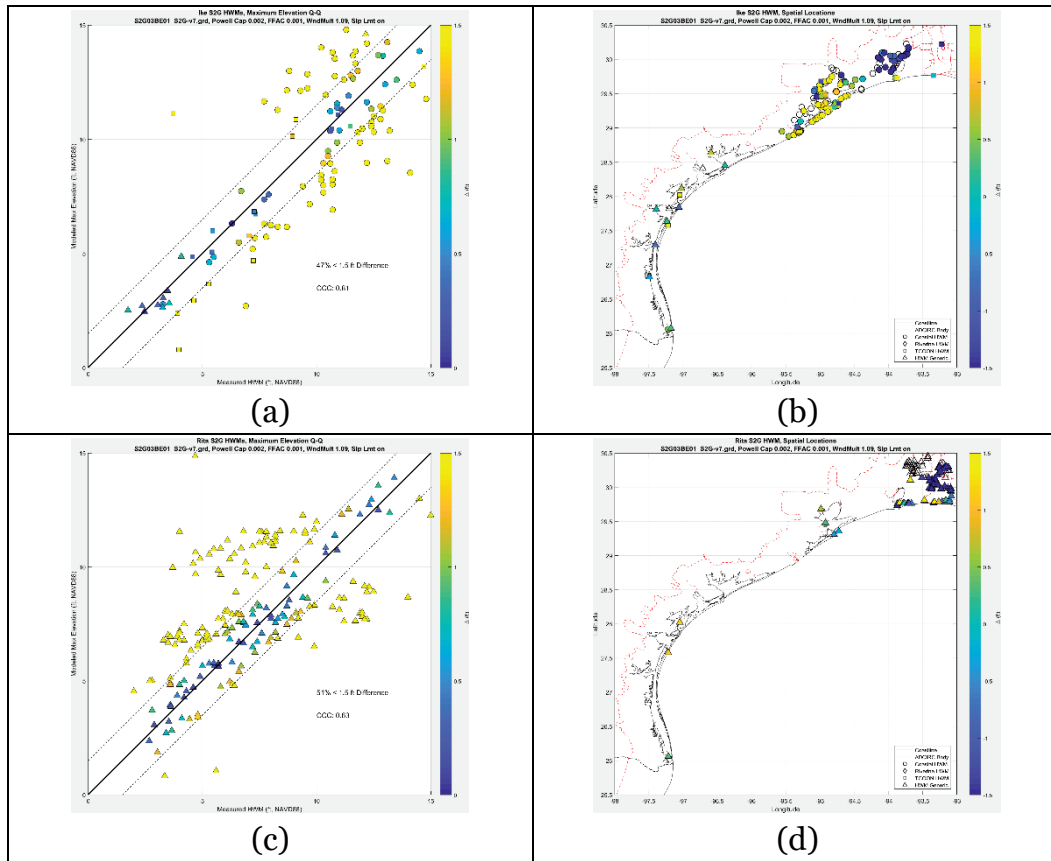
Bias correction

The results for all validation storms were used to determine model bias. There was a noticeable difference in bias between the Sabine area and the Galveston area, so the bias correction was split into two regional bias corrections with the two regions separated at longitude 94.4W deg. Figure B-5 shows the region to the west of 94.4W with the uncorrected QQ plot on the left and the corrected on the right. In this case, the corrected values were computed as Modeled SWL/0.853. Figure B-6 shows the region to the east of 94.4W with the uncorrected QQ plot on the left and the corrected on the right. In this case, the corrected values were computed as Modeled SWL/1.054. These corrections were applied to all CSTORM SWLs in the study.

Figure B-5. QQ plots for validation storms for region to the West of longitude 94.4W with uncorrected on left and corrected on right. Red dashed lines show 20% error limits.
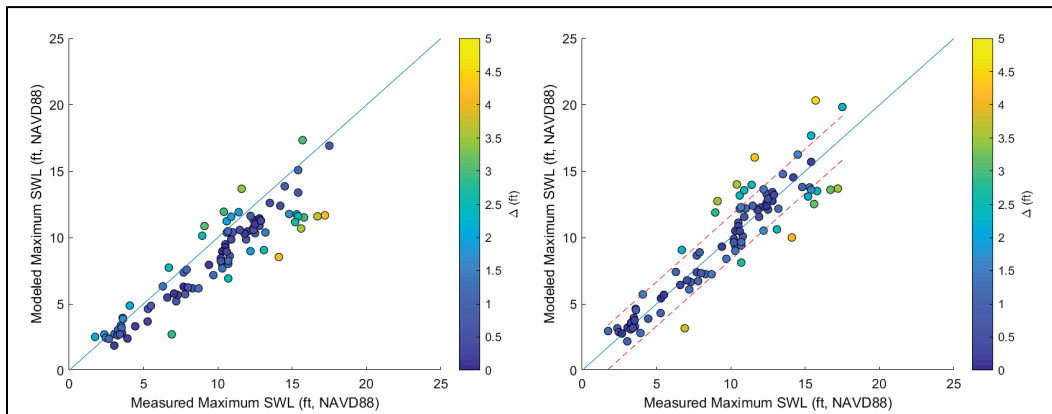
Figure B-6. QQ plots for validation storms for region to the East of longitude 94.4W with uncorrected on left and corrected on right. Red dashed lines show 20% error limits
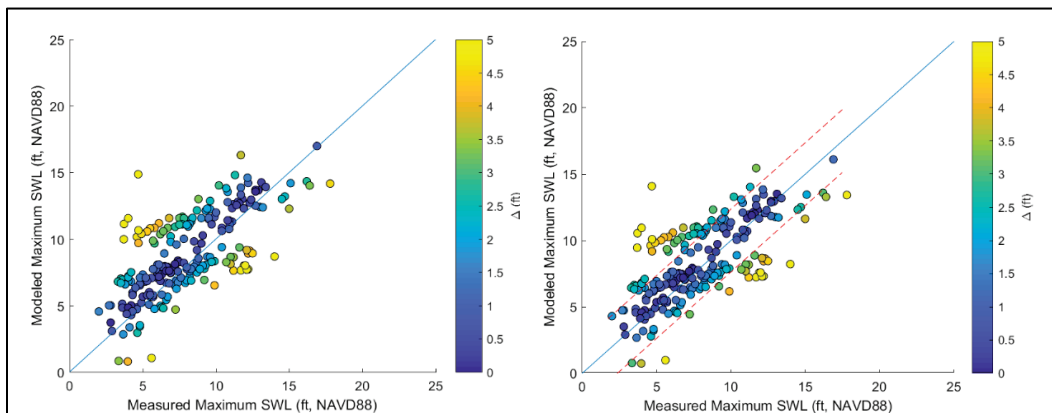
Sample CSTORM model results: without- and with-project

Under both the with- and without-project conditions, 189 synthetic tropical storm conditions were used in conjunction with three different starting water levels to compute storm surge and nearshore wave conditions using the CSTORM-MS. These were CSTORM fully coupled ADCIRC+STWAVE simulations. The three starting water levels used were adjusted for steric conditions and RSLC by adding (1) 1.52 ft, (2) 2.93 ft, and (3) 4.73 ft. Note that all model results have uniquely identifying file names and are stored on the ERDC High Performance Computing center's long-term archive storage system.

ADCIRC model results include time series of water levels and water currents at every node in the ADCIRC mesh and at all the SP locations along with a record of the interpolated winds and pressure fields used. At every computational node, ADCIRC also computes a maximum or minimum quantity value over the duration of the simulation, keeping track of those values at every computational time-step; in the CTXCS and S2G cases, the time-step size was 0.50 sec. Records for maximum water surface elevation, maximum water velocity, maximum wind velocity, and minimum sea surface pressure at every node are computed and output by ADCIRC. Then, a post-processing code linearly interpolates that information from the global solution files onto the SP locations.

STWAVE model results include time series of significant wave height, mean wave period, MWD, peak wave period, and wave stress gradients at every computational cell in the grid. An SP time-series file is also written to file and contains the following information at every SP location contained in a given STWAVE grid: significant wave height, mean wave period, MWD, peak wave period, wind speed, wind direction, and water level. A post-processing code computes for each computational cell, the maximum significant wave height achieved over the entire length of the simulation, over each wave snap, and writes the values to file along with the corresponding mean wave period and MWD. Similarly, the maximums at SP locations are also computed as a post-processing step.

The maximum water levels and wave heights at all the SP locations and all storms are collected into a single large comma-separated file (referred to as a maximum table) for each of the RSLC and structure scenarios. These maximum tables are then used in the stochastic simulations.

Quality control

Quality control of the CSTORM outputs included checking the peak time series for anomalies. The time series of the storm responses for each SP were plotted and visually analyzed. An example of SWL time series is shown in B-7. Wave height peaks are shown in Figure B-8.

Figure B-7. Peak SWL plot for SLC1 with-project, used for visual inspection during storm quality control.
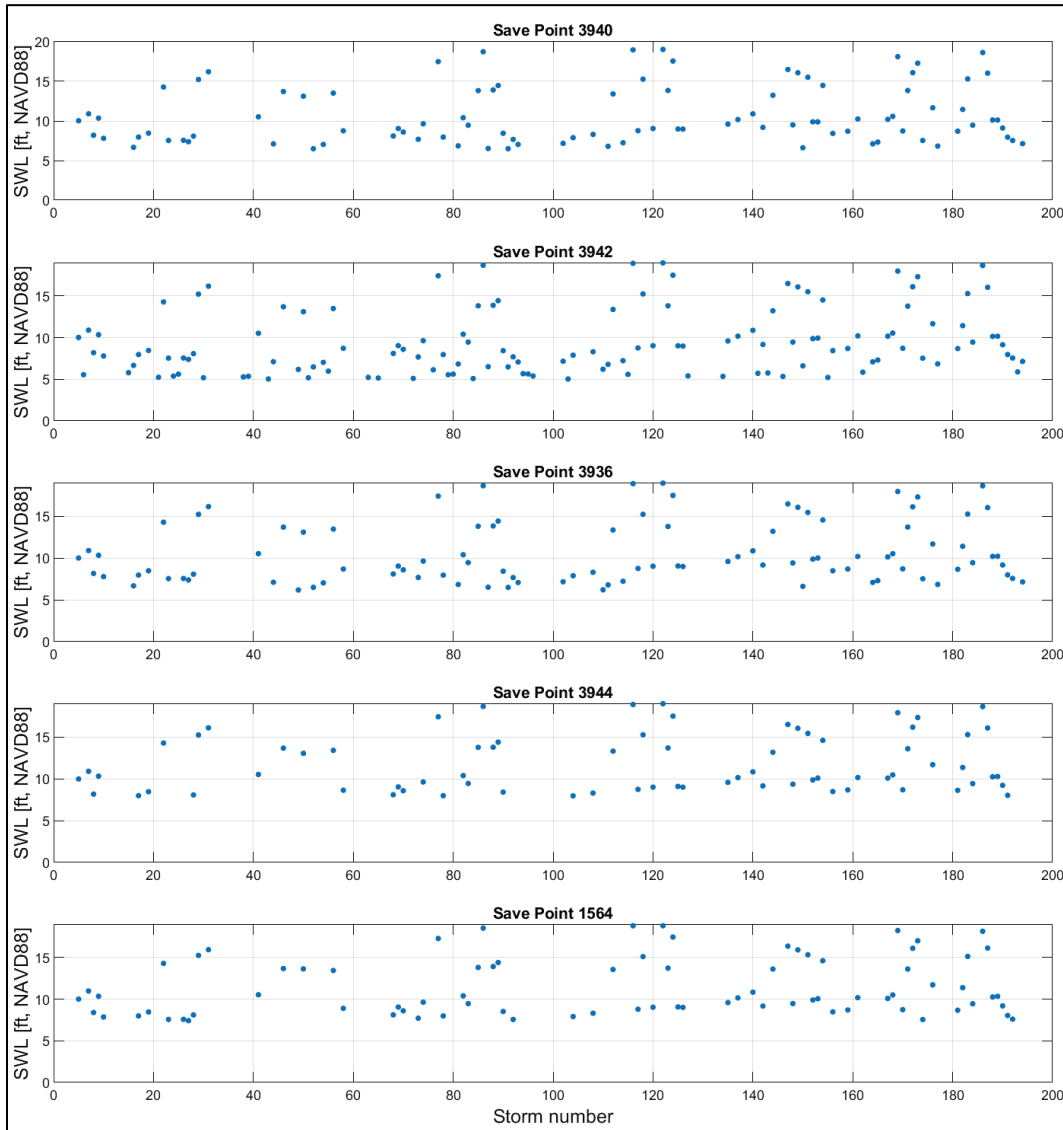
Figure B-8. Peak H_{m0} plot for SLC1 with-project, used for visual inspection during storm quality control.
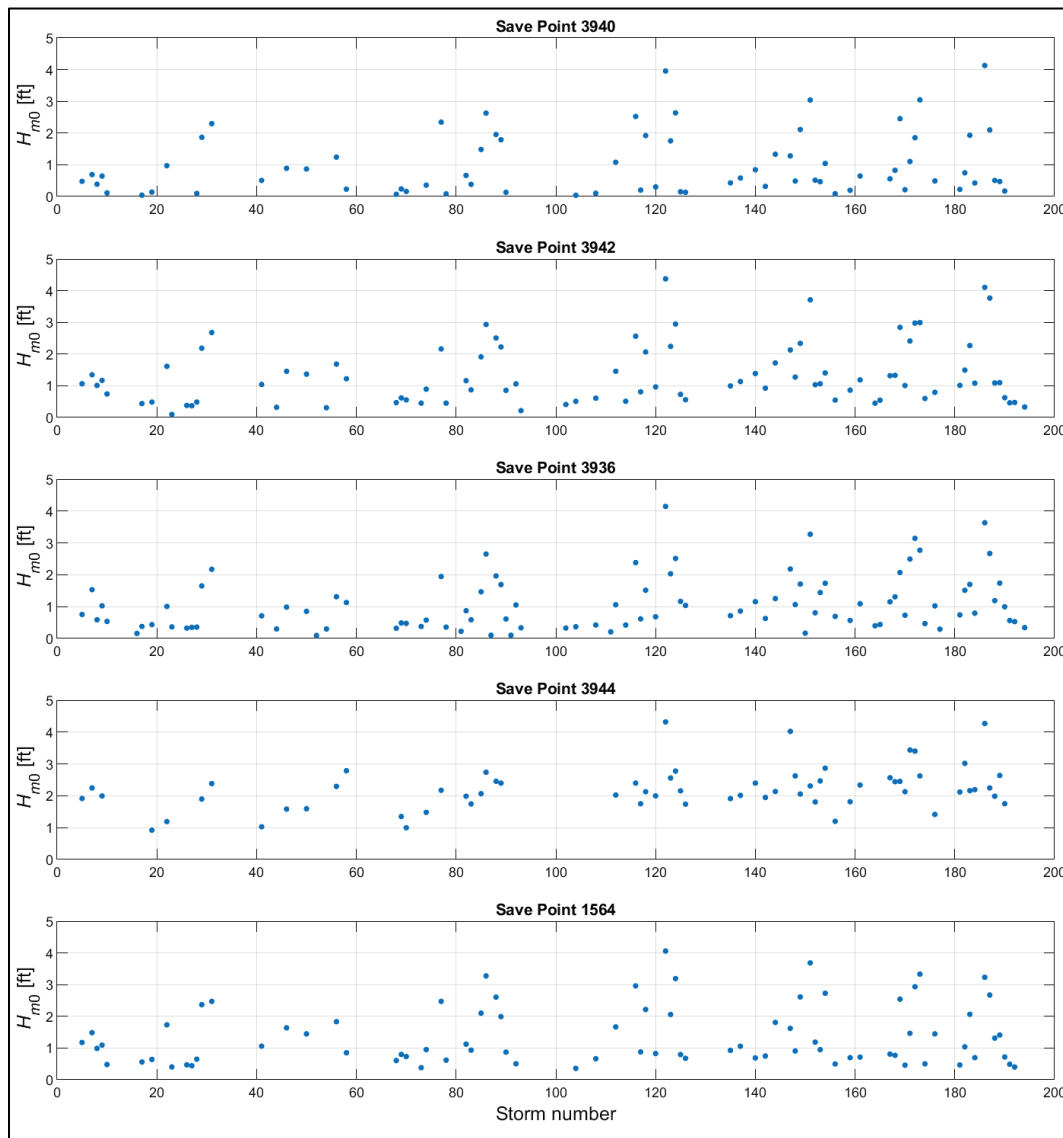
Parameter correlation

A simple correlation analysis was conducted using without-project SLC1 scenario. Two SPs were used: SP 1094 is in the center of Taylor's Bayou Turning Basin and always wet while SP 1564 is just seaward of transect 56 and is on dry land. Figure B-9 shows SWL versus H_{m0} in the top row for 1094 on left and 1564 on right and H_{m0} vs T_p in the bottom row for 1094 on left and 1564 on right. The correlation, as listed on the plots, suggests that the parameters are highly correlated with correlation higher for point 1564. This is probably due to greater depth dependency of the waves at point 1564 as a result of the water being shallow. This idea is confirmed in

Figure B-10 where Depth is plotted versus H_{m0}/Depth. Limited inter-
pretation can be done with this plot due to spurious correlation because
Depth is in both terms. At point 1094 on the left, it is deep water for the size
of the waves, so no depth-limited breaking occurs whereas at point 1564 on
the right there is depth-limited breaking for most storms. The effect of
correlation on overtopping is further described in Appendix F.

Figure B-9. SWL versus H_{m0} for S2G storm peaks for SP 1094 on left and 1564
on right.
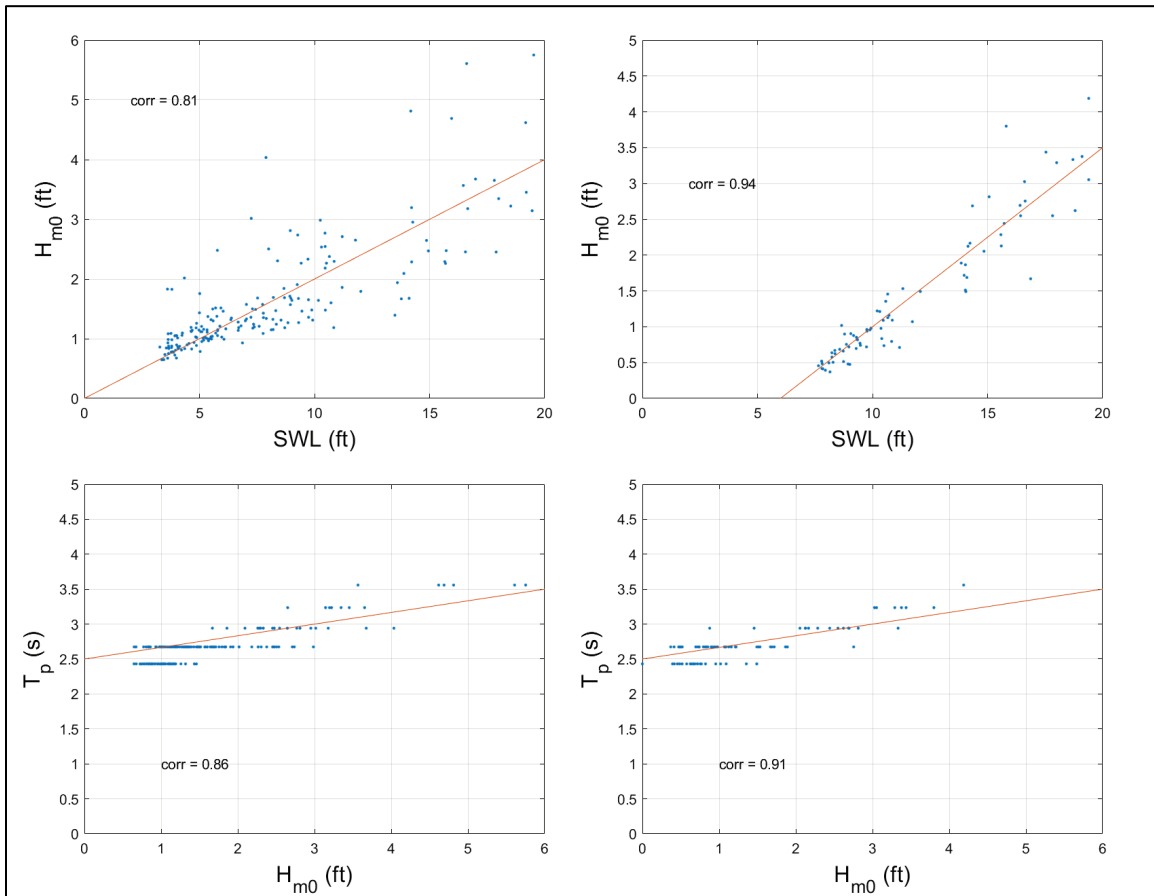
Figure B-10. Depth versus breaker parameter for S2G storm peaks for SP 1094 on left and 1564 on right.
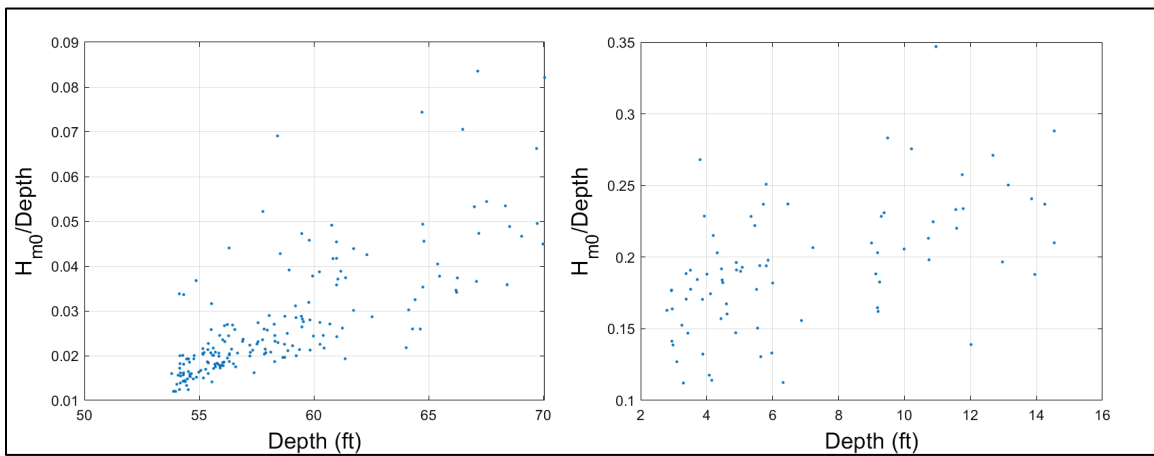
Appendix C: Storm Selection

Alex Taflanidis, PhD

University of Notre Dame

JPM-OS methods were adopted within the CTXCS to select the overall set of 660 tropical cyclones that spans the coast of Texas and neighboring regions that span the Texas coastal storm hazard. This set was reduced to 195 using a surrogate modeling approach as described herein in order to define a reduced suite of storms yet still match the SWL hazard curve. Consider an initial set of n_l storms with the lth storm having frequency weight (mean annual rate) of y_j^l for save point (SP) j. A total of n_j SPs are considered in the geographic domain of interest. The hazard curve for each SP is represented by the annual exceedance rate $\lambda_j(b)$ that the surge will exceed threshold b (considering different values of b), and is calculated as

$$\lambda_j(b) = \frac{1}{n_l} \sum_{l=1}^{n_l} \lambda_j^l I[y_j^l > b] \qquad (C.1)$$

where y_j^l denotes the surge at SP j for storm l and I is the indicator function corresponding to 1 if the quantity in the brackets is satisfied (else it is zero).

Consider now a subset of n_l' ($n_l' < n_l$) storms, with potentially adjusted rates $\lambda_j^{l'}$. The hazard curve is given by

$$\lambda_j'(b \mid \mathbf{s}) = \frac{1}{\sum_{l=1}^{n_l} s_l} \sum_{l=1}^{n_l} \lambda_j^{l'} I[y_j^l > b] s_l \qquad (C.2)$$

where s_l is an indicator index denoting whether storm belongs (s_l=1) or not (s_l=0) in the considered subset, and $\mathbf{s}$ is the n_l dimensional vector (vector of 1's and 0's) with components corresponding to s_l. Vector $\mathbf{s}$ uniquely defines the reduced subset of storms. The discrepancy between the original and adjusted hazard curves over a partitioning of the hazard curve $\{b_i=1,...,n_i\}$ is expressed as the weighted least squares

$$F(\mathbf{s}) = \sum_{j=1}^{n_j} \sum_{i=1}^{n_b} w_i (\lambda_j(b_i) - \lambda_j'(b_i \mid \mathbf{s}))^2 \qquad (\text{C.3})$$

where w_i is the weight for the discrepancy for threshold b_i, denoting the relative importance of the adjusted hazard curve matching the original one for that threshold. The partitioning of the hazard curve, i.e. selection of the threshold sequence $\{b_i=1,...,n_i\}$, is typically performed so that the sequence $\{b_i=i=1,...,n_i\}$ corresponds to specific rates of interest for the original hazard curve, that is, to specific values for $\lambda_j(b)$. The interior summation in Equation C.3 corresponds to calculation of the discrepancy of the hazard curves for each SP, considering the appropriate weights. The exterior summation corresponds to an averaging of this discrepancy over the desired group of SPs.

The optimal selection of the storms to belong in the adjusted set is then given by the optimization

$$\mathbf{s}^* = \underset{\mathbf{s} \in [0,1]^{n_l}}{\arg \min} F(\mathbf{s})$$
$$\text{such that } \sum_{l=1}^{n_l} s_l = n_l' \qquad (\text{C.4})$$

To address the computational challenges in Equation C.4 stemming from the fact that $\mathbf{s}$ includes binary variables (integer optimization), this problem is solved through genetic algorithms.

Hidden within the problem expressed through Equation C.4 is the subproblem of the selection of the adjusted rates $\lambda_j^{l'}$ and various implementations can be further distinguished based on the assumptions that range from (i) simply assigning the weights of the removed storms to the retained ones, maintaining proportionality of their relative likelihood, to (ii) explicitly optimizing the storm rates for a given $\mathbf{s}$. Implementation (i) leads to

$$\lambda_j^{l'} = s_l \lambda_j^l \frac{\displaystyle\sum_{l=1}^{n_l} \lambda_j^l}{\displaystyle\sum_{l=1}^{n_l} \lambda_j^l s_l} \qquad (\text{C.5})$$

which guarantees that the total rate for the retained storms is the same as the original

$$\sum_{l=1}^{n_l} \lambda_j^{l\,'} = \sum_{l=1}^{n_l} \lambda_j^{l} \tag{C.6}$$

and that the relative likelihood of each of the retained storms is the same as in the original set. Implementation (ii) corresponds to the optimization problem

$$[\lambda_j^{l\,'}]^* = \arg\min_{[\lambda_j^{l\,'}]} \sum_{i=1}^{n_b} w_i \, (\lambda_j(b_i) - \lambda_j^{'}(b_i \,|\, \mathbf{s}))^2 \tag{C.7}$$
$$\text{such that } \sum_{l=1}^{n_l} \lambda_j^{l\,'} = \sum_{l=1}^{n_l} \lambda_j^{l}$$

where $[\lambda_j^{l\,'}]$ denotes the vector composed of $\lambda_j^{l\,'}$ for the different storms.

Optimization of Equation C.7 identifies, for a given subset of storms, the optimal storm weights so that the hazard curve discrepancy is minimized for a specific SP. This implementation leads to a double loop optimization with the outer loop given by Equation C.4 and the inner loop, solved for every new $\mathbf{s}$ examined for the outer loop, given by Equation C.7. For this study, the optimization in Equation C.7 was employed using the genetic algorithm tool in Matlab.

Appendix D: Historical and Synthetic Tropical Cyclones

JPM-OS methodology is described in Appendix A. In this approach, historical tropical storms from 1938 to 2017 from the HURDAT2 database that impacted the Texas coastline were extracted. These storms are tropical cyclones and well parameterized by track (heading θ, landfall location), intensity (minimum central pressure, P), size (radius to maximum winds, R_{max}) and forward speed (V_r). Central pressure is further defined according to the deficit from far-field atmospheric pressure, $\Delta P = 1013$ mb - P_{min}. The historical tropical cyclones that impacted Texas are listed in Table D-1. The events that significantly impacted Freeport or Sabine areas are noted. A joint probability model of the tropical storm parameters was constructed and discretized to develop a suite of synthetic tropical storms that defines the entire hazard from low-intensity frequent storms to high-intensity very infrequent storms[1]. The upper limit of the storms extends beyond all historical events but only to reasonable extremes. The final storm list of 660 storms with track landfalls extending over the entire Texas coast and from well into Mexico to Florida is provided in Table D-2 for the Coastal Texas Study. Table D-3 provides a reduced list of 195 S2G storms that are a subset of the 660 storms and were determined to be optimal for SWL and overtopping hazard for the region spanning Freeport, Port Arthur, and Orange County.

---

[1] Nadal-Caraballo, N. C., A. B. Lewis, V. M. Gonzalez, T. C. Massey, and A. T. Cox. Draft. *Coastal Texas Protection and Restoration Feasibility Study, Probabilistic Modeling of Coastal Storm Hazards.* Unpublished. ERDC/CHL Technical Report. Vicksburg, MS: US Army Engineer Research and Development Center.

Table D-1. List of select historical TCs affecting the Coastal Texas study region.

Year	NHC ID	TC Name	Maximum Wind Speed (km/h)	Minimum Central Pressure (hPa)	Impact Freeport (F) or Sabine (S)
1938	3	UNNAMED	157	969	
1938	7	UNNAMED	93	996	
1940	2	UNNAMED	157	975	
1940	6	UNNAMED	83	999	S
1941	1	UNNAMED	93	996	
1941	2	UNNAMED	204	953	F
1942	2	UNNAMED	130	983	
1942	3	UNNAMED	185	962	
1943	1	UNNAMED	167	971	
1943	6	UNNAMED	157	972	
1944	5	UNNAMED	93	996	
1945	2	UNNAMED	65	1004	
1945	5	UNNAMED	185	962	F
1946	1	UNNAMED	65	1004	
1947	1	UNNAMED	83	999	
1947	3	UNNAMED	130	983	F
1949	11	UNNAMED	176	967	F
1950	8	HOW	74	1002	
1954	3	ALICE	176	967	
1954	5	BARBARA	93	997	
1955	5	UNNAMED	83	999	
1957	2	AUDREY	204	953	S
1957	3	BERTHA	102	994	
1958	1	ALMA	102	994	
1958	5	ELLA	176	969	
1958	7	GERDA	93	999	
1959	5	DEBRA	139	982	F
1960	1	UNNAMED	93	996	
1961	3	CARLA	278	909	SF
1963	4	CINDY	130	983	

Year	NHC ID	TC Name	Maximum Wind Speed (km/h)	Minimum Central Pressure (hPa)	Impact Freeport (F) or Sabine (S)
1964	3	ABBY	102	994	
1967	13	BEULAH	259	922	
1968	3	CANDY	111	992	
1970	4	CELIA	204	953	
1970	13	FELICE	111	992	
1971	11	FERN	148	976	
1971	13	EDITH	259	922	
1973	10	DELIA	111	990	
1975	7	CAROLINE	185	962	
1977	5	ANITA	278	909	
1978	4	AMELIA	83	999	
1978	9	DEBRA	93	997	
1979	6	CLAUDETTE	83	999	
1979	12	ELENA	65	1004	
1980	4	ALLEN	306	889	
1980	11	DANIELLE	93	997	
1980	16	JEANNE	157	975	
1982	5	CHRIS	102	994	
1983	3	ALICIA	185	962	SF
1983	4	BARRY	130	985	
1985	4	DANNY	148	979	
1985	12	JUAN	139	980	
1986	2	BONNIE	139	982	S
1987	3	UNNAMED	74	1002	
1988	2	BERYL	83	999	
1989	2	ALLISON	83	1000	
1989	4	CHANTAL	130	985	S
1989	14	JERRY	139	982	SF
1993	2	ARLENE	65	1004	
1995	4	DEAN	74	1002	
1998	3	CHARLEY	111	992	

Year	NHC ID	TC Name	Maximum Wind Speed (km/h)	Minimum Central Pressure (hPa)	Impact Freeport (F) or Sabine (S)
1998	6	FRANCES	102	994	
1999	3	BRET	232	937	
2000	5	BERYL	83	1000	
2001	1	ALLISON	93	996	
2002	6	FAY	93	997	
2002	13	LILI	232	938	
2003	4	CLAUDETTE	148	979	
2003	8	ERIKA	120	989	
2003	11	GRACE	65	1004	
2004	9	IVAN	269	917	
2005	5	EMILY	259	925	
2005	18	RITA	287	903	S
2007	5	ERIN	93	997	
2007	9	HUMBERTO	148	979	S
2008	4	DOLLY	157	975	
2008	5	EDOUARD	102	994	
2008	9	IKE	232	935	SF
2010	1	ALEX	176	967	
2010	10	HERMINE	111	990	
2011	4	DON	83	1000	
2011	13	LEE	93	996	
2015	2	BILL	93	997	
2017	3	CINDY	93	996	
2017	9	HARVEY	176	967	S

Table D-2. List of 660 storms for CTXCS that provided the basis for which storms were sampled. Cells are colored alternating blue and gray by Master Track group, for readability.

Storm Number	Texas Region	Master Track	Θ (deg)	ΔP(hPa)	R_{max} (km)	V_f (km/h)
1	2	1	-100	148	19.7	9.5
2	2	1	-100	128	19.4	30.9
3	2	1	-100	108	12.7	20.1
4	2	1	-100	88	74.7	15.3
5	2	1	-100	68	33.1	12.2
6	2	1	-100	48	14.9	33.7
7	2	1	-100	28	82.1	20.0
8	2	1	-100	8	22.6	10.6
9	2	2	-100	148	11.9	10.0
10	2	2	-100	128	33.9	38.3
11	2	2	-100	108	20.9	12.9
12	2	2	-100	88	9.1	19.8
13	2	2	-100	68	64.6	31.5
14	2	2	-100	48	95.6	11.2
15	2	2	-100	28	49.2	23.2
16	2	2	-100	8	18.4	9.3
17	2	3	-100	148	23.0	10.6
18	2	3	-100	128	29.2	23.0
19	2	3	-100	108	8.0	18.9
20	2	3	-100	88	16.8	8.0
21	2	3	-100	68	25.4	29.2
22	2	3	-100	48	70.5	19.2
23	2	3	-100	28	126.7	21.8
24	2	3	-100	8	42.2	11.4
25	2	4	-100	148	18.2	28.3
26	2	4	-100	128	8.5	11.5
27	2	4	-100	108	59.2	14.5
28	2	4	-100	88	46.0	15.8
29	2	4	-100	68	48.9	8.0
30	2	4	-100	48	44.4	20.3
31	2	4	-100	28	19.7	20.6
32	2	4	-100	8	86.6	29.6
33	2	5	-100	148	10.4	11.1
34	2	5	-100	128	24.1	21.0
35	2	5	-100	108	31.6	8.0
36	2	5	-100	88	20.2	27.8

Storm Number	Texas Region	Master Track	Θ (deg)	ΔP(hPa)	R_{max} (km)	V_f (km/h)
37	2	5	-100	68	73.3	13.2
38	2	5	-100	48	53.0	20.9
39	2	5	-100	28	9.9	9.8
40	2	5	-100	8	119.2	35.9
41	2	6	-100	148	13.2	18.2
42	2	6	-100	128	9.5	23.8
43	2	6	-100	108	22.7	22.7
44	2	6	-100	88	58.3	13.8
45	2	6	-100	68	70.2	9.8
46	2	6	-100	48	23.7	9.3
47	2	6	-100	28	64.1	34.6
48	2	6	-100	8	20.5	24.2
49	2	7	-100	148	8.6	32.6
50	2	7	-100	128	21.3	26.1
51	2	7	-100	108	19.2	10.4
52	2	7	-100	88	47.8	24.4
53	2	7	-100	68	15.1	18.3
54	2	7	-100	48	106.3	15.4
55	2	7	-100	28	58.9	11.1
56	2	7	-100	8	35.5	24.9
57	2	8	-100	148	27.3	44.6
58	2	8	-100	128	14.8	17.9
59	2	8	-100	108	37.7	9.5
60	2	8	-100	88	23.7	14.3
61	2	8	-100	68	10.8	30.3
62	2	8	-100	48	91.2	28.7
63	2	8	-100	28	44.7	23.9
64	2	8	-100	8	79.7	19.1
65	1	9	-100	148	12.5	25.7
66	1	9	-100	128	44.5	24.5
67	1	9	-100	108	15.9	30.3
68	1	9	-100	88	26.1	12.8
69	1	9	-100	68	8.0	24.8
70	1	9	-100	48	87.1	12.6
71	1	9	-100	28	69.7	29.1
72	1	9	-100	8	12.1	17.0
73	1	10	-100	148	14.9	8.0
74	1	10	-100	128	17.0	26.9
75	1	10	-100	108	8.8	15.0

Storm Number	Texas Region	Master Track	Θ (deg)	ΔP(hPa)	R_{max} (km)	V_f (km/h)
76	1	10	-100	88	70.5	14.8
77	1	10	-100	68	41.5	22.6
78	1	10	-100	48	34.6	19.7
79	1	10	-100	28	85.6	17.8
80	1	10	-100	8	37.7	11.0
81	2	11	-80	138	15.4	23.9
82	2	11	-80	118	19.3	13.0
83	2	11	-80	98	40.4	26.3
84	2	11	-80	78	79.8	10.3
85	2	11	-80	58	12.7	31.2
86	2	11	-80	38	30.6	10.7
87	2	11	-80	18	101.0	25.2
88	2	12	-80	138	33.8	14.2
89	2	12	-80	118	31.2	23.6
90	2	12	-80	98	14.6	13.4
91	2	12	-80	78	19.4	18.5
92	2	12	-80	58	27.3	34.0
93	2	12	-80	38	107.3	24.9
94	2	12	-80	18	58.2	8.9
95	2	13	-80	138	25.2	32.3
96	2	13	-80	118	16.5	22.2
97	2	13	-80	98	11.7	13.9
98	2	13	-80	78	40.9	20.8
99	2	13	-80	58	35.9	10.3
100	2	13	-80	38	97.2	25.7
101	2	13	-80	18	20.2	30.0
102	2	14	-80	138	14.5	38.7
103	2	14	-80	118	17.9	17.3
104	2	14	-80	98	37.5	9.4
105	2	14	-80	78	90.6	15.2
106	2	14	-80	58	17.5	16.1
107	2	14	-80	38	66.4	26.5
108	2	14	-80	18	53.2	19.3
109	2	15	-80	138	24.4	8.0
110	2	15	-80	118	23.0	24.3
111	2	15	-80	98	15.5	14.4
112	2	15	-80	78	30.3	8.0
113	2	15	-80	58	60.3	11.7
114	2	15	-80	38	81.6	22.0

Storm Number	Texas Region	Master Track	Θ (deg)	ΔP(hPa)	R_{max} (km)	V_f (km/h)
115	2	15	-80	18	12.0	12.4
116	2	16	-80	138	11.6	19.3
117	2	16	-80	118	40.5	8.0
118	2	16	-80	98	8.0	16.5
119	2	16	-80	78	20.7	36.5
120	2	16	-80	58	68.0	23.1
121	2	16	-80	38	56.2	15.8
122	2	16	-80	18	30.6	15.6
123	2	17	-80	138	30.5	19.9
124	2	17	-80	118	20.0	10.5
125	2	17	-80	98	28.9	27.1
126	2	17	-80	78	11.8	25.0
127	2	17	-80	58	45.2	35.8
128	2	17	-80	38	120.5	13.0
129	2	17	-80	18	48.4	12.8
130	2	18	-80	138	19.9	22.5
131	2	18	-80	118	8.0	19.6
132	2	18	-80	98	26.6	9.9
133	2	18	-80	78	24.7	33.2
134	2	18	-80	58	62.8	19.9
135	2	18	-80	38	32.5	18.5
136	2	18	-80	18	92.5	16.6
137	2	19	-80	138	12.4	33.7
138	2	19	-80	118	23.8	15.6
139	2	19	-80	98	69.3	23.2
140	2	19	-80	78	9.3	11.8
141	2	19	-80	58	47.2	8.9
142	2	19	-80	38	38.6	22.7
143	2	19	-80	18	60.8	26.9
144	1	20	-80	138	15.9	10.0
145	1	20	-80	118	14.5	27.6
146	1	20	-80	98	58.2	33.8
147	1	20	-80	78	34.6	21.5
148	1	20	-80	58	39.5	8.0
149	1	20	-80	38	72.1	23.4
150	1	20	-80	18	8.0	10.6
151	1	21	-80	138	21.0	15.2
152	1	21	-80	118	13.1	9.0
153	1	21	-80	98	53.1	8.0

Storm Number	Texas Region	Master Track	Θ (deg)	ΔP(hPa)	R_{max} (km)	V_f (km/h)
154	1	21	-80	78	58.1	19.0
155	1	21	-80	58	20.7	15.0
156	1	21	-80	38	44.9	19.0
157	1	21	-80	18	78.2	9.3
158	1	22	-80	138	12.0	20.5
159	1	22	-80	118	42.3	8.5
160	1	22	-80	98	8.9	15.9
161	1	22	-80	78	22.1	38.7
162	1	22	-80	58	70.9	23.8
163	1	22	-80	38	58.7	16.3
164	1	22	-80	18	32.7	16.1
165	1	23	-80	138	10.0	15.8
166	1	23	-80	118	9.3	14.0
167	1	23	-80	98	48.9	17.0
168	1	23	-80	78	31.7	30.6
169	1	23	-80	58	55.6	16.6
170	1	23	-80	38	11.7	14.9
171	1	23	-80	18	41.5	8.0
172	2	24	-60	148	23.8	11.6
173	2	24	-60	128	10.0	32.1
174	2	24	-60	108	30.5	42.9
175	2	24	-60	88	41.0	23.0
176	2	24	-60	68	19.5	12.7
177	2	24	-60	48	100.6	11.6
178	2	24	-60	28	46.9	18.3
179	2	24	-60	8	51.7	15.0
180	2	25	-60	148	15.3	17.0
181	2	25	-60	128	22.6	28.8
182	2	25	-60	108	14.3	27.4
183	2	25	-60	88	79.8	18.6
184	2	25	-60	68	18.0	15.1
185	2	25	-60	48	73.5	32.2
186	2	25	-60	28	66.8	10.2
187	2	25	-60	8	49.3	25.8
188	2	26	-60	148	8.3	30.3
189	2	26	-60	128	22.0	10.5
190	2	26	-60	108	20.1	19.5
191	2	26	-60	88	31.1	35.0
192	2	26	-60	68	22.4	15.6

Storm Number	Texas Region	Master Track	Θ (deg)	ΔP(hPa)	R_{max} (km)	V_f (km/h)
193	2	26	-60	48	112.9	15.9
194	2	26	-60	28	89.4	18.9
195	2	26	-60	8	26.8	15.5
196	2	27	-60	148	20.3	24.9
197	2	27	-60	128	13.7	40.7
198	2	27	-60	108	35.1	28.3
199	2	27	-60	88	21.4	8.9
200	2	27	-60	68	89.1	13.6
201	2	27	-60	48	67.7	13.5
202	2	27	-60	28	11.9	14.8
203	2	27	-60	8	59.3	30.9
204	2	28	-60	148	15.7	9.0
205	2	28	-60	128	12.6	21.7
206	2	28	-60	108	43.8	24.9
207	2	28	-60	88	27.3	36.9
208	2	28	-60	68	59.7	18.9
209	2	28	-60	48	40.4	16.5
210	2	28	-60	28	107.2	11.5
211	2	28	-60	8	8.0	11.9
212	2	29	-60	148	25.9	20.7
213	2	29	-60	128	15.9	18.5
214	2	29	-60	108	45.7	8.5
215	2	29	-60	88	13.5	28.7
216	2	29	-60	68	38.1	19.5
217	2	29	-60	48	16.6	8.4
218	2	29	-60	28	97.6	12.9
219	2	29	-60	8	67.5	22.8
220	2	30	-60	148	10.7	31.4
221	2	30	-60	128	26.5	12.0
222	2	30	-60	108	25.4	15.5
223	2	30	-60	88	38.0	39.1
224	2	30	-60	68	110.1	14.6
225	2	30	-60	48	13.2	22.2
226	2	30	-60	28	29.8	12.0
227	2	30	-60	8	76.5	27.5
228	2	31	-60	148	16.1	8.5
229	2	31	-60	128	24.9	16.2
230	2	31	-60	108	36.3	35.7
231	2	31	-60	88	35.2	10.4

Storm Number	Texas Region	Master Track	Θ (deg)	ΔP(hPa)	R_{max} (km)	V_f (km/h)
232	2	31	-60	68	16.6	23.3
233	2	31	-60	48	21.9	35.4
234	2	31	-60	28	54.0	15.2
235	2	31	-60	8	156.4	17.5
236	2	32	-60	148	17.3	14.2
237	2	32	-60	128	11.6	19.1
238	2	32	-60	108	55.5	24.1
239	2	32	-60	88	39.5	9.9
240	2	32	-60	68	43.3	32.8
241	2	32	-60	48	29.0	22.9
242	2	32	-60	28	27.7	13.3
243	2	32	-60	8	103.0	9.7
244	1	33	-60	148	20.9	34.0
245	1	33	-60	128	23.4	15.2
246	1	33	-60	108	9.6	16.6
247	1	33	-60	88	53.7	8.5
248	1	33	-60	68	23.9	8.5
249	1	33	-60	48	36.5	27.7
250	1	33	-60	28	102.2	30.3
251	1	33	-60	8	54.2	12.3
252	1	34	-60	148	13.5	12.6
253	1	34	-60	128	20.6	29.8
254	1	34	-60	108	10.3	23.4
255	1	34	-60	88	32.5	26.0
256	1	34	-60	68	67.3	8.9
257	1	34	-60	48	131.7	24.3
258	1	34	-60	28	42.5	13.8
259	1	34	-60	8	44.5	28.5
260	1	35	-60	148	13.9	19.4
261	1	35	-60	128	25.6	17.4
262	1	35	-60	108	28.4	10.9
263	1	35	-60	88	10.2	16.9
264	1	35	-60	68	94.6	21.9
265	1	35	-60	48	46.5	25.1
266	1	35	-60	28	51.6	8.0
267	1	35	-60	8	62.0	13.2
268	1	36	-60	148	17.7	12.1
269	1	36	-60	128	10.5	19.7
270	1	36	-60	108	29.4	13.9

Storm Number	Texas Region	Master Track	Θ (deg)	ΔP(hPa)	R_{max} (km)	V_f (km/h)
271	1	36	-60	88	42.6	42.0
272	1	36	-60	68	28.4	26.4
273	1	36	-60	48	30.9	23.6
274	1	36	-60	28	148.0	15.7
275	1	36	-60	8	16.3	12.8
276	1	37	-60	148	11.6	13.2
277	1	37	-60	128	39.0	10.0
278	1	37	-60	108	27.4	29.3
279	1	37	-60	88	12.4	30.9
280	1	37	-60	68	50.9	27.3
281	1	37	-60	48	11.4	9.8
282	1	37	-60	28	119.2	19.4
283	1	37	-60	8	24.7	18.0
284	2	38	-40	138	10.4	16.3
285	2	38	-40	118	9.9	16.1
286	2	38	-40	98	50.9	17.6
287	2	38	-40	78	33.1	31.8
288	2	38	-40	58	57.9	17.1
289	2	38	-40	38	13.5	15.3
290	2	38	-40	18	43.8	8.4
291	2	39	-40	138	16.3	10.5
292	2	39	-40	118	15.1	28.5
293	2	39	-40	98	61.3	28.0
294	2	39	-40	78	36.1	22.1
295	2	39	-40	58	41.4	8.5
296	2	39	-40	38	75.1	19.6
297	2	39	-40	18	10.0	11.0
298	2	40	-40	138	18.3	9.0
299	2	40	-40	118	26.4	34.5
300	2	40	-40	98	9.9	21.2
301	2	40	-40	78	63.1	16.3
302	2	40	-40	58	32.4	26.1
303	2	40	-40	38	24.8	8.9
304	2	40	-40	18	81.5	18.2
305	2	41	-40	138	8.0	12.6
306	2	41	-40	118	49.9	11.0
307	2	41	-40	98	30.0	39.5
308	2	41	-40	78	51.7	13.2
309	2	41	-40	58	24.0	12.1

Storm Number	Texas Region	Master Track	Θ (deg)	ΔP(hPa)	R_{max} (km)	V_f (km/h)
310	2	41	-40	38	19.1	33.3
311	2	41	-40	18	140.8	19.8
312	2	42	-40	138	21.7	24.7
313	2	42	-40	118	10.6	20.2
314	2	42	-40	98	41.9	10.4
315	2	42	-40	78	37.7	22.8
316	2	42	-40	58	98.1	21.1
317	2	42	-40	38	15.4	12.0
318	2	42	-40	18	34.9	36.3
319	2	43	-40	138	10.8	16.9
320	2	43	-40	118	37.3	29.5
321	2	43	-40	98	17.5	24.6
322	2	43	-40	78	46.0	8.5
323	2	43	-40	58	88.3	14.1
324	2	43	-40	38	61.2	30.6
325	2	43	-40	18	16.1	13.3
326	2	44	-40	138	8.8	44.2
327	2	44	-40	118	44.4	12.5
328	2	44	-40	98	21.4	19.3
329	2	44	-40	78	8.0	26.6
330	2	44	-40	58	77.1	30.0
331	2	44	-40	38	26.7	13.4
332	2	44	-40	18	111.0	21.6
333	2	45	-40	138	26.1	29.0
334	2	45	-40	118	11.8	31.8
335	2	45	-40	98	22.4	11.9
336	2	45	-40	78	27.5	13.7
337	2	45	-40	58	80.5	12.6
338	2	45	-40	38	85.1	37.1
339	2	45	-40	18	24.3	22.3
340	1	46	-40	138	12.8	35.1
341	1	46	-40	118	24.7	16.7
342	1	46	-40	98	75.0	23.9
343	1	46	-40	78	10.5	12.3
344	1	46	-40	58	49.2	9.4
345	1	46	-40	38	40.7	24.1
346	1	46	-40	18	63.5	27.8
347	1	47	-40	138	32.0	21.2
348	1	47	-40	118	20.7	10.0

Storm Number	Texas Region	Master Track	Θ (deg)	ΔP (hPa)	R_{max} (km)	V_f (km/h)
349	1	47	-40	98	31.2	29.0
350	1	47	-40	78	13.0	25.8
351	1	47	-40	58	51.3	37.9
352	1	47	-40	38	129.2	13.9
353	1	47	-40	18	50.8	13.7
354	1	48	-40	138	15.0	41.1
355	1	48	-40	118	18.6	17.8
356	1	48	-40	98	38.9	10.9
357	1	48	-40	78	98.4	15.7
358	1	48	-40	58	19.1	17.6
359	1	48	-40	38	69.2	27.4
360	1	48	-40	18	55.7	20.4
361	1	49	-40	138	20.5	23.2
362	1	49	-40	118	8.6	20.8
363	1	49	-40	98	27.7	11.4
364	1	49	-40	78	26.1	34.7
365	1	49	-40	58	65.3	20.5
366	1	49	-40	38	34.5	20.2
367	1	49	-40	18	96.6	17.1
368	1	50	-40	138	27.0	30.1
369	1	50	-40	118	15.8	18.4
370	1	50	-40	98	20.4	30.0
371	1	50	-40	78	42.5	9.4
372	1	50	-40	58	43.3	9.8
373	1	50	-40	38	140.7	16.9
374	1	50	-40	18	46.1	31.2
375	1	51	-40	138	8.4	13.1
376	1	51	-40	118	53.8	11.5
377	1	51	-40	98	32.4	42.5
378	1	51	-40	78	53.7	14.2
379	1	51	-40	58	25.6	13.1
380	1	51	-40	38	21.0	35.0
381	1	51	-40	18	153.3	21.0
382	1	52	-40	138	13.2	25.5
383	1	52	-40	118	29.1	14.5
384	1	52	-40	98	33.6	35.4
385	1	52	-40	78	72.1	16.8
386	1	52	-40	58	9.6	18.2
387	1	52	-40	38	49.3	9.8

Storm Number	Texas Region	Master Track	Θ (deg)	ΔP(hPa)	R_{max} (km)	V_f (km/h)
388	1	52	-40	18	66.3	23.7
389	2	53	-20	148	8.9	17.6
390	2	53	-20	128	35.4	9.0
391	2	53	-20	108	40.6	32.7
392	2	53	-20	88	15.7	26.9
393	2	53	-20	68	34.8	20.1
394	2	53	-20	48	55.2	14.0
395	2	53	-20	28	21.7	8.4
396	2	53	-20	8	133.9	19.7
397	2	54	-20	148	16.5	14.8
398	2	54	-20	128	8.0	16.8
399	2	54	-20	108	15.1	37.6
400	2	54	-20	88	51.6	25.2
401	2	54	-20	68	45.1	34.3
402	2	54	-20	48	62.5	10.3
403	2	54	-20	28	93.3	8.9
404	2	54	-20	8	14.2	18.6
405	2	55	-20	148	12.9	37.1
406	2	55	-20	128	20.0	12.5
407	2	55	-20	108	47.7	39.9
408	2	55	-20	88	33.8	23.7
409	2	55	-20	68	12.3	17.2
410	2	55	-20	48	25.4	29.7
411	2	55	-20	28	112.8	16.2
412	2	55	-20	8	39.9	20.2
413	2	56	-20	148	18.7	15.3
414	2	56	-20	128	32.6	43.8
415	2	56	-20	108	13.5	26.5
416	2	56	-20	88	24.9	20.4
417	2	56	-20	68	76.7	20.7
418	2	56	-20	48	79.9	8.0
419	2	56	-20	28	75.6	24.6
420	2	56	-20	8	10.1	16.0
421	2	57	-20	148	14.2	21.3
422	2	57	-20	128	37.0	9.5
423	2	57	-20	108	39.1	34.1
424	2	57	-20	88	14.6	21.0
425	2	57	-20	68	53.0	16.2
426	2	57	-20	48	18.4	8.9

Storm Number	Texas Region	Master Track	Θ (deg)	ΔP(hPa)	R_{max} (km)	V_f (km/h)
427	2	57	-20	28	36.0	36.7
428	2	57	-20	8	143.6	20.8
429	1	58	-20	148	8.0	20.0
430	1	58	-20	128	30.3	15.7
431	1	58	-20	108	16.7	9.9
432	1	58	-20	88	17.9	21.6
433	1	58	-20	68	30.0	38.3
434	1	58	-20	48	76.6	17.0
435	1	58	-20	28	38.1	10.6
436	1	58	-20	8	125.9	33.9
437	1	59	-20	148	16.9	26.5
438	1	59	-20	128	9.0	20.4
439	1	59	-20	108	26.4	11.9
440	1	59	-20	88	60.9	13.3
441	1	59	-20	68	26.9	11.3
442	1	59	-20	48	83.3	40.3
443	1	59	-20	28	23.7	31.5
444	1	59	-20	8	64.7	16.5
445	1	60	-20	148	9.2	27.4
446	1	60	-20	128	13.1	13.0
447	1	60	-20	108	64.0	16.0
448	1	60	-20	88	36.6	9.4
449	1	60	-20	68	62.1	36.1
450	1	60	-20	48	57.6	17.5
451	1	60	-20	28	33.9	16.7
452	1	60	-20	8	107.8	14.6
453	1	61	-20	148	21.5	15.9
454	1	61	-20	128	14.2	33.3
455	1	61	-20	108	18.4	17.1
456	1	61	-20	88	63.7	10.9
457	1	61	-20	68	9.4	16.7
458	1	61	-20	48	38.4	18.0
459	1	61	-20	28	78.8	27.1
460	1	61	-20	8	28.9	8.0
461	1	62	-20	148	29.1	22.0
462	1	62	-20	128	16.4	22.3
463	1	62	-20	108	11.1	20.7
464	1	62	-20	88	66.9	17.5
465	1	62	-20	68	31.5	28.2

Storm Number	Texas Region	Master Track	Θ (deg)	ΔP(hPa)	R_{max} (km)	V_f (km/h)
466	1	62	-20	48	60.0	12.1
467	1	62	-20	28	17.8	21.2
468	1	62	-20	8	70.4	38.5
469	1	63	-20	148	9.5	39.1
470	1	63	-20	128	27.3	34.8
471	1	63	-20	108	23.6	12.4
472	1	63	-20	88	86.6	11.3
473	1	63	-20	68	20.9	11.7
474	1	63	-20	48	65.1	25.9
475	1	63	-20	28	15.8	22.5
476	1	63	-20	8	56.7	8.4
477	1	64	-20	148	9.8	22.7
478	1	64	-20	128	41.4	13.6
479	1	64	-20	108	17.5	9.0
480	1	64	-20	88	44.3	29.8
481	1	64	-20	68	101.3	17.8
482	1	64	-20	48	48.6	21.6
483	1	64	-20	28	13.9	25.4
484	1	64	-20	8	73.4	10.1
485	1	65	-20	148	11.0	23.4
486	1	65	-20	128	31.4	11.0
487	1	65	-20	108	33.9	25.7
488	1	65	-20	88	29.9	22.3
489	1	65	-20	68	84.5	10.3
490	1	65	-20	48	42.4	10.7
491	1	65	-20	28	8.0	28.1
492	1	65	-20	8	90.3	26.6
493	2	66	0	138	22.3	17.5
494	2	66	0	118	13.8	9.5
495	2	66	0	98	55.5	8.5
496	2	66	0	78	60.5	19.6
497	2	66	0	58	22.3	15.5
498	2	66	0	38	47.1	20.8
499	2	66	0	18	85.0	9.7
500	2	67	0	138	17.3	11.0
501	2	67	0	118	33.4	40.3
502	2	67	0	98	23.5	19.9
503	2	67	0	78	15.6	27.5
504	2	67	0	58	111.5	24.6

Storm Number	Texas Region	Master Track	Θ (deg)	ΔP(hPa)	R_{max} (km)	V_f (km/h)
505	2	67	0	38	8.0	17.4
506	2	67	0	18	116.8	11.5
507	2	68	0	138	13.7	26.3
508	2	68	0	118	30.1	15.1
509	2	68	0	98	34.9	37.2
510	2	68	0	78	75.7	17.3
511	2	68	0	58	11.2	18.7
512	2	68	0	38	51.5	10.2
513	2	68	0	18	69.1	24.4
514	1	69	0	138	28.0	36.8
515	1	69	0	118	17.2	22.9
516	1	69	0	98	12.7	14.9
517	1	69	0	78	44.2	23.5
518	1	69	0	58	37.7	10.7
519	1	69	0	38	102.0	28.4
520	1	69	0	18	22.2	32.6
521	1	70	0	138	23.0	27.2
522	1	70	0	118	11.2	19.0
523	1	70	0	98	43.5	9.0
524	1	70	0	78	39.3	24.2
525	1	70	0	58	104.1	21.8
526	1	70	0	38	17.3	12.5
527	1	70	0	18	37.1	39.0
528	1	71	0	138	17.8	11.5
529	1	71	0	118	34.6	43.3
530	1	71	0	98	24.5	20.5
531	1	71	0	78	16.9	28.5
532	1	71	0	58	121.3	25.3
533	1	71	0	38	9.8	17.9
534	1	71	0	18	123.5	11.9
535	1	72	0	138	9.6	18.1
536	1	72	0	118	27.3	21.5
537	1	72	0	98	64.9	18.7
538	1	72	0	78	47.8	29.5
539	1	72	0	58	14.3	19.3
540	1	72	0	38	53.9	8.4
541	1	72	0	18	75.1	34.3
542	1	73	0	138	9.2	13.6
543	1	73	0	118	46.9	25.1

Storm Number	Texas Region	Master Track	Θ (deg)	ΔP(hPa)	R_{max} (km)	V_f (km/h)
544	1	73	0	98	36.2	31.2
545	1	73	0	78	68.8	9.9
546	1	73	0	58	8.0	27.0
547	1	73	0	38	22.9	8.0
548	1	73	0	18	39.3	14.2
549	1	74	0	138	29.2	31.2
550	1	74	0	118	12.5	33.0
551	1	74	0	98	25.6	12.4
552	1	74	0	78	28.8	14.7
553	1	74	0	58	84.2	13.6
554	1	74	0	38	88.8	39.9
555	1	74	0	18	26.4	23.0
556	1	75	0	138	18.8	9.5
557	1	75	0	118	28.2	36.1
558	1	75	0	98	10.8	21.8
559	1	75	0	78	65.8	17.9
560	1	75	0	58	34.1	27.9
561	1	75	0	38	28.6	9.3
562	1	75	0	18	88.6	18.7
563	1	76	0	138	11.2	18.7
564	1	76	0	118	38.8	30.6
565	1	76	0	98	18.4	25.4
566	1	76	0	78	49.7	8.9
567	1	76	0	58	92.9	14.5
568	1	76	0	38	63.8	31.9
569	1	76	0	18	18.1	14.7
570	2	77	20	148	19.2	35.4
571	2	77	20	128	11.1	14.1
572	2	77	20	108	21.8	17.7
573	2	77	20	88	55.9	18.0
574	2	77	20	68	47.0	10.8
575	2	77	20	48	20.1	18.6
576	2	77	20	28	25.7	39.4
577	2	77	20	8	94.3	23.5
578	1	78	20	148	22.2	41.5
579	1	78	20	128	15.3	8.0
580	1	78	20	108	42.1	13.4
581	1	78	20	88	8.0	19.2
582	1	78	20	68	39.8	21.3

Storm Number	Texas Region	Master Track	Θ (deg)	ΔP(hPa)	R_{max} (km)	V_f (km/h)
583	1	78	20	48	50.7	30.9
584	1	78	20	28	31.8	9.3
585	1	78	20	8	113.2	13.7
586	1	79	20	148	12.2	24.1
587	1	79	20	128	17.6	14.6
588	1	79	20	108	11.9	31.5
589	1	79	20	88	49.6	33.5
590	1	79	20	68	36.4	9.4
591	1	79	20	48	9.7	26.8
592	1	79	20	28	135.9	14.3
593	1	79	20	8	31.1	22.1
594	1	80	20	148	11.3	16.4
595	1	80	20	128	28.3	36.4
596	1	80	20	108	24.5	11.4
597	1	80	20	88	19.1	32.1
598	1	80	20	68	80.4	24.0
599	1	80	20	48	8.0	13.0
600	1	80	20	28	56.4	17.3
601	1	80	20	8	46.9	21.5
602	1	81	20	148	24.8	18.8
603	1	81	20	128	12.1	27.8
604	1	81	20	108	32.7	21.3
605	1	81	20	88	22.5	11.8
606	1	81	20	68	57.3	41.2
607	1	81	20	48	121.0	14.5
608	1	81	20	28	40.3	26.3
609	1	81	20	8	33.3	14.1
610	1	82	20	148	14.6	29.3
611	1	82	20	128	18.2	8.5
612	1	82	20	108	52.5	22.0
613	1	82	20	88	11.3	16.4
614	1	82	20	68	55.1	14.1
615	1	82	20	48	27.2	14.9
616	1	82	20	28	61.5	33.0
617	1	82	20	8	83.1	8.9
618	1	83	20	148	10.1	13.7
619	1	83	20	128	18.8	25.3
620	1	83	20	108	50.0	18.3
621	1	83	20	88	28.6	12.3

Storm Number	Texas Region	Master Track	Θ (deg)	ΔP (hPa)	R_{max} (km)	V_f (km/h)
622	1	83	20	68	13.7	25.6
623	1	83	20	48	32.7	37.5
624	1	83	20	28	72.6	12.4
625	1	83	20	8	98.4	32.3
626	1	84	40	138	14.1	8.5
627	1	84	40	118	22.3	26.7
628	1	84	40	98	47.0	12.9
629	1	84	40	78	14.3	12.7
630	1	84	40	58	53.4	22.4
631	1	84	40	38	92.9	21.4
632	1	84	40	18	14.1	15.1
633	1	85	40	138	36.3	14.7
634	1	85	40	118	32.3	25.9
635	1	85	40	98	16.5	15.4
636	1	85	40	78	23.4	20.2
637	1	85	40	58	29.0	40.7
638	1	85	40	38	113.4	29.4
639	1	85	40	18	72.0	10.2
640	1	86	40	138	19.3	12.1
641	1	86	40	118	35.9	38.0
642	1	86	40	98	19.4	22.5
643	1	86	40	78	55.9	11.3
644	1	86	40	58	30.7	11.2
645	1	86	40	38	42.8	11.1
646	1	86	40	18	131.3	28.8
647	1	87	40	138	23.7	21.8
648	1	87	40	118	25.5	12.0
649	1	87	40	98	13.6	18.1
650	1	87	40	78	18.1	41.6
651	1	87	40	58	73.9	28.9
652	1	87	40	38	78.3	14.4
653	1	87	40	18	28.5	17.6
654	1	88	40	138	16.8	28.1
655	1	88	40	118	21.5	13.5
656	1	88	40	98	45.2	32.4
657	1	88	40	78	84.7	10.8
658	1	88	40	58	15.9	32.5
659	1	88	40	38	36.5	11.6
660	1	88	40	18	105.7	26.0

Table D-3. List of 195 S2G storms with associated tropical cyclone parameters. Storm number is the same as storm number in Table D-1. Storms crossed out indicate that CSTORM simulation did not complete for all scenarios, so those storms were removed from analysis.

Storm Number	Texas Region	Master Track	θ (deg)	ΔP (hPa)	R_{max} (km)	V_f (km/h)
18	2	3	-100	128	18.14	14.29
49	2	7	-100	148	5.34	20.26
60	2	8	-100	88	14.73	8.89
63	2	8	-100	28	27.78	14.85
66	1	9	-100	128	27.65	15.22
68	1	9	-100	88	16.22	7.95
73	1	10	-100	148	9.26	4.97
74	1	10	-100	128	10.56	16.71
76	1	10	-100	88	43.81	9.20
77	1	10	-100	68	25.79	14.04
80	1	10	-100	8	23.43	6.84
87	2	11	-80	18	62.76	15.66
95	2	13	-80	138	15.66	20.07
108	2	14	-80	18	33.06	11.99
114	2	15	-80	38	50.70	13.67
120	2	16	-80	58	42.25	14.35
128	2	17	-80	38	74.88	8.08
129	2	17	-80	18	30.07	7.95
134	2	18	-80	58	39.02	12.37
135	2	18	-80	38	20.19	11.50
136	2	18	-80	18	57.48	10.31
~~139~~	~~2~~	~~19~~	~~-80~~	~~98~~	~~43.06~~	~~14.42~~
141	2	19	-80	58	29.33	5.53
143	2	19	-80	18	37.78	16.71
145	1	20	-80	118	9.01	17.15
147	1	20	-80	78	21.50	13.36
148	1	20	-80	58	24.54	4.97
149	1	20	-80	38	44.80	14.54
153	1	21	-80	98	32.99	4.97
157	1	21	-80	18	48.59	5.78

Storm Number	Texas Region	Master Track	θ (deg)	ΔP (hPa)	R_{max} (km)	V_f (km/h)
159	1	22	-80	118	26.28	5.28
167	1	23	-80	98	30.39	10.56
173	2	24	-60	128	6.21	19.95
178	2	24	-60	28	29.14	11.37
184	2	25	-60	68	11.18	9.38
187	2	25	-60	8	30.63	16.03
194	2	26	-60	28	55.55	11.74
210	2	28	-60	28	66.61	7.15
218	2	29	-60	28	60.65	8.02
219	2	29	-60	8	41.94	14.17
224	2	30	-60	68	68.41	9.07
227	2	30	-60	8	47.53	17.09
229	2	31	-60	128	15.47	10.07
230	2	31	-60	108	22.56	22.18
234	2	31	-60	28	33.55	9.44
238	2	32	-60	108	34.49	14.98
242	2	32	-60	28	17.21	8.26
~~243~~	~~2~~	~~32~~	~~-60~~	~~8~~	~~64.00~~	~~6.03~~
245	1	33	-60	128	14.54	9.44
247	1	33	-60	88	33.37	5.28
248	1	33	-60	68	14.85	5.28
249	1	33	-60	48	22.68	17.21
251	1	33	-60	8	33.68	7.64
252	1	34	-60	148	8.39	7.83
258	1	34	-60	28	26.41	8.57
261	1	35	-60	128	15.91	10.81
267	1	35	-60	8	38.53	8.20
269	1	36	-60	128	6.52	12.24
285	2	38	-40	118	6.15	10.00
290	2	38	-40	18	27.22	5.22
294	2	39	-40	78	22.43	13.73
296	2	39	-40	38	46.66	12.18
301	2	40	-40	78	39.21	10.13

Storm Number	Texas Region	Master Track	θ (deg)	ΔP (hPa)	R$_{max}$ (km)	V$_f$ (km/h)
304	2	40	-40	18	50.64	11.31
308	2	41	-40	78	32.12	8.20
309	2	41	-40	58	14.91	7.52
318	2	42	-40	18	21.69	22.56
323	2	43	-40	58	54.87	8.76
327	2	44	-40	118	27.59	7.77
330	2	44	-40	58	47.91	18.64
331	2	44	-40	38	16.59	8.33
332	2	44	-40	18	68.97	13.42
333	2	45	-40	138	16.22	18.02
337	2	45	-40	58	50.02	7.83
339	2	45	-40	18	15.10	13.86
341	1	46	-40	118	15.35	10.38
342	1	46	-40	98	46.60	14.85
344	1	46	-40	58	30.57	5.84
345	1	46	-40	38	25.29	14.98
346	1	46	-40	18	39.46	17.27
348	1	47	-40	118	12.86	6.21
349	1	47	-40	98	19.39	18.02
352	1	47	-40	38	80.28	8.64
353	1	47	-40	18	31.57	8.51
356	1	48	-40	98	24.17	6.77
357	1	48	-40	78	61.14	9.76
360	1	48	-40	18	34.61	12.68
363	1	49	-40	98	17.21	7.08
365	1	49	-40	58	40.58	12.74
366	1	49	-40	38	21.44	12.55
367	1	49	-40	18	60.02	10.63
368	1	50	-40	138	16.78	18.70
369	1	50	-40	118	9.82	11.43
371	1	50	-40	78	26.41	5.84
373	1	50	-40	38	87.43	10.50
374	1	50	-40	18	28.65	19.39

Storm Number	Texas Region	Master Track	θ (deg)	ΔP (hPa)	R_{max} (km)	V_f (km/h)
376	1	51	-40	118	33.43	7.15
387	1	52	-40	38	30.63	6.09
388	1	52	-40	18	41.20	14.73
396	2	53	-20	8	83.20	12.24
401	2	54	-20	68	28.02	21.31
407	2	55	-20	108	29.64	24.79
411	2	55	-20	28	70.09	10.07
417	2	56	-20	68	47.66	12.86
419	2	56	-20	28	46.98	15.29
427	2	57	-20	28	22.37	22.80
428	2	57	-20	8	89.23	12.92
434	1	58	-20	48	47.60	10.56
435	1	58	-20	28	23.67	6.59
437	1	59	-20	148	10.50	16.47
439	1	59	-20	108	16.40	7.39
440	1	59	-20	88	37.84	8.26
444	1	59	-20	8	40.20	10.25
445	1	60	-20	148	5.72	17.03
446	1	60	-20	128	8.14	8.08
447	1	60	-20	108	39.77	9.94
448	1	60	-20	88	22.74	5.84
449	1	60	-20	68	38.59	22.43
451	1	60	-20	28	21.06	10.38
459	1	61	-20	28	48.96	16.84
460	1	61	-20	8	17.96	4.97
461	1	62	-20	148	18.08	13.67
462	1	62	-20	128	10.19	13.86
464	1	62	-20	88	41.57	10.87
471	1	63	-20	108	14.66	7.71
474	1	63	-20	48	40.45	16.09
475	1	63	-20	28	9.82	13.98
476	1	63	-20	8	35.23	5.22
477	1	64	-20	148	6.09	14.11

Storm Number	Texas Region	Master Track	θ (deg)	ΔP (hPa)	R_{max} (km)	V_f (km/h)
484	1	64	-20	8	45.61	6.28
486	1	65	-20	128	19.51	6.84
490	1	65	-20	48	26.35	6.65
494	2	66	0	118	8.57	5.90
496	2	66	0	78	37.59	12.18
504	2	67	0	58	69.28	15.29
506	2	67	0	18	72.58	7.15
510	2	68	0	78	47.04	10.75
512	2	68	0	38	32.00	6.34
513	2	68	0	18	42.94	15.16
514	1	69	0	138	17.40	22.87
518	1	69	0	58	23.43	6.65
519	1	69	0	38	63.38	17.65
522	1	70	0	118	6.96	11.81
523	1	70	0	98	27.03	5.59
526	1	70	0	38	10.75	7.77
527	1	70	0	18	23.05	24.23
529	1	71	0	118	21.50	26.91
530	1	71	0	98	15.22	12.74
532	1	71	0	58	75.37	15.72
534	1	71	0	18	76.74	7.39
536	1	72	0	118	16.96	13.36
540	1	72	0	38	33.49	5.22
544	1	73	0	98	22.49	19.39
545	1	73	0	78	42.75	6.15
548	1	73	0	18	24.42	8.82
553	1	74	0	58	52.32	8.45
560	1	75	0	58	21.19	17.34
562	1	75	0	18	55.05	11.62
573	2	77	20	88	34.73	11.18
577	2	77	20	8	58.60	14.60
578	1	78	20	148	13.79	25.79
579	1	78	20	128	9.51	4.97

Storm Number	Texas Region	Master Track	θ (deg)	ΔP (hPa)	R_{max} (km)	V_f (km/h)
580	1	78	20	108	26.16	8.33
582	1	78	20	68	24.73	13.24
583	1	78	20	48	31.50	19.20
584	1	78	20	28	19.76	5.78
586	1	79	20	148	7.58	14.98
587	1	79	20	128	10.94	9.07
589	1	79	20	88	30.82	20.82
590	1	79	20	68	22.62	5.84
594	1	80	20	148	7.02	10.19
595	1	80	20	128	17.58	22.62
598	1	80	20	68	49.96	14.91
600	1	80	20	28	35.05	10.75
601	1	80	20	8	29.14	13.36
606	1	81	20	68	35.60	25.60
608	1	81	20	28	25.04	16.34
609	1	81	20	8	20.69	8.76
617	1	82	20	8	51.64	5.53
618	1	83	20	148	6.28	8.51
626	1	84	40	138	8.76	5.28
627	1	84	40	118	13.86	16.59
628	1	84	40	98	29.20	8.02
631	1	84	40	38	57.73	13.30
632	1	84	40	18	8.76	9.38
633	1	85	40	138	22.56	9.13
634	1	85	40	118	20.07	16.09
635	1	85	40	98	10.25	9.57
636	1	85	40	78	14.54	12.55
640	1	86	40	138	11.99	7.52
644	1	86	40	58	19.08	6.96
645	1	86	40	38	26.59	6.90
646	1	86	40	18	81.59	17.90
652	1	87	40	38	48.65	8.95
660	1	88	40	18	65.68	16.16

Appendix E: LiDAR Surveys

LiDAR surveys were conducted for the region in 2018 at very-high accuracy. The TWDB was responsible for the following metadata excerpts below that describe the data and processing. This description was taken verbatim from the metadata files that accompanied the data. These data and metadata can be found online at https://www.fisheries.noaa.gov/inport/item/58236.

> The Texas Water Development Board (TWDB) in cooperation with their project partners tasked Fugro Geospatial, Inc. (Fugro) under the Department of Information Resources (DIR) Geographic Information Systems (GIS) Hardware, Software and Services contract also known as the Texas Strategic Mapping (StratMap) Contract to acquire high resolution elevation data and associated products from airborne LiDAR systems during the 2017-2018 leaf-off season. The StratMap Program promotes inter-governmental collaboration and partnerships to purchase geospatial data products that provide cost savings and project efficiencies. Both the StratMap Program and the StratMap Contract are administered by the Texas Natural Resources Information System (TNRIS), a division of TWDB. Project partners include: Houston-Galveston Area Council (H-GAC), Harris County Flood Control District (HCFCD), and the United States Geological Survey (USGS). This Coastal Texas project consists of approximately 9,758 DO4Q tiles and is located on the Texas Coast covering much of Orange to Matagorda County along with Harris County and the surrounding area. The project includes large metropolitan areas as well as coastal areas. The Urban and Coastal AOIs consist of approximately 4.045 square miles and were acquired between January 12 and March 22, 2018 utilizing both Riegl LMS-Q680i and Riegl LMS-Q780 sensors; collecting multiple return x, y, and z as well as intensity data. Specialized in-house and commercial software processes the native LiDAR data into 3-dimensional positions that can be imported into GIS software for visualization and further analysis. The horizontal datum for the data is the North American Datum of 1983 (NAD83, 2011) in meters and the vertical datum is the North

American Vertical Datum of 1988 (NAVD88) in meters realized with GEOID12B.

During LiDAR data collection the airborne GPS receiver was collecting data at 2 Hz frequency and the Dilution of Precision (PDOP) was monitored. GPS base stations were also running at the operational airports and were recording data at 1 Hz. The airborne GPS data was post-processed in DGPS mode together with the base station data to provide high accuracy aircraft positions. The GPS trajectory then was combined with the IMU data using loosely coupled approach to yield high accuracy aircraft positions and attitude angles. Then the LiDAR data was processed using the aircraft trajectory and raw LiDAR data. After boresighting the LiDAR data, the ground control points were measured against the LiDAR data by technicians using TerraScan and proprietary software and the LiDAR data was adjusted vertically to the ground control. The horizontal datum is NAD83(2011) in meters and the vertical datum is the North American Vertical Datum of 1988 (NAVD88) in meters. The vertical datum was realized through the use of the published/calculated ellipsoidal heights of the base station to process the aircraft trajectory and then later applying the GEOID12B model to the processed LiDAR data to obtain orthometric heights.

Fugro collected Riegl-derived LiDAR over the Coastal Texas project AOI with a 0.5 meter Nominal Pulse Spacing (NPS). Data was collected when environmental conditions met the specified criteria: leaf-off and no significant snow cover or flood conditions; cloud, smoke, dust, and fog-free between the aircraft and ground. The collection was accomplished on January 13, 14, 15, 17, 18, 22, 23, 24, 25, 28, 29, 30, and 31, February 2, 8, 19, 23, and 26, and March 1, 2, 3, 6, 7, 8, 11, 12, 13, 14, 19, 20, 21, and 22 2018; 982 flight lines were acquired in 117 lifts. The lines were flown at an average of 3,250 feet above mean terrain. The collection was performed using the Riegl LMS-Q680i and Riegl LMS-Q780i LiDAR systems, serial numbers 163, 165, 421, and 961.

All acquired LiDAR data went through a preliminary review to assure that complete coverage had been obtained and that there were no gaps between flight lines before the flight crew left the project site. Once back in the office, the data was run through a complete iteration of processing to ensure that it is complete, uncorrupted, and that the entire project area has been covered without gaps between flight lines. There are essentially three steps to this processing: 1) GPS/IMU Processing - Airborne GPS and IMU data was processed using the airport GPS base station data. 2) Raw Lidar Data Processing - Technicians processed the raw data to LAS format flight lines with full resolution output before performing QC. A starting configuration file is used in this process, which contains the latest calibration parameters for the sensor. The technicians also generated flight line trajectories for each of the flight lines during this process. 3) Verification of Coverage and Data Quality - Technicians checked the trajectory files to ensure completeness of acquisition for the flight lines, calibration lines, and cross flight lines. The intensity images were generated for the entire lift at the required 0.5 meter NPS. Visual checks of the intensity images against the project boundary were performed to ensure full coverage to the 300 meter buffer beyond the project boundary. The intensity histogram was analyzed to ensure the quality of the intensity values. The technician also thoapproximately reviewed the data for any gaps in project area. The technician generated a sample TIN surface to ensure no anomalies were present in the data. Turbulence was inspected for each flight line; if any adverse quality issues were discovered, the flight line was rejected and re-flown. The technician also evaluated the achieved post spacing against project specified 0.5 meter NPS as well as making sure no clustering in point distribution.

The boresight for each lift was done individually as the solution may change slightly from lift to lift. The following steps describe the Raw Data Processing and Boresight process: 1) Technicians processed the raw data to LAS format flight lines using the final GPS/IMU solution. This LAS data set was used as source data for boresight. 2) Technicians first

used Fugro proprietary and commercial software to calculate initial boresight adjustment angles based on sample areas within the lift. These areas cover calibration flight lines collected in the lift, cross tie and production flight lines. These areas are well distributed in the lift coverage and cover multiple terrain types that are necessary for Once boresighting was completed, the project was set up for automatic classification. First, the LiDAR data was cut into production tiles and the flight line overlap points, noise points, ground points, and building points were classified automatically. Fugro utilized commercial software, as well as proprietary, in-house developed software for automatic filtering. The parameters used in the process were customized for each terrain type to obtain optimum results. These parameters were also customized to capture multiple categories of vegetation based on height (low, medium, and high vegetation). After all "low" points are classified, points remaining are reclassified automatically based on height from the ground. Once the automated filtering was completed, the files were run through a visual inspection to ensure that the filtering was not too aggressive or not aggressive enough. In cases where the filtering was too aggressive and important terrain were filtered out, the data was either run through a different filter within local area or was corrected during the manual filtering process. Bridge deck points and culvert points were classified as well during the interactive editing process. Interactive editing was completed in visualization software that provides manual and automatic point classification tools. Fugro utilized commercial and proprietary software for this process. All manually inspected tiles went through a peer review to ensure proper editing and consistency. After the manual editing and peer review, all tiles went through another final automated classification routine. This process ensures only the required classifications are used in the final product (all points classified into any temporary classes during manual editing will be re-classified into the project specified classifications). Once manual inspection, QC and final autofilter is complete for the LiDAR tiles, the LAS data was packaged to the project specified tiling scheme, cut to the approved tile layout, and formatted to LAS v1.4. It was

also re-projected to UTM Zone 15 north; NAD83(2011), meters; NAVD88(GEOID12B), meters. The file header was formatted to meet the project specification. This Classified Point Cloud product was used for the generation of derived products. This product was delivered in fully compliant LAS v1.4, Point Record Format 6 with Adjusted Standard GPS Time. Georeferencing information is included in all LAS file headers. Each tile has File Source ID assigned to zero. The Point Source ID matches to the flight line ID in the flight trajectory files. Intensity values are included for each point, normalized to 16-bit. The following classifications are included: Class 1 – Processed, but unclassified; Class 2 – Bare earth ground; Class 3 – Low Vegetation (0.01m to 1.00m above ground); Class 4 – Medium Vegetation (1.01m to 3.00m above ground); Class 5 – High Vegetation (greater than 3.01m above ground); Class 6 – Building; Class 7 – Low Point (Noise); Class 9 – Water; Class 10 – Ignored Ground; Class 13 – Bridges; and Class 14 – Culverts. The classified point cloud data was delivered in tiles without overlap using the project tiling scheme.</boresight angle calculation. The technician then analyzed the results and made any necessary additional adjustment until it is acceptable for the selected areas. 3) Once the boresight angle calculation was completed for the selected areas, the adjusted settings were applied to all of the flight lines of the lift and checked for consistency. The technicians utilized commercial and proprietary software packages to analyze the matching between flight line overlaps for the entire lift and adjusted as necessary until the results met the project specifications. 4) Once all lifts were completed with individual boresight adjustment, the technicians checked and corrected the vertical misalignment of all flight lines and also the matching between data and ground truth. The relative accuracy was ? 3 cm RMSDz within swath overlap (between adjacent swaths) with a maximum difference of ± 17 cm. 5) The technicians ran a final vertical accuracy check of the boresighted flight lines against the surveyed ground control points after the z correction to ensure the requirement of RMSEz (non-vegetated) ? 10 cm, NVA ? 19.6 cm 95% Confidence Level was met.

Upon the completion of LiDAR point cloud product creation, First Return points were used for intensity image generation automatically. The software considers points from neighboring tiles while creating the images for seamless edge matching. The intensity images were generated at 0.5 meter resolution in 16-bit. Georeferencing information was assigned to all images. The technician QC'ed the final intensity images before delivery. The intensity images were delivered in GeoTIFF format.

Hydro linework is produced by heads-up digitizing using classified LiDAR datasets. Additionally, products created from LiDAR including intensity images, shaded-relief TIN surfaces, and contours are used. Hydrographic features were collected as separate feature classes: 1) Inland Ponds and Lakes nominally larger than 2 acres in area (Ponds_and_Lakes) and 2) Inland Streams and Rivers nominally larger than 15.25 meters (Stream_and_River)(1_Acre_Islands). After initial collection, features were combined into working regions based on watershed sub-basins. Linework was then checked for the following topological and attribution rules: 1) Lines must be attributed with the correct feature code and 2) Lake and stream banklines must form closed polygons. Hydro features were collected as vector linework using LiDAR and its derived products listed above. This linework is initially 2D, meaning that it does not have elevation values assigned to individual line vertices. Vertex elevation values were assigned using a distance weighted distribution of LiDAR points closest to each vertex. This is similar to draping the 2D linework to a surface modeled from the LiDAR points. After the initial 'drape', the linework elevation values were further adjusted based on the following rules: 1) Lake feature vertices were re-assigned (flattened) to lowest draped vertex value, and 2) Double stream bankline vertices were re-assigned based on the vertices of the closest adjusted double stream connector line. Fugro proprietary software was used to create profiles to ensure bank to bank flatness, monotonicity check, and lake flatness. The hydro breaklines were delivered as polygons in Esri ArcGIS version 10.3 geodatabase format.

The hydro-flattened bare earth DEM was generated using the LiDAR bare earth points and 3D hydro breaklines to a resolution of 1 meter. The bare earth points that fell within 1*NPS along the hydro breaklines (points in class 10) were excluded from the DEM generation process. This is analogous to the removal of mass points for the same reason in a traditional photogrammetrically compiled DTM. This process was done in batch using proprietary software. The technicians then used Fugro proprietary software for the production of the LiDAR-derived hydro-flattened bare earth DEM surface in initial grid format at 1 meter GSD. Water bodies (inland ponds and lakes), inland streams and rivers, and island holes were hydro-flattened within the DEM. Hydro-flattening was applied to all water impoundments, natural or man-made, nominally larger than 2 acres in area and to all streams nominally wider than 15.25 meters. This process was done in batch. Once the initial, hydro-flattened bare earth DEM was generated, the technicians checked the tiles to ensure that the grid spacing met specifications. The technicians also checked the surface to ensure proper hydro-flattening. The entire data set was checked for complete project coverage. Once the data was checked, the tiles were then converted to .IMG format. Georeference information is included in the raster files.

Appendix F: Wave Runup and Overtopping

The computations of runup and overtopping are considered in the design of an HFP structure. These parameters are computed from empirical equations. The structure is designed to withstand a specified overtopping tolerance, or limit state.

Wave runup

Wave runup on coastal structures and beaches has historically been used to determine the landward extent of wave action for coastal flood-risk mapping. FEMA[1] continues to use runup to delineate the flood extent. Empirical equations are still standard engineering practice. However, numerical models can model the extent of runup and are increasingly being used. This former method is standard engineering practice, so herein, empirical equations are the focus.

The crest height of a structure can be designed to be coincident with the maximum runup associated with some rare storm condition. This is still a widely used technique. However, it does not provide any indication of the erosion safety level. Therefore, designs for erodible structures, like levees, have moved more towards overtopping for design. Runup still provides some useful information, so it is described herein and quantified for the S2G levees.

Wave runup and setup are illustrated in Figure F-1 where η_{max} = maximum setup and R = runup. Wave setup is the increase of the still water level as a result of radiation stresses from wave breaking in the nearshore zone. Wave runup and rundown are the time-varying vertical extent of the water level along the shoreline. Wave runup is a useful parameter to define the crest height of structures or to use as an indicator of incipient overtopping in a simulation. Wave runup typically includes wave setup. Because runup is a time-varying quantity, a representative statistical value is required. Usually, runup is represented as a relatively extreme probability of exceedance (e.g., $R_{1\%}$ or $R_{2\%}$) computed from

---

[1] FEMA (Federal Emergency Management Agency). 2011 (Unpublished). *Flood Insurance Study: Coastal Counties, Texas. Intermediate Submission 2: Scoping and Data Review.* Joint Report prepared for Federal Emergency Management Agency by the Department of the Army, US Army Corps of Engineers, Washington, DC.

approximately one-half hour of continuous water surface recordings, where 1% and 2% indicated percent exceedance values. For coastal structures, the runup statistic is typically computed as the sum of runups divided by the number of waves as opposed to the number of runups, primarily because the number of waves is more consistent and definitive.

Figure F-1. Illustration of wave setup and runup from Melby (2012).
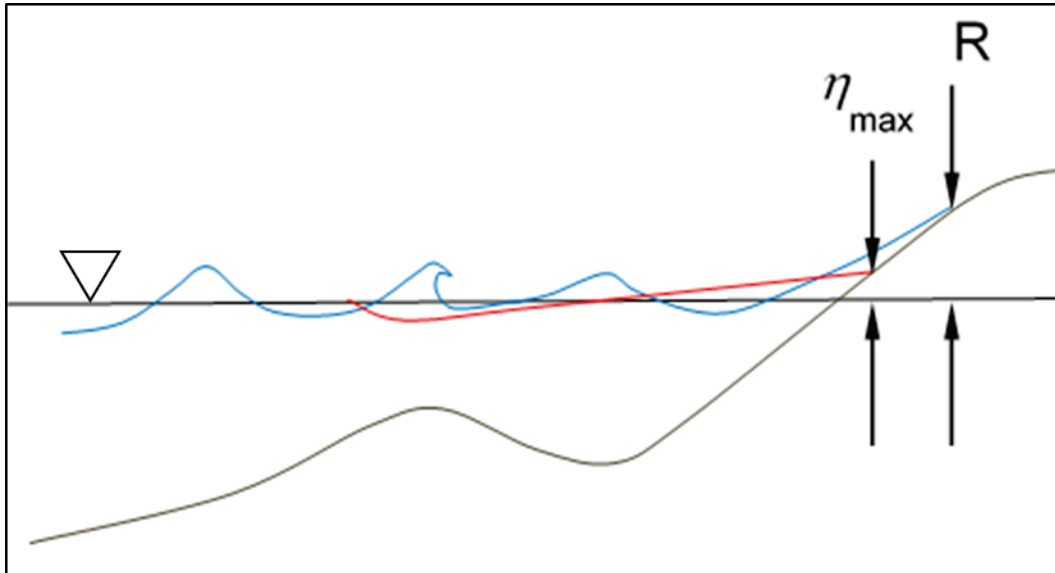
Impermeable slopes

Wave runup has been quantified primarily using small-scale laboratory experiments, and most of these were done using smooth impermeable slopes. These tests correspond to earthen levees. Runup height above the still water level exceeded by 2% of incident irregular waves defined at the toe of the structure is denoted as $R_{2\%}$ and is commonly used to define runup. The CEM (USACE 2008) provides several equations for runup, and these are similar to other formulas developed. Most of the runup equations for generalized structures are supported by a large number of small- to large-scale experiments. The latest formula in international guidance is similar to that given in the CEM and is found in the EurOtop (2018) manual. This formula can be written as

$$\frac{R_{2\%}}{H_{m0}} = 1.65\gamma_b\gamma_f\gamma_\beta\xi_{m-1,0}$$

$$\frac{R_{2\%}}{H_{m0}} \leq \gamma_b\gamma_{fsurging}\gamma_\beta(4 - 1.5/\xi_{m-1,0})$$

(F.1)

This equation is valid for structures with a slope of cotα =1:8 and steeper. The coefficients 1.65 and 1.0 can be considered normally distributed with means of 1.65 and 1.0 and standard deviations of 0.10 and 0.07, respectively.

The runup height $R_{2\%}$ is similar in scale to the spectral significant wave height H_{m0} at the toe of the slope. The surf similarity parameter $\xi_{m-1,0}$ is given as

$$\xi_{m-1,0} = \tan \alpha / \sqrt{s_{m-1,0}}, \; s_{m-1,0} = H_{m0}/L_{m-1,0}, \; L_{m-1,0} = g(T_{m-1,0})^2/2\pi \quad \text{(F.2)}$$

where α = angle of the seaward slope from the horizontal; $L_{m-1,0}$ = deepwater wavelength based on the spectral wave period $T_{m-1,0}$ at the toe of the slope. The reduction coefficients γ are described below.

The calculation for runup on very gradual slopes can be reduced to

$$\frac{R_{u2\%}}{H_{m0}} = 3.6 \quad \text{(F.3)}$$

This assumes that there is a very shallow foreshore that causes breaking and a surf similarity parameter greater than 15.

The calculation for runup on vertical walls can be reduced to

$$\frac{R_{u2\%}}{H_{m0}} = 1.8 \quad \text{(F.4)}$$

This equation assumes that there is minimal effect of a foreshore.

For slopes between cotα=2 and vertical walls, modified equation is used:

$$\frac{R_{u2\%}}{H_{m0}} = 0.8 \cot \alpha + 1.6 \; ; 1.8 \; \leq \frac{R_{u2\%}}{H_{m0}} \leq 3.0 \quad \text{(F.5)}$$

The coefficients of 0.8 and 1.6 are assumed to be normally distributed with standard deviations of 0.056 and 0.112, respectively.

Runup reduction factors

The reduction factor γ in Equation F.1 is equal to 1 for wave runup on a smooth uniform slope with normally incident waves. It is decomposed into several components as

$$\gamma = (\gamma_f \, \gamma_b \, \gamma_\beta) \le 1 \tag{F.6}$$

where γ_f is the reduction factor associated with slope roughness, γ_b is for a berm, and γ_β is for oblique waves. Table F-1 provides a summary of some friction coefficients. In addition,

$$\gamma_{f\,surging} = \gamma_f + (\xi_{m-1,0} - 1.8)(1-\gamma_f)/8.2 \text{ and } \gamma_{f\,surging} = 1.0 \text{ for } \xi_{m-1,0} > 10. \tag{F.7}$$

Table F-1. Friction coefficients for use in runup and overtopping equations.

Type of Armor Layer	γ_f
Rocks (1 layer, impermeable core)	0.60
Rocks (1 layer, permeable core)	0.45
Rocks (2 layers, impermeable core)	0.55
Rocks (2 layers, permeable core)	0.40
Cubes (1 layer, random positioning)	0.50
Cubes (2 layers, random positioning)	0.47
Steps	0.60
Grass with $H_{m0}<0.75$	$1.15\sqrt{H_{m0}}$

Equation F.1 predicts the increase of $R_{2\%} / (\gamma \, H_{m0}) = 0.8$ to 3.3 with the increase of $\xi_{m-1,0} = 0.5$ to 5.0, which may be regarded as a typical range for inclined impermeable structures. $R_{2\%}$ is a maximum of approximately $2H_{m0}$.

Levees are normally covered with grass, reinforced turf, asphalt, or concrete blocks. Grass has a relatively greater hydraulic roughness for thin wave runup depths. Therefore, $\gamma_f = 1$ will typically be conservative for grass. A small H_{m0} may affect roughness for all types of material, so the friction coefficients will be conservative in this case (EurOtop 2018)

A levee slope may include a berm with different slopes seaward and landward of the berm. The formulas given above are normally used for berms with an appropriate reduction in runup using γ_b. However, the guidance is for berms that are near the SWL. These assumptions constitute an oversimplification of complex physics from waves breaking on a compound slope. Therefore, generally, these recommendations tend to be conservative. Different methods have been proposed to estimate the equivalent uniform slope $tan\alpha$ for different composite slopes (e.g., Kobayashi and Jacobs 1985; Mase et al. 2013). The EurOtop (2018) manual presents complicated methods to estimate $tan\alpha$ and γ_b for

different composite slopes. No single method is expected to work for different composite slopes because wave dynamics depend on the actual bottom geometry.

Oblique directional (short-crested) waves generally result in lower wave runup than normally incident waves. The reduction factor γ_β is given as

$$
\begin{aligned}
\gamma_\beta &= 1.0 \quad \text{for } |\beta| \leq 20° \\
\gamma_\beta &= 1 - 0.0022|\beta| \quad \text{for } 20° < |\beta| \leq 80° \\
\gamma_\beta &= 0.82 \quad \text{for } |\beta| < 80°
\end{aligned}
\tag{F.8}
$$

where β is the incident wave angle in degrees at the toe of the slope (Figure F-2). For normally incident waves, $\beta = 0$. Equation F.8 is from the EurOtop (2018) manual. There is a discontinuity at $|\beta| = 20°$. The range of $\gamma_\beta = 0.82 - 1.0$ for directional random waves turns out to be relatively small perhaps because directional wave spectra include waves of nearly normal incidence.

Figure F-2. Definition sketch for wave direction.
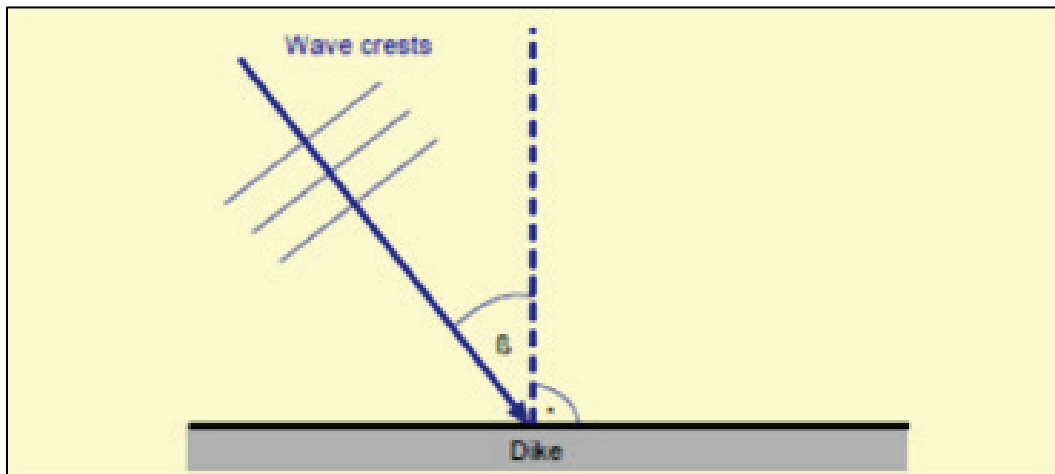
Equation F.1 is based on a best fit to primarily laboratory physical model measurements, and these data include significant scatter. The uncertainty in the best fit coefficients is assumed to be normally distributed with the mean value corresponding to the value calculated using Equation F.1. The standard deviation of the scattered data points for smooth uniform slopes ($\gamma = 1$) is 7% of the mean value implying that the error is within

approximately 20%. There is a reduction of wave height and period for wave angles greater than 80°. This reduces H_{m0} and T_p to zero for wave angles greater than 110°.

Permeable slopes

Equation F.1 applies to wave runup on the seaward slope of a rubble mound structure as well. The EurOtop manual includes guidance for Equation F.1 for permeable slopes. The calibrated values of the reduction factor γ_f for breaking waves are γ_f = 0.55 for two layers of rock on impermeable core and γ_f = 0 40 for two layers of rock on permeable core. The reduction factor γ_{fsurge} for surging waves was expressed as

$$\gamma_{fsurge} = \gamma_f \quad \text{for } \xi_{\text{m-1,0}} \leq 1.8$$
$$\gamma_{fsurge} = \gamma_f + (\xi_{\text{m-1,0}} - 1.8)(1 - \gamma_f)/8.2 \quad \text{for } 1.8 < \xi_{\text{m-1,0}} < 10 \qquad \text{(F.10)}$$
$$\gamma_{fsurge} = 1.0 \quad \text{for } \xi_{\text{m-1,0}} \geq 10$$

The EurOtop (2018) manual provides a procedure to compute γ_b that can be complicated in practice. The berm effect is included by computing the effective slope and influence factor. Figure F-3 shows an idealized definition sketch for the berm parameterization. Berms are defined as slopes shallower than 1:15 while the levee slope is defined as slopes steeper than 1:8. Interpolation is recommended for slopes between. For effective slope, there is a two-step process. An initial estimate is made as the average of the slopes between $1.5H_{m0}$ above and below the SWL over the width between the intersections of these two points less the berm width.

$$tan\alpha = \frac{3H_{m0}}{L_{slope} - B} \qquad \text{(F.11)}$$

A second estimate is made by computing the runup using the slope above.

$$tan\alpha = \frac{1.5H_{m0} + R_{u2\%(1st\ estimate)}}{L_{slope} - B} \qquad \text{(F.12)}$$

If $1.5\ H_{m0}$ or $R_{2\%}$ is above the crest level, then the crest level is the characteristic point above SWL. The influence factor is given by

$$\gamma_b = 1 - r_B(1 - r_{db})\ for\ 0.6 \leq \gamma_b \leq 1.0 \qquad \text{(F.13)}$$

where the berm width influence is given by

$$r_b = \frac{B}{L_{Berm}} \tag{F.14}$$

and the influence of the vertical distance between the middle of the berm and the SWL, d_b, is governed by

$$r_{db} = 0.5 - 0.5\cos\left(\pi\frac{d_b}{R_{2\%}}\right) \text{ for berm above SWL}$$

$$r_{db} = 0.5 - 0.5\cos\left(\pi\frac{d_b}{2H_{m0}}\right) \text{ for berm below SWL} \tag{F.15}$$

$$r_{db} = 1 \text{ for berm outside the area of influence.}$$

Figure F-3. Definition sketch for berm coefficient (EurOtop 2018).
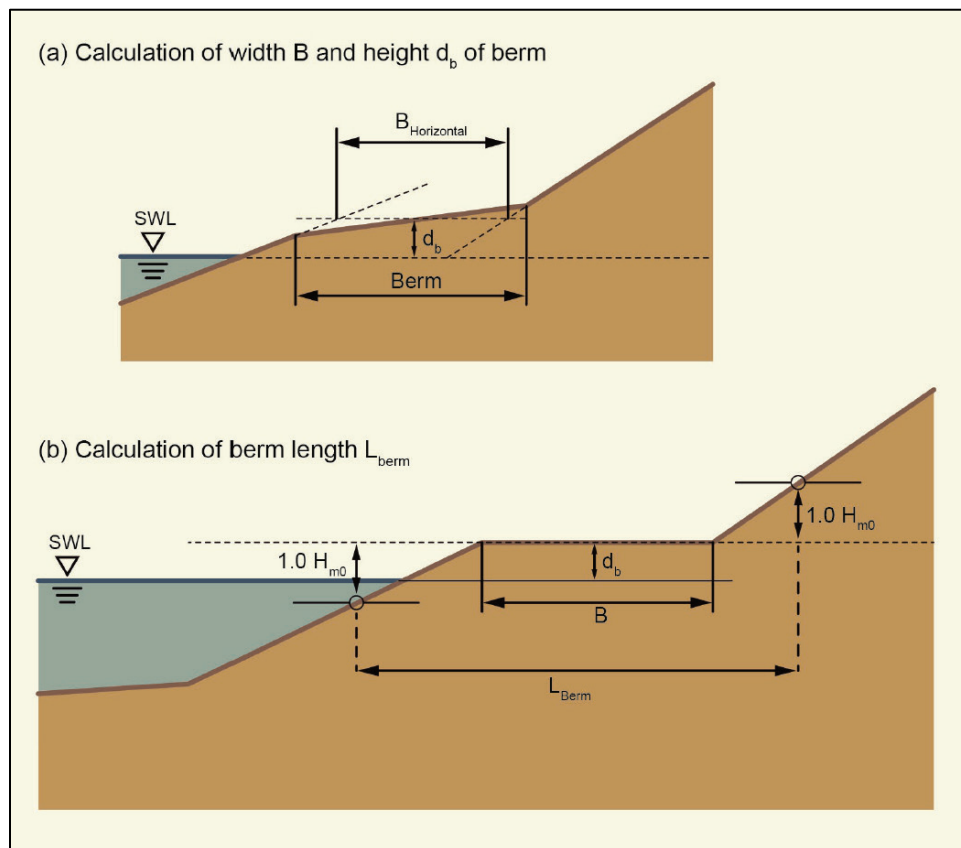
The coefficient 1.65 in Equation F.1 can be considered normally distributed with mean of 1.65 and standard deviation of 0.12. The modification from prior versions of Equation F.1 is to decrease the empirical coefficients by slightly less than 10% and change T_p to $T_{m-1,0}$. This modification represents a slight decrease in predicted runup over prior versions. Figure F-4 shows Equation F.1 plotted with additional large-scale data referenced in the EurOtop (2018) manual and provided to

the author by J. van der Meer.[1] These data are published in many reports, including Dutch and German language reports or proprietary reports, so the details of the various studies may not be available.

Figure F-4. Equation F.1 runup prediction plotted with large-scale measurements referenced in the EurOtop manual (EurOtop 2018).
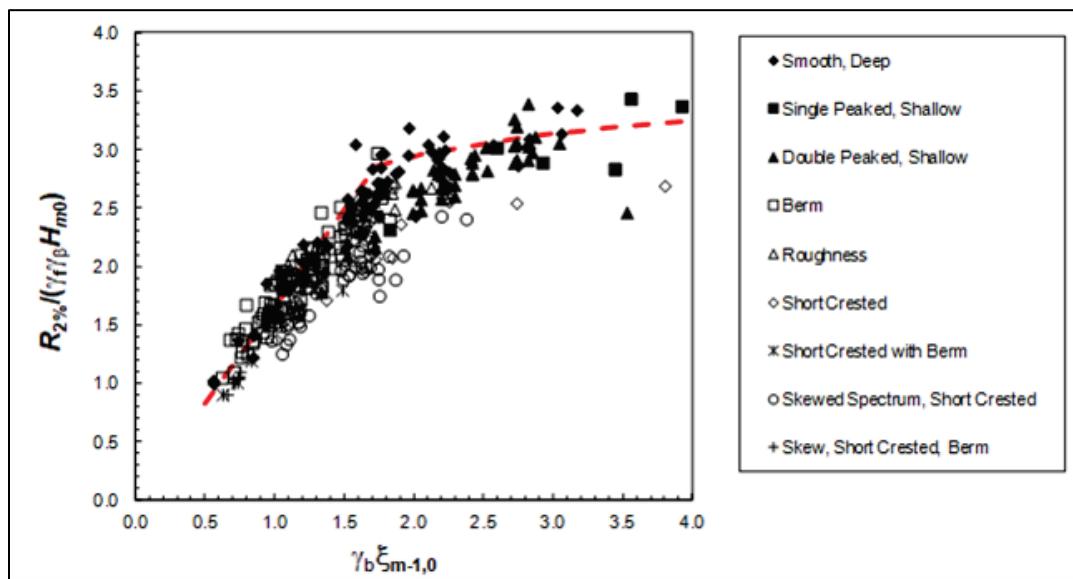
In Figure F-4, a wide variety of structure and wave and water level conditions are represented including shallow and deep water at the structure toe, single-peaked and double-peaked spectra, short-crested and long-crested seas, skewed spectra, smooth impermeable and rubble structures, varied roughness, and bermed structures. For all cases, the appropriate influence coefficients were applied. As shown in Figure F-4, Equation F.1 fit includes an over-prediction bias, presumably to provide some conservativeness.

An important consideration within this chapter is that fits to the data are generally mean fits. As such, they are not necessarily conservative. Conservativism is achieved through application of a reliability scheme or application at CL above 50%. This is described below.

---

[1] Personal Communication between J. Melby and J. van der Meer (Van der Meer Consulting B.V.), January 2011,

Steady flow overtopping

Steady flow overtopping occurs on a coastal structure when the crest height is lower than the water level (i.e., there is a negative freeboard, R_c). The rate at which water is overflowing landward of the structure is defined using the weir formula as

$$q_{overflow} = 0.54 \sqrt{g \, |-Rc^3|} \qquad \text{(F.16)}$$

where g is gravity and $q_{overflow}$ is the overflow rate per unit alongshore length of the structure crest. The coefficient 0.54 varies with structure type and is generally accepted for flow over a weir (Hughes and Nadal 2009). The coefficient of 0.54 is used as-is for a wall. For a levee, this coefficient can be reduced for friction but is usually not reduced because the frictional losses are very small (a few percent) and it is usually applied with this small amount of added conservativism.

Wave overtopping

The crest height of a coastal structure is designed using allowable wave overtopping criteria instead of the wave runup height. Damage can be related to the amount or rate of wave overtopping on the structure crest and landward area, but no reliable method exists to predict damage initiation and progression. For design, the average wave overtopping rate q per unit alongshore length of the structure crest is used to describe the intermittent wave overtopping during a given sea state. Wave overtopping discharge for sloping structures is based on a mean fit to primarily laboratory data and is given in the EurOtop (2018) manual as

$$\frac{q}{\sqrt{gH_{m0}^3}} = \frac{0.023}{\sqrt{tan\alpha}} \gamma_b \xi_{m-1,0} exp\left[-2.7\left(\frac{R_C}{\xi_{m-1,0}H_{m0}\gamma_b\gamma_f\gamma_\beta\gamma_v}\right)^{1.3}\right]$$

$$\frac{q}{\sqrt{gH_{m0}^3}} \leq 0.09 exp\left[-1.5\left(\frac{R_C}{H_{m0}\gamma_f\gamma_\beta\gamma_*}\right)^{1.3}\right] \qquad \text{(F.17)}$$

where γ coefficients were primarily described earlier except γ_v and γ_* are coefficients to account for a vertical wall. The coefficients 2.7 and 1.5 can be considered normally distributed with standard deviations of 0.2 and 0.15, respectively. The coefficients 0.023 and 0.09 can also be considered normally distributed with standard deviations of 0.003 and 0.0135, respectively. These equations are approximately valid for a surf similarity

parameter less than 5. Like Equation F.1, Equation F.17 is only slightly different from prior published versions.

Shallow and very shallow foreshores are considered when the zero-moment wave steepness is less than 0.01 or where h/H_{m0} is less than 1 and h is the toe depth. The overtopping equation is modified to

$$\frac{q}{\sqrt{g\,H_{m0}}} = 10^{-0.79} \exp\left(-\frac{Rc}{\gamma_f\,\gamma_\beta\,H_{m0}\,(0.33+0.022\,\xi_{m-1,0})}\right) \tag{F.18}$$

The coefficient -0.79 can be considered normally distributed with a standard deviation of 0.29. This equation is approximately valid for surf similarity parameters between 5 and 7.

Overtopping on vertical walls can be determined using

$$\frac{q}{\sqrt{g\,H_{m0}^3}} = 0.047 \exp\left[-\left(2.35\frac{Rc}{H_{m0}\,\gamma_f\,\gamma_\beta}\right)^{1.3}\right] \tag{F.19}$$

The coefficients 0.047 and 2.35 can be considered normally distributed with standard deviations of 0.007 and 0.23, respectively.

Slopes steeper than $\cot\alpha = 2$, but not vertical, require an iteration between the overtopping formula for gradual slopes and the overtopping formula for vertical slopes shown as

$$\frac{q}{\sqrt{g\,H_{m0}^3}} = a \exp\left[-\left(b\frac{Rc}{Hm0}\right)^c\right] \tag{F.20}$$

where $a = 0.09 - 0.01(2 - \cot\alpha)^{2.1}$ for $\cot\alpha < 2$ and $a = 0.09$ for $\cot\alpha \geq 2$, $b = 1.5 + 0.42(2 - \cot\alpha)^{1.5}$ with a maximum of $b = 2.35$, for $\cot\alpha < 2$ and $b = 1.5$ for $\cot\alpha \geq 2$.

This set of equations assumes that the waves are not breaking. If there are breaking waves, the equation for gradual slopes should be used. The coefficients a and b can be considered normally distributed with coefficients of variation as 0.15 and 0.10, respectively. This equation assumes a relatively low freeboard and smooth slopes and has only been validated for $\cot\alpha$ between 0.36 and 2.75. The influence factor for oblique waves is interpolated between the vertical wall and gradual slope to obtain γ_β.

Combined overflow and wave overtopping

Combined overflow and wave overtopping for a submerged structure can be calculated using

$$q_{total} = q_{(Overtopping, where\ Rc=0)} + q_{overflow} \qquad \text{(F.21)}$$

where $q_{overtopping}$ is calculated for a zero freeboard. As the structure becomes more submerged, the wave overtopping becomes negligible, approximately at R_c / H_{mo} <-0.3.

Project parameters

The input parameters for runup and overtopping equations require understanding of the structure geometry and wave and water level forcings. The structure geometry for with-project was defined by SWG, such as the slope, design elevation, and crest width. The existing structure geometry was extracted from transects that were developed from a high-resolution DEM.

Transect data

Critical cross sections were approximately 800 ft long at critical points along the structure, with approximate location defined by SWG. The topography was defined by the LiDAR described in Appendix E, and the bathymetry was defined from the NOAA database and SWG surveys. These sets of data were meshed together to allow a transect profile to be computed at each critical cross section.

Each transect was individually analyzed. An idealized structure was created over the topography and bathymetry of each transect. A semi-automated Matlab routine was developed to allow the user to select specific points on each measured profile. An example is shown in Figure F-5. The user selects points along the measured transect; then, the routine creates a new fitted transect using straight line segments between the points. Figure F-6 shows an example of the measured transect and the idealized transect.

Figure F-5. Example of points selected by user on measured profile using Matlab semi-automated software.
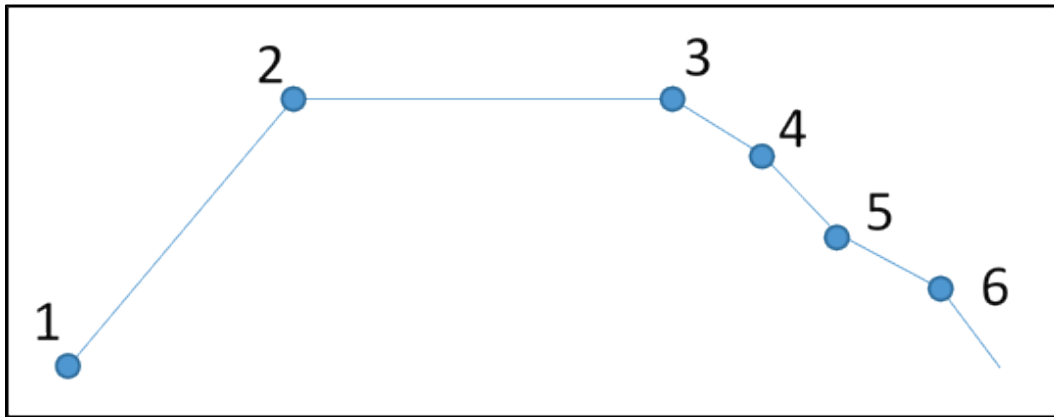
Figure F-6. Example of transect with measured profile and idealized transect fit with straight line segments.
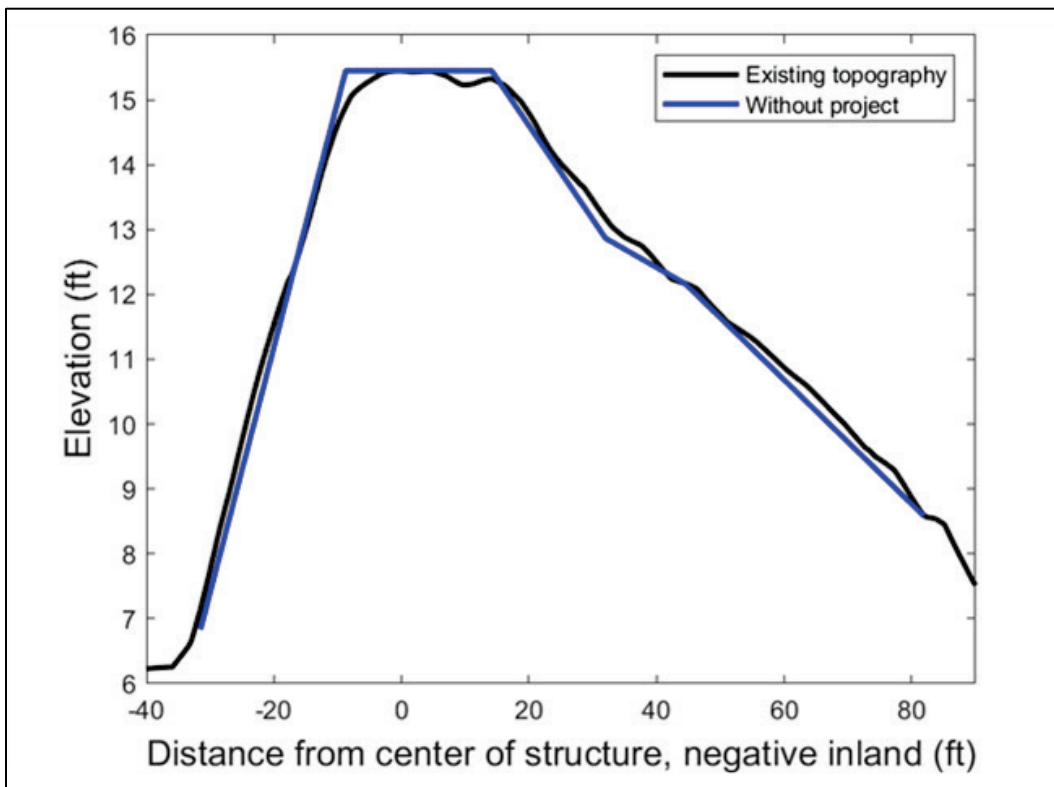
Structure slope

Melby (2012) suggested defining the seaward slope of the structure for runup between SWL$\pm H_{m0}$. The EurOtop II (2018) manual suggests using the slope between $-1.5*H_{m0}$ and $R_{2\%}$; however, this requires an iterative process to determine $R_{2\%}$ as discussed above. The runup and overtopping

routine applies a weighted slope over the four seaward points of the idealized structure with respect to the SWL±H_{mo}, shown in Figure F-7.

Figure F-7. Transect segments for defining slope for use in runup and overtopping equations.
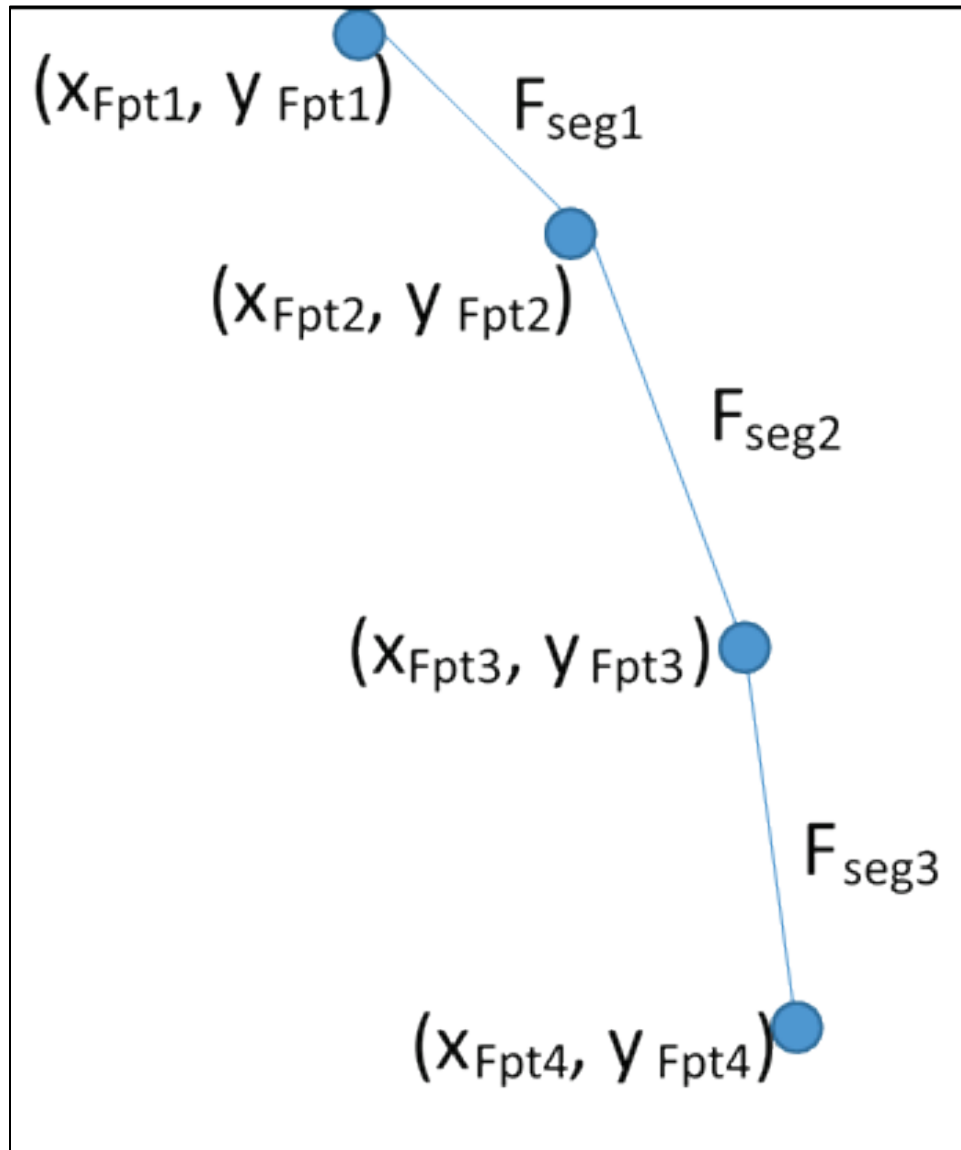
The slope of each seaward segment, $F_{seg(i)}$, is defined by

$$Slope_{Fseg(i)} = \frac{y_{Fpt(i)} - y_{Fpt(i+1)}}{x_{Fpt(i)} - x_{Fpt(i+1)}} \qquad \text{(F.22)}$$

where i and $i+1$ correspond to the two F_{pt} on each end of the segment. The length of each segment, L_{Fseg}, is defined by

$$L_{Fseg} = abs(x_{Fpt(i)} - x_{Fpt(i+1)}) \qquad \text{(F.23)}$$

Equation F.23 is also used to define the length of the structure transect between SWL±H_{m0}. The weight of a segment of slope between SWL±H_{m0} is defined by

$$Weight_{slope} = \frac{\sum (L_{Fseg(i)} * Slope_{Fseg})}{\sum L_{Fseg\_Total}} \qquad \text{(F.24)}$$

Wave and water level forcings

The wave and water level forcings applied to the runup and overtopping equations are ADCIRC and STWAVE outputs near the toe of each structure transect. The wave height should already account for any transformations.

Floodwall overtopping

The crest height of a coastal structure is designed using allowable wave overtopping criteria. Damage can be related to the amount or rate of wave overtopping on the structure crest and landward area, but no reliable method exists to predict damage initiation and progression. For design, the average wave overtopping rate q per unit alongshore length of the structure crest is used to describe the intermittent wave overtopping rate during a given sea state. Wave overtopping discharge rate for floodwalls is based on a mean fit to primarily laboratory data and is given in the EurOtop (2018) manual as

$$\frac{q}{\sqrt{g\,H_{m0}^3}} = 0.047 \exp\left[-\left(2.35\frac{R_c}{H_{m0}}\right)^{1.3}\right] \qquad \text{(F.25)}$$

where g is gravity, R_c is structure freeboard, and H_{m0} is wave height. The coefficients 0.047 and 2.35 can be considered normally distributed with standard deviations of 0.007 and 0.23, respectively. Equation F.25 is valid

for plain vertical walls with the absence of an influencing foreshore. The presence of an influencing foreshore is considered when the depth at the toe of the wall is less than $4*H_{m0}$, then the overtopping discharge rate is given by

$$\frac{q}{\sqrt{g\,H_{m0}^3}} = 0.05 \exp\left[-\left(2.78\frac{R_c}{H_{m0}}\right)^{1.3}\right] \tag{F.26}$$

The coefficients 0.05 and 2.78 can be considered normally distributed with standard deviations of 0.012 and 0.17, respectively.

Overflow occurs when the crest height is lower than the water level. The rate at which water is overflowing landward of the structure is defined as

$$q_{overflow} = 0.54\sqrt{g\,|-Rc^3|} \tag{F.27}$$

where $q_{overflow}$ is the overflow rate per unit alongshore length of the structure crest. Total overtopping for a submerged structure can be calculated using

$$q_{total} = q_{(Overtopping,where\ Rc=0)} + q_{overflow} \tag{F.28}$$

where $q_{overtopping}$ is calculated from wave overtopping Equations for a zero freeboard.

Floodwall nappe geometry

The design of leeside protection from the overtopping free-falling jet of water can be determined using the nappe profile, which describes the extent of the jet influence, shown in Figure F-8. It is assumed that the floodwall is high, where the total head above the wall crest is near the height of surge above the wall and the upstream velocity is near zero. The lower nappe is closest to the backside of the floodwall, and the upper nappe is an extension of the flow overtopping. The impact locations of the lower and upper nappe, x_L, and x_U, on the horizontal ground on the protected side of a wall are defined as

$$\frac{x_L}{h_1} = \frac{-B-\sqrt{B^2-4A\left(C-\frac{-H_w}{h_1}\right)}}{2A} \tag{F.29}$$

$$\frac{x_U}{h_1} = \frac{-B - \sqrt{B^2 - 4A\left(C + D - \frac{-H_w}{h_1}\right)}}{2A} \tag{F.30}$$

where H_w is the height of the floodwall, and h_1 is defined as the difference between H_w and the total water depth, h. The coefficients in the nappe geometry equations are $A = -0.425$; $B = 0.055$; $C = 0.150$; and $D = 0.559$. The distance from the floodside of the wall to the center of the jet at impact is

$$x_c = \frac{x_L + x_U}{2} \tag{F.31}$$

Figure F-8. Flow over a sharp-crested weir.
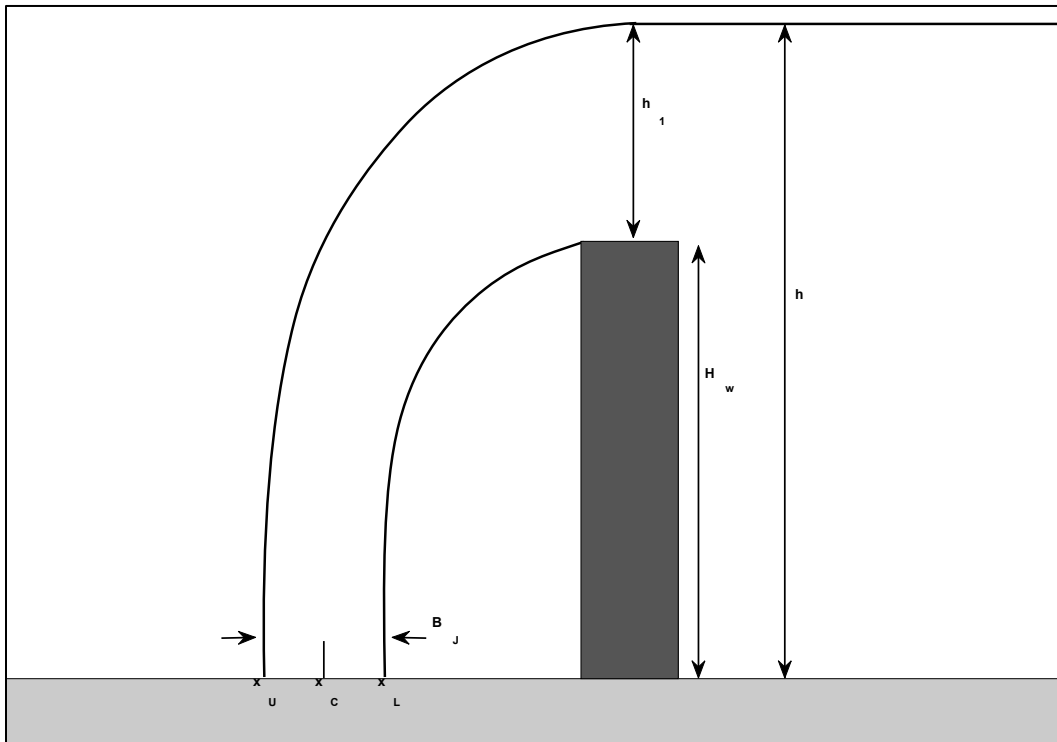
The overtopping jet angle, θ_J, is the average of the lower and upper geometry angles, θ_L and θ_U, where 0 degrees is to the leeside horizontal of the structure:

$$\theta_L = \tan^{-1}\left(\frac{2A\, x_L}{h_1} + B\right) \tag{F.32}$$

$$\theta_U = \tan^{-1}\left(\frac{2A\, x_U}{h_1} + B\right) \tag{F.33}$$

The width of the impinging jet normal to the flow streamlines is estimated as

$$B_J = B_x * \sin(-\theta_J) \tag{F.34}$$

where B_x is the difference between x_L, and x_U. The jet entry velocity can be estimated using the overtopping rate per unit length by

$$V_J = \frac{q}{B_J} \tag{F.35}$$

The total force exerted by the overtopping jet on the scour protection per unit length along the wall is given by

$$F_J = \rho * B_J * V_J^2 \tag{F.36}$$

Fluid density, ρ, is assumed to be that of saltwater.

Pressure on floodwall

The pressures on a structure are calculated using Goda (2010) methods. The pressure distribution is described in Figure F-9 and Figure F-10. The pressure at SWL can be calculated using Equation F.37. The pressure at the crest of the structure is calculated using Equation F.38. The pressure at the toe of the structure is calculated using Equation F.39. For a wall with negative freeboard, only p_2 and p_3 are used, as shown in Figure F-10.

$$p_1 = 0.5 * (1 + cos\beta) * (\lambda_1\alpha_1 + \lambda_2\alpha_* \cos^2\beta) * \rho * g * H_{design} \tag{F.37}$$

$$p_2 = \begin{cases} \left(1 - \frac{R_c}{\eta^*}\right) p_1 \ for \ \eta^* > R_c \\ 0 \ for \ \eta^* \leq R_c \end{cases} \tag{F.38}$$

$$p_3 = \alpha_3 p_1 \tag{F.39}$$

Figure F-9. Wave pressure distribution.
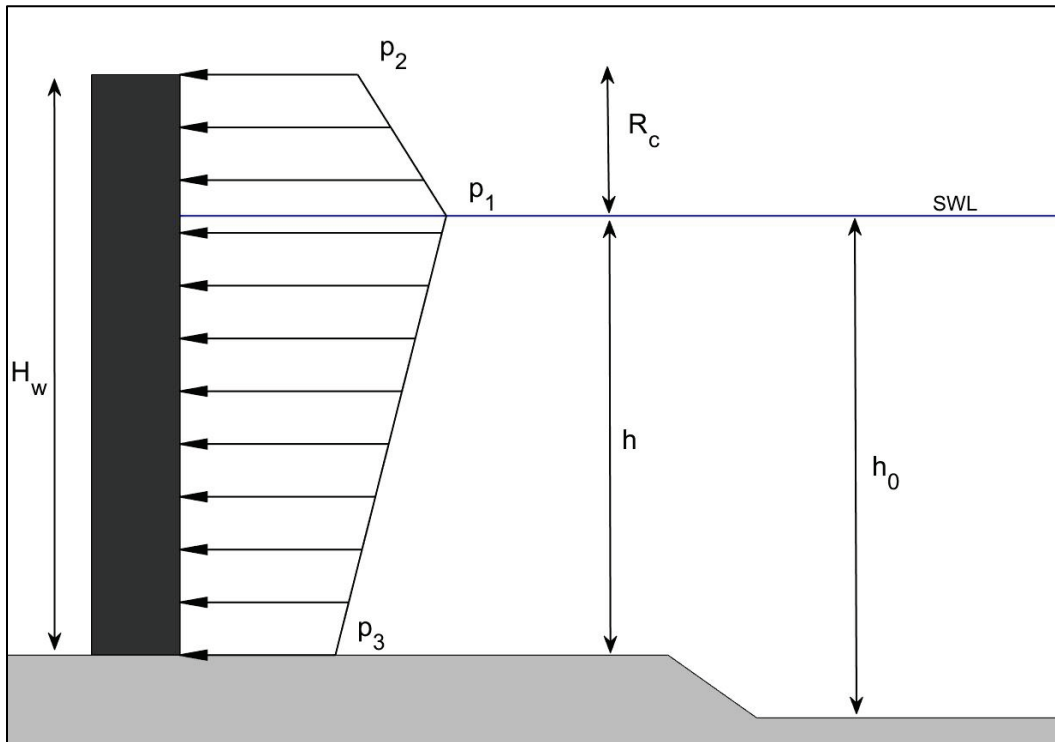
Figure F-10. Wave pressure distribution for SWL above crest.
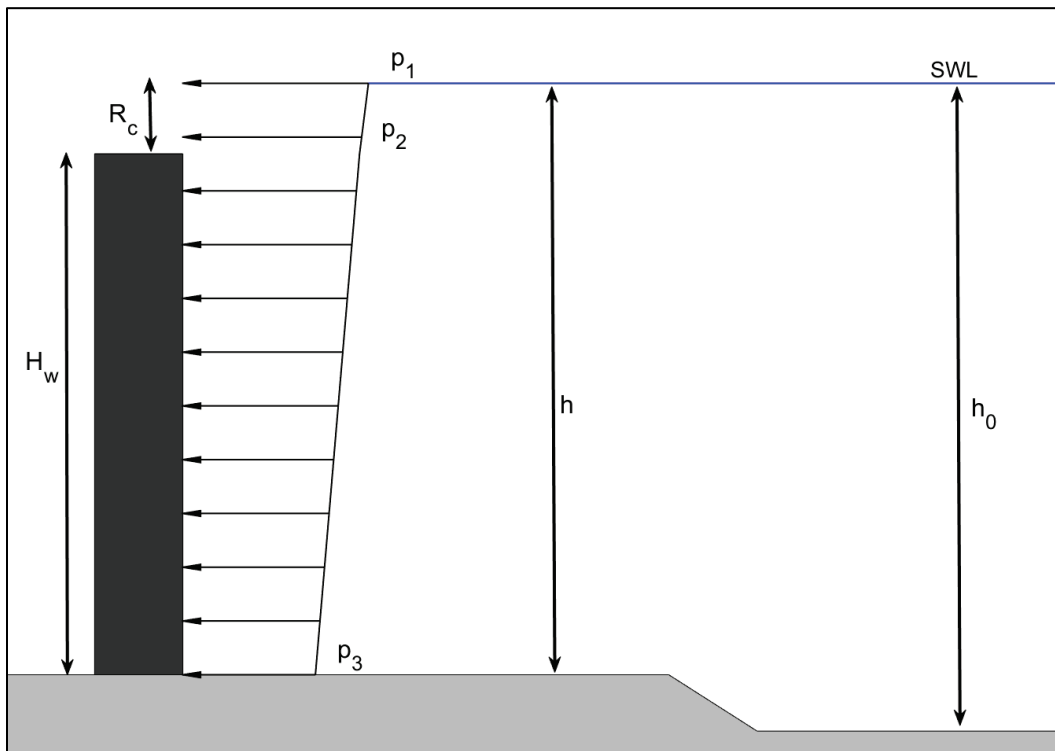
The λ coefficients in the pressure equations are modification factors, taken as 1 for conventional vertical walls. The angle of wave incidence, β, is taken as 0 for wave crests parallel to walls. The design wave height for non-breaking waves, H_{design}, is 1.8*H_{m0}. Breaking waves are not considered in this analysis. The free surface design elevation, η^*, is calculated with respect to the design wave height using

$$\eta^* = 0.75 * (1 + cos\beta) * \lambda_1 * H_{design} \tag{F.40}$$

The alpha coefficients used in the pressure equations are computed using Equations F.41 to F.44. The deep water depth is h_o, the water depth in front of the structure is h, the wave length in deep water is L, and the height of the wall is H_w. Here, L is computed using linear wave theory. Goda (2010) prescribes using $T_{1/3}$ but T_p is used herein as a conservative estimate.

$$\alpha_1 = 0.6 + 0.5 \left[\frac{\frac{4\pi h_0}{L}}{\sinh\left(\frac{4\pi h_0}{L}\right)} \right]^2 \tag{F.41}$$

$$\alpha_2 = \frac{2*h}{H_{design}} \tag{F.42}$$

$$\alpha_3 = 1 - \frac{H_w - R_c}{h_0} \left[1 - \frac{1}{\cosh\left(\frac{2\pi h_0}{L}\right)} \right] \tag{F.43}$$

$$\alpha_* = \alpha_2 \tag{F.44}$$

Appendix G: Stochastic Structure Response Simulations

Several approaches for stochastic structure response were evaluated. This appendix summarizes and compares these approaches. The methods fall into two classes: event-based (EB) and response-based (RB). EB approaches are also referred to as frequency-based. RB is commonly referred to in literature as a "structure variable" approach.

In <u>EB stochastic simulation</u>, the forcing (SWL, H_{m0}, T_p, wave direction) is characterized for a single statistic (100 yr ARI or 1% AEP), and then the response is computed for this "event." A range of statistical events can be evaluated to define a hazard curve. Uncertainty can either be included in the semi-deterministic calculation (1% AEP SWL defined at the 90% confidence limit), or uncertainty can be sampled using Monte Carlo simulation to define confidence intervals about the mean hazard curve. This latter method was used for the US Army Corps of Engineers, New Orleans District, LACPR and HDRRS studies.

In <u>RB stochastic simulation</u>, the storm forcing is characterized for each storm, and then the peak responses computed for all events, and finally the hazard curve of response is computed. Uncertainty can be added for each storm and thousands of storms evaluated to define confidence limits.

Herein, there is an evaluation of two EB approaches and three RB approaches ranging from quasi-deterministic to full probabilistic with time-dependency.

Event-based (EB) approach

Designing for a single statistical event is a traditional civil engineering approach. Unfortunately, in coastal levee and floodwall engineering, it can be difficult to define a single critical statistical event because the forcing, as well as the structure response (e.g., overtopping rate), are multivariate. For example, forcing based on SWL, H_{m0}, T_p, and wave direction produces a multi-variate probabilistic surface. Further, the wave and water level parameters are interdependent, with waves and storm water levels being a strong function of wind speed and direction. There are an infinite number of combinations of these parameters that lie along the 1% AEP probability surface. A maximum of maximums can be defined, but this is typically

overly conservative and results in a poor definition of risk. Also, a 1% AEP event does not necessarily equate to a 1% AEP response (e.g., overtopping rate). Third, the 1% AEP is not a safety standard. It is a standard for requirement of flood insurance. Unfortunately, this standard for flood insurance has unintentionally resulted in communities targeting this as a level of safety. In this regard, the 1% AEP represents a relatively low level of safety for life-and-death decisions related to flooding. This safety level is a standard minimum for Gulf of Mexico CSRM projects. Because it is a relatively low standard, it is crucial that computation be done in a reasonably conservative and accurate manner.

The present state of practice utilizes the 90% CL. This is easy to understand for a single parameter such as SWL but becomes complex when considering a multivariate probability model. It is likely that EB and RB approach solutions will diverge (EB less accurate) with increasing confidence level because of the increased influence of high-uncertainty contributors like overtopping rate. If the structure response (e.g., overtopping rate) hazard curve is steeply sloping near the design limit state, then the EB solution is likely to produce wildly inaccurate solutions. Unfortunately, this is more often than not the situation because north Texas regions are inundated only by hazards that are near to or greater than the design condition. EB approaches are attractive because they have a historical basis in civil engineering and are simpler, so they are easier to comprehend, particularly when dealing with complex multi-variate probabilistic problems like threshold flooding associated with CSRM features. There are tradeoffs that are valuable to understand and this chapter illustrates the differences.

The typical flood risk study EB approach is consistent with the FEMA National Flood Insurance Program approach to characterize flooding in terms of the 1% AEP SWL. Wave effects are added in but on a somewhat ad hoc basis to maintain a relatively simple approach. Simplifying assumptions about the multi-variate statistical characteristics of forcing (waves and water levels) limits the accuracy of the studies. These assumptions include simplifying assumptions about the multivariate probabilistic models, such as uncorrelated or fully correlated peak wave height and water level or neglecting wave period, storm duration and hydrograph shape in the multi-variate probability model. As shown in Appendix B, for S2G the wave and water level parameters are highly correlated. Further, the above assumptions are not necessarily consistent

with nearshore coastal storm physics where the hydraulic hazard is primarily driven by wind suggesting that all primary wave and water level parameters should be partially correlated. Within the present study, all influential parameters are included within the multivariate probability model. This is a multi-valued problem, so simulation is required to define reasonable but conservative RB designs. This is not a significant complication over the LACPR and HSDRRS approach since those studies used Monte Carlo simulation to sample epistemic uncertainties. Two EB approaches considered in the present analysis are described below.

Response-based (RB) approach

RB stochastic simulation computes responses for all storms and then computes response hazard curves. RB approaches are more likely to produce a spatially consistent risk estimate than EB because the response statistic is consistent. This can be compared to EB where only the forcing statistic is consistent and the response statistic is not. An RB risk assessment is usually more accurate than an EB one because RB models are less likely to rely on subjective judgment about, or make arbitrary simplifications to, the complex multi-variate statistical relationships. In addition, events based on 1% AEP parameters may be contrary to physics. Wave overtopping rate is sensitive to SWL and H_{m0}, so any error in the multi-variate probability model will be reflected in the structure response computation. The RB simulation approach overcomes these limitations but requires running thousands of storms to achieve a statistically stable solution. Therefore, while results are provided for both EB and RB approaches herein, the RB results are considered more accurate especially when associated with an AEP of the response (e.g., overtopping rate) that reflects the level of protection of the CSRM system.

For the RB modeling approach, storms are sampled according to their relative probabilities and structure responses (in this case, overtopping rate) are computed for response modes of interest. The final outputs are probability distributions of response and specific statistical values, such as the 1% AEP value of each parameter at 50% and 90% CLs.

Many potential workflows are possible with a wide range of complexities. The most complex is time-dependent analysis where, for each sampled storm, structure response is computed at every time-step and uncertainty associated with the storm peak is applied across all time-steps. Peak structure response is selected for each storm to compute statistics. A

second, somewhat simpler, peaks-based RB approach is to use peak SWL and peak H_{m0} (independent of SWL) with T_p and MWD selected at the same time step as the peak H_{m0}. A third approach with complexity between the prior two, called quasi-time dependent herein, deterministically computes the response for every storm time step (189 storms) and identifies the time-step of peak structure response (q). The values of SWL, H_{m0}, T_p, and MWD that produce this peak response are saved for each storm, and then the stochastic simulation uses these values in the same way as the peaks-based method. It is expected that the fully time-dependent would be the most accurate, the quasi time-dependent next, and the peaks-based solution the least accurate of these RB approaches.

Treatment of uncertainty in stochastic simulation

Uncertainty in flood risk studies is usually grouped according to natural variations in physical processes (aleatory) and errors in the understanding and prediction of these processes (epistemic). This grouping is a simplification and not intended to be a rigorous categorization of all uncertainties. However, it serves the primary purpose for dealing with uncertainty herein. The primary natural variability of hurricane extreme responses is dealt with through the JPM-OS approach and is quantified through the use of the multivariate probability relation Equation A.1, repeated in Equation G.1.

The joint probability of coastal tropical storm hazards can be summarized by means of the JPM integral:

$$\lambda_{r(\hat{x})>r} = \lambda \int P[r(\hat{x}) + \sigma > r | \hat{x}, \sigma] \, f_{\hat{x}}(\hat{x}) f_\sigma(\sigma) d\hat{x} d\sigma$$

$$\approx \sum_i^n \lambda_i \, P[r(\hat{x}) + \sigma > r | \hat{x}, \sigma] \tag{G.1}$$

where $\lambda_{r(\hat{x})>r}$= AEP of storm response r due to forcing vector $\hat{x}$; σ =unbiased error term; $P[r(\hat{x}) + \sigma > r | \hat{x}, \sigma]$ = conditional probability that storm i with parameters $\hat{x}$ generates a response larger than r. The primary tropical cyclone parameters commonly accounted for in the forcing vector $\hat{x}$ are: distance to reference location (x_0); central pressure deficit (Δp); radius of maximum winds (R_{max}), translation speed (V_f); and heading direction (θ). Secondary parameters may include Holland B and astronomical tide.

Tides are normally part of the aleatory uncertainty, but herein they are combined with the epistemic because they are relatively small and, as shown in the main report, can be treated as a normally distributed error. All errors from modeling, including those associated with sampling within the stochastic simulation, are considered to be epistemic in nature and are addressed in this section.

It is routine in coastal flood risk studies to consider epistemic uncertainties as normally distributed, and this results in significant simplifications of the statistical math. However, it is a common argument that probability distributions pertaining to hurricane flooding have "fat tails," so normal distributions will not be conservative. This is definitely the case for probability distributions associated with aleatory uncertainty and is addressed well within the JPM-OS approach where there is no normality assumption made. However, for epistemic uncertainty, the assumption of normality for the types of epistemic uncertainty that are important to flood risk is reasonable. As well, for large sample sets, the assumption of normality is not crucial according to the central limit theorem. This issue is addressed in the many JPM-OS-specific references provided in Appendix A.

Epistemic uncertainty that is considered in the overtopping rate stochastic simulation is a combination of multiple discrete component uncertainties. Herein, these are characterized as standard deviations corresponding to normally distributed parameters. The discrete uncertainties are generally considered probabilistically independent and are aggregated accordingly. However, wave and water level parameters are not independent, so correlation of these parameter uncertainties was included where it was considered influential. This is described in Appendix B and further below. The following uncertainties have been estimated and accounted for:

1. Random variations in the Holland B parameter.
2. Random astronomical tide phase.
3. Errors in hydrodynamic modeling and grids associated with epistemic uncertainty.
4. Errors in meteorological modeling associated with simplified PBL winds.
5. Storm track variations not captured in synthetic storm set.
6. Sampling errors (both JPM-OS distributions and Monte Carlo).
7. Overtopping rate empirical equation uncertainty.

These errors associated with the hazard are described in Nadal-Caraballo et al. (2015) and Melby et al. (2017). More detailed analysis of errors in probabilistic coastal hazards studies has been recently completed[1].

The astronomical tide in the Gulf of Mexico is shown in the main report to be small enough to allow it to be considered an uncertainty associated with the total water level response. This is common practice in Gulf of Mexico flood risk studies. This uncertainty captures the aleatory variability arising from the possibility of the tropical cyclone arriving during any tide phase. The uncertainty is computed as the standard deviation of the predicted tide at a given location and is approximately equal to MHHW[2] - MSL[3]. The tidal uncertainty of 0.83 ft was applied to SWL, computed as the standard deviation of the hourly record of NOAA water level gage Texas Point, Sabine Pass, TX 8770822, for the predicted tide time series between 2012 and 2019.

Each hazard component uncertainty is assumed to be unbiased and normally distributed. The uncertainties are represented as standard deviations, and their effects are generally combined additively. The total uncertainty is represented by the standard deviation of errors (σ_ε), where the total associated uncertainty is computed as the square root of the sum of the squares of the standard deviations of each component uncertainty (σ_i):

$$\sigma_\varepsilon = \sqrt{\sum_i^n \sigma_i^2} \qquad \text{(G.2)}$$

The following breakdown of hazard uncertainty for stochastic simulation is based on Nadal-Caraballo et al. (2015), which was based, in-part, on Resio et al. (2013) and Jacobsen et al. (2015). The coefficient of variation, given by $\nu = \sigma_\varepsilon/\mu$, where σ_ε and μ, for example, are the standard deviation and mean SWL from the validation study, is usually approximately 20%, and this is further divided into a 15% component that is applied within the integration of Equation G.1 and a second component of 13.2% applied

---

[1] Nadal-Caraballo, N. C., V. M. Gonzalez, J. A. Melby, and A. B. Lewis. Draft. *Approaches for Probabilistic Modeling of Numerical Surge Simulation Errors.* ERDC/CHL Technical Report. Vicksburg, MS: US Army Engineer Research and Development Center.

[2] Mean Higher High Water

[3] Mean Sea Level

to compute confidence limits. This separate grouping of uncertainties is required to assure a smooth uniform storm forcing hazard curves:

1. Mean Hazard Curve

$$\lambda_{r(\hat{x})>r} \approx \sum_{i}^{n} \lambda_i \, P[\{(r(\hat{x}) * 1.15) \leq \sigma_c\} > r | \hat{x}, \sigma] \qquad \text{(G.3)}$$

2. 90% Confidence Limit

$$\text{CL}_{90\%} = \lambda_{r(\hat{x})>r} + 1.2816 * (\lambda_{r(\hat{x})>r} \leq \sigma_c) * 0.132 \qquad \text{(G.4)}$$

where $\sigma_c = 3$ ft for H_{mo} and $\sigma_c = \sqrt{2.5^2 + 0.83^2} \, ft$ for SWL. Here, 3.0 ft for H_{mo} and 2.5 ft for SWL are from the validations of ADCIRC and STWAVE (Nadal-Caraballo et al. 2015), and 0.83 ft is the standard deviation of tidal fluctuations, as described above. Usually, the Holland B parameter uncertainty is proportional while other uncertainties are constant; however, the ADCIRC model error has also been shown to be proportional to SWL. Wave period uncertainty is estimated as a function of H_{mo} uncertainty, assuming constant wave steepness, to maintain wave physics. The SWL uncertainty values were determined from high water mark data throughout the region, so these uncertainty values apply to the entire region.

For stochastic simulation, the typical EB approach to incorporate uncertainty is as follows:

1. Compute AEP SWL and H_{mo} using Equation G.1 and associated T_p and MWD based on averaging about $H_{mo} \pm 1$ m. Open averaging range as needed if no storms are found in range. Include 0.15 proportion of uncertainty to produce smooth mean hazard curve.
2. To compute overtopping rate hazard curve, enter Monte Carlo simulation loop and for each discrete AEP value.
   a. Generate a random number between 0 and 1 that represents the probability and select uncertainties for SWL, H_{mo} and associated T_p and MWD.
   b. Apply remaining uncertainty proportion 0.132 to SWL and $H_{mo.}$
   c. Compute overtopping rate including uncertainty of equations.
   d. Repeat for ~10^5 total samples = 189 storms * Number of simulations.
3. Sort results and compute 50% and 90% exceedance probability values.

In the following, two versions of EB simulation were adopted:

- EB1: Step 1 was used with Equations G.3 and G.4 for wave and water level parameters, and these values were then input directly into deterministic versions of the overtopping rate empirical equations.
- EB2: Steps 1, 2, and 3 were followed to compute q hazard curves.

For RB approaches, the steps required are as follows:

1. Start with individual storm values of SWL and H_{m0} and associated T_p and MWD (for example peaks).
2. Separately compute q uncertainty using 0.132 portion of SWL, H_{m0}, and associated T_p and MWD uncertainty combined with stochastic overtopping rate empirical equations.
3. Enter Monte Carlo simulation loop.
   a. Apply 0.15 portion of uncertainty to SWL, H_{m0}, and associated T_p and MWD.
   b. Compute mean hazard curve using deterministic overtopping rate equations.
   c. Use bootstrap resampling and Equation G.4 to compute overtopping rate confidence limit curves including uncertainty calculated in step 2 with ~10^5 samples = 189 storms * Number of simulations.

The three RB approaches included the following simulation scenarios:

- RB1: Peaks method: SWL and H_{m0} peaks and associated T_p and MWD used to compute overtopping rate response.
- RB2: Quasi time-dependent method: SWL, H_{m0}, T_p, and MWD at time-step of maximum q used to compute overtopping rate response.
- RB3: Time dependent method: q computed at all time-steps and maximum from each storm selected for integration in step 3-c.

The only difference between the three RB methods was in how the wave parameters were processed before calculating q.

In the methods above, the standard normal distribution was discretized into 444 values, and 444 replicates were computed rather than the alternative of brute-force Monte Carlo looping. This is a much more efficient way to compute ~10^5 samples in Matlab by taking advantage of

the Matlab vectorization capability, reducing computation time by orders of magnitude.

The methods were checked to determine the sensitivity of q to tide. The approaches were

1. Tide σ was combined with the SWL=2.5 ft as an upper limit to uncertainty.
2. Tide σ was combined with SWL proportional uncertainty.

The results are shown in Figure G-1 where RB1 method is plotted for Port Arthur Transect 58 using the feasibility crest elevation and SLC1 storm forcing conditions. There was no significant difference in q between the different computation methods.

Figure G-1. Treatment of tide within proportional part of uncertainty or as an adjustment to the upper limit of uncertainty.
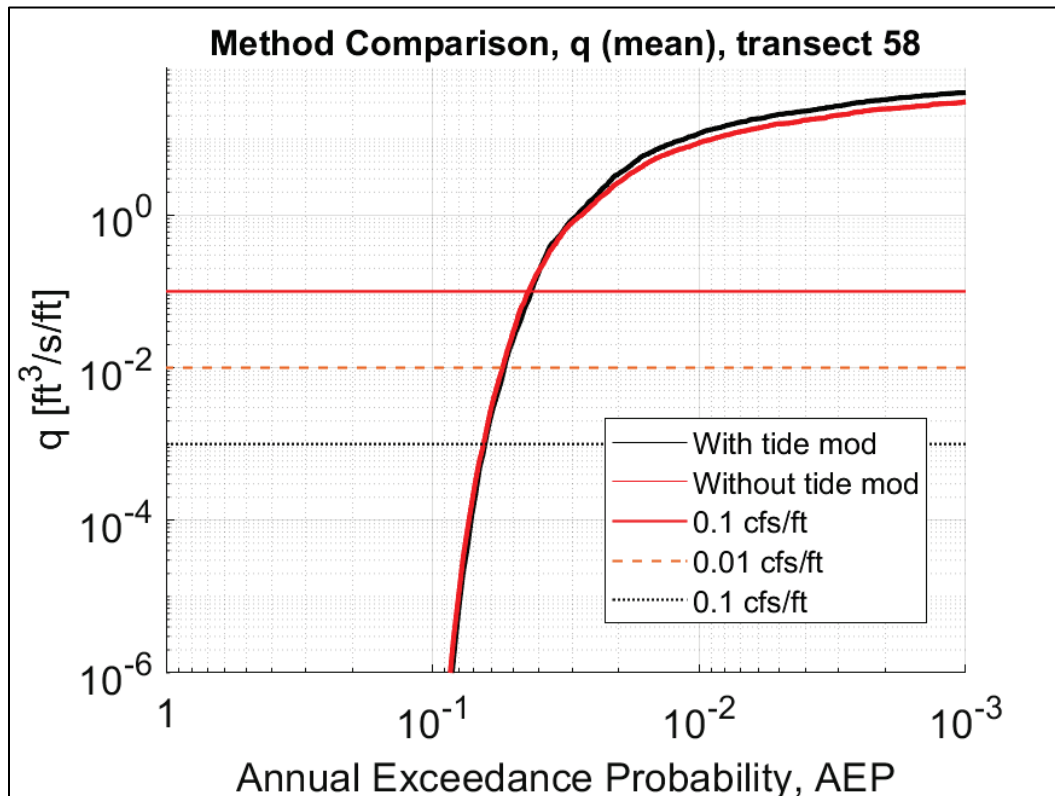
Evaluation of stochastic simulation approaches

The full evaluation of the stochastic simulation approaches was completed using preliminary storm data at Port Arthur Transect 150, with corresponding S2G SP 2591, shown in Figure G-2. An idealized slope of 1:10 and a crest elevation of 15 ft, NAVD88, were used for the comparison of the stochastic simulations. Additionally, multiple S2G SPs with a variety of wave and water level exposures were used to evaluate the methodology effects on the optimized crest elevation using an idealized levee with a slope of 1:6.

EB1 is the simplest and easiest workflow to apply but can lose relevance with respect to risk. For RB approaches, RB1 with storm peaks is easier to apply than RB2 or RB3 but may yield overly conservative results because H_{m0} and SWL do not peak at the same time for most storms. Additionally, peak H_{m0} and SWL may occur between time-steps; therefore, the time-series forcings will not reflect the absolute maximum H_{m0} and SWL during a storm. These errors are relatively small for the most intense storms where SWL and H_{m0} hydrographs are in phase in the areas of the CSRM systems, as shown in Figure G-3.

Figure G-2. Location of transect 150 and SP 2591 at the north end of SNWW.
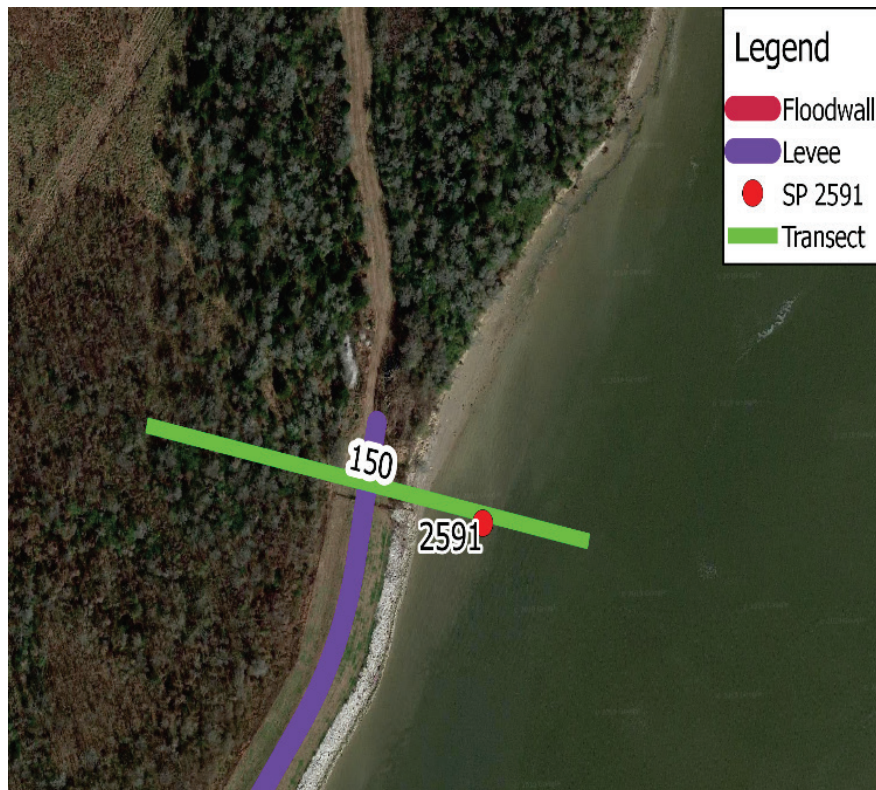
Figure G-3. Time series for storm 606 at S2G SP 2591, corresponding to Transect 150.
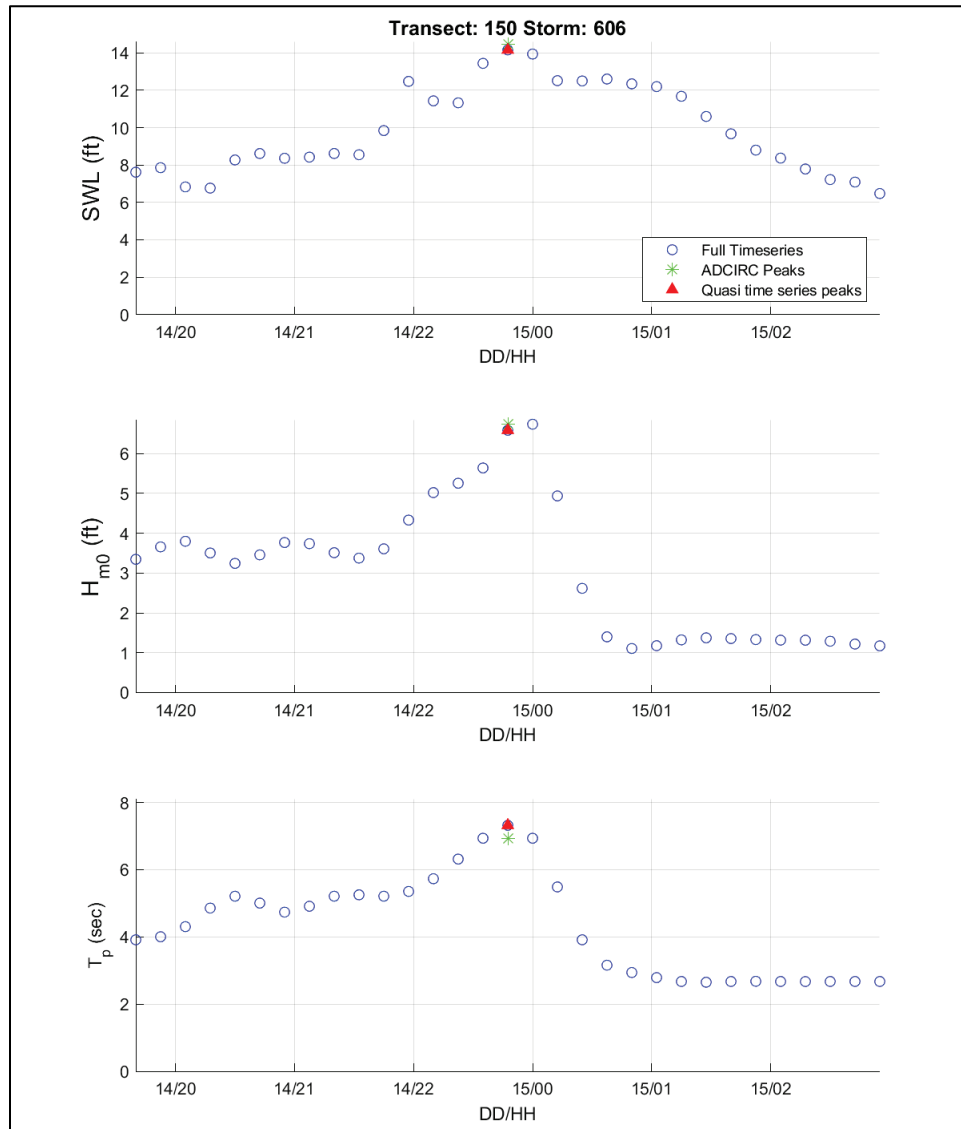
RB2 evaluated the storm forcings in the time series that produced the maximum overtopping rate. The SWL and H_{m0} used in RB2 were compared to peak SWL and H_{m0} used in RB1. The results are shown in Figures G-4 for SWL and G-5 for H_{m0}. Overall, most of the storms have the same value for both approaches. There is a slight high bias for RB1 because peak SWL and H_{m0} are more often higher than that of RB2. The peak SWL trends slightly higher. There are a few values where the peaks are significantly higher than the quasi-time-dependent values for both SWL and H_{m0} but these tend to be for relatively lower intensity storms and these outliers are not influential for the hazard curve.

Figure G-4. Peak value of SWL that produces peak q vs. storm peak SWL for 189 S2G storms at S2G SP 2591 corresponding to Transect 150.
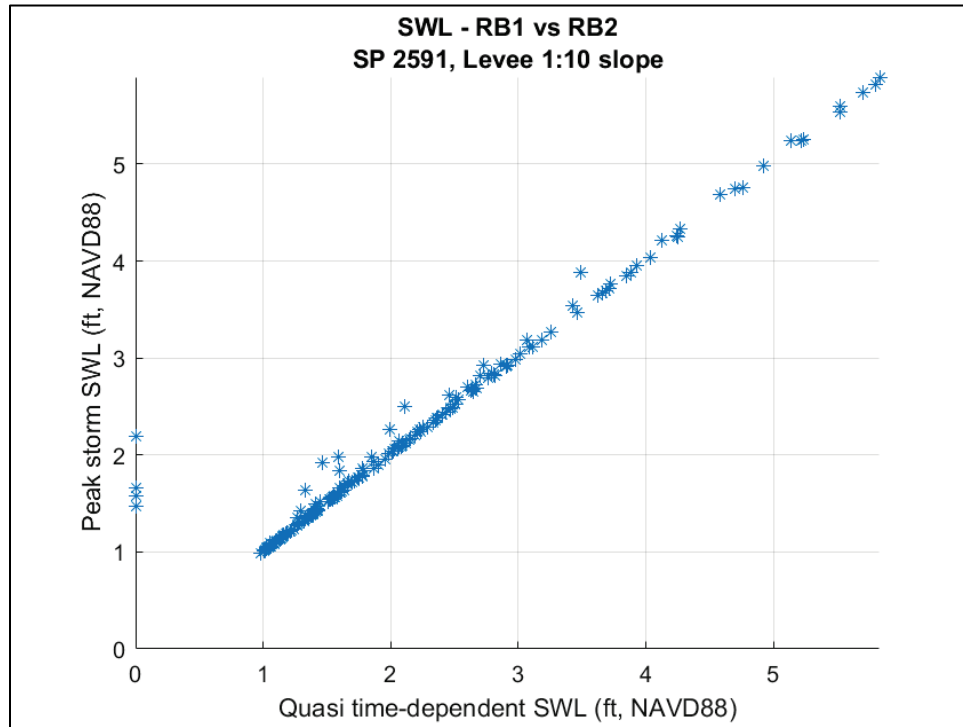
Figure G-5. Peak value of H_{m0} that produces peak q vs. storm peak H_{m0} for 189 S2G storms at S2G SP 2591 corresponding to Transect 150.
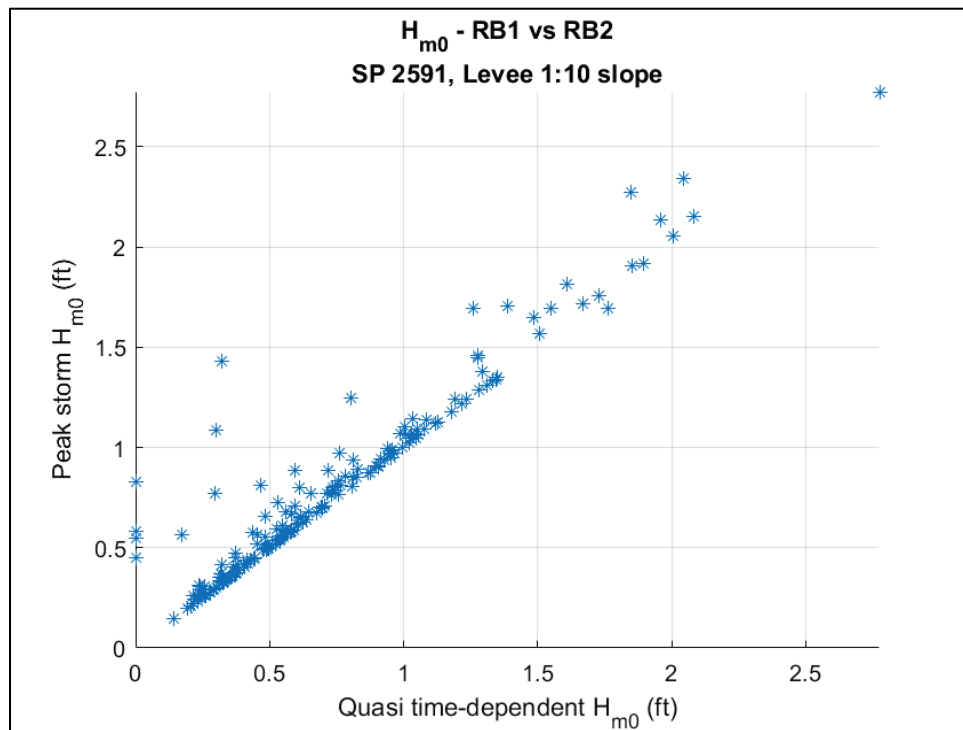
Figure G-6 shows the overtopping hazard curves for an idealized transect 150 with a slope of 1:10 and crest elevation of 15 ft, NAVD88. The RB methods are virtually identical at both the 50% and 90% CL. Similarly, the EB methods are nearly identical for the entire AEP range at the 50% CL but deviate at the 90% CL. The EB methods are significantly different from the RB methods. Stehno (2021) showed that RB1 is similar to RB3, but EB2 can result in either overestimation or underestimation of overtopping, and the over/underestimations did not correlate to either structure geometries or coastal hazards. A full error analysis was done in Stehno (2021) and showed that there was large scatter in EB2 clearly illustrating this method provides poor estimates of overtopping rate hazard.

Note that RB3 simulation takes nearly an order of magnitude more computational time than the other two RB approaches; however, the results of this comparison show that RB1 produces a reasonable approximation of the overtopping rate hazard curve. The quasi-time-dependent method is more efficient than RB3 when computing the hazard due to its relatively low computational requirements. The peaks-based method was even more efficient than both RB2 and RB3 when computing the hazard; therefore, the peak-based method (RB1) was most efficient of the RB methods.

Figure G-6. Method comparison of q 50% and 90% CL for Transect 150, SP 2591, 1:10 slope and 15 ft NAVD88 crest elevation, SLC1 with-project.
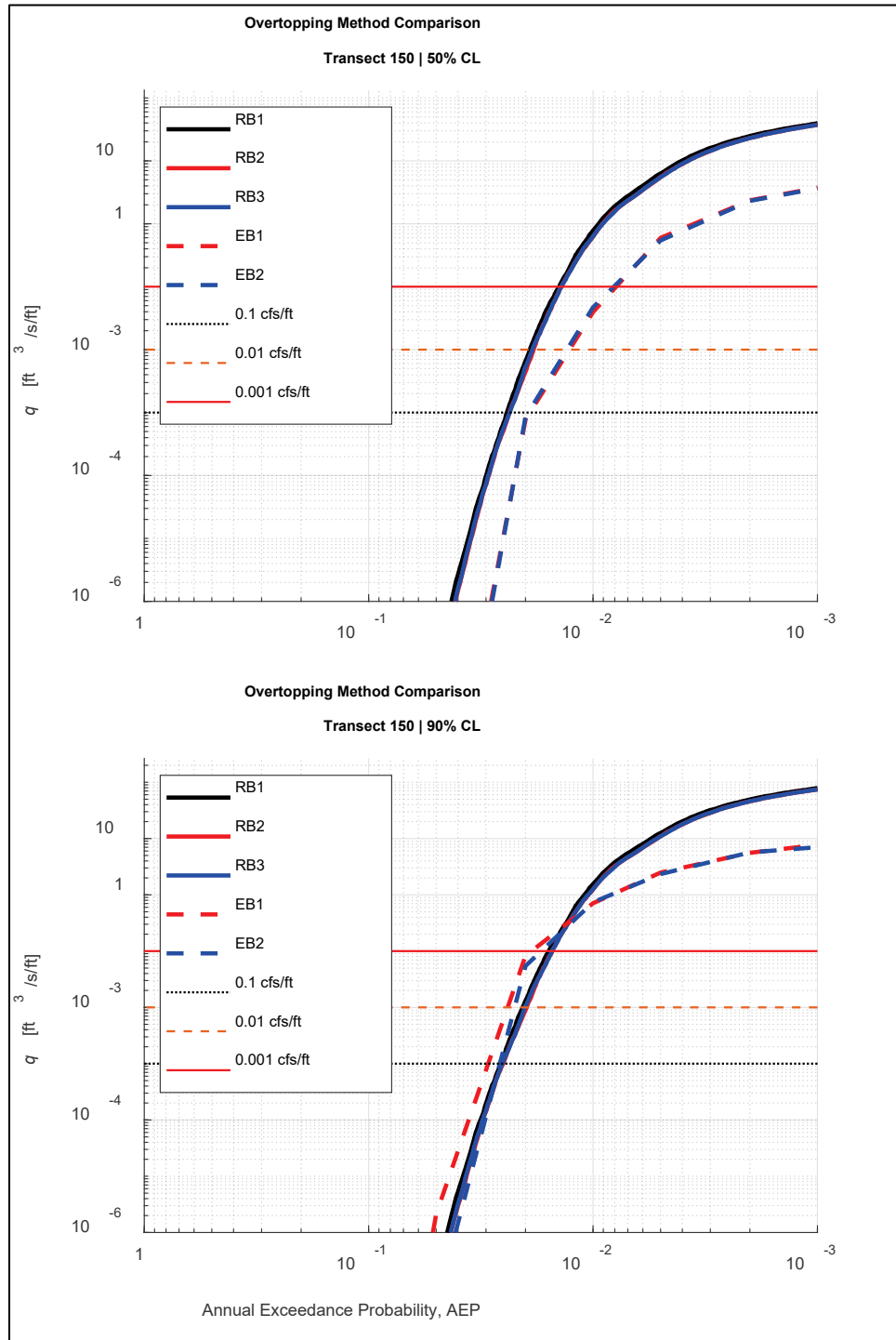
The methods were also compared for determining optimized levee crest elevation. For each method, an overtopping rate was computed for a low crest elevation. If the overtopping rate for a 1% AEP was less than the overtopping rate limit state of $q=0.1$ cfs/ft for a 90% CL, then 0.5 ft elevation was added to the crest, and the overtopping rate was re-computed. This was repeated until the overtopping rate limit state was satisfied. The resulting crest elevations for an idealized levee with a 1:6 slope are listed in Table G-1 for six S2G SPs representing a variety of exposures. Note that the SPs presented below may correspond to an analysis transect on the CSRM system, but the structure geometry may be different and result in a different elevation than those presented in the data reports. Only the SCL1 condition is presented.

Optimized crest elevations are considered equal between methods if they are within 0.5 ft, which was used as the elevation step increase during the optimization routine. The three RB methods resulted in identical crest elevations for the SPs in this analysis.

Table G-1. Design crest elevations in feet, NAVD88, for 1:6 levee using S2G SPs under with-project SLC1 storm forcing conditions.

Save Point	RB1	RB2	RB3	EB1	EB2
2591	20.5	20.5	20.5	21.0	20.0
1324	15.5	15.5	15.5	17.0	17.0
1682	15.0	15.0	15.0	18.5	16.5
1741	15.5	15.5	15.5	18.0	18.0
3830	15.0	15.0	15.0	16.0	16.0
4472	16.5	16.5	16.5	17.5	17.0

The EB analyses resulted in -0.5 to 3.5 ft error compared to RB3. This result is consistent with Stehno (2021) who found large scatter in overtopping rate using the EB methods. Although the EB analysis is less complex and computationally less demanding than the RB, the overtopping results are not very reliable and result in potential over- or underdesign of the structure with large potential cost implications for overprediction or lower safety levels for underprediction.

The idealized levee structure with a 1:10 slope for transect 150 was evaluated under SLC2 with-project storm forcing conditions. The resulting crest elevations are listed in Table G-2.

Table G-2. Design crest elevations in feet, NAVD88, for Transect 150 (feet, NAVD88) using SP 2591 under with-project SLC2 storm forcing conditions. The structure included an idealized levee with a 1:10 seaward slope.

Save Point	RB1	RB2	RB3	EB1	EB2
2591	23.0	23.0	22.5	26.0	25.0

The EB methods greatly over-estimated the optimized crest elevation by 2.5 and 3.5 ft for EB2 and EB1, respectively. RB1 and RB2 were within the 0.5 ft of RB3; however, the above analysis suggests that there is some error from using the storm peaks or quasi-time series. A comparison of AEP was accomplished, and it was found that the error is not large enough to warrant using the more complicated RB3 method for S2G. This was further supported during the design elevation analysis where the three RB methods resulted in similar design elevations. An additional error term was added to account for the uncertainty in overtopping from using the simplified peaks-only method, but it was found that this error term had no measurable impact on the results.

Impact of SWL and H_{m0} correlation

In Appendix B, a correlation analysis was summarized that showed that SWL and H_{m0} were highly correlated for shallow locations. Herein, an analysis of correlated and uncorrelated uncertainties was performed to determine the impact on the final response results. Figure G-7 shows the q results for Port Arthur Transects 56 and 58. It is clear from the figures that there is no significant difference between assuming uncorrelated uncertainties or using the full correlation.

Figure G-7. *q* at 50% and 90% confidence limits using RB1 and with-project SLC1 scenario showing impact of uncorrelated and fully correlated SWL and H_{m0} uncertainties.
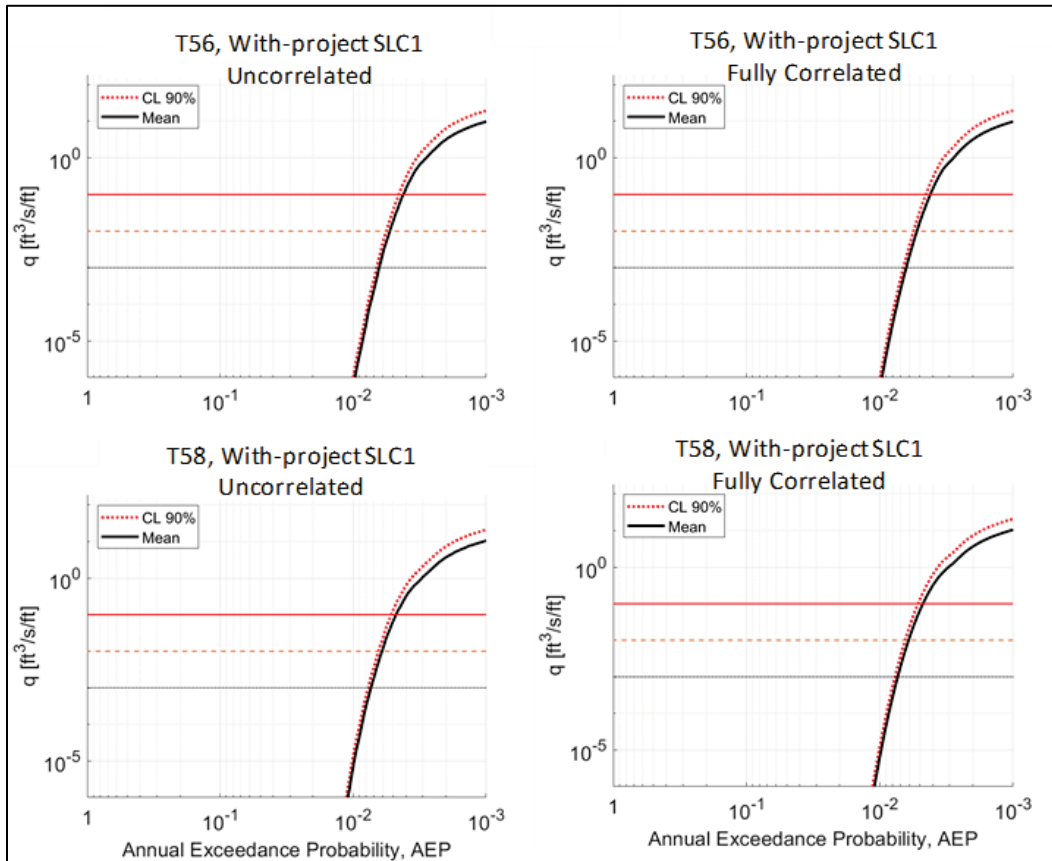
Appendix H: Relative Sea Level Rise

This chapter presents a slide deck compiled by Shubhra Misra (SWG) to support SLC values used in this study within geoid offsets in CSTORM simulations.

Review of Previously Adopted RSLC Values

S2G Final Integrated Feasibility Report Environmental Impact Study (2017)

- RSLC results based on USACE ER 1100-2-8162 and ETL 1100-2-1.
- Base year for calculations: **1992** (midpoint of the last National Tidal Datum Epoch, 1983-2001)
  - Governing equation:

$$E(t) = 0.0017t + bt^2$$

where: 0.0017 corresponds to the observed 1.7 mm/yr global GMSL change presented at IPCC (2007a), t is time in years, and b is a coefficient corresponding to the scenario being considered (low, intermediate, or high).
  - **Note: The sea level change magnitudes presented in the feasibility report are relative to the base year 1992, not the beginning of the S2G service life.**

Methodology

- RSLC calculations were performed with the USACE Sea-Level Change Curve Calculator (Ver. 2017.55), based on ER 1100-2-8162 (2013), with the governing equation:

$$E(t_2) - E(t_1) = 0.0017(t_2 - t_1) + b(t_2^2 - t_1^2)$$

where 0.0017 corresponds to the observed 1.7 mm/yr global GMSL change presented at IPCC (2007a), t_1 is the number of years from 1992 to the beginning of the project service life, t_2 is the service period under consideration, and b corresponds to the scenario under consideration.
- Base year for calculations: **2027** (Beginning of S2G service life)
- Scenarios
  - **Low**: Linear prediction based on historically-recorded data sets (b = 0.00)
  - **Intermediate**: Modified NRC Curve I (b = 2.71E-5)
  - **High**: Modified NRC Curve III (b = 1.13E-4)

Procedures

- To allow for a comparison between the values generated for this presentation and those contained in previous reports, all results were regenerated for the updated time spans considering originally adopted base years.
- To accomplish this, the following steps were taken:
  1. The previously adopted S2G base year was entered into the Sea-Level Change Curve Calculator (Ver. 2017.55).
  2. It was ensured that identical results were produced for the years reported within previous publications. Therefore, the new values generated are representative of the conclusions made in the aforementioned reports.
  3. The results produced by this effort and the S2G FIFR were compiled for comparison.

Results: RSLC After 20-Year Service Age (Start of Service Life : 2027)

Estimated RSLC from 2027 to 2047 (20-year service age)

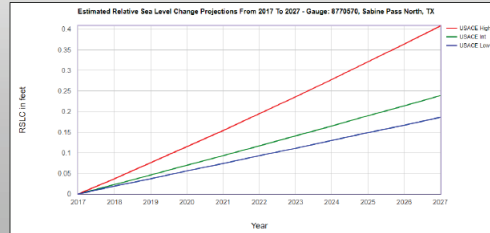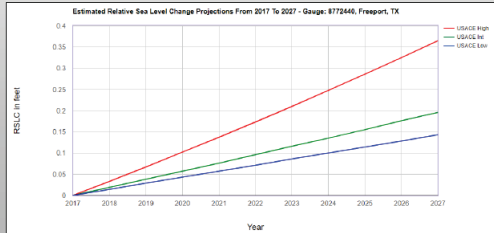| Project Area	Tidal Gage	Relative Sea Level Change Values (USACE)					
		Low (ft)		Intermediate (ft)		High (ft)	
		Historic Rate	Sabine to Galveston FIFR EIS (2017)	NRC Curve I	Sabine to Galveston FIFR EIS (2017)	NRC Curve III	Sabine to Galveston FIFR EIS (2017)
Port Arthur, TX Orange, TX	Sabine Pass North	0.37	1.02	0.53	1.29	1.04	2.14
Freeport, TX	Freeport	0.28	0.79	0.45	1.05	0.95	1.91
Base (Start) Year for RSLC Cal		2027	1992	2027	1992	2027	1992
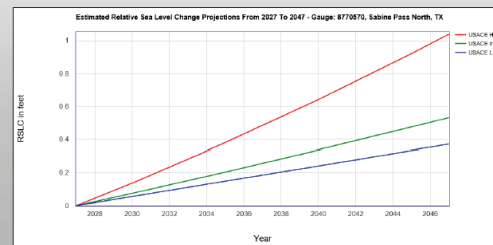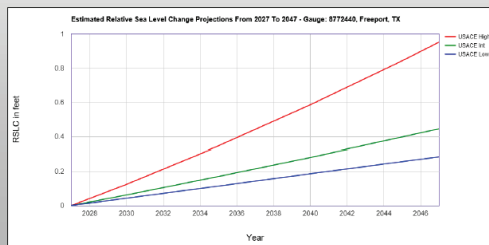
Results: RSLC After 50-Year Service Age (Start of Service Life : 2027)

Estimated RSLC from 2027 to 2077 (50-year service age)

Project Area	Tidal Gage	Relative Sea Level Change Values (USACE)					
		Low (ft)		Intermediate (ft)		High (ft)	
		Historic Rate	Sabine to Galveston FIFR EIS (2017)	NRC Curve I	Sabine to Galveston FIFR EIS (2017)	NRC Curve III	Sabine to Galveston FIFR EIS (2017)
Port Arthur, TX Orange, TX	Sabine Pass North	0.93	1.58	1.46	2.22	3.15	4.26
Freeport, TX	Freeport	0.71	1.21	1.25	1.86	2.94	3.89
Base (Start) Year for RSLC Cal		2027	1992	2027	1992	2027	1992
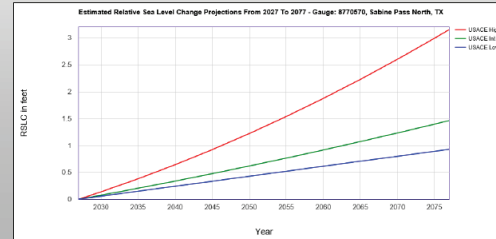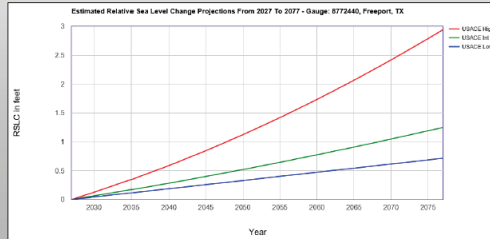
Results: RSLC After 100-Year Service Age (Start of Service Life : 2027)

Estimated RSLC from 2027 to 2127 (100-year service age)

Project Area	Tidal Gage	Relative Sea Level Change Values (USACE)					
		Low (ft)		Intermediate (ft)		High (ft)	
		Historic Rate	Sabine to Galveston FIFR EIS (2017)	NRC Curve I	Sabine to Galveston FIFR EIS (2017)	NRC Curve III	Sabine to Galveston FIFR EIS (2017)
Port Arthur, TX Orange, TX	Sabine Pass North	1.86	2.51	3.37	4.13	8.16	9.26
Freeport, TX	Freeport	1.43	1.93	2.94	3.55	7.73	8.68
Base (Start) Year for RSLC Cal		2027	1992	2027	1992	2027	1992

RSLC for S2G (continued)
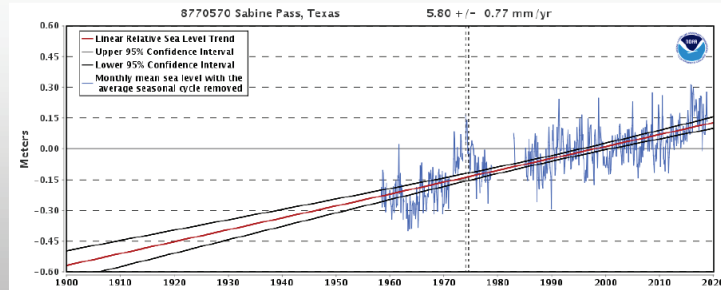
- Scenario 1 (Beginning of Service Life; Low) : 0.17 ft

- Scenario 2 (50-year Service Life; Intermediate) : RSLC = 0.22 + 1.36 = 1.58 ft

- Scenario 3 (100-year Service Life; Intermediate) : RSLC = 0.22 + 3.16 = 3.38 ft

Mean Sea Level to NAVD88 at Sabine Pass North (8770570)
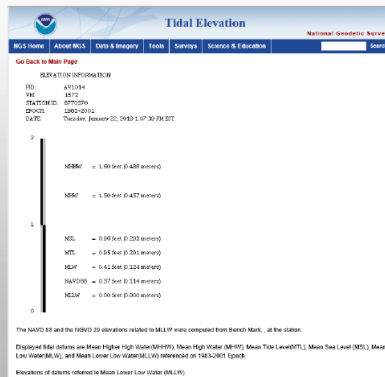
MSL (1992, ft, NAVD1988) = 0.96 – 0.37 = 0.59 ft (NAVD 1988)

Mean Sea Level Trend at Sabine Pass North (8770570)

MSL (2017, ft, NAVD1988) = MSL (1992, ft, NAVD1988) + 5.8 mm/yr x 0.00328084 ft/mm x 25 yrs = 0.59 ft + 5.8 mm/yr x 0.00328084 ft/mm x 25 yrs = 1.07 ft (NAVD 1988)

Mean Sea Level to NAVD at Freeport (8772440)

MSL (1992, ft, NAVD1988) = 0.95 – 0.46 = 0.49 ft (NAVD 1988)

Mean Sea Level Trend at Freeport
(8772440)

Apparent Datum Shift
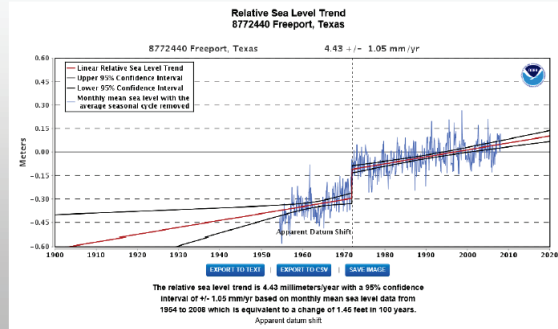
MSL (2017, ft, NAVD1988) = MSL (1992, ft, NAVD1988) + 4.43 mm/yr x 0.00328084 ft/mm x 25 yrs = 0.49 ft + 4.43 mm/yr x 0.00328084 ft/mm x 25 yrs = 0.85 ft (NAVD 1988)

2017 Mean Sea Level (ft, NAVD1988) for ADCIRC simulations

[MSL (2017, ft, NAVD1988) at Sabine Pass North] + [MSL (2017, ft, NAVD 1988) at Freeport] / 2

=

(1.07 + 0.85)/2

=

0.96 ft (NAVD 1988)

Appendix I: Nonlinear Residual

CSTORM is a coupled modeling system that includes wind and pressure forcing and coupled wave and surge responses. Therefore, SWL responses include the effects of wind setup, currents, and wave setup, among others. These effects are often larger in confined areas, such as in relatively narrow canals and near structures. A common practice in coastal engineering is to linearly superimpose modeled surge with sea level rise, tide, and other SWL offsets. There is an error introduced in the responses from linearly adding an offset to the SWL that is known as a nonlinear residual, and this error is due to the exclusion of the complex interaction between wind, currents, waves, and water levels. This nonlinear residual is computed here as the difference between the full CSTORM simulation SWL (with wind, waves, and different geoid offsets) and that computed with offsets added linearly in post-processing. An analysis of nonlinear residual was done for several storms that significantly impacted the study area. Three levels of geoid offset were used to simulate the entire S2G 189 storm suite: SLC0 = 1.52 ft, SLC1 = 2.93, and SLC2 = 4.73 ft. For the purposes of this nonlinear analysis, a fourth value, SLC3=1.10 ft, was simulated for three storms of record (532, 598, and 634) for the purpose of examining a smaller linear difference between geoid offsets.

In the following, color contour plots of maximum water surface elevations and the spatial distribution of nonlinear residual are presented for storms 532, 598, and 634 and the four geoid offsets: SLC0 = 1.52 ft, SLC1 = 2.93 ft, SLC2 = 4.73 ft, and SLC3 = 1.10 ft. ft. The NLR is computed as NLR = (Max Surge SLCA) - ((Max Surge SLCB) + (SLCA - SLCB)) where A and B = 0, 1, 2, 3. Table I-1 shows the values of the linear difference in geoid offsets for each of the four cases.

Table I-1. List of SLC values and the linear difference combinations used for making comparisons of nonlinear residual impacts to water levels.

Case	SLC1 - SLC0	SLC2 - SLC1	SLC2 - SLC0	SLC0 - SLC3
Linear Difference	(2.93-1.52) = 1.41 ft	(4.73-2.93) = 1.80 ft	(4.73-1.52) = 3.21 ft	(1.52-1.10) = 0.42 ft

Figure I-1 shows four maximum water surface elevation contour maps for storm 532 under the various geoid offset conditions. These results are from the full CSTORM simulation results and offer a regional view of the Port Arthur and Orange County region of the Texas coast. The black lines

in the maps represent the Port Arthur CSRM structures as represented in the ADCIRC mesh. Notice that under the SLC2 condition, the area is almost completely inundated with water surface elevations in the range of 20+ ft. Figure I-2 shows NLR contour maps for storm 532 under four different linear difference plots. The figures illustrate that over most of the region, the NLR is small, but in the vicinity of the structures, the NLR can be 2 to 3 times the linear offset difference. Furthermore, the NLR is also dependent on the water levels (meaning with larger offsets, there may be more NLR in the same area than when a smaller offset was considered). This is illustrated behind the flood protection structures in the NLR plot for SLC2 – SLC1.

Color contour plots of maximum water surface elevations for storm 598 are shown in Figure I-3, and the associated NLR spatial distribution is shown in Figure I-4. Similar results to those shown for storm 532 are observed in areas that were inundated by both storms.

Finally, color contour plots of maximum water surface elevations for storm 634 are shown in Figure I-5 and plots for the NLR spatial distribution are shown in Figure I-6. The results for storm 634 are similar to those shown for storms 532 and 598 in areas that were inundated by both storms.

Figure I-1. Color contour plots of maximum water surface elevation for storm 532, for SLC0, SLC1, SLC2, and SLC3. Note that the color scales are the same for each SLC case plotted here.
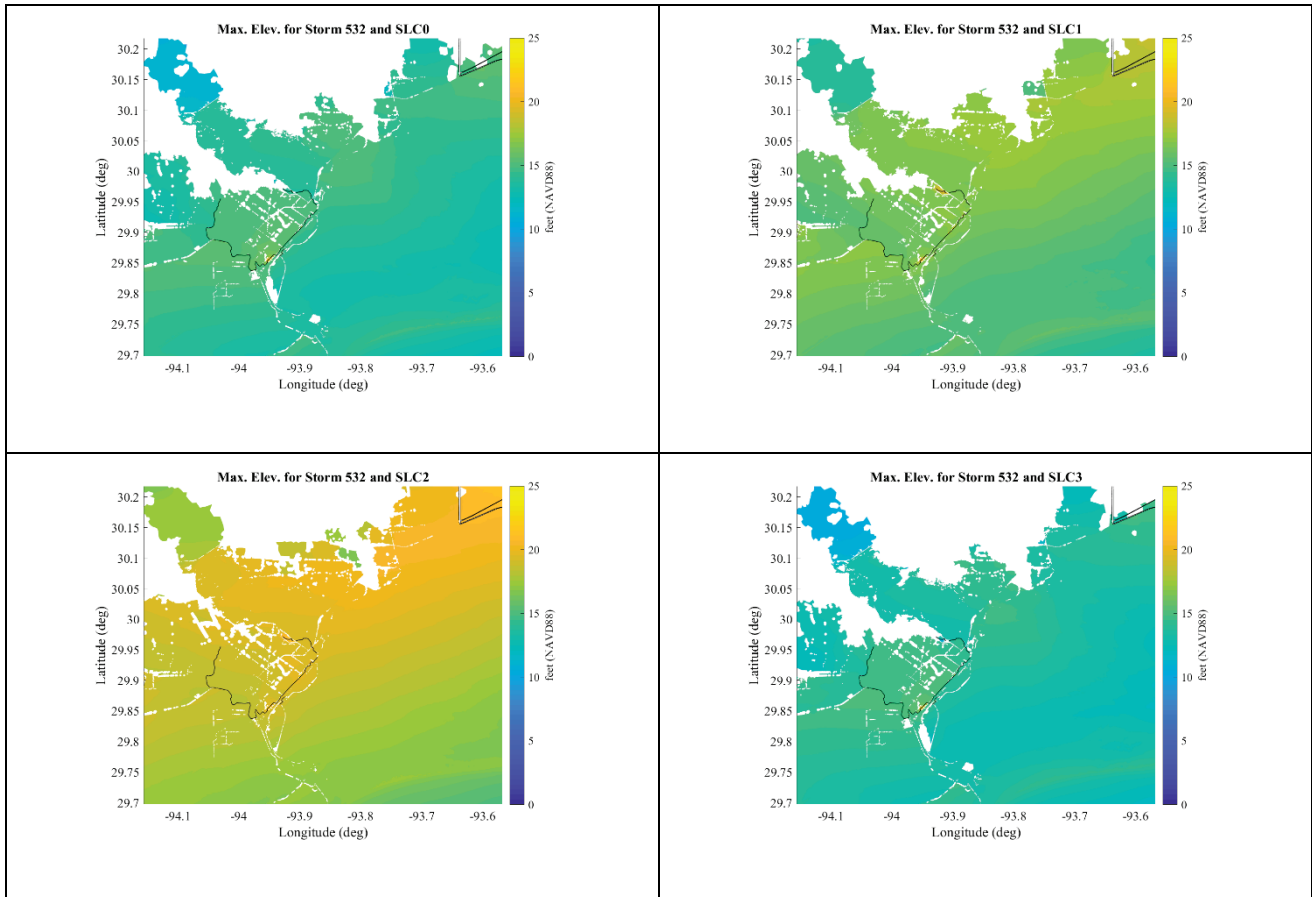
Figure I-2. Spatial distribution of NLR for storm 532 for four linear offsets. Left column is regional view of Port Arthur and Orange County. Right column is the area near Taylor Bayou Turning Basin in Port Arthur. Note color scales change from one row to the next.
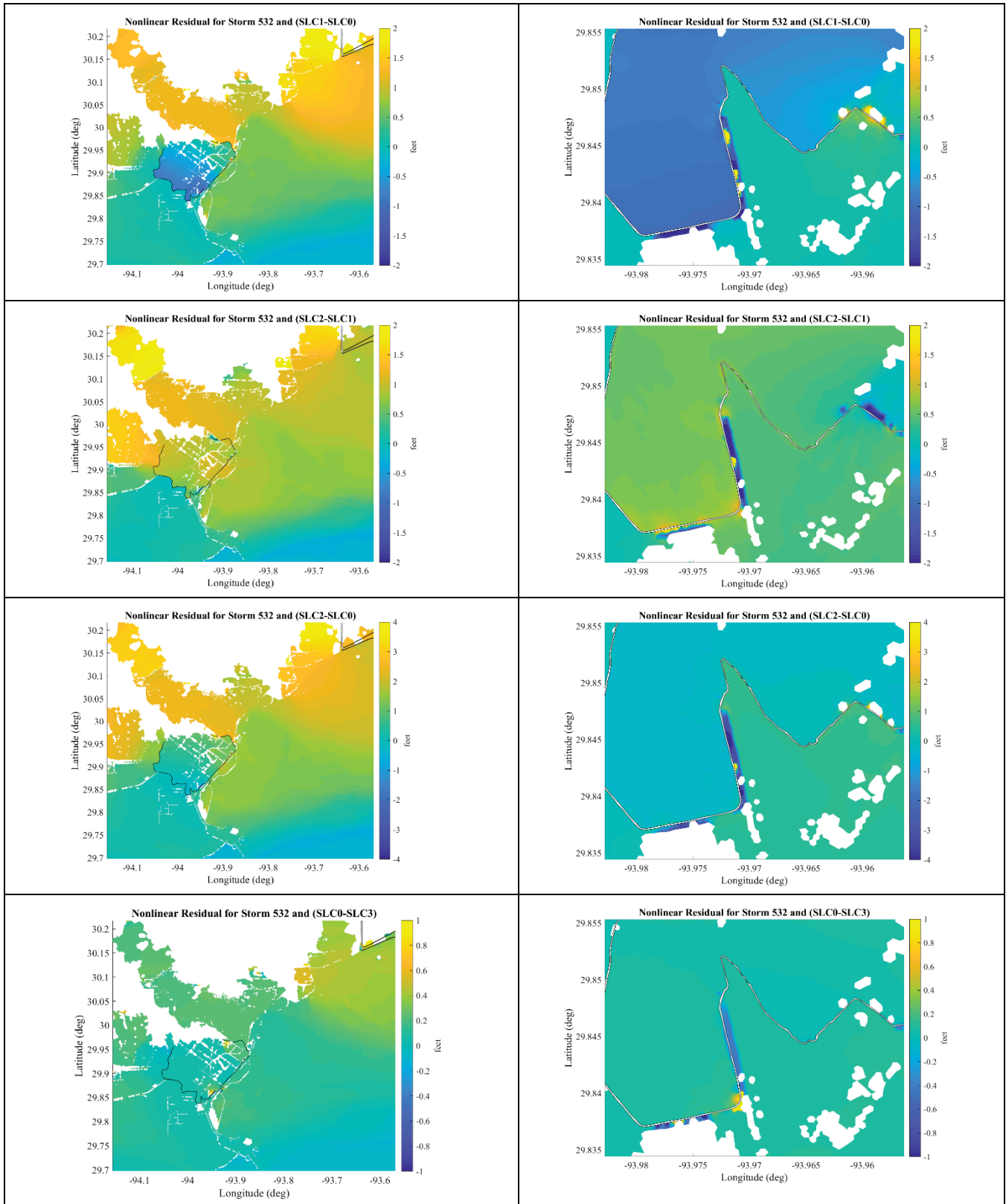
Figure I-3. Maximum water surface elevation for storm 598, for SLC0 (upper left), SLC1 (upper right), SLC2 (lower left), and SLC3 (lower right). Note color scales are the same for each SLC case plotted here.
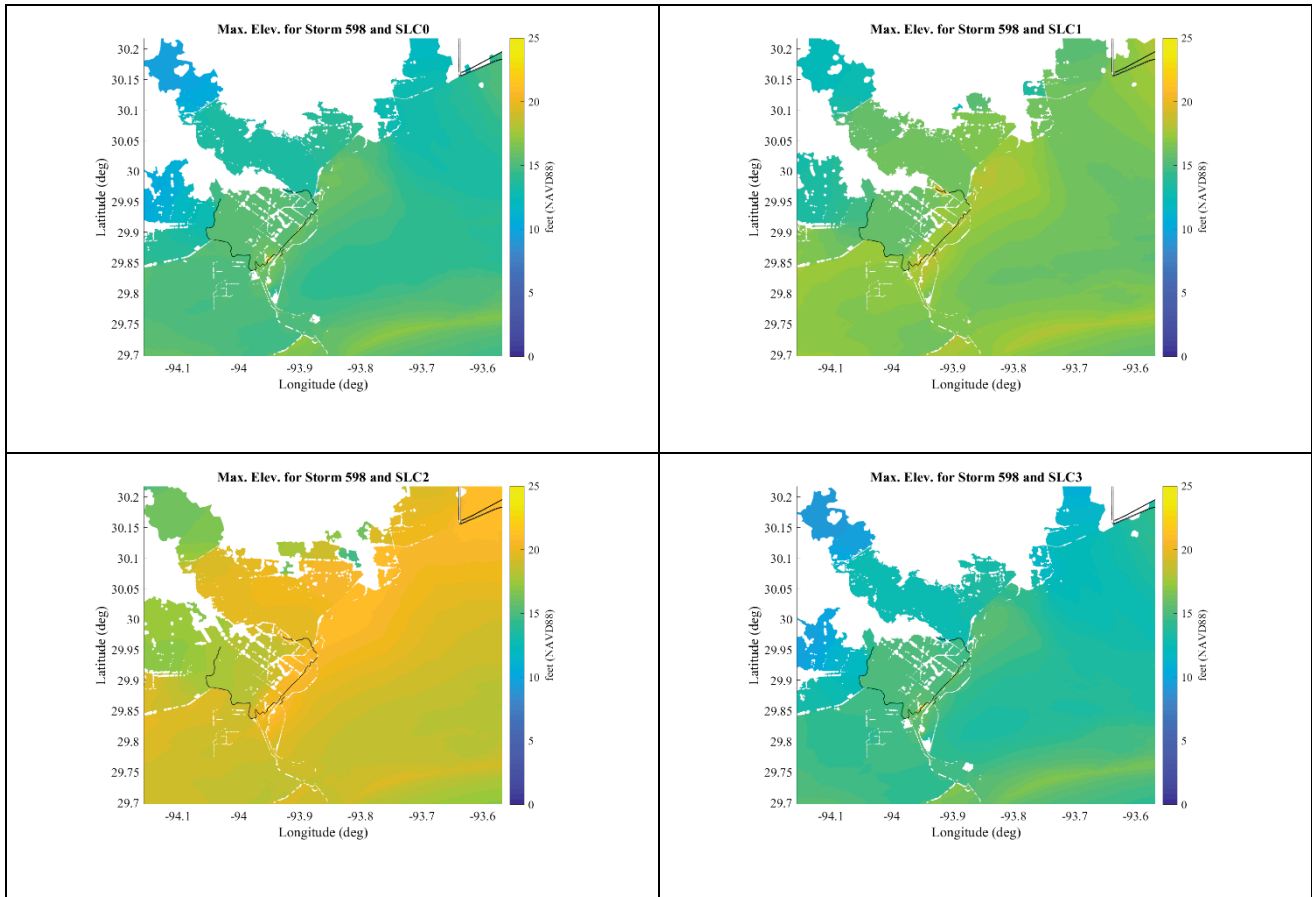
Figure I-4. Spatial distribution of the NLR for storm 598 among four different water level combinations. Left column is regional view of Port Arthur and Orange County while right column is the area near Taylor Bayou Turning Basin in Port Arthur.
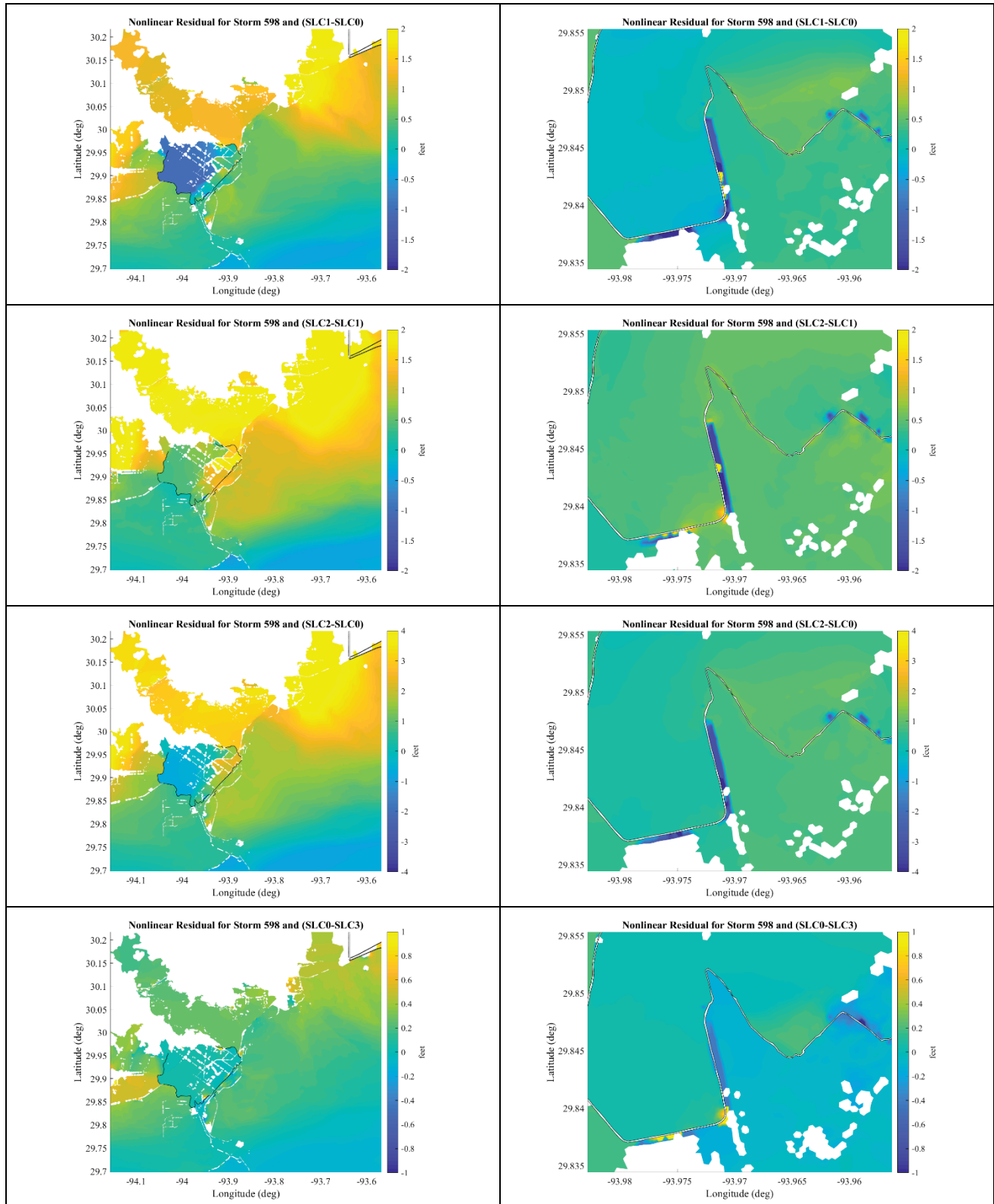
Figure I-5. Maximum water surface elevation for storm 634 for SLC0 (upper left), SLC1 (upper right), SLC2 (lower left), and SLC3 (lower right). Note color scales are the same for each SLC case plotted here.
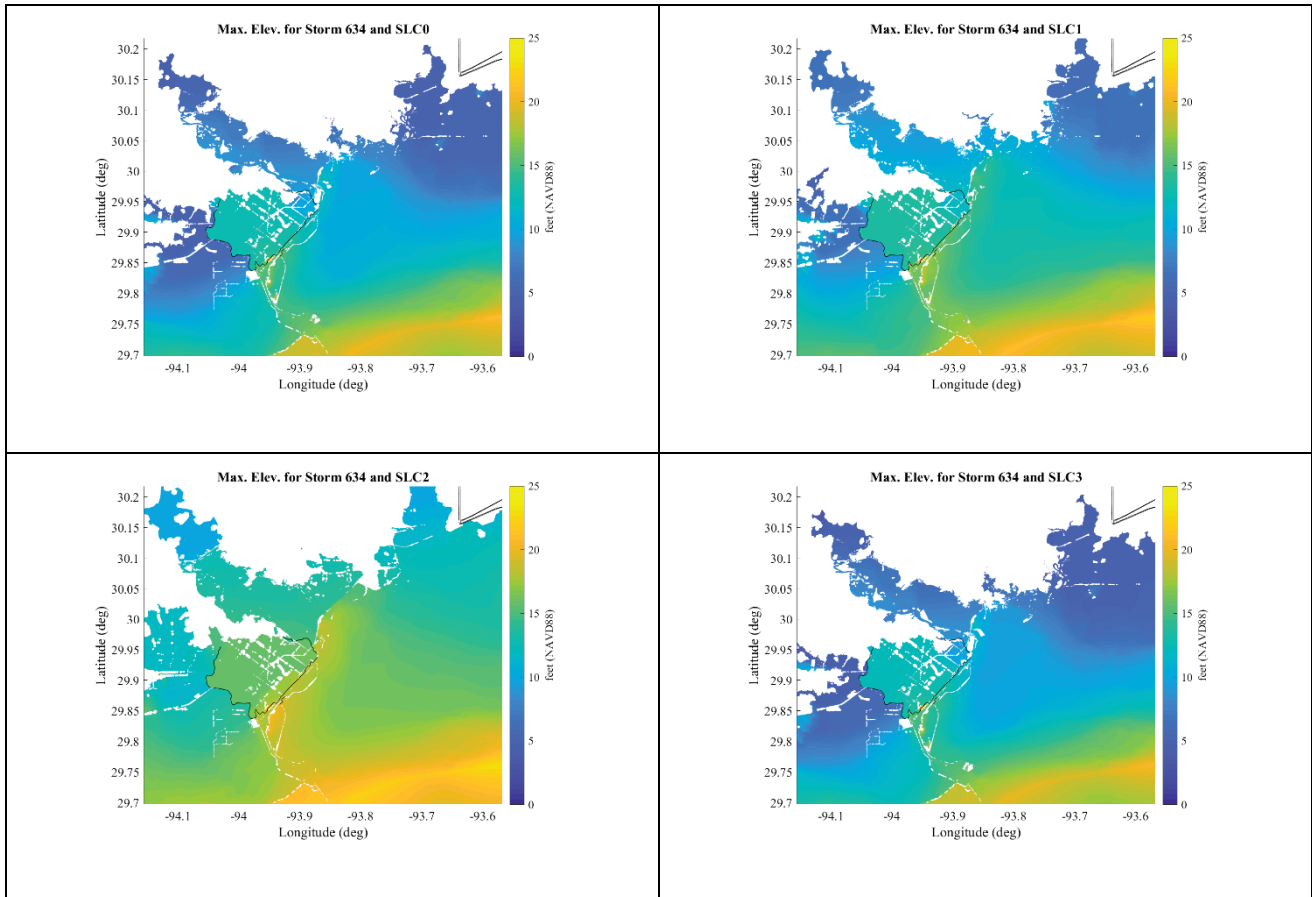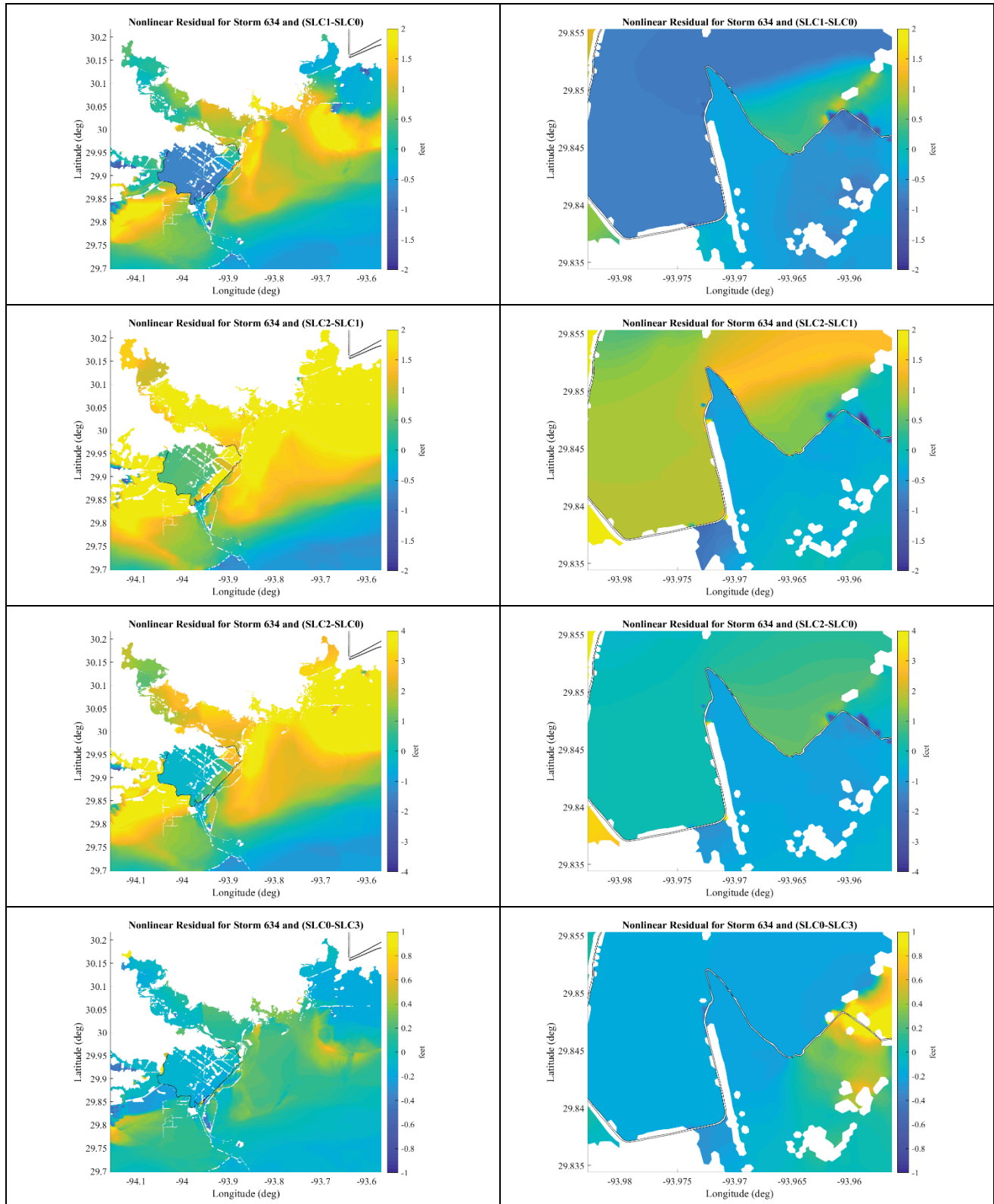
Figure I-6. Spatial distribution of the NLR for storm 634 among four different water level combinations. Left column is regional view of Port Arthur and Orange County while right column is the area near Taylor Bayou Turning Basin in Port Arthur.

Appendix J: Chief of Engineers S2G Report

DEPARTMENT OF THE ARMY
CHIEF OF ENGINEERS
2600 ARMY PENTAGON
WASHINGTON, DC 20310-2600

DAEN   DEC 0 7 2017

THE SECRETARY OF THE ARMY

SUBJECT: Sabine Pass to Galveston Bay, Texas, Coastal Storm Risk Management and
Ecosystem Restoration Study

1. I submit for transmission to Congress my report on Coastal Storm Risk Management (CSRM)
and Ecosystem Restoration (ER) within six counties of the upper Texas coast (Orange, Jefferson,
Chambers, Harris, Galveston, and Brazoria Counties). It is accompanied by the report of the
Galveston District Engineer and the Southwestern Division Engineer. These reports are a partial
response to a resolution from the Committee on Environment and Public Works dated June 23,
2004, entitled "Coastal Texas Protection and Restoration Study." The resolution requested that
this study be undertaken to "develop a comprehensive plan for severe erosion along coastal
Texas for the purposes of shoreline erosion and coastal storm damages, providing for
environmental restoration and protection, increasing natural sediment supply to coast, restoring
and preserving marshes and wetlands, improving water quality, and other related purposes to the
interrelated ecosystem along the coastal Texas area." The project area was hit by a Category 4
hurricane, Hurricane Harvey, on August 25, 2017. At the time of signature of this Report of the
Chief of Engineers damage assessments are still underway. Early reports indicate extensive
flooding and damages across the project area in addition to the loss of 10 lives in Orange County
and four lives in Jefferson County. Preconstruction engineering and design (PED) activities, if
funded, would be continued under the authorities provided by the resolution cited above.

2. The reporting officers' recommendation for the upper Texas coastal region encompassing the
six counties along 120 miles of coastline include authorization of a plan to reduce the risks of
tropical storm surge impacts in Orange, Jefferson and Brazoria Counties through the construction
of structural measures and the continuation of the study of the Galveston region (Galveston,
Harris, and Chambers Counties) for CSRM. Continuation of the study of ER alternatives
assessed in the six counties will be conducted under the comprehensive Coastal Texas Protection
and Restoration feasibility study. The recommended plan was developed utilizing a region-wide
systems approach to achieve the full range of benefits, although the CSRM plans are separable
and able to function individually. The plan includes (i) increasing the level of performance and
resiliency of the existing Port Arthur and Vicinity Hurricane Flood Protection (HFPP) project in
Jefferson County, Texas (the Port Arthur and Vicinity CSRM Plan); (ii) the construction of a
new levee/floodwall system (the Orange 3 CSRM Plan) along the edge of the Sabine and Neches
River floodplains from Orange, Texas to the vicinity of Orangefield, Texas that is approximately
26.7-miles; and (iii) increasing the level of performance and resiliency of the existing Freeport
and Vicinity HFPP project in Brazoria County, Texas (the Freeport and Vicinity CSRM Plan).

DAEN
SUBJECT: Sabine Pass to Galveston Bay, Texas, Coastal Storm Risk Management and
Ecosystem Restoration Study

3. Based on October 2017 price levels, the estimated project first cost of the recommended plan,
which includes three separable elements, is $3,318,772,000. All construction work will be cost
shared in accordance with the cost sharing provisions of Section 103 of the Water Resources
Development Act (WRDA) of 1986, as amended (33 U.S.C. 2213). The Federal share of the
project first costs of the hurricane and storm damage risk reduction features is estimated to be
$2,157,202,000 (65 percent) and the total non-Federal share is estimated to be $1,161,570,000
(35 percent). The total cost of non-Federal contribution of lands, easements, rights-of-way,
relocations, and dredged or excavated material disposal areas (LERRDs) is estimated to be
$52,451,000. The total annual cost of Operation, Maintenance, Repair, Replacement and
Rehabilitation (OMRR&R) of the project is currently estimated to be $5,585,000 per year. The
OMRR&R estimate includes $41,000 per year for monitoring of the environmental mitigation
component after the commencement of OMRR&R. Based on a 2.75 percent discount rate and a
50-year period of analysis, the total equivalent average annual costs of the three separable
elements for the project are estimated to be $141,799,000 including OMRR&R. Additionally,
the non-Federal sponsors would be fully responsible for removing and relocating utilities and
discharge pipelines on the project site that are non-compensable, at a total cost estimated to be
$128,320,000. The equivalent average annual benefits for the three separable elements are
estimated to be $452,633,000 with net average annual benefits of $310,834,000. The
recommended plan is the National Economic Development plan.

   a. The first element of the recommended plan is the Port Arthur and Vicinity CSRM Plan.

      (1) The Port Arthur and Vicinity CSRM Plan would raise approximately 5.5 miles of the
existing 27.8 miles of earthen levee to elevations ranging from 14.4 to 17.2 feet North American
Vertical Datum (NAVD 88), and construct or reconstruct approximately 5.7 miles of floodwall
to elevations ranging from about 14.4 to 19.4 feet NAVD 88. A separate 1,830 feet of new
earthen levee would be constructed in the Port Neches area northwest of the existing northern
terminus. Additionally, 26 vehicle closure structures would be replaced and erosion protections
would be added.

      (2) The existing Port Arthur HFPP local sponsor, Jefferson Country Drainage District
No. 7, will be the non-Federal cost-sharing sponsor for the Port Arthur and Vicinity CSRM Plan.
Based on October 2017 price levels, the estimated project first cost of the recommended plan is
$744,865,000. All construction work will be cost shared in accordance with the cost sharing
provisions of Section 103 of WRDA 1986, as amended. The Federal share of the project first
costs of the hurricane and storm damage risk reduction features is estimated to be $484,162,000
(65 percent) and the total non-Federal share is estimated to be $260,703,000 (35 percent). The
non-Federal contribution of LERRDs for the improvements associated with the Port Arthur and
Vicinity CSRM Plan would be about $8,376,000. The non-Federal sponsor's cost for removing
and relocating utilities and discharge pipelines associated with the Port Arthur and Vicinity
CSRM Plan that are non-compensable would be about $38,544,000. The non-Federal sponsor
would be responsible for the OMRR&R of the project after construction. OMRR&R is currently
estimated at $199,000.

DAEN
SUBJECT: Sabine Pass to Galveston Bay, Texas, Coastal Storm Risk Management and
Ecosystem Restoration Study

(3) Based on a 2.75 percent discount rate and a 50-year period of analysis, the total
average annual costs of the project are estimated to be $29,757,000, including OMRR&R. The
recommended plan would reduce average annual coastal storm damages by about 76 percent and
would leave average total equivalent annual residual damages estimated at $42,604,000. The
equivalent average annual benefits for Port Arthur and Vicinity CSRM Plan is estimated to be
$139,106,000 with net average annual benefits of $109,349,000, which results in a BCR of
approximately 4.7 to 1. The recommended plan is the National Economic Development plan.

b. The second element of the recommended plan is the Orange 3 CSRM Plan.

(1) This element includes 15.6 miles of newly constructed levee ranging from 12.0 to
17.5 feet NAVD 88 in elevation and 10.7 miles of newly constructed floodwalls and gates
ranging from 13.5 to 16 feet NAVD 88. Seven pump stations, 56 drainage structures, and 32
closure gates located at road and railway crossings would be constructed to mitigate interior
flooding during surge events. Finally, two navigable sector gates with adjacent vertical lift
floodgates for normal channel flows would be constructed in Adams and Cow Bayous to reduce
surge penetration. Unavoidable direct and indirect environmental impacts to 2,409 acres of
forested wetlands and estuarine marsh associated with the Orange 3 CSRM Plan would be fully
compensated by the implementation of the mitigation plan. Monitoring and adaptive
management of the mitigation areas will be conducted until the mitigation measures have been
demonstrated to be successful.

(2) Orange County, Texas will be the non-Federal cost-sharing sponsor for the Orange 3
CSRM Plan. Based on October 2017 price levels, the estimated first cost of the recommended
Orange 3 CSRM Plan is $1,967,826,000. All construction work will be cost shared in
accordance with the cost sharing provisions of Section 103 of WRDA 1986, as amended. The
Federal share of the first costs of the hurricane and storm damage risk reduction features is
estimated to be $1,279,087,000 (65 percent) and the total non-Federal share is estimated to be
$688,739,000 (35 percent). The non-Federal contribution of LERRDs for the newly constructed
levee/floodwall system associated with the Orange 3 CSRM Plan would be about $33,199,000.
The non-Federal sponsor's cost for removing and relocating utilities and discharge pipelines
associated with the Orange 3 CSRM Plan that are non-compensable would be about
$62,387,000. The non-Federal sponsor would be responsible for OMRR&R of the project after
construction. OMRR&R is currently estimated at $4,663,000.

(3) Based on a 2.75 percent discount rate and a 50-year period of analysis, the total
average annual costs of the Orange 3 CSRM Plan are estimated to be $87,268,000, including
OMRR&R. The recommended plan would reduce average annual coastal storm damages by
about 64 percent and would leave average total equivalent annual residual damages estimated at
$60,496,000. The equivalent average annual benefits for Orange 3 CSRM Plan is estimated to
be $105,919,000 with net average annual benefits of $18,651,000, which results in a benefit-cost
ratio (BCR) of approximately 1.2 to 1. The recommended plan is the National Economic
Development plan.

3

DAEN
SUBJECT: Sabine Pass to Galveston Bay, Texas, Coastal Storm Risk Management and
Ecosystem Restoration Study

c. The third element of the recommended plan is the Freeport and Vicinity CSRM Plan.

(1) The recommended Freeport and Vicinity CSRM Plan would raise approximately 13.1
miles of the existing earthen levee system and construct or reconstruct approximately 5.5 miles
of floodwall, improving approximately 43 percent of the existing 43-mile long system. Final
elevations would range from 15.8 to 23.8 feet NAVD 88. Navigable sector gates would be
installed in the Dow Barge Canal to reduce surge penetration in that area. Ten vehicle closure
structures at road and railroad crossings would be replaced and erosion protection would be
added. Other project features include raising and reconstructing the Highway 332 crossing,
installation of four drainage structures, including one at the head of the Dow Barge Canal, and
raising the floodwall at Port Freeport's Berth 5 dock.

(2) The existing Freeport Harbor Flood Protection Project local sponsor, the Velasco
Drainage District, will be the non-Federal cost-sharing sponsor for the Freeport and Vicinity
CSRM Plan. Based on October 2017 price levels, the estimated project first cost of the
recommended plan is $606,313,000. All construction work will be cost shared. In accordance
with the cost sharing provisions of Section 103 of WRDA 1986, as amended, the Federal share
of the project first costs of the hurricane and storm damage risk reduction features is estimated to
be $393,953,000 (65 percent) and the total non-Federal share is estimated to be $207,660,000 (35
percent). The non-Federal contribution of LERRDs for the improvements associated with the
Freeport and Vicinity CSRM Plan would be about $10,876,000. The non-Federal sponsor's cost
for removing and relocating utilities and discharge pipelines associated with the Freeport and
Vicinity CSRM Plan that are non-compensable would be about $27,389,000. The non-Federal
sponsor would be responsible for the OMRR&R of the project after construction. OMRR&R is
currently estimated at $723,000.

(3) Based on a 2.75 percent discount rate and a 50-year period of analysis, the total
average annual costs of the Freeport Harbor CSRM Plan are estimated to be $24,774,000,
including OMRR&R. The recommended plan would reduce average annual coastal storm
damages by about 66 percent and would leave average total equivalent annual residual damages
estimated at $107,006,000. The equivalent average annual benefits for Freeport and Vicinity
CSRM Plan is estimated to be $207,608,000 with net average annual benefits of $182,834,000,
which results in a BCR of approximately 8.4 to 1. The recommended plan is the National
Economic Development plan.

d. The recommended plan is intended to prevent damages to structures and content and
critical infrastructure from coastal storm surge and waves. It should be noted, however, that
reducing the risk of loss of life during major storm events can only be achieved by adhering to
existing procedures for evacuation of residents and visitors well before expected hurricane
landfall, thus removing people from harm's way. This study recommends continuation of the
evacuation policy both with and without the project.

4

DAEN
SUBJECT: Sabine Pass to Galveston Bay, Texas, Coastal Storm Risk Management and
Ecosystem Restoration Study

4. In accordance with USACE Sea Level Change (SLC) Guidance, Engineer Regulation (ER)
1100-2-8162, the study evaluated potential impacts in SLC in its plan formulation and
engineering of the recommended plan. Three levels of Relative Sea Level Change (RSLC) were
considered for both the without-project and with-project conditions. The risk reduction system
has been designed to provide a risk reduction against a 1 percent annual chance exceedance
probability storm event based on the 2070 intermediate RSLC forecast condition. In recognition
of the uncertainty presented by sea level rise, adaptation capacity has been incorporated into the
final feasibility-level design to maximize the systems' overall usefulness over the life of the
project. The adaptability will allow for limited overtopping of wave and minor still water
overtopping that would then be mitigated for using interior drainage features or height increases
to the floodwall if required. The equivalent average annual benefits are estimated to range from
nearly $55,000,000 to $164,000,000 under the low SLC scenario, $104,000,000 to $203,000,000
under the intermediate SLC scenario, and to nearly $157,000,000 to $291,000,000 under the high
SLC scenario. Corresponding annual net benefits for the recommended plan range from
approximately $16,000,000 to $178,000,000 with BCRs ranging from 1.2 to 8.2. The
recommended plan also shows high project performance with a 99 percent conditional non-
exceedance probability over a 50-year period under all SLC scenarios.

5. The goals and objectives included in the Campaign Plan of the USACE have been fully
integrated into the Sabine Pass to Galveston Bay study process. The recommended plan was
developed in coordination and consultation with various Federal, state, and local agencies using
a systematic and regional approach to formulating solutions and evaluating the benefits and
impacts that would result. The feasibility study evaluated shoreline erosion and coastal storm
damage problems as well as opportunities for environmental restoration and protection. Risk and
uncertainty were addressed during the study by sensitivity analysis that evaluated the potential
impacts of sea level change and economic assumptions as well as cost uncertainties.
6. In accordance with the USACE Engineer Circular (EC) 1165-2-214 on review of decision
documents, all technical, engineering and scientific work underwent an open, dynamic and
rigorous review process to ensure technical quality. This included District Quality Control
review, Agency Technical Review, Major Subordinate Command review, Independent External
Peer Review, Public Review, and a USACE Headquarters policy and legal review. All
comments from the above referenced reviews have been addressed and incorporated into the
final documents. Overall, the reviews resulted in improvements to the technical quality of the
report.

7. Washington-level review indicates that the project recommended by the reporting officers is
technically sound, environmentally and socially acceptable, and economically justified. The plan
complies with all essential elements of the 1983 U.S. Water Resources Council's *Economic and
Environmental Principles and Guidelines for Water and Land Related Resources Implementation
Studies* and complies with other administrative and legislative policies and guidelines. Also the
views of interested parties, including Federal, state and local agencies have been considered.

DAEN
SUBJECT: Sabine Pass to Galveston Bay, Texas, Coastal Storm Risk Management and Ecosystem Restoration Study

8. Federal implementation of the project would be subject to the non-Federal sponsors agreeing in a binding written agreement to comply with applicable Federal laws and policies, and to perform the following non-Federal obligations, including, but not limited, to the following:

a. Provide 35 percent of initial project costs assigned to hurricane and storm damage reduction, and 100 percent of initial project costs assigned to protecting undeveloped private lands and other private shores which do not provide public benefits, as further specified below:

(1) Enter into an agreement that provides, prior to construction, 35 percent of design costs;

(2) Provide all lands, easements, and rights-of-way, and perform or ensure the performance of any relocations determined by the Federal Government to be necessary for the initial construction or the operation and maintenance of the project, all in compliance with applicable provisions of the Uniform Relocation and Assistance and Real Property Acquisition Policies Act of 1970, as amended (42 U.S.C. 4601-4655) and the regulations contained n 49 C.F.R. Part 24;

(3) Provide, during construction, any additional amounts as are necessary to make the total contribution equal to 35 percent of initial project costs assigned to hurricane and storm damage reduction, and 100 percent of initial project costs assigned to protecting undeveloped private lands and other private shores which do not provide public benefits;

b. For so long as the project remains authorized, operate, maintain, repair, rehabilitate, and replace the project, or functional portion of the project, including any mitigation features, at no cost to the Federal Government, in a manner compatible with the project's authorized purposes and in accordance with applicable Federal and State laws and regulations and any specific, directions prescribed by the Federal Government;

c. Inform affected interests, at least annually, of the extent of protection afforded by the project; participate in and comply with applicable Federal floodplain management and flood insurance programs; comply with Section 402 of the Water Resources Development Act of 1986, as amended (33 U.S.C. 701b-12); and publicize floodplain information in the area concerned and provide this information to zoning and other regulatory agencies for their use in adopting regulations, or taking other actions, to prevent unwise future development and to ensure compatibility with protection levels provided by the project;

d. Prevent obstructions or encroachments on the project (including prescribing and enforcing regulations to prevent such obstructions or encroachments) that might reduce the level of protection the project affords, hinder operation and maintenance of the project, or interfere with the project's proper function;

e. Give the Federal Government a right to enter, at reasonable times and in a reasonable manner, upon property that the non-Federal sponsors own or control for access to the project for

6

DAEN
SUBJECT: Sabine Pass to Galveston Bay, Texas, Coastal Storm Risk Management and
Ecosystem Restoration Study

the purpose of completing, inspecting, operating, maintaining, repairing, rehabilitating, or
replacing the project;

f. Hold and save the United States free from all damages arising from design, construction,
operation, maintenance, repair, rehabilitation, and replacement of the project, except for damages
due to the fault or negligence of the United States or its contractors;

g. Perform, or ensure performance of, any investigations for hazardous substances that are
determined necessary to identify the existence and extent of any hazardous substances regulated
under the Comprehensive Environmental Response, Compensation, and Liability Act
(CERCLA), Public Law 96-510, as amended (42 U.S.C. 9601-9675), that may exist in, on, or
under lands, easements, or rights-of-way that the Federal Government determines to be required
for construction, operation, and maintenance of the project. However, for lands that the Federal
government determines to be subject to the navigation servitude, only the Federal Government
shall perform such investigations unless the Federal Government provides the non-Federal
sponsors with prior specific written direction, in which case the non-Federal sponsors shall
perform such investigations in accordance with such written direction;

h. Assume, as between the Federal Government and the non-Federal sponsors, complete
financial responsibility for all necessary cleanup and response costs of any hazardous substances
regulated under CERCLA that are located in, on, or under lands, easements, or rights-of-way that
the Federal Government determines to be required for construction, operation, and maintenance
of the project; and

i. Agree, as between the Federal Government and the non-Federal sponsors, that the non-
Federal sponsors shall be considered the operator of the project for the purpose of CERCLA
liability, and to the maximum extent practicable, operate, maintain, repair, rehabilitate, and
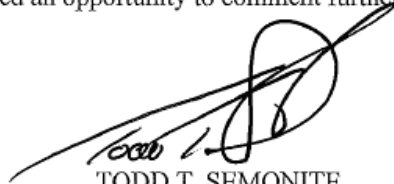replace the project in a manner that will not cause liability to arise under CERCLA.

9. I concur in the findings, conclusions, and recommendations of the reporting officers.
Accordingly, I recommend that the plan to reduce the risks of tropical storm surge impacts in
Orange, Jefferson and Brazoria Counties, Texas be authorized in accordance with the reporting
officers' recommended plan at an estimated project first cost of $3,318,772,000, with such
modifications as in the discretion of the Chief of Engineers may be advisable. My
recommendation is subject to cost sharing, financing, and other applicable requirements of
Federal and state laws and policies, including Section 103 of WRDA 1986, as amended.

10. The recommendation contained herein reflects the information available at this time and
current departmental policies governing formulation of individual projects. It does not reflect
program and budgeting priorities inherent in the formulation of a national civil works
construction program or the perspective of higher review levels within the executive branch.

7

DAEN
SUBJECT: Sabine Pass to Galveston Bay, Texas, Coastal Storm Risk Management and
Ecosystem Restoration Study

Consequently, the recommendation may be modified before it is transmitted to the Congress as a
proposal for authorization and implementation funding. However, prior to transmittal to
Congress, the state, interested Federal agencies, and other parties will be advised of any
significant modifications and will be afforded an opportunity to comment further.

TODD T. SEMONITE
Lieutenant General, USA
Chief of Engineers

Acronyms and Abbreviations

ACE	Annual chance exceedance
ADCIRC	Advanced Circulation
AEP	Annual exceedance probabilities
ANN	Artificial neural network
ARI	Average recurrence intervals
CEM	Coastal Engineering Manual
CHS	Coastal Hazards System
CL	Confidence limits
CSRM	Coastal Storm Risk Management
CTXCS	Coastal Texas Comprehensive Study
DEM	Digital elevation model
DGPS	Digital global positioning system
DTM	Digital terrain model
EB	Event-based
ERDC	US Army Engineer Research and Development Center
FEMA	Federal Emergency Management Agency
FIS	Flood information study
GIS	Geographical information system
GKF	Gaussian Kernel Function
GLCC	Global Land Cover Characterization
GMSL	Global mean sea level
GOM	Gulf of Mexico
GPM	Gaussian Process Metamodeling
GPS	Global Positioning System

HFP	Hurricane Flood Protection
HPTRM	High performance turf reinforcement mats
HSDRRS	Hurricane Storm Damage Risk Reduction System
ID	Identifier
JPM	Joint probability method
JPM-OS	JPM with Optimal Sampling
LACPR	Louisiana Coastal Protection and Restoration Project
LCLU	Land cover and land use
LMSL	Local mean sea level
LTEP	Long-term exceedance probability
MGC	Multivariate Gaussian Copula
MWD	Mean wave direction
NACCS	North Atlantic Coast Comprehensive Study
NAD83	North American Datum of 1983
NAVD88	North American Vertical Datum of 1988
NCLD	National Land Cover Database
NFIP	National Flood Insurance Program
NLR	Nonlinear residual
NOAA	National Oceanic and Atmospheric Administration
NRC	National Research Council
NTR	Nontidal residual
PBL	Planetary Boundary Layer
PCHA	Probabilistic coastal hazard analysis
PED	Pre-construction, Engineering, and Design
QC	Quality control
RANS	Reynolds averaged Navier-Stokes

RB   response-based

RS   Response surface

RSLC   Relative sea level change

S2G   Sabine Pass to Galveston Bay

SLC   Sea level change

SLC0   Sea level change corresponding to beginning of service life

SLC1   Sea level change corresponding to 50 yr service life

SLC2   Sea level change corresponding to 100 yr service life

SLR   Sea level rise

SNWW   Sabine-Neches Waterway

SP   Save point

SRR   Storm recurrence rate

StratMap   Texas Strategic Mapping

STWAVE   Steady State Wave

SWG   Galveston District

SWL   Storm water level

TC   Tropical cyclone

TWDB   Texas Water Development Board

USACE   US Army Corps of Engineers

USGS   US Geological Survey

WAM   Wave model

WNAT   Western North Atlantic

REPORT DOCUMENTATION PAGE

1. REPORT DATE	2. REPORT TYPE	3. DATES COVERED (From - To)
August 2021	Report 1 of a series	

4. TITLE AND SUBTITLE
Sabine Pass to Galveston Bay, TX
Pre-Construction, Engineering and Design (PED): Coastal Storm Surge and Wave Hazard Assessment: Report 1 – Background and Approach

5a. CONTRACT NUMBER

5b. GRANT NUMBER

5c. PROGRAM ELEMENT NUMBER

6. AUTHOR(S)
Jeffrey A. Melby, Thomas C. Massey, Abigail L. Stehno, Norberto C. Nadal-Caraballo, Shubhra Misra, and Victor Gonzalez

5d. PROJECT NUMBER

5e. TASK NUMBER

5f. WORK UNIT NUMBER

7. PERFORMING ORGANIZATION NAME(S) AND ADDRESS(ES)
Coastal and Hydraulics Laboratory
US Army Engineer Research and Development Center
3909 Halls Ferry Road
Vicksburg, MS 39180-6199

US Army Engineer District, Galveston
CESWG-EC-H
2000 Fort Point Road
Galveston, TX 77550

8. PERFORMING ORGANIZATION REPORT NUMBER
ERDC/CHL TR-21-15

9. SPONSORING/MONITORING AGENCY NAME(S) AND ADDRESS(ES)
US Army Engineer District, Galveston
Galveston, TX

10. SPONSOR/MONITOR'S ACRONYM(S)
SWG

11. SPONSOR/MONITOR'S REPORT NUMBER(S)

12. DISTRIBUTION/AVAILABILITY STATEMENT
Approved for public release; distribution is unlimited.

13. SUPPLEMENTARY NOTES
Funding provided via Galveston District CCLC.

14. ABSTRACT
The US Army Corps of Engineers, Galveston District, is executing the Sabine Pass to Galveston Bay Coastal Storm Risk Management (CSRM) project for Brazoria, Jefferson, and Orange Counties regions. The project is currently in the Pre-construction, Engineering, and Design phase. This report documents coastal storm water level and wave hazards for the Port Arthur CSRM structures. Coastal storm water level (SWL) and wave loading and overtopping are quantified using high-fidelity hydrodynamic modeling and stochastic simulations. The CSTORM coupled water level and wave modeling system simulated 195 synthetic tropical storms on three relative sea level change scenarios for with- and without-project meshes. Annual exceedance probability (AEP) mean values were reported for the range of 0.2 to 0.001 for peak SWL and wave height (Hm0) along with associated confidence limits. Wave period and mean wave direction associated with Hm0 were also computed. A response-based stochastic simulation approach is applied to compute AEP runup and overtopping for levees and overtopping, nappe geometry, and combined hydrostatic and hydrodynamic fluid pressures for floodwalls. CSRM structure crest design elevations are defined based on overtopping rates corresponding to incipient damage. Survivability and resilience are evaluated. A system-wide hazard level assessment was conducted to establish final recommended system-wide CSRM structure elevations.

15. SUBJECT TERMS
Flood control, Flood forecasting, Galveston Bay (Tex.), Hurricanes, Sabine Pass (La. And Tex.), Storm surges, Water waves

16. SECURITY CLASSIFICATION OF:			17. LIMITATION OF ABSTRACT	18. NUMBER OF PAGES	19a. NAME OF RESPONSIBLE PERSON
a. REPORT	**b. ABSTRACT**	**c. THIS PAGE**			Jeffrey A. Melby
Unclassified	Unclassified	Unclassified	SAR	249	**19b. TELEPHONE NUMBER** (Include area code) 601-634-2026